

Doctoral Thesis

Thesis Title

Conversion of Methyl Glycosides to
Valuable Chemicals via Rhenium-
Catalyzed Deoxydehydration

Department of Applied Chemistry
Graduate School of Engineering,
TOHOKU UNIVERSITY

JI CAO

(ID No. B6TD9402)

Advising Professor at Tohoku Univ.	Professor Keiichi, Tomishige
Research Advisor at Tohoku Univ.	Assistant professor Masazumi, Tamura
Dissertation Committee Members Name marked with “○” is the Chief Examiner	<div>○ <u>Prof. Keiichi, Tomishige</u></div> <div>1 <u>Prof. Tetsutaro, Hattori</u> 2 <u>Prof. Hitoshi, Kasai</u></div>

Conversion of Methyl Glycosides to Valuable Chemicals via Rhenium-Catalyzed Deoxydehydration

ABSTRACT: Even though fossil fuels are necessary in our daily life, their clearly limited reserves and the growth of energy demand promote the development of renewable biomass increasingly significant. Carbohydrates are major component of lignocellulosic biomass, and have been used as important building blocks in organic synthesis because of their structural diversity and high density of functional groups, in order to obtain valuable chemicals such as medicines, biomaterials and agrichemicals. But conventionally, by organic method for carbohydrates transformation are multistep with high cost and low yield, while catalytic methods for carbohydrates transformation lose their original stereostructure. Deoxydehydration (DODH) reaction is a potential method to decrease the oxygen content effectively. It can particularly remove two vicinal OH groups, which are frequently observed in biomass-based products, to form corresponding C=C bond. Recently, our laboratory found that Pd- or Au- modified CeO₂ supported Re catalysts (ReO_x-Pd/CeO₂ or ReO_x-Au/CeO₂) were effective for transformation of vicinal OH groups in polyols by using gaseous H₂, providing the corresponding saturated or unsaturated dideoxy polyols via DODH + hydrogenation (DODH + HG) or DODH reactions, respectively.

Methyl glycosides are structurally stable, and can be easily obtained by methanolysis of lignocellulosic biomass or methylation of monosaccharides. The main object of this research is to develop an effective catalytic system for conversion of methyl glycosides with vicinal *cis*-OH groups without protection of the OH groups to valuable dideoxy products, particularly chiral polyols with keeping their original stereostructure.

[Chapter 2: Deoxydehydration + hydrogenation of *cis*-vicinal OH groups over ReO_x-Pd/CeO₂ catalyst and mechanistic study] ReO_x-Pd/CeO₂ (Re=2 wt%, Pd/Re=0.25) was an effective catalyst for the direct and selective transformation of methyl glycosides having *cis*-vicinal OH groups into the corresponding dideoxy products in high yields with maintaining the original structure using H₂ as a reductant. From the kinetic results, the reactivity of methyl glycosides is lower than that of simple cyclic diols, which can be attributed to the presence of the substituents in the methyl glycosides except the *cis*-vicinal diols. Moreover, the reactivity of the methyl glycosides depended on the structure, and the low activity is related to the direction of the substituents adjacent to the *cis*-vicinal diols in methyl glycosides. The kinetic parameters regarding substrate concentration and H₂ pressure are almost zero in DODH+HG of methyl glycosides and simple cyclic diols over ReO_x-Pd/CeO₂ catalyst, suggesting that the reaction mechanisms of the methyl glycosides and simple cyclic diols is similar. DFT calculations of the adsorption state and the transition state of methyl glycosides on isolated Re species over CeO₂ showed that the activation energy of these methyl glycosides is different, which was also supported by Arrhenius plots based on the experimental results. The reactivity difference of methyl glycosides may be due to their activation energy differences, and the

difference of these substrates is derived from the intricate interactions between the adjacent functional groups to *cis*-vicinal OH groups and the surface hydroxy groups

[Chapter 3: Deoxydehydration of *cis*-vicinal OH groups on methyl glycosides over $\text{ReO}_x\text{-Au/CeO}_2$ catalyst^[1]] Transformation of sugars without protection of the OH groups is an ideal method and a powerful tool for biomass utilization, and particularly, unsaturated sugars are a promising target because they can be transformed to versatile chemicals owing to the olefin group in molecular.

Herein, we demonstrated direct transformation of various methyl glycosides, without protection of the OH groups to the corresponding unsaturated sugars with maintaining their original stereostructure in high selectivities (61-93%) and yields (up to 90%) using $\text{ReO}_x\text{-Au/CeO}_2$ catalyst by deoxydehydration. $\text{ReO}_x\text{-dpAu}^{0.3}/\text{CeO}_2$ catalyst prepared by deposition-precipitation method was a reusable heterogeneous catalyst and was applied to DODH of methyl glycosides. It can selectively remove the *cis*-vicinal OH groups in various methyl glycosides, providing the corresponding olefin products in high selectivity and high yield even at low H_2 pressure (0.2-1.7 MPa at 413 K). Moreover, maximum turnover number (TON) per total Re atom of 270 was obtained.

[Chapter 4: One-pot selective synthesis of chiral polyols from methyl glycosides via deoxydehydration^[2,3]] Chiral polyols are important intermediates and chemicals in the synthesis of fine chemistry, such as perfume and alcoholic beverage, cosmetics, food additives, polymers and medicines. The consecutive reaction (ring opening + hydrogenation of C=O) of dideoxy products in the DODH + HG of methyl glycosides over $\text{ReO}_x\text{-Pd/CeO}_2$ catalyst, was investigated using various hydrogenation and/or hydrolysis catalysts. This is because such dideoxy products have asymmetric carbon atoms, fixed hydroxyl group positions and original stereostructure in the molecules.

The results showed that the combination of $\text{ReO}_x\text{-Pd/CeO}_2$ catalyst and hydrogenation catalyst ($\text{Rh-ReO}_x/\text{SiO}_2$, $\text{Ir-ReO}_x/\text{SiO}_2$, Pt/SiO_2 ^[5], $\text{Pt/SiO}_2\text{-Al}_2\text{O}_3$ ^[5] and commercial Ru/C catalyst) showed high selectivity of their corresponding chiral polyols. For example, (2*S*)-1,2,5-pentantriol was obtained with 97% yield and 96% e.e from methyl β -D-ribofuranoside over $\text{ReO}_x\text{-Pd/CeO}_2$ and $\text{Ir-ReO}_x/\text{SiO}_2$ catalyst.

[Conclusion] Methyl glycosides with *cis*-vicinal OH groups could be directly and selectively transformed to the corresponding saturated dideoxy products over $\text{ReO}_x\text{-Pd/CeO}_2$ catalyst via DODH +HG reaction, and the methyl glycosides could be transformed to the corresponding unsaturated dideoxy products in high yields over $\text{ReO}_x\text{-Au/CeO}_2$ catalyst via DODH reaction without protection of the OH groups and with keeping the original stereostructure. Chiral polyols were selectively synthesized from methyl glycosides in high total yield and high e.e. by DODH, hydrolysis, and hydrogenation reactions.

[References] [1] J. Cao, M. Tamura, Y. Nakagawa, K. Tomishige, *ACS Catal.* 2019, 3725-3729; [2] M. Tamura, N. Yuasa, J. Cao, Y. Nakagawa, K. Tomishige, *Angew. Chem. Int. Ed.* 2018, 57, 8058-8062; [3] S. Krishna, J. Cao, M. Tamura, Y. Nakagawa, M. De bruyn, G. S. Jacobson, B. M. Weckhuysen, J. A. Dumesic, K. Tomishige, and G. W. Huber, *ACS Sustainable Chem. Eng.* 2019, <https://doi.org/10.1021/acssuschemeng.9b04634>.

Contents

Chapter 1 General Introduction

1.1	Energy demands and fossil fuels	1
1.2	Biomass in renewable resources	5
1.3	Carbohydrates in biomass	8
1.4	Deoxydehydration reaction	13
1.5	Research purpose and strategy	18
1.6	Outline of this thesis	20
	References	23

Chapter 2 Mechanistic study on deoxydehydration + hydrogenation of methyl glycosides to the dideoxy sugars over $\text{ReO}_x\text{-Pd/CeO}_2$ catalyst

2.2	Introduction	27
2.2	Experimental	28
2.3	Results and Discussion	33
2.4	Conclusions	42
	References	44

Chapter 3 Direct synthesis of unsaturated sugars from methyl glycosides

3.1	Introduction	77
3.2	Experimental	79
3.3	Results and Discussion	85
3.4	Conclusions	89
	References	90

Chapter 4 One-pot selective synthesis of chiral polyols from methyl glycosides via deoxydehydration

4.1	Introduction	149
4.2	Experimental	150
4.3	Results and Discussion	154
4.4	Conclusions	158
	References	159

Chapter 5 Summary and conclusion

	Acknowledgements	172
	List of Publications	174

Chapter 1

General Introduction

1.1 Energy demands and Fossil fuels

Energy drives human society and it is extremely important to continue human development. The total demand for energy in the world is rapidly increasing with the increase of the human population, and the development of modern society. In 2017, almost 80% of the global energy demands was survived by fossil fuels for heating, electricity, transportation, and so on^[1]. On the other hand, renewable energy is only contributing 13.5% of the global energy demands, and the rest 6.5% of global energy need is survived by nuclear power^[2]. In 2018, the world consumed about 13200 million tonnes (Mtoe) of primary energy, which is about 27 times larger than that in 1800 (Figure 1.1^[1, 3-4]). And due to the rapid increase of the world population, global energy consumption will increase by more than 25% from 2018 to 2040^[5-6].

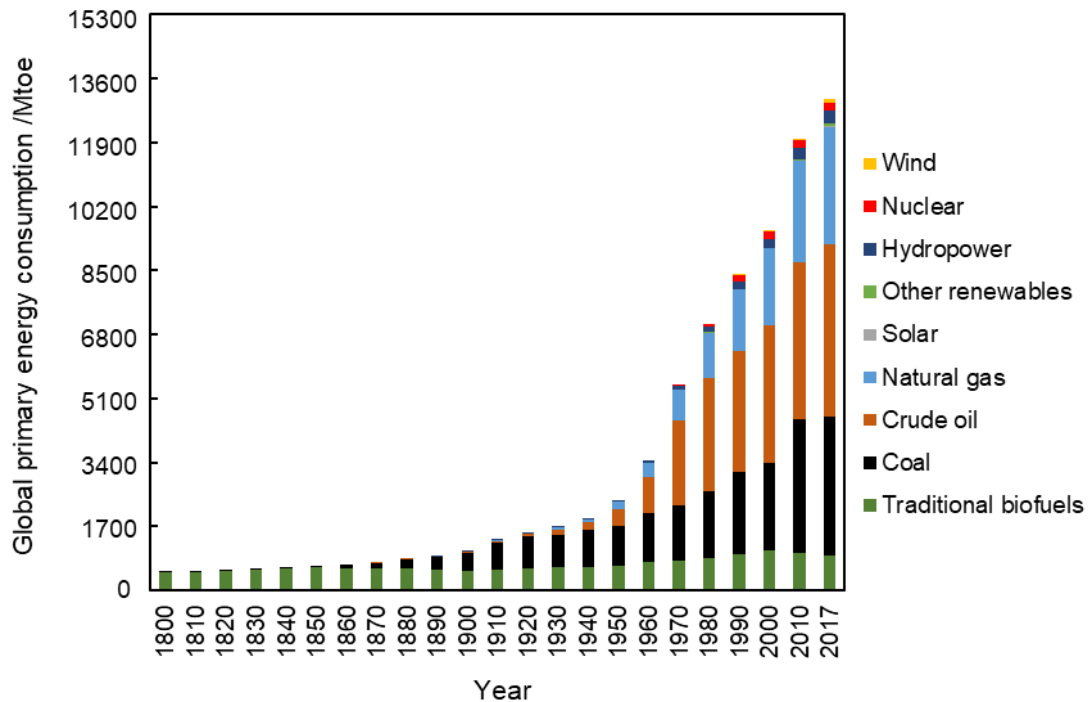


Figure 1.1 Primary energy consumption by source in the world (1800-2018) ^[1, 3-4]

Fossil fuels are non-renewable resources, including petroleum, natural gas (shale gas) and coal, and are the worldwide energy resources and feedstocks formed from carbohydrates in millions of years. They have advantages such as low cost, easy collection and convenient transportation.

Petroleum is a naturally formed liquid, which can be found in geological formations beneath the earth's surface, and it is a mixture of various hydrocarbons. The common molecules in petroleum are alkanes, cycloalkanes, aromatic hydrocarbons, or complicated chemicals like asphaltenes. Petroleum is generally used for transports (in U.S., about 89% of petroleum was used for transportation in 2018^[3]), heating, and electricity. The petrochemical industry uses petroleum as a raw feedstock to make products such as plastics, solvents, and hundreds of other chemicals and end-user goods. Figure 1.2 showed the predicted petroleum demand under stated policies scenario (existing policy frameworks) and sustainable development scenario (an integrated approach to achieving internationally agreed objectives on climate change, air quality and universal access to modern energy)^[5]. It was predicted that petroleum demand growth is robust to 2030, but the growth may get slow down greatly from 2030 to 2040 because the demand can be controlled by the development of electric cars.

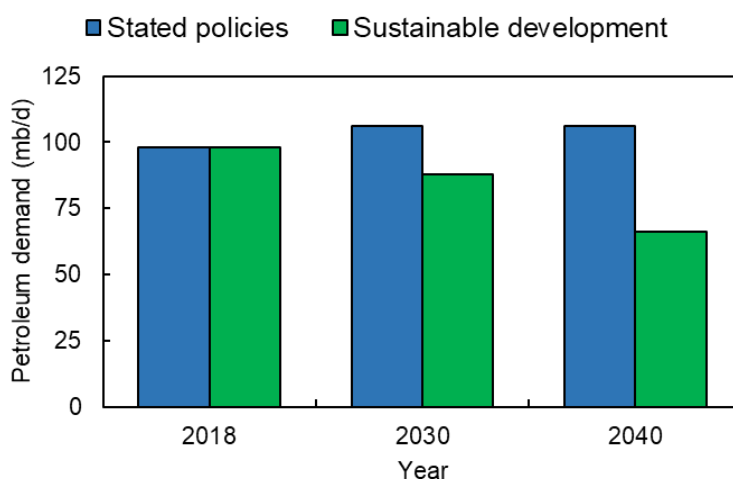


Figure 1.2 Global petroleum demand from 2018 to 2040^[5]

Coal is a combustible black or brownish-black sedimentary rock, which is formed as rock strata called coal seams. The content of coal is mostly carbon with H, S, O and N. Coal is most

abundant and affordable fossil fuel in the world, and annual world coal consumption amount is about 5800 Mtoe. About 75% of coal is used as thermal coal^[7], and in 2019, the coal is responsible for about 40% of global electricity generation^[5]. The demand outlook (from 2018 to 2040) of coal under the stated policies scenario and sustainable development scenario is shown in Figure 1.3^[5]. It is predicted that the global coal demand is essentially flat under stated policies scenario, and the demand falls rapidly under sustainable development scenario, there is a stark variation between these two scenarios in the next 20 years (2018 to 2040).

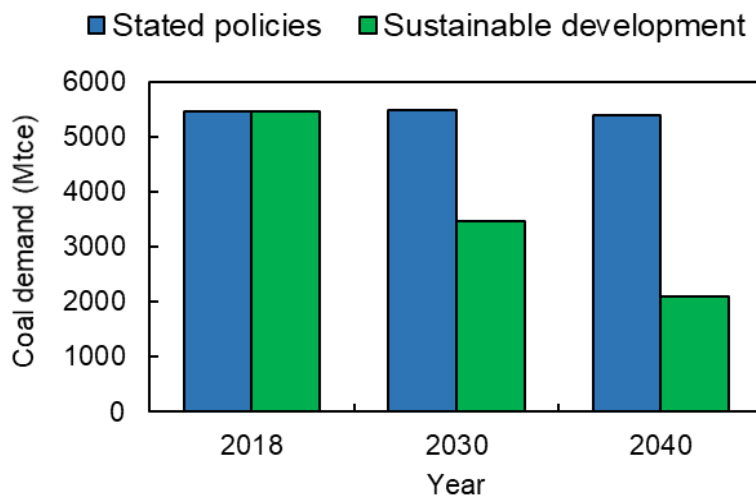


Figure 1.3 Global coal demand from 2018 to 2040^[5]

Natural gas is a naturally occurring hydrocarbon gas mixture, which mainly consists of CH_4 , and commonly includes various higher alkanes, and a small amount of CO_2 , N_2 , H_2S , or He. Most natural gas is used for heating (including industrial and residential), electricity generating, and transportation. In U.S., about 35% of natural gas was used for electricity, and about 50% of natural was used for industrial and residential heating, and 3% of natural gas was used for transportation in 2018^[5]. The demand outlook (to 2040) of natural gas under the stated policies scenario and sustainable development scenario is shown in Figure 1.4^[5]. It is predicted that the natural gas demand is keeping growth under stated policies scenario, and the demand falls slightly from 2030 under sustainable development scenario.

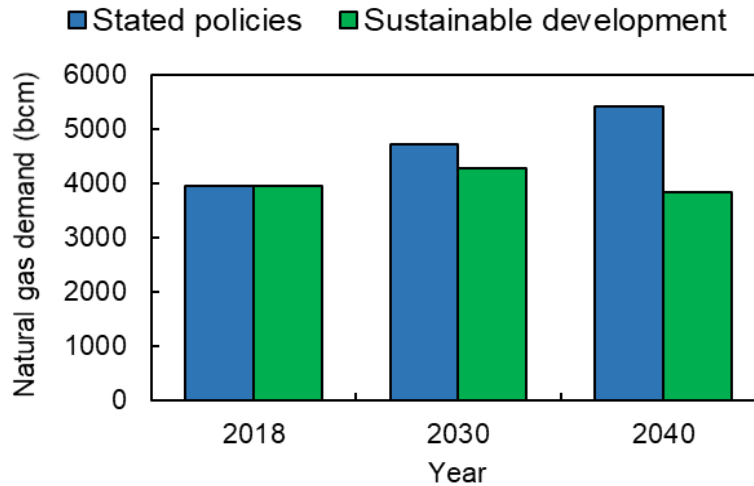


Figure 1.4 Global natural gas demand from 2018 to 2040^[5]

Even though fossil fuels are necessary for our daily life, they still have disadvantages such as their reservation is limited and they could not be regenerated in a short time. It was predicted that the petroleum, natural gas, and coal may deplete by 2040, 2042, and 2112, respectively^[8]. Due to the population pressure and the depletion of fossil fuels, the price of petroleum and natural gas increased dramatically since 2000 and reached the highest price in 2008, and then kept fluctuated since 2009^[9]. In addition, the increasing energy demand has imposed the increase of conventional fuel prices, declining the economy of the countries which are dependent on the fossil fuel import.

The use of fossil fuel also causes many severe global environmental. In 2018, the emission of CO₂ into atmosphere through the consumption of fossil fuels (oil, natural gas and coal) were 33890.8 Mtoe, occupying 82% of total carbon dioxide emission. China (28%), U.S. (15%) and India (7%) produced about half of the CO₂ emission in the world (Figure1.5^[6]). Among the several kinds of fossil fuels, coal units produce the highest emission amount of CO₂ per unit electric energy produced (about 0.1 tons of CO₂ per toe), while natural gas units produce on about 0.06 tons of CO₂ per toe^[10]. The emission of CO₂ would cause global warming. It was analyzed that the average global surface temperature has increased approximately 1.0°C since 1880, and it has a trend to rise up to 1.5°C from 2030 to 2052^[11]. Furthermore, burning fossil fuels also emit other pollutants such as SO₂, NO_x, toxic particulate matters, and smoke into the

air.

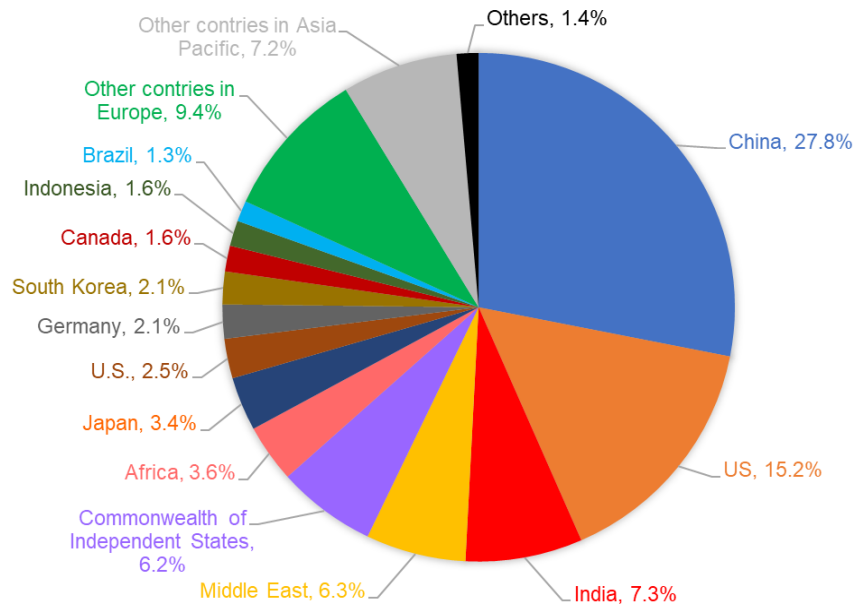


Figure 1.5 Global CO₂ emissions in 2018^[6]

The collection and production of fossil fuels such as oil fields or coal mines also may cause unrecoverable damages to the surrounding environment including air, water, and soil pollutions. And the unearthing, processing, and moving of oil, natural gas, and coal, which are stored underground, also would take enormous damage on our landscapes.

Therefore, renewable carbon energy resources and feedstocks as alternatives for fossil-based carbon sources are increasingly significant and attract more attentions in the 21st century.

1.2 Biomass in renewable resources

1.2.1 The development of renewable resources

In recent years, alternative energy resources instead of current fossil fuels are urgently required, in other words, the production of energy (electricity, heat, fuels, chemicals as well as other products) should be strongly based on renewable resources because they have little/none environmental hazards. Renewable energy resources include solar, hydropower, wind, tide and geotherm, as well as biomass. In fact, the total contribution of renewable resources remains small now, even though we include modern biofuels and hydropower, the energy generation amount of

renewable resources is still less than five percent among all sources. So, we have a long way to transit from a non-renewable-based (fossil fuels) energy to a renewable one.

It was reported that renewable energy excluding hydropower (solar, wind, geothermal, biomass and others) in energy generation increased by over 15 times from 1990 to 2018 (28 years), which is two times higher than the average growth from 1965 to 1990 (7.5 times in these 25 years). Wind (12.2 Mtoe) contributed more to renewable generation growth than solar (11.3 Mtoe), and it has accounted for around 50% of renewables generation in the last few years (from 2010). Solar has constantly increased its share in renewable energy generation, and represents 24% in 2018, 13% higher than the 11% in 2013 (Figure 1.6)^[6]. Meanwhile, the hydropower energy generation showed steady growth (15% per year).

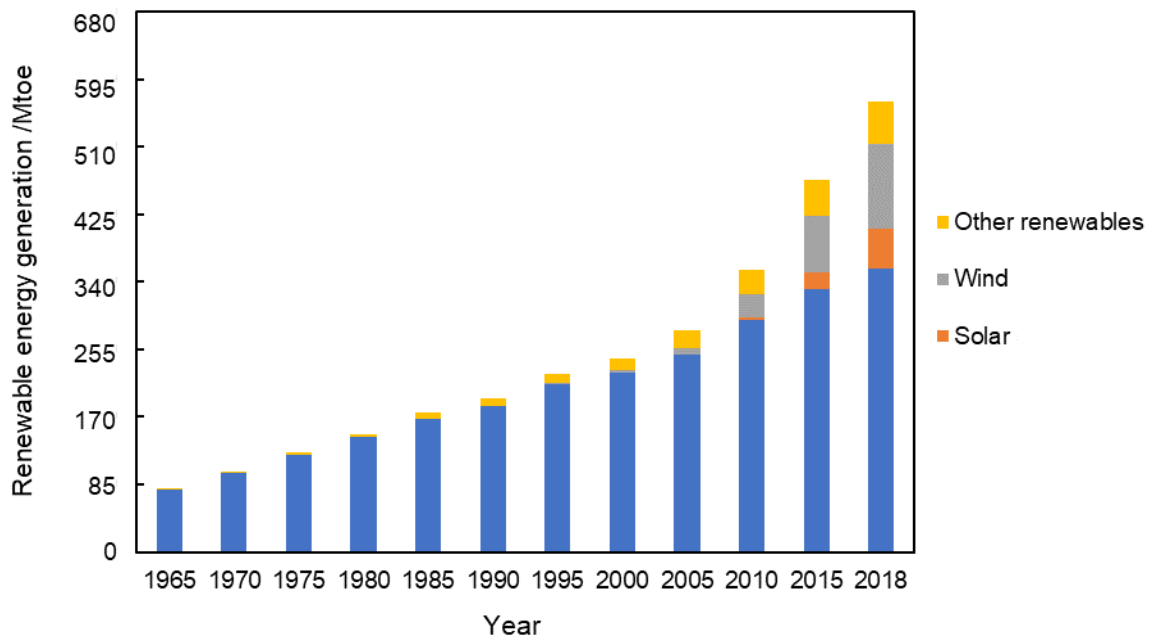


Figure 1.6 Renewable energy generation by source (Others includes electricity generated from geothermal, biomass and other sources of renewable energy).

Among these renewable resources, recyclable and abundant biomass plays special roles for the sustainable development scenario since it can provide us food sources, renewable materials, and energy production.

Biomass is an abundant, cheap and biodegradable resource with low initial ignition structural organic component, which could help the transition to the low carbon economy. It contains moisture, C, H, O elements, water-soluble nutrient elements and alkaline-earth elements. Biomass including woods, plants, agricultural crops, foods, yards, wood wastes and animal manures has become an important part of the world's chemical feedstock and energy resource. It was reported that the world biomass production amounts to 170,000 Mtoe per annum of which only 3% is used for food and non-food human consumption. However, biomass also has some disadvantages, for example, it contains 42 wt% of oxygen based on the dry weight, and the high oxygen content is unwanted, moreover, it has high values of moisture, halogen, and some hazardous trace elements; therefore, it has low values of energy density (bulk density and calorific value)^[12].

The most traditional utilization of biomass is directly burning for heating. Actually, even neglecting the massive use of wood as a construction material, 55% of biomass was used in burning with very low efficiency^[5]. Biomass also can be converted into biofuels, fertilizers, neutralizing alkaline reagents, building materials, as well as some biochemicals. On the one hand, biomass can increase the burning efficiency by increasing the bulk density like pelleting or densification^[13]. The heating value of biomass can be improved by thermal pretreatment such as torrefaction, pyrolysis, and gasification to increase the carbon content and decrease the unnecessary oxygen content^[14].

Biofuels are suitable for the production of bioethanol, biogas and biodiesel as renewable low-carbon energy resources, which have been increasingly demanded. "First generation biofuels" typically are bioethanol from sugar fermentation and biodiesel from vegetable oil transesterification. And "second generation biofuels" or "advanced biofuels" are non-food-based biofuels that can be produced from various kinds of biomass^[15]. In 2018, the world energy consumption by biomass increased by 18% from 2017, and 88 Mtoe of biofuels was produced globally, which growth averaged 9.7% from 2017^[5]. Brazil (3.1 Mtoe) and Indonesia (2.2 Mtoe) together accounted for about two-thirds of global growth (8.5 Mtoe). In 2018, as fuels, the production amount of ethanol was 60.4 Mtoe in North America, accounting for 56% of total

production amount. And biodiesel production in Europe amounted to 34.9 Mtoe, representing 37%^[6] of total production amount. Although biofuels are becoming essential energy resources, the world energy consumption by biomass was still under 13% nowadays because of the higher cost of biofuels production than that of fossil fuels^[16].

1.3 Carbohydrates in biomass

Carbohydrates are naturally present in biomass of plants and animals. They are mainly formed by green plants in a multitude of bio-synthetic pathways, for example, the photosynthetic process^[17]. They makeup 70-75% of dried plants but are present only 5-10% in dried animal bodies as glycogen, sugars and their derivatives^[18]. Carbohydrates are divided into three subgroups on the basis of their degree of polymerization: monosaccharides (including sugar alcohols), oligosaccharides and polysaccharides. Monosaccharides are simple sugars, oligosaccharides comprise a few monosaccharide units (2-9) linked together with glycosidic bonds formed by expelling water molecules, and polysaccharides are abundant in nature, such as cellulose, starch and hemicelluloses.

Lignocellulosic biomass, which is composed of cellulose, hemicellulose and lignin, is the most important polymer component in carbohydrates, such as woody and agricultural feedstocks (Figure 1.7). Cellulose is the main part of woody biomass (40-60%), has the chain structure composed of D-glucose and it functioned as the support for cell walls in biomass. Commonly, it is not soluble in water or organic solvents at room temperature. Hemicellulose is the second largest component in biomass (20-40%), and is composed of polymers of pentoses (xylose, arabinose), hexoses (glucose, mannose, galactose), and sugar acids^[19]. Cellulose and hemicellulose as polysaccharides can be degraded into smaller molecules for further production of value-added chemicals with less oxygen content. Biorefinery is a process of fractionating and/or converting biomass into bio-products in solid, liquid, and gaseous forms, in an eco-friendly way through advanced technologies^[17]. Compared with petroleum refinery, the biorefinery using cellulose and hemicellulose as feedstocks, has many advantages such as sustainability, easy accessibility, and large supply.

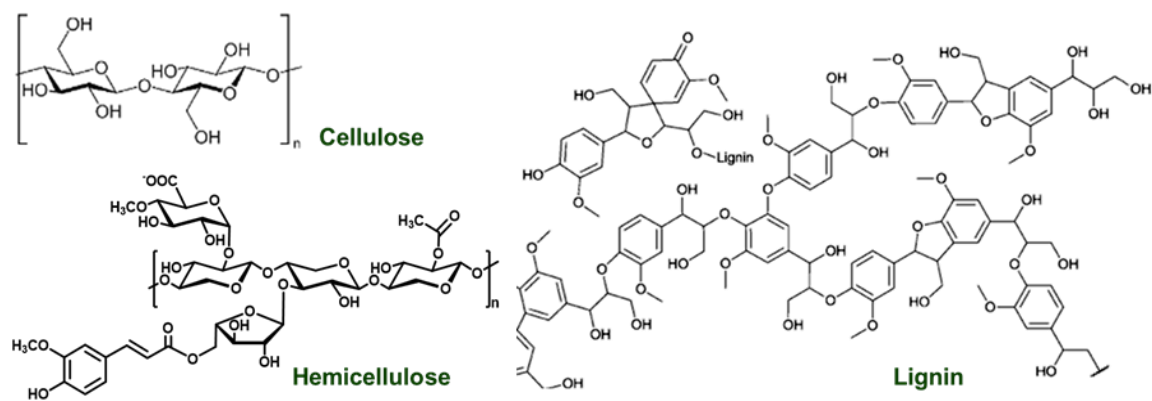


Figure 1.7 Chemical structures of lignocellulose (cellulose, hemicellulose, and lignin)

Conventionally, highly functionalized renewable biomass feedstocks (saccharides and polyols) could be converted to various value-added chemicals via thermal conversion, hydrolysis, hydrogenolysis, deoxygenation, dehydration, decarbonylation, reforming, oxidation and so on^[20-23].

1.3.1 Thermal or thermochemical conversion of carbohydrates

Energy products can be obtained from cellulosic biomass (polysaccharides) by thermal or thermochemical conversion. There are four processes for thermal or thermochemical conversion, such as combustion, pyrolysis, gasification, and liquefaction (Figure 1.8)^[24].

Pyrolysis process is the process of conversion of specific biomass into tars (bio-oil), chars, and combustible gas products through partial combustion under the oxygen environment. In the gasification process, solid biomass was transformed into synthesis gas (syngas) by heating, the syngas was mainly composed of CO, H₂, and N₂. In the combustion process, biomass was reacted with oxygen to form CO₂, H₂O, and was heat in a high temperature environment. The liquefaction of biomass is conducted in water, it can convert biomass into fertilizer or biofuels and syngas. However, these methods lose the original stereostructure of carbohydrates despite that the stereostructure was useful for the synthesis of valuable chemicals.

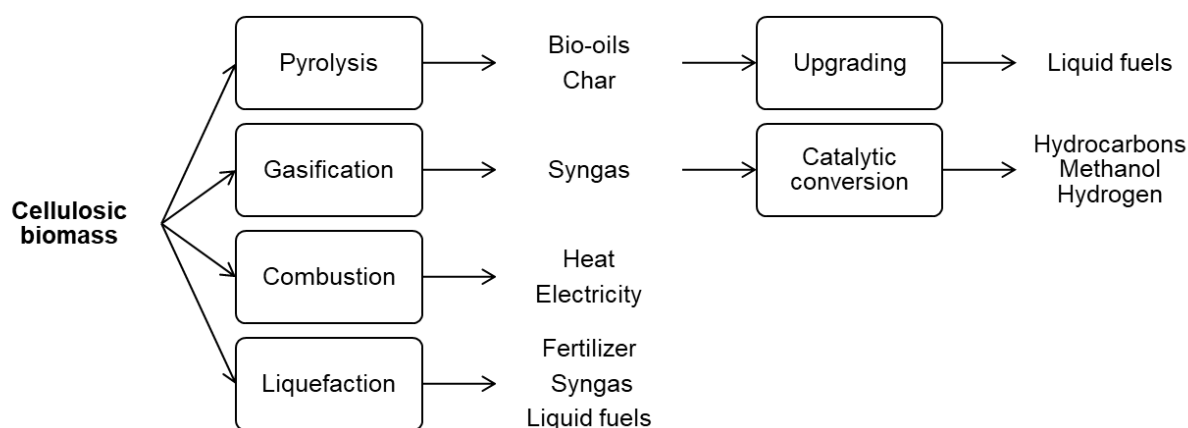


Figure 1.8 Thermochemical conversion of cellulosic biomass into energy products

Among the above four thermal conversion processes of biomass, pyrolysis and gasification are widely used two. Pyrolysis is generally carried out at lower temperatures (typically at 773 K) than gasification (typically higher than 1073 K). Pyrolysis provides complex fractions of combustible gases, tars and chars by thermal degradation, in the absence of oxidizing agent, such as air and oxygen, while gasification mainly provides a simple gaseous phase by heating, in the presence of controlled amounts of oxidizing agents, such as air, oxygen or steam.

1.3.2 Chemical conversion processes of carbohydrates ~hydrolysis

As introduced above, biomasses are usually complex feedstocks because lignocellulosic materials (polysaccharides) are the most important component in them. The most common chemical pretreatment method of these carbohydrates is hydrolysis, useful monosaccharides (glucose, galactose, arabinose, xylose and others) can be obtained by hydrolysis, and it can be accomplished by chemical or biochemical treatment (Figure1.9).

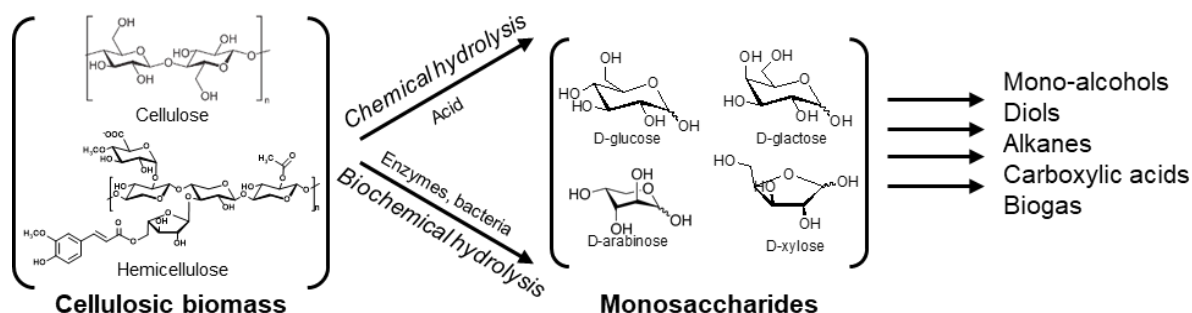


Figure 1.9 Process scheme for the hydrolysis of biomass-derived carbohydrates into various valuable products

Chemical treatment was acid hydrolysis (pretreat with acids like H_2SO_4 or HCl), it can be accomplished either by concentrated mineral acids at low temperatures^[25] or by dilute acid at high temperatures^[26]. During the acid hydrolysis process, depolymerization of carbohydrates to their monosaccharide moieties reactions take place. The major hydrolysis products are glucose, others are aldohexoses (mannose and galactose) and aldopentoses (xylose and arabinose).

Biochemical treatment allows the decomposition of biomass to available carbohydrates, using biological agents such as bacteria, enzymes, and so on^[27]. Anaerobic digestion and fermentation are the most widely used biochemical technologies for biomass hydrolysis. Anaerobic digestion is a multi-step biological process, it is useful for the proper management of waste and the generation of renewable energy. The fermentation process contains multiple biochemical reactions, it could convert monosaccharides (hexoses and pentoses) into ethanol and CO_2 by microorganisms such as yeasts, under anaerobic conditions.

1.3.3 Chemical conversion processes of carbohydrates ~dehydration

Dehydration is commonly carried out in the reaction of carbohydrates due to their large amount of OH groups, especially by using acid catalysts or acid conditions^[21-22, 28]. As a dehydration product of monosaccharides (fructose or glucose), 5-hydroxymethylfurfural (5-HMF) is an important and renewable platform chemical in the bio-based production. The production and application of 5-HMF and the reaction mechanism of the dehydration reaction

had been reviewed by Kuster and his co-workers in 1990^[29] and Lewkowski and his co-workers in 2001^[30]. It is an useful intermediate for the production of 2,5-dimethylfuran (DMF), which could be used as biofuel, and other important molecules such as levulinic acid, 2,5-furandicarboxylic acid, 3,5-dihydroxymethylfuran and so on (Figure 1.10)^[22, 31]. Besides, dehydration is also used for the conversion of sugar alcohols combined with hydrogenolysis and/or dehydration reaction. For example, 1,2-propanediol can be produced from glycerol by this process^[32].

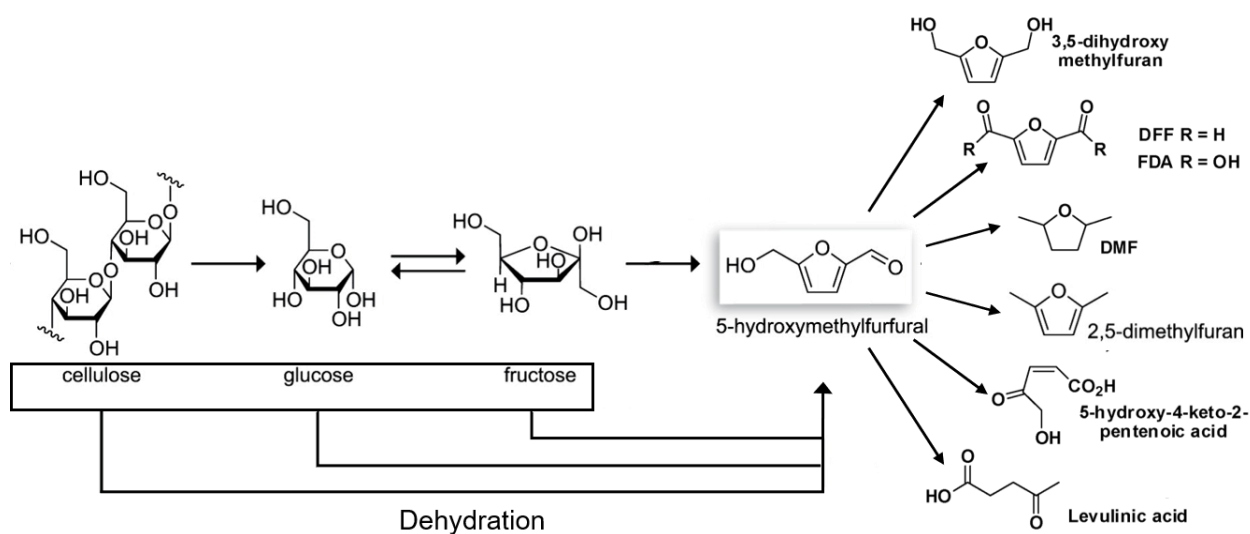


Figure 1.10 Dehydration of saccharides to valuable chemicals

1.3.4 Chemical conversion processes of carbohydrates ~others

Some other common chemical conversion processes of carbohydrates (for example, glucose) are illustrated in Figure 1.11. Glucose can be oxidized, either under acidic or alkaline conditions, to mono- and dicarboxylic acids, or reduced to various polyhydroxy compounds by means of hydrogenation or hydrogenolysis. Other possibilities include dehydration and isomerization.

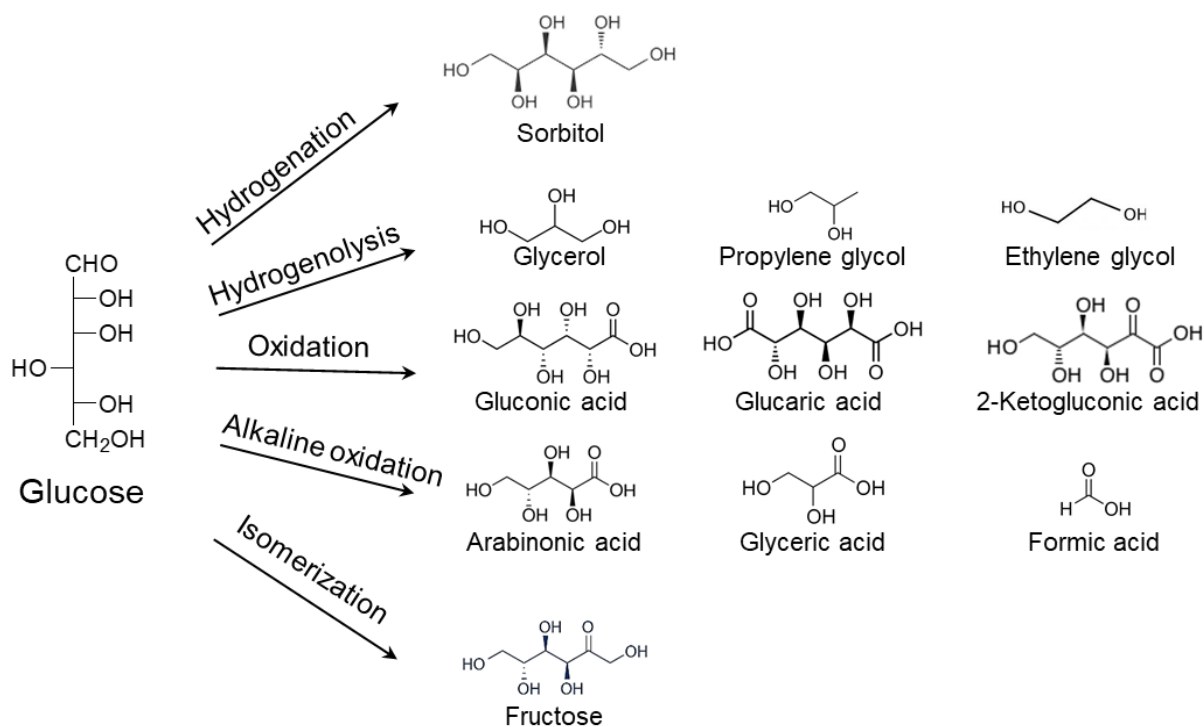


Figure 1.11 Common chemical conversion process of glucose.

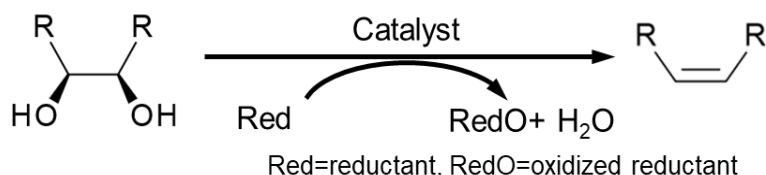
Recently, some effective transformation methods of sugars with keeping their original stereostructure have been developed. Gagné and co-workers^[33-35] reported effective reaction system of $B(C_6F_5)_3^+$ tertiary silane and $B(C_6F_5)_3^+$ catecholborane for the selective transformation of silyl-protected polyols to chiral polyol synthons and reductive carbocyclization of unsaturated carbohydrates, where selective C–O bond cleavage of saccharide derivatives was achieved. Huber and co-workers demonstrated a novel transformation route of cellulose via the formation of levoglucosenone, providing tetrahydrofurandimethanol and 1,6-hexanediol in high selectivity^[36-38].

1.4 Deoxydehydration reaction

1.4.1 Deoxydehydration (DODH) process

It is very important to develop a system for removal of the unwanted high oxygen content (hydroxyl groups) in carbohydrate-derived feedstocks to synthesize value-added chemicals. Deoxydehydration (DODH) is a simple, direct and potential method to effectively decrease the

OH groups in biomass-based products. DODH can remove two vicinal hydroxyl groups which are frequently observed in biomass-based molecules, especially sugars and sugar alcohols, to form a corresponding C=C bond (Scheme 1.1, R = alkyl, aryl, or H) without changing the other part of this molecular. Catalyzed DODH reactions have been actively investigated in recent years, including homogeneous and heterogeneous catalysts.

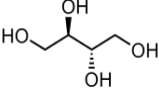
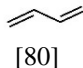
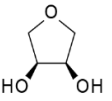
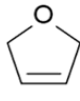
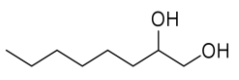
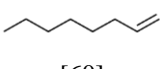
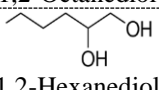
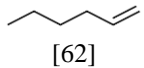
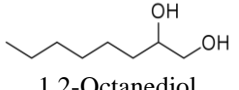
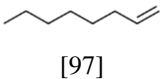
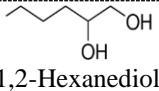
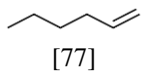
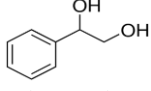
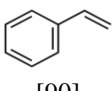


Scheme 1.1 Generalized Scheme for deoxydehydration (DODH) Reaction

1.4.2 Homogeneous DODH catalysts

Typical DODH systems use homogeneous catalysts, and some typical examples are shown in Table 1.1. Effective Re-^[39-57], W-^[58], Mo-^[59-63] Ru-^[64], and V-^[65] based homogeneous catalysts were developed. In 1996, Cook and Andrews firstly reported an Re-based catalyst, where Cp*ReO₃ (Cp* = pentamethylcyclopentadienyl) can catalyze the DODH reaction of erythritol to form 1,3-butanediene with the reductant of triphenylphosphine (PPh₃)^[39]. Recently, researchers became interested in Re-catalyzed DODH reaction because of their high reaction yields to the target product. Methyltrioxorhenium (CH₃ReO₃) has been the most common homogeneous catalyst in DODH reaction since Ziegler and co-workers reported it as an effective catalyst^[40] for the DODH system of epoxides and diols. Then, Toste and co-workers reported a seminal work on the DODH of various saccharide derivatives with CH₃ReO₃ catalyst to afford the corresponding polyenes in moderate to high yields^[41-42], moreover, this effective catalyst was also reported by other groups ^[51, 56]. Generally, DODH reaction over homogeneous catalyst has some problems. For example, PPh₃, Na₂SO₃ and secondly alcohols are commonly used as reductants in the reaction; the turnover number (TON) of these homogeneous catalysts are not so high (typically lower than 100); and homogeneous catalysts are commonly difficult to separate, which may lead the high cost.

Table 1.1 Homogeneous catalyst for DODH reaction

Substrate	Catalyst	Reductant	Reaction conditions	Product [Yield / %]	TOF ^a /h ⁻¹	TON ^a	Ref
 Erythritol	Cp*ReO ₃	PPh ₃	408 K 28 h	 [80]	1.9	54	[39]
 1,4-Anhydroerythritol	CH ₃ ReO ₃	3-Octanol	443 K 2.5 h	 [90]	14	36	[41]
 1,2-Octanediol	CH ₃ ReO ₃	NaSO ₃	423K 20 h	 [60]	2	30	[66]
 1,2-Hexanediol	<i>cis</i> -[Ru(TMSO/DMSO) ₄]	H ₂	393 K 3 h	 [62]	21	62	[64]
 1,2-Octanediol	[n-Bu ₄ N](dipic [#]) VO ₂	PPh ₃	423K 48 h	 [97]	0.2	10	[65]
 1,2-Hexanediol	(NH ₄) ₆ Mo ₇ O ₂₄ ·4H ₂ O	<i>i</i> PrOH	523 K 18 h	 [77]	0.9	15	[60]
 Phenyl-1,2-ethanediol	Cp''ReO ₃	PPh ₃	408 K 15 h N ₂	 [90]	3.0	47	[57]

^aper active metal (Re, V, Mo and Ru) atom, calculated from the product yield. Cp* = pentamethylcyclopentadienyl. Cp'' = 1,3-ditert-butylcyclopentadienyl. dipic[#]=2,6-pyridinedicarboxylate

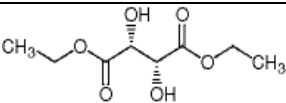
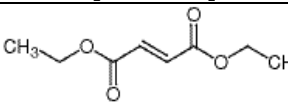
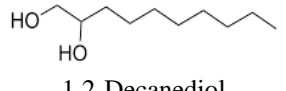
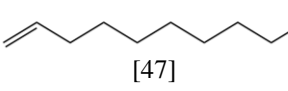
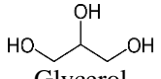
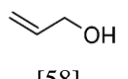
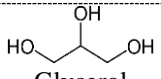
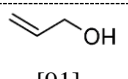
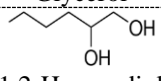
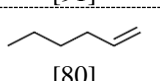
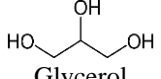
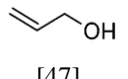
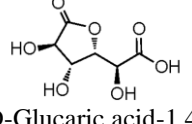
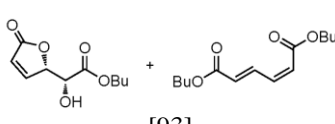
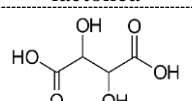
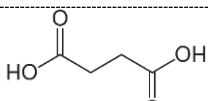
1.4.3 Heterogeneous DODH catalysts

The application of heterogeneous catalysts and H₂ reductant is under development, some results were listed in Table 1.2. In 2013, Nicholas and Jentoft reported the first heterogeneous rhenium example, ReO_x/C catalyst, which has the activity for DODH of glycols to their corresponding olefins^[67]. Recently, Sharkey and co-workers stabilized the ReO_x and MoO_x on solid supports such as Fe₂O₃, TiO₂, Al₂O₃, SiO₂, and ZrO₂, the obtained catalysts were effective for the DODH of 1,2-diols to olefins^[68]. Moreover, other supported ReO_x catalysts^[67-72], supported MoO_x catalysts^[68, 73], unsupported Re nanoparticles (ReO_x NPs)^[74] and bimetallic Pt-Re catalyst^[75] were also reported to be effective for the DODH reaction. H₂, PPh₃ and secondary alcohols were used as reductants.

Otherwise, some pieces of literature have reported on application of the DODH reaction to the transformation of sugars: Toste demonstrated conversion of sugar acids to dicarboxylic acids

with a combination catalyst system of Pd/C, KReO₄ and NH₄ReO₄^[48]. Moreover, MoO_x/Carbon black was also applied to the conversion of sugar acids to dicarboxylic acids^[73].

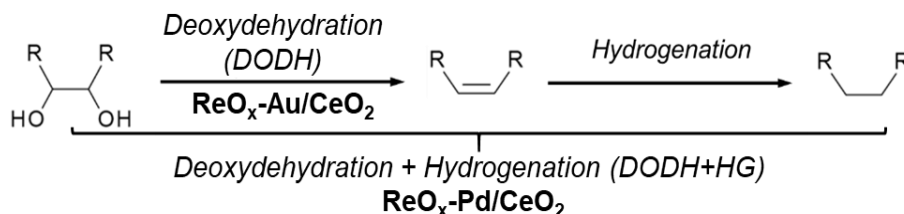
Table 1.2 Heterogeneous catalyst for DODH reaction

Substrate	Catalyst	Reductant	Reaction conditions	Product [Yield / %]	TOF /h ⁻¹ *TON*	Ref
 (+)-Diethyl tartrate	ReO _x /C	H ₂	423 K 48 h	 [95]	0.7 32	[67]
 1,2-Decanediol	(NH ₄) ₆ Mo ₇ O ₂₄	PPh ₃	423 K 24 h	 [47]		[68]
 Glycerol	ReO _x /TiO ₂	3-Octanol	443 K 1 h	 [58]	11 272	[69]
 Glycerol	ReO _x /Al ₂ O ₃	2-Hexanol	443 K 2.5 h	 [91]	16 186	[70]
 1,2-Hexanediol	ReO _x NPs	3-Octanol	433 K 10 h	 [80]	1.7 40	[74]
 Glycerol	Pt-Re Nanoporous	H ₂	433 K 12 h N ₂	 [47]	33 327	[75]
 D-Glucaric acid-1,4-lactone	ReO _x /ZrO ₂	Butanol	393 K 24 h N ₂	 [93]	0.7 32	[72]
 Tartaric acid	MoO _x /C	H ₂	443 K 24 h	 [87]	17 44	[73]

*per active metal (Re, V, Mo and Ru) atom, calculated from the product yield.

1.4.4 Previous DODH study in Tomishige lab

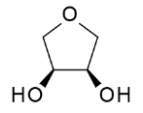

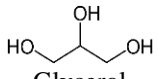
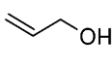
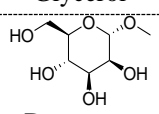
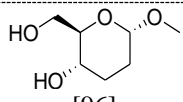
Recently, our lab found that Pd-modified CeO₂-supported Re (ReO_x-Pd/CeO₂)^[76] and Au-modified CeO₂-supported Re (ReO_x-Au/CeO₂)^[77] were effective heterogeneous catalysts for direct and selective transformation of the *cis*-vicinal OH groups in polyols by using gaseous H₂, providing the corresponding saturated and unsaturated dideoxy product, respectively, via DODH reaction with retention of the original stereostructure and without protection of OH groups (Scheme 1.2).



Scheme 1.2 Dehydration and dehydration + hydrogenation over Re-catalyst.

These results are based on our previous finding of heterogeneous $\text{ReO}_x\text{-Pd/CeO}_2$ or $\text{ReO}_x\text{-Au/CeO}_2$ catalysts effective for DODH + hydrogenation^[78-79] (DODH + HG) and DODH^[80-81] of polyols, respectively (Table 1.3).

Table 1.3 DODH reaction over $\text{ReO}_x\text{-M/CeO}_2$ catalyst

Substrate	Catalyst	Reductant	Reaction conditions	Product [Yield / %]	Ref
 1,4-Anhydroerythritol	$\text{ReO}_x\text{-Pd/CeO}_2$	H_2	8 MPa 413 K 64 h	 [>99]	[78]
 Glycerol	$\text{ReO}_x\text{-Au/CeO}_2$	H_2	8 MPa 413 K 51 h	 [91]	[80]
 Methyl α -D-mannopyranoside	$\text{ReO}_x\text{-Pd/CeO}_2$	H_2	8 MPa 413 K 51 h	 [96]	[76]

On these catalysts, isolated Re species attached on CeO_2 surface can be catalytically active and Pd and Au metals work as promoters for the formation of the active Re^{4+} species by reduction via the activation of H_2 molecule. The reaction mechanism was proposed to have four elementary reaction steps. The first step is the reduction of isolated Re^{6+} species to Re^{4+} species by activated H_2 , then the substrate with vicinal OH groups is coordinated to the Re^{4+} species with the two OH groups as diolate; after that, alkene is formed and eliminated with the regeneration of Re^{6+} center, and the catalytic cycle is completed by re-reduction of Re^{6+} species and coordination of substrate (Figure 1.12).

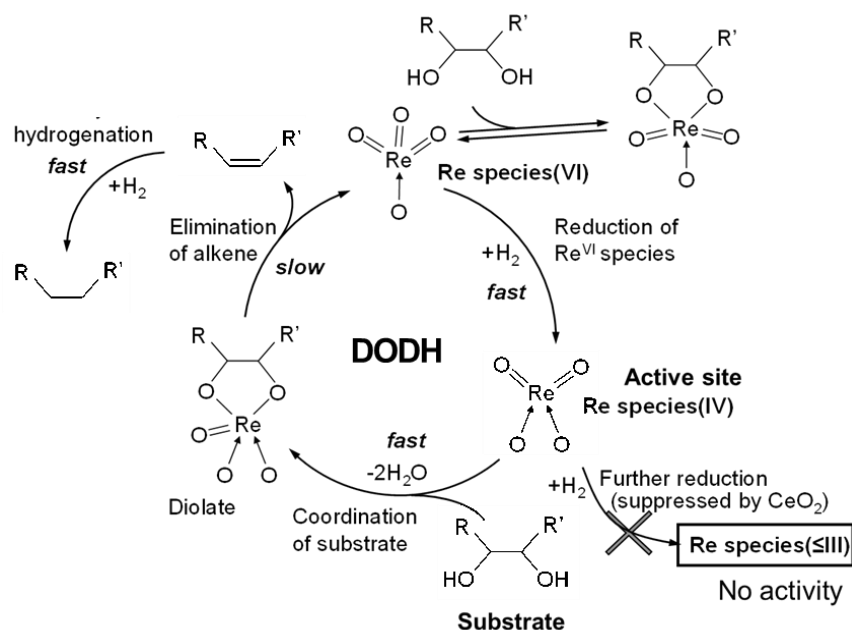


Figure 1.12 Reaction mechanism of Re-catalyzed DODH reaction over CeO_2 support

1.5 Research object and strategies

Biomass-derived compounds such as saccharides and sugar alcohols which can be easily obtained from cellulose or hemicellulose are important building blocks in biomass refinery. As chemical platforms, monosaccharides such as glucose, mannose or ribose have original stereostructure and contain high oxygen content. Carbohydrate structures often contain numerous asymmetric carbon atoms (chiral centers) whose four substituents are different.

Conventional transformation methods of saccharides into valuable chemicals such as dehydration and reforming lose their original stereostructure in spite of the chiral and stereostructure being useful for the synthesis of valuable chemicals such as medicines, biomaterials and agrichemicals^[31, 82-89]. And traditionally, valuable chiral chemicals are synthesized by multistep syntheses including protection and deprotection steps, leading to the high cost and low yield^[90-93].

In practice, a common monosaccharide will usually exist as an equilibrium mixture of six tautomeric forms in neutral or mildly acid or basic aqueous solutions (2 open-chain aldehyde and 4 heterocyclic ring forms). Under equilibrium state, the relative concentrations of these tautomeric forms are based on their thermodynamic stabilities, and cyclic forms are clearly

avored over acyclic form, and pyranose ring are favored over furanose forms. Their chemical structures of the tautomeric forms in aqueous solution and the percentage compositions of these forms and D-glucose as a model saccharide are shown in Figure 1.13.

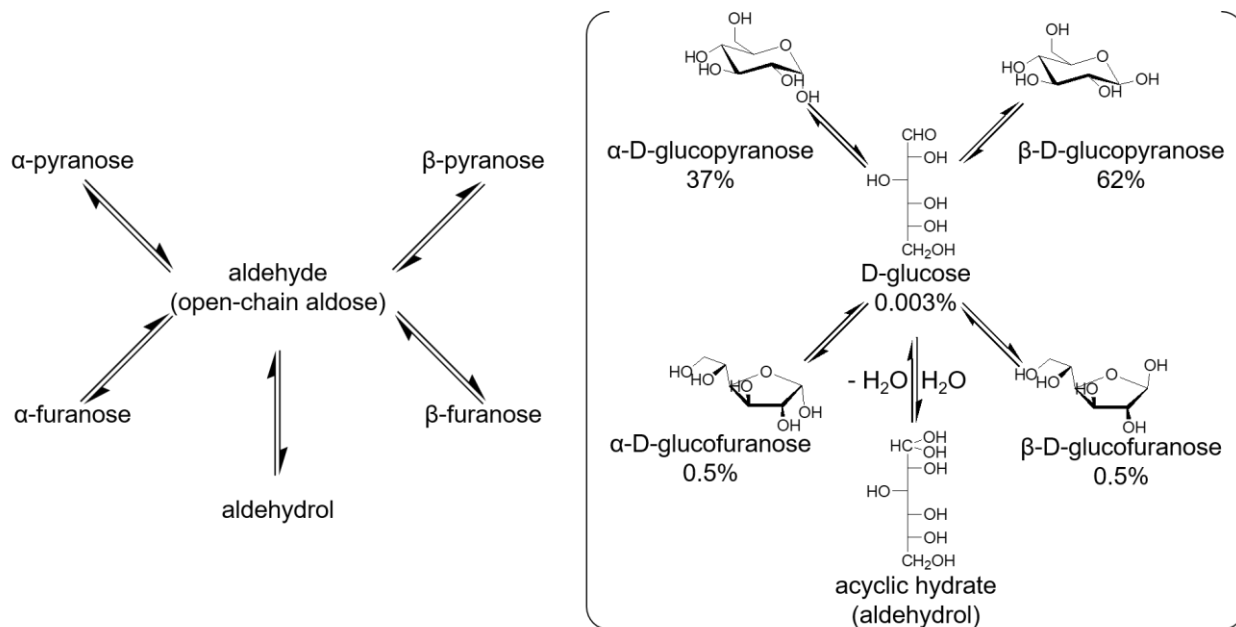
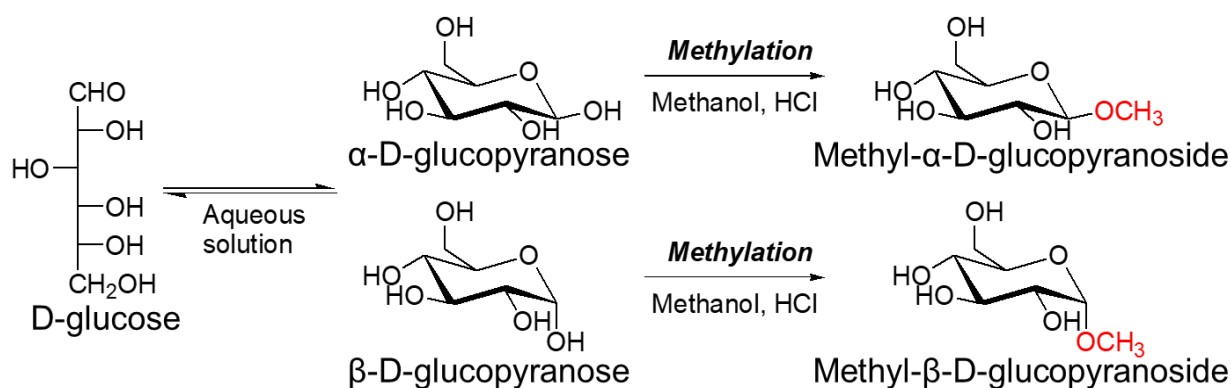


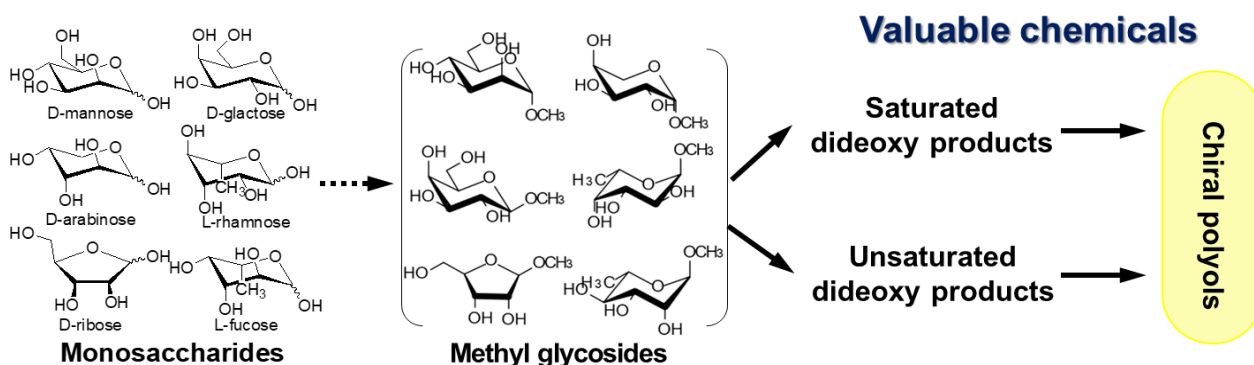
Figure 1.13 Introduction of various tautomeric forms of open-chain aldose (ex. D-glucose) in aqueous solution

To fix the stereostructure (hydroxy group position) of monosaccharides in the aqueous solution during the reaction, it is necessary to maintain the ring of monosaccharide and prevent it from equilibrating with other isomeric structures. Glycosides have “protected anomeric centers”, so they are stable under neutral or basic conditions, and the mutarotation (reducing sugars may undergo structural changes in solution, for example between α - and β -anomers via an open-chain aldehyde containing form)^[94] does not occur spontaneously on them. Hence, chemical reactions can be carried out at other sites in the glycosides. Methyl glycosides can be easily obtained by methanolysis of lignocellulosic biomass^[32] or methylation of monosaccharides with methanol and HCl^[95]. The methylation of D-glucose to methyl glycosides was shown in Scheme 1.3.



Scheme 1.3 Methylation of D-glucose to methyl glycoside.

Therefore, development of direct and selective transformation of monosaccharides without protection of the OH groups and keeping the original stereostructure is an ideal method for sugar transformation and a powerful tool for biomass transformation, and particularly dideoxy saccharides are promising target because they can be transformed to versatile chiral chemicals due to their stereostructure and multiple functional groups. The main object of this research is to develop an effective catalytic system for the conversion of methyl glycosides from monosaccharides with vicinal *cis*-OH groups to valuable dideoxy products particularly chiral polyols with original stereostructure using H_2 as a reductant (Scheme 1.4, including saturated and unsaturated product).



Scheme 1.4 Transformation of monosaccharides to valuable chemicals

1.6 Outline of the thesis

This thesis presents the results of the conversion of methyl glycosides to valuable chemicals via rhenium-catalyzed deoxydehydration.

Chapter 1 is a general introduction of fossil fuels, biomass, biomass-derived carbohydrates and the techniques for sugar conversion and DODH reaction. It also introduces the objects of this study and the strategies for the research.

Chapter 2 investigated the reaction mechanism on the deoxydehydration + hydrogenation (DODH + HG) of methyl glycosides over $\text{ReO}_x\text{-Pd/CeO}_2$ catalyst. Six kinds of methyl glycosides (such as methyl β -D-ribofuranoside, methyl α -L-rhamnopyranoside, methyl α -D-mannopyranoside, methyl β -L-arabinopyranoside, methyl β -D-galactopyranoside and methyl α -L-fucopyranoside) and the related simple cyclic diols (such as *cis*-1,2-cyclopentanediol, *cis*-1,2-cyclohexanediol and 1,4-anhydroerythritl) were selected as model substrates. Reaction conditions were optimized firstly, then time-courses of related substrates over the optimized $\text{ReO}_x\text{-Pd/CeO}_2$ catalyst were conducted and selectivities to products were compared. The kinetic parameters in the reaction of DODH + HG of methyl glycosides with vicinal OH groups and related substrates were determined. The structure of the diolate intermediate and its transition state is determined by the DFT calculations on the basis of the property of monomeric Re species on CeO_2 surface. The activation energies obtained by the experimental data and DFT calculation are compared.

Chapter 3 presents the study of the direct transformation of methyl glycosides (such as methyl α -L-rhamnopyranoside, methyl α -D-mannopyranoside, methyl β -L-arabinopyranoside, methyl β -D-galactopyranoside and methyl α -L-fucopyranoside) to corresponding unsaturated dideoxy products without protection of the OH groups where the *cis*-vicinal OH groups in the substrate were selectively converted to C=C bond with keeping the original stereostructure using heterogeneous $\text{ReO}_x\text{-Au/CeO}_2$ catalyst by DODH. The catalyst preparation method effect and H_2 pressure effect were investigated, the suitable catalyst was found out and characterized.

Chapter 4 further conducted the hydrolysis and hydrogenation of dideoxy product which obtained from methyl glycosides (such as methyl α -L-rhamnopyranoside, methyl α -D-mannopyranoside, methyl β -L-arabinopyranoside and methyl β -D-ribofuranoside) via DODH reaction, because such dideoxy have asymmetric carbon atoms, fixed hydroxyl group positions and original stereostructure in the molecules. The combinations of $\text{ReO}_x\text{-Pd/CeO}_2$ catalyst with

hydrogenation catalyst (Rh–ReO_x/SiO₂, Ir–ReO_x/SiO₂, Pt/SiO₂, Pt/SiO₂-Al₂O₃ and commercial Ru/C catalyst) were conducted under different temperature. Furthermore, one-pot synthesis of chiral polyols from methyl glycosides was also investigated.

Chapter 5 summarizes the results in chapter 2-4 and make a general conclusion of this thesis.

Reference

- [1]. Balachandar, G.; Khanna, N.; Das, D., Biohydrogen production from organic wastes by dark fermentation. In *Biohydrogen*, Elsevier: 2013; pp 103-144.
- [2]. Tiwari, G. N.; Dubey, S., *Fundamentals of photovoltaic modules and their applications*. Royal Society of Chemistry: 2009.
- [3]. , U.S. Energy Information Administration (EIA)-Energy use for transportation; Available from: <https://www.eia.gov/energyexplained/use-of-energy/transportation.php>.
- [4]. Ritchie, H.; Roser, M., **2020**.
- [5]. International Energy Agency (IEA) (2019), W. E. O., IEA, Paris, Available from: <https://www.iea.org/reports/world-energy-outlook-2019>.
- [6]. BP Statistical Review of World Energy, Available from: <https://www.bp.com/en/global/corporate/energy-economics/statistical-review-of-world-energy>.
- [7]. Riazi, M.; Gupta, R., *Coal production and processing technology*. CRC press: 2015.
- [8]. Shafiee, S.; Topal, E., *Energy Policy* **2009**, 37 (1), 181-189.
- [9]. Chen, H.; Liao, H.; Tang, B.-J.; Wei, Y.-M., *Energy Economics* **2016**, 57, 42-49.
- [10]. Leonard, M. D.; Michaelides, E. E.; Michaelides, D. N., *Renewable Energy* **2020**, 145, 951-962.
- [11]. Rull, V.; Vegas-Vilarrúbia, T.; Huber, O.; Señaris, C., *Biodiversity of Pantepui: The Pristine "Lost World" of the Neotropical Guiana Highlands*. Academic Press: 2019.
- [12]. Vassilev, S. V.; Vassileva, C. G.; Vassilev, V. S., *Fuel* **2015**, 158, 330-350.
- [13]. Miedema, J. H.; Benders, R. M. J.; Moll, H. C.; Pierie, F., *Applied Energy* **2017**, 187, 873-885.
- [14]. Chew, J. J.; Doshi, V., *Renewable and Sustainable Energy Reviews* **2011**, 15 (8), 4212-4222.
- [15]. Inderwildi, O. R.; King, D. A., *Energ. Environ. Sci.* **2009**, 2 (4), 343.
- [16]. Popp, J.; Lakner, Z.; Harangi-Rákos, M.; Fári, M., *Renewable and Sustainable Energy Reviews* **2014**, 32, 559-578.
- [17]. Al, R., *Carbohydrate chemistry: Fundamentals and applications*. World Scientific Publishing Company: 2018.
- [18]. Alén, R., *Biorefining of Forest Resources* **2011**, 20, 56-115.
- [19]. Girio, F. M.; Fonseca, C.; Carvalheiro, F.; Duarte, L. C.; Marques, S.; Bogel-Lukasik, R., *Bioresour. Technol.* **2010**, 101 (13), 4775-800.
- [20]. Huber, G. W.; Iborra, S.; Corma, A., *Chem. Rev.* **2006**, 106 (9), 4044-98.
- [21]. Binder, J. B.; Raines, R. T., *J. Am. Chem. Soc.* **2009**, 131 (5), 1979-85.
- [22]. Tong, X.; Ma, Y.; Li, Y., *Applied Catalysis A: General* **2010**, 385 (1-2), 1-13.
- [23]. Palkovits, R.; Delidovich, I., *Philos Trans A Math Phys Eng Sci* **2018**, 376 (2110).
- [24]. Tursi, A., *Biofuel Research Journal* **2019**, 6 (2), 962-979.
- [25]. ALEXANDER, C., PROCESS OF CONVERTING CELLULOSE INTO SUGAR. US Patent App. 695,795: 1901.
- [26]. Ewen, M. F.; Tomlinson, G. H., Process of producing from ligno-cellulose fermentable sugar. Google Patents: 1909.

- [27]. Behera, S.; Arora, R.; Nandhagopal, N.; Kumar, S., *Renewable and Sustainable Energy Reviews* **2014**, *36*, 91-106.
- [28]. Yi, G.; Teong, S. P.; Zhang, Y., *ChemSusChem* **2015**, *8* (7), 1151-5.
- [29]. Kuster, B., *Starch-Stärke* **1990**, *42* (8), 314-321.
- [30]. Lewkowski, J., *Arkivoc* **2001**, *2001* (1), 17-54.
- [31]. Rosatella, A. A.; Simeonov, S. P.; Frade, R. F. M.; Afonso, C. A. M., *Green Chem.* **2011**, *13* (4), 754.
- [32]. Nakagawa, Y.; Tamura, M.; Tomishige, K., *J. Mater. Chem. A* **2014**, *2* (19), 6688-6702.
- [33]. Bender, T. A.; Dabrowski, J. A.; Gagné, M. R., *ACS Catal.* **2016**, *6* (12), 8399-8403.
- [34]. Bender, T. A.; Dabrowski, J. A.; Zhong, H.; Gagné, M. R., *Org. Lett.* **2016**, *18* (16), 4120-41233.
- [35]. Lowe, J. M.; Seo, Y.; Gagné, M. R., *ACS Catal.* **2018**, *8* (9), 8192-8198.
- [36]. Cao, F.; Schwartz, T. J.; McClelland, D. J.; Krishna, S. H.; Dumesic, J. A.; Huber, G. W., *Energ. Environ. Sci.* **2015**, *8* (6), 1808-1815.
- [37]. Karanjkar, P. U.; Burt, S. P.; Chen, X. L.; Barnett, K. J.; Ball, M. R.; Kumbhalkar, M. D.; Wang, X. H.; Miller, J. B.; Hermans, I.; Dumesic, J. A.; Huber, G. W., *Catal. Sci. Technol.* **2016**, *6* (21), 7841-7851.
- [38]. Krishna, S. H.; McClelland, D. J.; Rashke, Q. A.; Dumesic, J. A.; Huber, G. W., *Green Chem.* **2017**, *19* (5), 1278-1285.
- [39]. Cook, G. K.; Andrews, M. A., *J. Am. Chem. Soc.* **1996**, *118* (39), 9448-9449.
- [40]. Ziegler, J. E.; Zdilla, M. J.; Evans, A. J.; Abu-Omar, M. M., *Inorg. Chem.* **2009**, *48* (21), 9998-10000.
- [41]. Shiramizu, M.; Toste, F. D., *Angew. Chem. Int. Ed. Engl.* **2012**, *51* (32), 8082-6.
- [42]. Shiramizu, M.; Toste, F. D., *Angew. Chem. Int. Ed. Engl.* **2013**, *52* (49), 12905-9.
- [43]. Li, X.; Wu, D.; Lu, T.; Yi, G.; Su, H.; Zhang, Y., *Angew. Chem. Int. Ed. Engl.* **2014**, *53* (16), 4200-4.
- [44]. Michael McClain, J.; Nicholas, K. M., *ACS Catal.* **2014**, *4* (7), 2109-2112.
- [45]. Raju, S.; Moret, M.-E.; Klein Gebbink, R. J. M., *ACS Catal.* **2014**, *5* (1), 281-300.
- [46]. Dethlefsen, J. R.; Fristrup, P., *ChemSusChem* **2015**, *8* (5), 767-75.
- [47]. Li, X.; Zhang, Y., *ChemSusChem* **2016**, *9* (19), 2774-2778.
- [48]. Larson, R. T.; Samant, A.; Chen, J.; Lee, W.; Bohn, M. A.; Ohlmann, D. M.; Zuend, S. J.; Toste, F. D., *J. Am. Chem. Soc.* **2017**, *139* (40), 14001-14004.
- [49]. Petersen, A. R.; Fristrup, P., *Chemistry* **2017**, *23* (43), 10235-10243.
- [50]. Morris, D. S.; van Rees, K.; Curcio, M.; Cokoja, M.; Kuhn, F. E.; Duarte, F.; Love, J. B., *Catal. Sci. Technol.* **2017**, *7* (23), 5644-5649.
- [51]. Shin, N.; Kwon, S.; Moon, S.; Hong, C. H.; Kim, Y. G., *Tetrahedron* **2017**, *73* (32), 4758-4765.
- [52]. Ricciardi, M.; Passarini, F.; Capacchione, C.; Proto, A.; Barrault, J.; Cucciniello, R.; Cespi, D., *ChemSusChem* **2018**, *11* (11), 1829-1837.
- [53]. Wozniak, B.; Li, Y. H.; Tin, S.; de Vries, J. G., *Green Chem.* **2018**, *20* (19), 4433-4437.
- [54]. Jefferson, A.; Srivastava, R. S., *Polyhedron* **2019**, *160*, 268-271.

- [55]. Donnelly, L. J.; Thomas, S. P.; Love, J. B., *Chem Asian J* **2019**, *14* (21), 3782-3790.
- [56]. Zhang, H. F.; Li, X. K.; Su, X. Y.; Ang, E. L.; Zhang, Y. G.; Zhao, H. M., *Chemcatchem* **2016**, *8* (8), 1500-1506.
- [57]. Li, J.; Lutz, M.; Otte, M.; Klein Gebbink, R. J. M., *ChemCatChem* **2018**, *10* (20), 4755-4760.
- [58]. Fang, Z.; Zetterholm, P.; Dixon, D. A., *J. Phys. Chem. A* **2016**, *120* (11), 1897-907.
- [59]. Dethlefsen, J. R.; Lupp, D.; Oh, B. C.; Fristrup, P., *ChemSusChem* **2014**, *7* (2), 425-8.
- [60]. Dethlefsen, J. R.; Lupp, D.; Teshome, A.; Nielsen, L. B.; Fristrup, P., *ACS Catal.* **2015**, *5* (6), 3638-3647.
- [61]. Lupp, D.; Christensen, N. J.; Dethlefsen, J. R.; Fristrup, P., *Chemistry* **2015**, *21* (8), 3435-42.
- [62]. Robertson, J.; Srivastava, R. S., *Molecular Catalysis* **2017**, *443*, 175-178.
- [63]. Stalpaert, M.; De Vos, D., *ACS Sustain. Chem. Eng.* **2018**, *6* (9), 12197-12204.
- [64]. Murru, S.; Nicholas, K. M.; Srivastava, R. S., *J. Mol. Catal. A: Chem.* **2012**, *363-364*, 460-464.
- [65]. Chapman, G., Jr.; Nicholas, K. M., *Chem Commun (Camb)* **2013**, *49* (74), 8199-201.
- [66]. Vkuturi, S.; Chapman, G.; Ahmad, I.; Nicholas, K. M., *Inorg. Chem.* **2010**, *49* (11), 4744-6.
- [67]. Denning, A. L.; Dang, H.; Liu, Z.; Nicholas, K. M.; Jentoft, F. C., *ChemCatChem* **2013**, *5* (12), 3567-3570.
- [68]. Sharkey, B. E.; Denning, A. L.; Jentoft, F. C.; Gangadhara, R.; Gopaladasu, T. V.; Nicholas, K. M., *Catal. Today* **2018**, *310*, 86-93.
- [69]. Sandbrink, L.; Klindtworth, E.; Islam, H.-U.; Beale, A. M.; Palkovits, R., *ACS Catal.* **2015**, *6* (2), 677-680.
- [70]. Kon, Y.; Araque, M.; Nakashima, T.; Paul, S.; Dumeignil, F.; Katryniok, B., *Chemistryselect* **2017**, *2* (30), 9864-9868.
- [71]. MacQueen, B.; Barrow, E.; Rivera Castro, G.; Pagan-Torres, Y.; Heyden, A.; Lauterbach, J., *Industrial & Engineering Chemistry Research* **2019**.
- [72]. Lin, J.; Song, H.; Shen, X.; Wang, B.; Xie, S.; Deng, W.; Wu, D.; Zhang, Q.; Wang, Y., *Chem Commun (Camb)* **2019**, *55* (74), 11017-11020.
- [73]. Fu, J. Y.; Vasiliadou, E. S.; Goulas, K. A.; Saha, B.; Vlachos, D. G., *Catal. Sci. Technol.* **2017**, *7* (21), 4944-4954.
- [74]. Jang, J. H.; Sohn, H.; Camacho-Bunquin, J.; Yang, D. L.; Park, C. Y.; Delferro, M.; Abu-Omar, M. M., *ACS Sustain. Chem. Eng.* **2019**, *7* (13), 11438-11447.
- [75]. Nijem, S.; Dery, S.; Carmiel, M.; Horesh, G.; Garrevoet, J.; Spiers, K.; Falkenberg, G.; Marini, C.; Gross, E., *The Journal of Physical Chemistry C* **2018**, *122* (43), 24801-24808.
- [76]. Tamura, M.; Yuasa, N.; Cao, J.; Nakagawa, Y.; Tomishige, K., *Angew. Chem. Int. Ed. Engl.* **2018**, *57* (27), 8058-8062.
- [77]. Cao, J.; Tamura, M.; Nakagawa, Y.; Tomishige, K., *ACS Catal.* **2019**, 3725-3729.
- [78]. Ota, N.; Tamura, M.; Nakagawa, Y.; Okumura, K.; Tomishige, K., *Angew. Chem. Int. Ed. Engl.* **2015**, *54* (6), 1897-900.
- [79]. Ota, N.; Tamura, M.; Nakagawa, Y.; Okumura, K.; Tomishige, K., *ACS Catal.* **2016**, *6* (5), 3213-3226.

- [80]. Tazawa, S.; Ota, N.; Tamura, M.; Nakagawa, Y.; Okumura, K.; Tomishige, K., *ACS Catal.* **2016**, 6 (10), 6393-6397.
- [81]. Nakagawa, Y.; Tazawa, S.; Wang, T.; Tamura, M.; Hiyoshi, N.; Okumura, K.; Tomishige, K., *ACS Catal.* **2017**, 8 (1), 584-595.
- [82]. Danishefsky, S. J.; Bilodeau, M. T., *Angew. Chem. Int. Ed. Engl.* **1996**, 35 (13-14), 1380-1419.
- [83]. Harris, J. M.; Keranen, M. D.; O'Doherty, G. A., *J. Org. Chem.* **1999**, 64 (9), 2982-2983.
- [84]. Allen, J. R.; Harris, C. R.; Danishefsky, S. J., *J. Am. Chem. Soc.* **2001**, 123 (9), 1890-7.
- [85]. Montero, A.; Mann, E.; Herradón, B., *Eur. J. Org. Chem.* **2004**, 2004 (14), 3063-3073.
- [86]. Boysen, M. M., *Chemistry* **2007**, 13 (31), 8648-59.
- [87]. Willfor, S.; Sundberg, K.; Tenkanen, M.; Holmbom, B., *Carbohydr. Polym.* **2008**, 72 (2), 197-210.
- [88]. Luley-Goedl, C.; Nidetzky, B., *Biotechnol J* **2010**, 5 (12), 1324-38.
- [89]. Nahain, A. A.; Ignjatovic, V.; Monagle, P.; Tsanaksidis, J.; Ferro, V., *Med Res Rev* **2018**, 38 (5), 1582-1613.
- [90]. Angerbauer, R.; Schmidt, R. R., *Carbohydr. Res.* **1981**, 89 (2), 193-201.
- [91]. Shan, M.; Xing, Y.; O'Doherty, G. A., *J. Org. Chem.* **2009**, 74 (16), 5961-6.
- [92]. Guaragna, A.; D'Alonzo, D.; Paoletta, C.; Napolitano, C.; Palumbo, G., *J. Org. Chem.* **2010**, 75 (11), 3558-68.
- [93]. Song, W.; Wang, S.; Tang, W., *Chem. Asian J.* **2017**, 12 (10), 1027-1042.
- [94]. Rudd, T.; Skidmore, M. A.; Yates, E. A., Surface-Based Studies of Heparin/Heparan Sulfate-Protein Interactions: Considerations for Surface Immobilisation of HS/Heparin Saccharides and Monitoring Their Interactions with Binding Proteins. In *Chemistry and Biology of Heparin and Heparan Sulfate*, Elsevier: 2005; pp 345-366.
- [95]. Ouellette, R. J.; Rawn, J. D., **2018**, 889-928.

Chapter 2

Mechanistic study on deoxydehydration + hydrogenation of methyl glycosides to the dideoxy sugars over $\text{ReO}_x\text{-Pd/CeO}_2$ catalyst

2.1 Introduction

Carbohydrates are the main component of biomass and are also important intermediates for medicines, biomaterials, agrichemicals^[1-9], hence the development of effective transformation methods of them is essential. Since there are high density of functional groups in sugars and they present poor solubility in organic solvents, and limited scope for functionalization, which properties limit their industrial scale transformation^[10].

Deoxydehydration (DODH) reaction can selectively transform vicinal OH groups to the corresponding C=C bond in a single step^[11-13], and it is a promising method to lower the oxygen content in sugars. Recently, we found that Pd-modified CeO_2 -supported Re ($\text{ReO}_x\text{-Pd/CeO}_2$)^[14] and Au-modified CeO_2 -supported Re ($\text{ReO}_x\text{-Au/CeO}_2$)^[15] were effective heterogeneous catalysts for direct and selective transformation of the *cis*-vicinal OH groups in methyl glycosides by using gaseous H_2 , providing the corresponding saturated dideoxy methyl glycosides and unsaturated dideoxy glycosides, respectively, via DODH reaction with retention of the original stereostructure and without protection of OH groups. These results are based on our previous finding of heterogeneous $\text{ReO}_x\text{-Pd/CeO}_2$ or $\text{ReO}_x\text{-Au/CeO}_2$ catalysts effective for DODH + hydrogenation^[16-17] (DODH + HG) and alkenes by DODH^[18-19] of polyols, respectively. On these catalysts, isolated Re species attacked on CeO_2 surface can be catalytically active and Pd and Au metals work as promoters for formation of the active Re^{4+} species by reduction via the activation of H_2 molecule. The reaction mechanism was proposed to have four elementary reaction steps. First step is the reduction of isolated Re^{6+} species to Re^{4+} species by activated H_2 , then the substrate with vicinal OH groups is coordinated to the Re^{4+} species with the two OH groups as diolate; after that, alkene is formed and eliminated with the regeneration of Re^{6+} center, and the catalytic cycle is completed by re-reduction of Re^{6+} species and coordination of substrate.

According to the previous active results, the reactivity of the methyl glycosides is much lower than that of simple diols, and the reactivity of methyl glycosides seems to strongly depend on the kind of methyl glycosides^[14]. However, now the cause for the reactivity difference between substrates is unclear, and to the best of our knowledge, there are no systematic research on the effect of the substituents of pyranose and furanose- ring such as functional groups (-OH, -CH₂OH, OCH₃, -CH₃, etc.) except vicinal OH groups, and their configurations in the substrates on the reactivity in DODH reaction. In order to elucidate the reaction mechanism, the kinetic parameters in the reaction of DODH + HG of methyl glycosides with vicinal OH groups and related substrates were determined. In most cases, the reaction orders with respect to the substrate concentrates and H₂ pressure were both about zero, indicating the rate determining step is the DODH of diolate of the reduced Re species. The structure of the diolate intermediate and its transition state is determined by the DFT calculations on the basis of the property of monomeric Re species on CeO₂ surface. The activation energies obtained by the experimental data and DFT calculation are compared. Therefore, clarification of the decisive factors to dominate the reactivity of the methyl glycosides is of great importance to elucidate the reaction mechanism of methyl glycosides, and it will provide useful information for the design of the catalysts in transformation of sugars.

Herein, we conducted kinetic studies and DFT calculations on DODH + HG of six kinds of methyl glycosides (such as methyl β -D-ribofuranoside, methyl α -L-rhamnopyranoside, methyl α -D-mannopyranoside, methyl β -L-arabinopyranoside, methyl β -D-galactopyranoside and methyl α -L-fucopyranoside) and the related simple cyclic diols (such as *cis*-1,2-cyclopentanediol, *cis*-1,2-cyclohexanediol and 1,4-anhydroerythritl) over the optimized ReO_x-Pd/CeO₂ catalyst.

2.2 Experimental

2.2.1 Reagent information

All the sugar alcohols and methyl glycosides were analytic reagents from chemical product corporations and were used without treatment: *cis*-1,2-cyclopentanediol (>99%, Sigma-Aldrich Co., LLC.), *cis*-1,2-cyclohexanediol (>97%, Sigma-Aldrich Co., LLC.), *trans*-1,2-cyclohexanediol (>98%, Sigma-Aldrich Co., LLC.), 1,4-anhydroerythritol (>98%, Tokyo Chemical Industry Co., Ltd.),

methyl α -D-mannopyranoside (>98%, FUJIFILM Wako Pure Chemical Co.), methyl β -D-galactopyranoside (>95% (NMR), FUJIFILM Wako Pure Chemical Co.), methyl β -L-arabinopyranoside (>97% (NMR), FUJIFILM Wako Pure Chemical Co.), methyl α -L-fucopyranoside (>98% (HPLC), Tokyo Chemical Industry Co., Ltd.), methyl α -L-rhamnopyranoside (>97% (NMR), FUJIFILM Wako Pure Chemical Co.) and methyl α -D-glucopyranoside (>98% (GC), Tokyo Chemical Industry Co., Ltd.).

All metal precursors for catalyst preparation were analytic reagents from chemical product corporations: CeO_2 (Daiichi Kigenso Kagaku Kogyo Co., Ltd.), NH_4ReO_4 (Mitsuwa Chemicals Co., Ltd.), $(\text{NH}_4)_6\text{H}_2\text{W}_{12}\text{O}_{40}\cdot\text{H}_2\text{O}$ (Strem Chemicals, Inc.), $(\text{NH}_4)_6\text{Mo}_7\text{O}_{24}\cdot 4\text{H}_2\text{O}$ (FUJIFILM Wako Pure Chemical Co.), NH_4VO_3 (FUJIFILM Wako Pure Chemical Co.), $\text{Mn}(\text{NO}_3)_2\cdot 6\text{H}_2\text{O}$ (FUJIFILM Wako Pure Chemical Co.), $(\text{NH}_4)\text{NbO}(\text{C}_2\text{O}_4)_2\cdot x\text{H}_2\text{O}$ (FUJIFILM Wako Pure Chemical Co.), $\text{Cr}(\text{NO}_3)_3\cdot 9\text{H}_2\text{O}$ (FUJIFILM Wako Pure Chemical Co.), $\text{Pd}(\text{NO}_3)_2$ (Sigma-Aldrich Co., LLC.), $\text{Ru}(\text{NO})(\text{NO}_3)_{3-x}(\text{OH})_x$ (Sigma-Aldrich Co., LLC.), $\text{Pt}(\text{NH}_3)_4(\text{NO}_3)_2$ (Sigma-Aldrich Co., LLC.), H_2IrCl_6 (Furuya Metal Co., Ltd.), $\text{RhCl}_3\cdot 3\text{H}_2\text{O}$ (FUJIFILM Wako Pure Chemical Co.), $\text{Co}(\text{NO}_3)_2\cdot 6\text{H}_2\text{O}$ (FUJIFILM Wako Pure Chemical Co.), $\text{Ni}(\text{NO}_3)_2\cdot 6\text{H}_2\text{O}$ (FUJIFILM Wako Pure Chemical Co.), $\text{HAuCl}_4\cdot 4\text{H}_2\text{O}$ (FUJIFILM Wako Pure Chemical Co.), AgNO_3 (FUJIFILM Wako Pure Chemical Co.), $\text{Cu}(\text{NO}_3)_2\cdot 3\text{H}_2\text{O}$ (FUJIFILM Wako Pure Chemical Co.).

All solvents were from chemical product corporations and were used without treatment: 1,4-dioxane (>99.5%, FUJIFILM Wako Pure Chemical Co.), diisopropyl ether (>99.0%, Nacalai Tesque, Inc.), 2-octanol (>98.0%, Tokyo Chemical Industry Co., Ltd.), diethylene glycol dimethyl ether (>99.0% Tokyo Chemical Industry Co., Ltd.) and methanol (>96%, FUJIFILM Wako Pure Chemical Co.)

2.2.2 Catalyst preparation

The $\text{ReO}_x/\text{CeO}_2$ ($\text{Re}=2$ wt%) and Pd/CeO_2 ($\text{Pd}=0.3$ wt%) catalyst were prepared by impregnating CeO_2 powder (calcined at 873 K for 1 h, BET surface area: $84\text{ m}^2\text{ g}^{-1}$) with a 0.1 M aqueous solution of NH_4ReO_4 or $\text{Pd}(\text{NO}_3)_2$, respectively. After drying and stirring over a 353 K hot plate, the obtained mixture was dried at 383 K for 12 h. Then, the mixture was calcined in air at 773 K for 3 h.

The $\text{MO}_x\text{-Pd/CeO}_2$ ($\text{M}_1 = \text{W, Mo, Re, V, Mn, Nb, Cr}$, $\text{M}_2 = 2 \text{ wt\%}$, $\text{Pd}/\text{M}_2 = 0.25 \text{ mol mol}^{-1}$) catalysts were prepared by impregnating CeO_2 powder (calcined at 873 K for 1 h) with a 0.1 M aqueous solution of NH_4VO_3 , $\text{Cr}(\text{NO}_3)_3 \cdot 9\text{H}_2\text{O}$, $\text{Mn}(\text{NO}_3)_2 \cdot 6\text{H}_2\text{O}$, $(\text{NH}_4)\text{NbO}(\text{C}_2\text{O}_4)_2 \cdot x\text{H}_2\text{O}$, $(\text{NH}_4)_6\text{Mo}_7\text{O}_{24} \cdot 4\text{H}_2\text{O}$, $(\text{NH}_4)_6\text{H}_2\text{W}_{12}\text{O}_{40} \cdot \text{H}_2\text{O}$ or NH_4ReO_4 , respectively. After drying and stirring over a 353 K hot plate and drying at 383 K for 12 h, the obtained mixture was impregnating with a 0.1 M aqueous solution of $\text{Pd}(\text{NO}_3)_2$. After drying and at 353 K over a hot plate, the catalysts were further dried at 383 K for 12 h. Then, the mixture was calcined in air at 773 K for 3 h.

The $\text{ReO}_x\text{-M}_2/\text{CeO}_2$ ($\text{M}_2 = \text{Pd, Ru, Pt, Ir, Rh, Ni, Co, Au, Ag, Cu}$, $\text{Re} = 2 \text{ wt\%}$, $\text{M}/\text{Re} = 0.25 \text{ mol mol}^{-1}$) catalysts were prepared by impregnating the CeO_2 powder (calcined at 873 K for 1 h) with a 0.1 M aqueous solution of NH_4ReO_4 , after drying and stirring over a 353 K hot plate and drying at 383 K for 12 h, the obtained mixture was impregnating with corresponding 0.1 M solution of $\text{HAuCl}_4 \cdot 4\text{H}_2\text{O}$, $\text{Ru}(\text{NO})(\text{NO}_3)_{3-x}(\text{OH})_x$, $\text{Pt}(\text{NH}_3)_4(\text{NO}_3)_2$, H_2IrCl_6 , $\text{RhCl}_3 \cdot 3\text{H}_2\text{O}$, $\text{Co}(\text{NO}_3)_2 \cdot 6\text{H}_2\text{O}$, $\text{Ni}(\text{NO}_3)_2 \cdot 6\text{H}_2\text{O}$, $\text{HAuCl}_4 \cdot 4\text{H}_2\text{O}$, AgNO_3 , $\text{Cu}(\text{NO}_3)_2 \cdot 3\text{H}_2\text{O}$, respectively. After drying and at 353 K over a hot plate, the catalysts were further dried at 383 K for 12 h. Then, the mixture was calcined in air at 773 K for 3 h.

All of these catalysts were used in powdery form.

2.2.3 Activity test

Activity tests were performed in a 190 mL stainless steel autoclave. The substrate, catalyst and 1,4-dioxane were put into the autoclave with a spinner. After sealing the reactor, the air content was purged three times with H_2 (>99.99%; Takachiho Trading Co., Ltd.), and the pressure was raised to appropriate value (typically 5.5 MPa) by H_2 at room temperature (RT). Autoclaves were then heated to the reaction temperature and its temperature was monitored using a thermocouple inserted in the autoclave. The pressure at reaction temperature was recorded (typically 8.0 MPa at 413 K). The reaction time zero (0 h) was defined as the time when the temperature reached the set value (typically 413 K) and the heating-up time was about 40 mins. The stirring rate was fixed at 500 rpm (magnetic stirring).

After an appropriate reaction time, the autoclave was cooled down to RT in cold water bath. The gases in the autoclave were collected in a gas bag. The autoclave contents and the washing solvent (10 g mixed solution including 8 g distilled water and 2 g 1,4-dioxane) were transformed to vials, and the catalysts were separated by filtration.

2.2.4 Kinetic test

Kinetic tests were performed in a 190 mL stainless steel autoclave. The substrate, catalyst and 1,4-dioxane were put into the autoclave with a spinner. After sealing the reactor, the air content was purged three times with H_2 , and the initial pressure was fixed in 1.0 MPa by H_2 at RT. Autoclaves were then heated to the reaction temperature and its temperature was monitored using a thermocouple inserted in the autoclave. The pressure was raised to appropriate value and the reaction time zero (0 h) was defined as the time when the temperature reached the set value (typically 413 K) and the heating-up time was about 15 mins. The stirring rate was fixed at 500 rpm.

After an appropriate reaction time, the autoclave was cooled down to RT in cold water bath. The gases were collected in a gas bag. The autoclave contents and the washing solvent (10 g mixed solution including 8 g distilled water and 2 g 1,4-dioxane) with internal standard (2-octanol, diisopropyl ether or diethylene glycol dimethyl ether) were transformed to vials, and the catalysts were separated by filtration.

2.2.5 Product analysis

The both of gas and liquid products were collected and analyzed by FID-GC (Shimadzu GC-2014) and GC-MS (QP5050, Shimadzu) equipped with TC-WAX capillary column (diameter 0.25 mm, 30 m), and HPLC (Shimadzu LC-10A, refractive index detector) with Aminex HPX-87C column (diameter 7.8 mm, 300 mm) using water as the eluent. The amount of unreacted substrate was based on the HPLC result, and the amounts of products was based on the GC result. The calibration curves were obtained by using corresponding chemicals and isolated products.

The conversion and the selectivity were calculated on the methyl glycoside basis. The carbon balance was also confirmed in each result and the difference in carbon balance was always in the range of the allowed experimental error within $\pm 5\%$.

All the formulas were listed as follow:

$$\text{Conversion (\%)} = [1 - \text{unreacted substrate (mol)} / \text{substrate (mol)}] \times 100$$

$$\text{Conversion (Product basis) (\%)} = \sum \text{product (mol)} / \text{substrate (mol)} \times 100$$

$$\text{Selectivity (\%)} = \text{product (mol)} \times n_{\text{carbon}} / \sum (\text{product (mol)} \times n_{\text{carbon}}) \times 100$$

$$\text{Carbon balance (\%)} = (\sum (\text{product (mol)} \times n_{\text{carbon}}) + \text{unreacted substrate (mol)} \times n_{\text{carbon}}) / (\text{substrate (mol)} \times n_{\text{carbon}}) \times 100$$

$$\text{Formation amount (mmol g}_{\text{cat}}^{-1}) = (\text{dideoxy product (mmol)} + \text{DODH product (mmol)}) / \text{catalyst amount (g)}$$

$$\text{Reaction rate (mmol g}_{\text{cat}}^{-1} \text{ h}^{-1}) = \Delta \text{ Formation amount (mmol g}_{\text{cat}}^{-1}) / \Delta \text{ reaction time (h)}.$$

2.2.6 Computational Details

All DFT calculations were carried out by the spin-polarized periodic-boundary DFT with the projector-augmented wave (PAW) method and plane-wave basis set using the Vienna *Ab initio* simulation package (VASP)^[20-21]. The generalized-gradient approximation by the Perdew–Burke–Ernzerhof (PBE) functional models was employed as the exchange and correlation potential, and the valence electrons were expanded in plane waves with a cutoff energy of 500 eV. The fractional occupancies of bands were allowed using the Gaussian smearing with a value of 0.2 eV. In order to correctly represent the nature of 4*f* orbitals of Ce atoms, the DFT+*U* approach was employed, and the *U* value was set to 5.0 eV, which gives reasonable accuracy in the previous works^[22-23]. The surface of $\text{CeO}_2(111)$ was modeled as a periodic *p* (3×3) hexagonal slab of 27 CeO_2 unit with three O–Ce–O tri-layers. The bottom O–Ce–O tri-layers were fixed at the bulk positions during the geometry optimization. The Brillouin zone integration was performed with a reciprocal space mesh consisting of only the Γ -point, which was tested to converge.

The dimensions of a simulation cell were set to $a = b = 11.67$, $c = 24.53$ Å and $\alpha = \beta = 90$, $\gamma = 60$ degrees, and this slab is separated by ~ 15 Å of vacuum space in the direction perpendicular to the

surface. The lattice parameters of the CeO₂(111) slab were determined by the cell optimization of the bulk CeO₂ with $7 \times 7 \times 7$ Monkhorst–Pack mesh for the k-point sampling, and the optimized lattice constant of 5.50 Å is in good agreement with the experimental value of 5.41 Å^[24-25], and also with other theoretical works^[26-27]. When the energies of the gas-phase molecules are calculated, the simulation cell of the cubic box with $a = b = c = 15.0$ Å is used.

The adsorption energy E_A of diolate structure of methyl glycosides over ReO/CeO₂ catalysts is calculated according to

$$E_A = E_{\text{Diolate}} + E_{\text{H}_2\text{O}} - E_{\text{Methylglycosides}} - E_{\text{surf}}$$

where E_{Diolate} is the total electronic energy of diolate structure while $E_{\text{H}_2\text{O}}$ and $E_{\text{Methylglycosides}}$ are the energies of the isolated water molecule and methyl glycosides, respectively, and E_{surf} is the energy of ReO/CeO₂ catalysts (**model-I** or **model-II**). In this definition, the more negative value of adsorption energy indicates a stronger binding to the catalysts. For geometry optimization, the forces on all atoms were minimized to less than 0.03 eV/Å, and transition states were located by the climbing image nudged elastic band (CI-NEB) method.

We first model the ReO_{*x*} species ($x = 2$) over CeO₂ where two Re=O bonds are formed above the surface. The calculated energy is found to be 1.14 eV higher than ReO species ($x = 1$) using energy of an isolate molecular oxygen as a reference, i.e. half the energy of molecular oxygen is used. Also, the energy of Re species ($x = 0$) is 1.41 eV higher than ReO species ($x = 1$), and therefore ReO is the most stable structure over the surface.

In calculating the activation energy for the DODH reaction of methyl glycosides with CH₃ReO₃ catalyst in the gas phase, the Gaussian 09 package is used. The B3LYP functionals is used, and the SDD effective core potential and associated basis set were used for the Re atom, and a 6-31G(d,p) basis set was employed for all other atoms.

2.3 Results and discussion

2.3.1 Optimization of reaction conditions in DODH + HG of methyl α -D-mannopyranoside and comparison of time-courses of related substrates

At first, catalyst composition such as main active metal oxides, noble metals and supports, was optimized in deoxydehydration + hydrogenation (DODH + HG) of methyl α -D mannopyranoside as a model reaction (Scheme 2.1, Figures 2.1-2.5). The tendency of the composition effects was similar to that in DODH+HG of 1,4-anhydroerythritol^[16-17]: Re oxide is the most effective metal oxide among tested MO_x ($\text{M}=\text{V}$, Cr, Mn, Nb, Mo, W and Re) in terms of conversion and selectivity (Figure 2.1), Pd metal is the most effective metal among various hydrogenation-active metals (Co, Ni, Ru, Rh, Pd, Ag, Ir, Pt and Au) in terms of conversion and selectivity (Figure 2.2), and CeO_2 was the most effective supports among various metal oxides (MgO , $\gamma\text{-Al}_2\text{O}_3$, SiO_2 , CaO , TiO_2 , ZnO , ZrO_2 and CeO_2) (Figure 2.3). Moreover, the optimized Re loading amount (2 wt%) (Figure 2.4) and Pd loading amount (Pd/Re ratio = 1/4) (Figure 2.5) of $\text{ReO}_x\text{-Pd/CeO}_2$ catalyst were also confirmed as the same as those in DODH+HG of 1,4-anhydroerythritol.

Next, the solvent effect was investigated in the same reaction with the optimized $\text{ReO}_x\text{-Pd/CeO}_2$ catalyst with Re=2 wt%, Pd/Re=1/4 (Figure 2.6), and this catalyst used for all the following studies. Typical ether solvents such as 1,4-dioxane, 1,2-dimethoxyethane and THF, alcohols such as 1-pentanol, 3-pentanol and methanol, and dodecane showed similar conversion with high selectivity to the target dideoxy product, although the conversion is a little low in the case of methanol. On the other hand, water solvent provided almost no conversion. The tendency is similar to that in our previous work on DODH+HG of 1,4-anhydroerythritol over $\text{ReO}_x\text{-Pd/CeO}_2$ catalyst^[17]. Considering that the solubility of sugar derivatives is typically low in organic solvents, in contrast high in water solvent, applicability of water-contained solvent will be important. The mixed solvents of 1,4-dioxane and water was tested in the same reaction. In the case of 10 wt% water containing 1,4-dioxane solvent (1,4-dioxane : water = 9 : 1), the reaction did not almost proceed. When the water content decreased to 3 wt% (1,4-dioxane : water = 29 : 1), the reaction occurred, and the conversion (18%) was about half as low as that of only 1,4-dioxane (35%), although the selectivity to the dideoxy product was a little low. The catalyst system is tolerated with a small amount of water, however, in general, water is not a suitable solvent.

As above, the optimized catalyst, $\text{ReO}_x\text{-Pd/CeO}_2$ (Re=2 wt%, Pd/Re=0.25) in DODH + HG of methyl α -D mannopyranoside is the same as that in DODH + HG of 1,4-anhydroerythritol, which

suggests that the active species and reaction mechanism of these substrates are fundamentally similar. These results are also supported by our previous preliminary work on the characterization of the catalyst structure of $\text{ReO}_x\text{-Pd/CeO}_2$ ^[16-17], where the catalyst structure of $\text{ReO}_x\text{-Pd/CeO}_2$ was stable and similar to that in DODH + HG of 1,4-anhydroerythritol.

However, as reported in our previous report, the reactivity of the methyl glycosides was clearly lower than that of simple diols such as 1,4-anhydroerythritol and 1,2-butanediol^[16-17], and obvious difference in reactivity were also observed among various methyl glycosides^[14].

In order to clarify the reaction tendency, time-courses of six kinds of methyl glycosides such as methyl β -D-ribofuranoside, methyl α -L-rhamnopyranoside, methyl α -D-mannopyranoside, methyl β -L-arabinopyranoside, methyl β -D-galactopyranoside and methyl α -L-fucopyranoside, and simple cyclic diols such as *cis*-1,2-cyclopentanediol and *cis*-1,2-cyclohexanediol, were investigated by adjusting the catalyst amount and reaction time (Figure 2.7, and the detailed data were shown in Tables 2.1-2.8). All of the substrates could smoothly react to give high conversion (\sim >99%). The reactivities of these substrates based on catalyst amount and \sim 99% conversion reaction time were in order of *cis*-1,2-cyclopentanediol > *cis*-1,2-cyclohexanediol > methyl β -D-ribofuranoside > methyl α -L-rhamnopyranoside > methyl α -D-mannopyranoside \approx methyl β -L-arabinopyranoside > methyl β -D-galactopyranoside > methyl α -L-fucopyranoside. The selectivity to the corresponding dideoxy product is totally high (>85%), however, the tendency of the selectivities is a little different among these substrates.

In the case of *cis*-1,2-cyclohexanediol (Figure 2.7 (b), Table 2.2), the selectivity to cyclohexane is a little low even at low conversion level and decreased with increasing the reaction time (85% at >99% conversion), which is due to the isomerization of *cis*-1,2-cyclohexanediol to *trans*-1,2-cyclohexanediol. However, *cis*-1,2-cyclopentanediol (Figure 2.7 (a), Table 2.1) provided almost complete selectivity to the cyclopentane (>99%), and the isomerization also did not occur in the cases of methyl glycosides as substrates over $\text{ReO}_x\text{-Pd/CeO}_2$ catalyst, which is different behavior from the result of 1,2-cyclohexanediol. This result may be due to the existence of the other functional groups except the *cis*-vicinal OH groups. As for the methyl glycosides, methyl β -D-ribofuranoside (Figure 2.7 (c), Table 2.3), a five-membered ring methyl glycoside, did not provide complete

selectivity, and furfuryl alcohol was formed as a main byproduct, which can be produced by demethanolysis of DODH product. On the other hand, in the case of the DODH + HG of six-membered ring methyl glycosides, the selectivity trend depended on the methyl glycosides. Focusing on the selectivity at low conversion level below 30%, methyl α -D-mannopyranoside and methyl β -D-galactopyranoside showed a little low selectivity ($\sim 90\%$) and some selectivity to DODH product as a main byproduct (5~11%) (Figure 2.7 (e), (g), Tables 2.5, 2.7). In contrast, methyl α -L-rhamnopyranoside, methyl β -L-arabinopyranoside and methyl α -L-fucopyranoside provided high selectivity ($>99\%$) to the dideoxy product at low conversion level (Figure 2.7 (d), (f), (h), Tables 2.4, 2.6, 2.8). The difference can be attributed to that the existence of hydroxymethyl group on the ring suppressed the hydrogenation of produced DODH product. On the other hand, focusing on the selectivity at high conversion level, DODH product was decreased with increasing the reaction time in the case of methyl α -L-rhamnopyranoside, methyl α -D-mannopyranoside and methyl β -D-galactopyranoside (Figure 2.7 (d), (e), (g), Tables 2.4, 2.5, 2.7), and the selectivity to others including hydrolysis, hydration and over-hydrogenation products was gradually increased in the case of the six-membered ring methyl glycosides except methyl β -L-arabinopyranoside (Figure 2.7 (f), Table 2.6).

As above, in addition to the difference of the reactivities, the selectivity tendency is also a little different among the methyl glycosides, which can be derived from the structure of methyl glycosides and the functional groups except *cis*-vicinal diols.

2.3.2 Kinetic studies on DODH + HG of various methyl glycosides and the related diols over $\text{ReO}_x\text{-Pd/CeO}_2$ catalyst.

To clarify the difference of the reactivity and selectivity among these methyl glycosides, it is essential to measure the reaction rate precisely in the kinetic region. Three kinds of cyclic diols such as *cis*-1,2-cyclopentanediol, 1,4-anhydroerythritol and *cis*-1,2-cyclohexanediol and six kinds of methyl glycoside such as methyl β -D-ribofuranoside, methyl α -L-rhamnopyranoside, methyl α -D-mannopyranoside, methyl β -L-arabinopyranoside, methyl β -D-galactopyranoside and methyl α -L-fucopyranoside were used as substrates, and the reaction rates ($\text{mmol g}_{\text{cat}}^{-1} \text{ h}^{-1}$) were estimated

with $\text{ReO}_x\text{-Pd/CeO}_2$ catalyst from three data points with different reaction time by the following equation: The reaction rate ($\text{mmol g}_{\text{cat}}^{-1} \text{ h}^{-1}$) = (Formation amount of DODH and dideoxy products [mmol]) / (Catalyst amount [g]) / (Reaction time [h]). The reaction rate was determined at low conversion level where the conversion was below 40% (Figure 2.8), and the results are shown in Table 2.9. The order of the reaction rates is *cis*-1,2-cyclopentanediol > 1,4-anhydroerythritol > *cis*-1,2-cyclohexanediol > methyl β -D-ribofuranoside > methyl α -L-rhamnopyranoside > methyl α -D-mannopyranoside \approx methyl β -L-arabinopyranoside > methyl β -D-galactopyranoside > methyl α -L-fucopyranoside, which agrees well with that of the time-courses results (Figure 2.7). The cyclic diols showed clearly higher reaction rate ($7.2\sim 20 \text{ mmol g}_{\text{cat}}^{-1} \text{ h}^{-1}$, entries 1-3) than the methyl glycosides ($0.38\sim 4.5 \text{ mmol g}_{\text{cat}}^{-1} \text{ h}^{-1}$, entries 4~9). Among the cyclic diols, *cis*-1,2-cyclopentanediol having a five-membered ring showed the highest reactivity ($20 \text{ mmol g}_{\text{cat}}^{-1} \text{ h}^{-1}$, entry 1). The reactivity of 1,4-anhydroerythritol having a tetrahydrofuran ring ($9.0 \text{ mmol g}_{\text{cat}}^{-1} \text{ h}^{-1}$, entry 2) is about 1/2-fold lower than that of *cis*-1,2-cyclopentanediol (entry 1), which will be related to the presence of the O atom in the five-membered ring. Moreover, the reactivity of *cis*-1,2-cyclohexanediol having a six-membered ring ($7.2 \text{ mmol g}_{\text{cat}}^{-1} \text{ h}^{-1}$, entry 3) is about 1/3-fold lower than that of *cis*-1,2-cyclopentanediol (entry 1), which will be associated with the difference of the ring structure, six-membered ring or five-membered one.

As for the reaction rate of the methyl glycosides, methyl β -D-ribofuranoside, which has a tetrahydrofuran ring, showed $4.5 \text{ mmol g}_{\text{cat}}^{-1} \text{ h}^{-1}$ (entry 4), which is 1/2-fold as small as that of 1,4-anhydroerythritol ($9.0 \text{ mmol g}_{\text{cat}}^{-1} \text{ h}^{-1}$, entry 2). The decrease of the reactivity will be derived from the methoxy group at C2 position and/or hydroxymethyl group at C5 position of the tetrahydrofuran ring. Otherwise, the reactivity of five-membered ring methyl β -D-ribofuranoside is about 3-times higher than the six-membered ring methyl glycosides methyl α -L-rhamnopyranoside, methyl α -D-mannopyranoside and methyl β -L-arabinopyranoside ($1.7\sim 1.9 \text{ mmol g}_{\text{cat}}^{-1} \text{ h}^{-1}$, entries 5-7), which are six-membered ring methyl glycoside (entry 4), which can be explained by the difference of the ring structure because the reactivity difference is similar to that in the case of *cis*-1,2-cyclopentanediol and *cis*-1,2-cyclohexanediol (entries 1 and 3). Therefore, the influence of the functional groups at the β -position of the *cis*-vicinal OH groups on the reactivity will be small.

Among the six-membered ring methyl glycosides, methyl α -L-rhamnopyranoside, methyl α -D-mannopyranoside and methyl β -L-arabinopyranoside (entries 5-7) showed similar reactivity ($1.7\text{-}1.9\text{ mmol g}_{\text{cat}}^{-1}\text{ h}^{-1}$) and methyl β -D-galactopyranoside and methyl α -L-fucopyranoside (entries 8 and 9) showed lower reactivity (0.73 and $0.38\text{ mmol g}_{\text{cat}}^{-1}\text{ h}^{-1}$, respectively). Here, the relation of the reactivity to the functional groups adjacent to the *cis*-vicinal OH groups and their configuration is discussed. The adjacent functional groups to the *cis*-vicinal OH groups in more reactive three six-membered ring methyl glycosides (entries 5-7) are at the opposite side to the *cis*-vicinal OH groups, and more unreactive two ones (entries 8 and 9) has a functional group at the same side to the *cis*-vicinal OH groups; the hydroxymethyl group (methyl β -D-galactopyranoside, entry 8) and methyl group (methyl α -L-fucopyranoside, entry 9) at C6 position. The position of the adjacent functional groups can affect the reactivities of DODH + HG. Particularly, focusing on methyl β -L-arabinopyranoside (entry 7) and methyl α -L-fucopyranoside (entry 9), these methyl glycosides have the same functional groups in the opposite direction except the functional group at C6 position, H (methyl β -L- arabinopyranoside, entry 7) and methyl group (methyl α -L-fucopyranoside, entry 9), however, the reaction rate of methyl β -L-arabinopyranoside is quite higher ($1.7\text{ mmol g}_{\text{cat}}^{-1}\text{ h}^{-1}$) than that of methyl α -L-fucopyranoside ($0.38\text{ mmol g}_{\text{cat}}^{-1}\text{ h}^{-1}$), indicating that the methyl group at the same side to *cis*-vicinal OH groups decreased the reactivity.

According to our previous works on hydrogenolysis of glycerol over metal oxide-modified noble metal catalysts^[28], primary OH groups can be more easily adsorbed on the metal oxide species than secondary OH groups, which may influence change the reactivity of substrates. Focusing on the structure of methyl α -L-rhamnopyranoside (entry 5) and methyl α -D-mannopyranoside (entry 6), these methyl glycosides have the same functional groups in the opposite direction except for the functional group at the C6 position, methyl group (methyl α -L-rhamnopyranoside, entry 5) and hydroxymethyl group (methyl α -D-mannopyranoside, entry 6). The reactivities of these methyl glycosides are similar, suggesting that the effect of the primary OH group of the hydroxymethyl group on the reactivity is not so large, which is also supported by the reaction of the mixed substrates of 1,4-anhydroerythritol and tetrahydrofurfuryl alcohol, a model primary alcohol (Scheme 2.2). The reaction rate of 1,4-anhydroerythritol was not so changed by addition of tetrahydrofurfuryl alcohol.

Next, the reaction order with respect to the substrate concentration and H_2 pressure was investigated with all the model substrates. The results are also listed in Table 2.9, and the details are shown in the supporting information (Figures 2.9-2.12). The reaction orders with respect to the substrate concentration of all the substrates were estimated to be almost zero, which suggests that the adsorption of the substrates on the monomeric Re species to form the diolate are strong and the coverage is almost saturated. The reaction orders with respect to the H_2 pressure of all substrates were estimated to be also almost zero, suggesting that the reaction steps associated with hydrogen are not included in the rate-determining step. This result is not in contradiction with the proposed reaction mechanism of ReO_x -Pd/CeO₂ catalyst^[17], where the rate-determining step is the elimination of alkene from the diolate adspecies on ReO_x -Pd/CeO₂ catalyst. Therefore, the reaction order with respect to the substrate concentration and H_2 pressure was not dependent on the substrates, suggesting the same rate-determining step.

In order to check the effect of the dideoxy product in the DODH reaction, DODH reaction of methyl α -D-mannopyranoside was conducted by addition of the half amount of methyl α -D-2,3-dideoxy-mannopyranoside, the corresponding dideoxy product (Scheme 2.3, the detailed data are shown in Table 2.10). The conversion was similar to that in the case of methyl α -D-mannopyranoside ((I) and (III)), which indicates that the dideoxy product did not affect the reaction. Considering that the dideoxy product has 1,3-diol structure, which can be adsorbed on the active site of Re^{4+} species, the adsorption of 1,2-diol in the methyl glycosides on the active site is stronger than that of 1,3-diol. Moreover, the reaction of methyl α -D-mannopyranoside by addition of the half amount of methyl α -D-3,4-dideoxy-galactopyranoside, the dideoxy product of methyl β -D-galactopyranoside, was performed (Scheme 2.3-(II), the detailed data is shown in Table 2.10), providing similar conversion to that of only methyl α -D-mannopyranoside ((II) and (III)). This result also supports the result that the effect of the primary OH group on the reactivity is not large as discussed above (Scheme 2.2).

In order to clarify the reactivity difference among the methyl glycosides, we selected methyl α -L-rhamnopyranoside (entry 5) and methyl α -L-fucopyranoside (entry 9) as model substrates because these substrates are stereoisomers and the difference of the reactivities is very large among

the 6-membered methyl glycosides (methyl α -L-rhamnopyranoside: $1.9 \text{ mmol g}_{\text{cat}}^{-1} \text{ h}^{-1}$, methyl α -L-fucopyranoside: $0.38 \text{ mmol g}_{\text{cat}}^{-1} \text{ h}^{-1}$).

The effect of the reaction temperature was investigated with methyl α -L-rhamnopyranoside and methyl α -L-fucopyranoside as substrates. Arrhenius plots of these substrates provided linear lines (Figure 2.13) and similar frequency factors (19 for methyl α -L-rhamnopyranoside and 20 for methyl α -L-fucopyranoside). The apparent activation energy of methyl α -L-rhamnopyranoside and methyl α -L-fucopyranoside was estimated to be 63 and 73 kJ mol^{-1} , respectively. Therefore, the difference of the reactivities between methyl α -L-rhamnopyranoside and methyl α -L-fucopyranoside can be derived from that of the apparent activation energy, indicating that the transition state of methyl α -L-rhamnopyranoside and methyl α -L-fucopyranoside is different by the difference of the structures.

2.3.3 DFT calculation of DODH reaction of methyl α -L-rhamnopyranoside and methyl α -L-fucopyranoside over $\text{ReO}_x\text{-Pd/CeO}_2$ catalyst

From the kinetic studies, the functional groups adjacent to *cis*-vicinal OH groups can affect the reactivity of the methyl glycoside, which means that they can influence the adsorption structure and/or transition state of the substrate. Therefore, the adsorption state of methyl glycoside and the transition state of DODH was calculated by DFT. DFT calculations were performed for methyl α -L-rhamnopyranoside and methyl α -L-fucopyranoside as model methyl glycosides over the isolated Re^{4+} species on CeO_2 , which is the main active site of $\text{ReO}_x\text{-Pd/CeO}_2$ catalyst^[17].

Since the CeO_2 surface is exposed to high H_2 pressure, fully hydrogenated surface is considered in this investigation. To accommodate the monomeric ReO_x species on the surface, three hydrogen atoms are removed from the surface and ReO_x species is placed on it to bind to three surface O atoms. When comparing the stability of various ReO_x species with the different number of oxygen atoms ($x = 0 \sim 2$), we found that the ReO_x ($x = 1$) species on three O atom of CeO_2 is the most stable structure over the surface (see the computational details), which is in accordance with the recent work^[29]. In this structure, which we refer to model-I hereafter, the oxidation state of Re atom is estimated as +7 based on the number of reduced Ce^{3+} atoms in the system. This oxidation state is

different from the experimental observations, where the active Re species involves the oxidation state of +4. Because of this, we also consider the model where one of the three bridging O atoms is removed from model-I. In this model, which is referred to as model-II, the Re atom is bound to two surface O atoms, and the oxidation state of Re is calculated to be +4, which is in accordance with the experimental findings (see Figure 2.14 for both structures). Using these two active site models, we compare the stability of intermediate diolate adspecies of the substrate. In the case of methyl α -L-rhamnopyranoside, we found that the adsorption energy of the most stable diolate adspecies over model-II is -32 kJ mol^{-1} , while it is 126 kJ mol^{-1} for model-I (structures are given in Figure 2.14). Therefore, model-II would be the most plausible structure of active species of the $\text{ReO}_x/\text{CeO}_2$ catalyst. Note that there are two conformations for diolate structure deriving from *cis*-vicinal OH groups depending on the orientation, and we focus only on the most stable conformation hereafter, which is referred to as *cis*-A (Figure 2.14). The adsorption energy for the other conformation and also those of diolate structures deriving from *trans*-vicinal OH groups for methyl α -L-rhamnopyranoside and methyl α -L-fucopyranoside are summarized in Figure 2.15, Figure 2.16 and Table 2.13.

Figure 2.17(a) shows the structure of diolate adspecies of methyl α -L-rhamnopyranoside, and it is reclined to the surface involving the hydrogen bond with the surface hydroxy groups. The transition state structure for the cleavage of two C-O bonds is given in Figure 2.17 (b), and it exhibits asymmetric structure with respect to the dissociation of the two C-O bonds, and one bond length is 1.71 \AA and the other is 2.01 \AA . This could mainly due to the stabilization of O₂ (shown in the figure) which fills the vacancy site after releasing the DODH product, in addition to the hydrogen bond with the surface. The activation energy is calculated as 65 kJ mol^{-1} , which is in good agreement with the experimental value of 63 kJ mol^{-1} activation energy of methyl α -L-rhamnopyranoside. After releasing the DODH product, the ReO species is bound to three surface O atoms (Figure 2.17(c)).

Figure 2.17 (d-f) shows the structures of diolate adspecies, transition state, and the final product for methyl α -L-fucopyranoside. The structures of ReO/CeO_2 catalyst are similar to those of methyl α -L-rhamnopyranoside. The adsorption energies of diolate adspecies are very close, -32 kJ mol^{-1} for methyl α -L-rhamnopyranoside and -30 kJ mol^{-1} for methyl α -L-fucopyranoside. A closer look into the transition structure of methyl α -L-fucopyranoside shows that asymmetry with respect to the

cleavage of the two C-O bonds is less pronounced, and the O2 atom is less stabilized in comparison to methyl α -L-rhamnopyranoside. The calculated activation energy of 77 kJ mol⁻¹ is slightly higher than that of α -L-rhamnopyranoside, which is also in good agreement with the experimental value of 73 kJ mol⁻¹ activation energy of methyl α -L-fucopyranoside.

As a model calculation, the gas-phase DODH reaction of methyl glycosides with CH₃ReO₃ catalyst is investigated by using the Gaussian 09 package (computational details are given in Figure 2.18). The activation energies of methyl α -L-rhamnopyranoside and methyl α -L-fucopyranoside are calculated as 87 kJ mol⁻¹ and 83 kJ mol⁻¹, respectively, indicating that the transition state of these substrates on the single active site is almost the same. Therefore, the difference in the transition structures comes over the active sites of ReO/CeO₂ from the intricate interactions between the adjacent functional groups to *cis*-vicinal OH groups and the surface hydroxy groups, resulting in changing the stability of the transition state of these substrates.

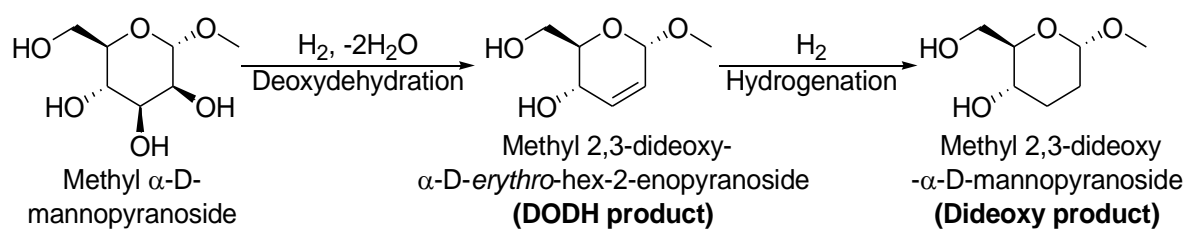
2.4 Conclusions

The screening of the active metal oxides, noble metals, supports and solvents in the DODH+HG of methyl glycosides showed that the same catalyst of ReO_x-Pd/CeO₂ (Re=2 wt%, Pd/Re=0.25) was effective for the reaction as in the case of DODH+HG of 1,4-anhydroerythritol. The reaction mechanism of DODH+HG of methyl glycosides such as methyl β -D-ribofuranoside, methyl α -L-rhamnopyranoside, methyl α -D-mannopyranoside, methyl β -L-arabinopyranoside, methyl β -D-galactopyranoside and methyl α -L-fucopyranoside and simple cyclic diols such as *cis*-1,2-cyclopentanediol, 1,4-anhydroerythritol and *cis*-1,2-cyclohexanediol was investigated with the optimized ReO_x-Pd/CeO₂ catalyst, and moreover DFT calculation was also conducted with structure isomers such as methyl α -L-rhamnopyranoside and methyl α -L-fucopyranoside, the reactivity difference of which is large (~5-fold), to clarify the difference of the reactivity by optimization of the adsorption state and calculation of the transition state. From the kinetic results, the reactivity of methyl glycosides is lower than that of simple cyclic diols, which can be attributed to the presence of the substituents in the methyl glycosides except the *cis*-vicinal diols. Moreover, the reactivity of the methyl glycosides depended on the structure, and the methyl glycosides with low

activity is related to the direction of the substituents adjacent to the *cis*-vicinal diols. The kinetic parameters regarding substrate concentration and H₂ pressure are similar in all substrates, that is the reaction order with respect to the substrate concentration was almost zero, and that with respect to the H₂ pressure was also almost zero, which are similar to that in our previous work on DODH+HG of 1,4-anhydroerythritol over ReO_x-Pd/CeO₂ catalyst. Therefore, these results suggest that the reaction mechanisms of the methyl glycosides and simple cyclic diols is similar. The adsorption state and the transition state of methyl α -L-rhamnopyranoside and methyl α -L-fucopyranoside was estimated by DFT calculations, which showed that the activation energy of these substrates is different (65 kJ mol⁻¹ and 77 kJ mol⁻¹ for methyl α -L-rhamnopyranoside and methyl α -L-fucopyranoside), which was also supported by the results of the Arrhenius plots (63 kJ mol⁻¹ and 73 kJ mol⁻¹ for methyl α -L-rhamnopyranoside and methyl α -L-fucopyranoside) from the experiment results. Based on the result of the activation energy of these substrates on the single active site of CH₃ReO₃ catalyst, where the activation energies are similar (87 kJ mol⁻¹ and 83 kJ mol⁻¹ for methyl α -L-rhamnopyranoside and methyl α -L-fucopyranoside), the difference of these substrates is derived from the intricate interactions between the adjacent functional groups to *cis*-vicinal OH groups and the surface hydroxy groups

References

- [1]. Danishefsky, S. J.; Bilodeau, M. T., *Angew. Chem. Int. Ed. Engl.* **1996**, *35* (13-14), 1380-1419.
- [2]. Harris, J. M.; Keranen, M. D.; O'Doherty, G. A., *J. Org. Chem.* **1999**, *64* (9), 2982-2983.
- [3]. Allen, J. R.; Harris, C. R.; Danishefsky, S. J., *J. Am. Chem. Soc.* **2001**, *123* (9), 1890-7.
- [4]. Montero, A.; Mann, E.; Herradón, B., *Eur. J. Org. Chem.* **2004**, *2004* (14), 3063-3073.
- [5]. Boysen, M. M., *Chemistry* **2007**, *13* (31), 8648-59.
- [6]. Willfor, S.; Sundberg, K.; Tenkanen, M.; Holmbom, B., *Carbohydr. Polym.* **2008**, *72* (2), 197-210.
- [7]. Luley-Goedl, C.; Nidetzky, B., *Biotechnol J* **2010**, *5* (12), 1324-38.
- [8]. Rosatella, A. A.; Simeonov, S. P.; Frade, R. F. M.; Afonso, C. A. M., *Green Chem.* **2011**, *13* (4), 754.
- [9]. Nahain, A. A.; Ignjatovic, V.; Monagle, P.; Tsanaktsidis, J.; Ferro, V., *Med Res Rev* **2018**, *38* (5), 1582-1613.
- [10]. Dimakos, V.; Taylor, M. S., *Chem. Rev.* **2018**, *118* (23), 11457-11517.
- [11]. Dethlefsen, J. R.; Fristrup, P., *ChemSusChem* **2015**, *8* (5), 767-75.
- [12]. Petersen, A. R.; Fristrup, P., *Chemistry* **2017**, *23* (43), 10235-10243.
- [13]. Donnelly, L. J.; Thomas, S. P.; Love, J. B., *Chem Asian J* **2019**, *14* (21), 3782-3790.
- [14]. Tamura, M.; Yuasa, N.; Cao, J.; Nakagawa, Y.; Tomishige, K., *Angew. Chem. Int. Ed. Engl.* **2018**, *57* (27), 8058-8062.
- [15]. Cao, J.; Tamura, M.; Nakagawa, Y.; Tomishige, K., *ACS Catal.* **2019**, 3725-3729.
- [16]. Ota, N.; Tamura, M.; Nakagawa, Y.; Okumura, K.; Tomishige, K., *Angew. Chem. Int. Ed. Engl.* **2015**, *54* (6), 1897-900.
- [17]. Ota, N.; Tamura, M.; Nakagawa, Y.; Okumura, K.; Tomishige, K., *ACS Catal.* **2016**, *6* (5), 3213-3226.
- [18]. Tazawa, S.; Ota, N.; Tamura, M.; Nakagawa, Y.; Okumura, K.; Tomishige, K., *ACS Catal.* **2016**, *6* (10), 6393-6397.
- [19]. Nakagawa, Y.; Tazawa, S.; Wang, T.; Tamura, M.; Hiyoshi, N.; Okumura, K.; Tomishige, K., *ACS Catal.* **2017**, *8* (1), 584-595.
- [20]. Kresse, G.; Furthmüller, J., *Comp Mater Sci* **1996**, *6* (1), 15-50.
- [21]. Kresse, G.; Furthmüller, J., *Physical Review B* **1996**, *54* (16), 11169-11186.
- [22]. Fabris, S.; Vicario, G.; Balducci, G.; de Gironcoli, S.; Baroni, S., *J. Phys. Chem. B* **2005**, *109* (48), 22860-7.
- [23]. Farra, R.; Wrabetz, S.; Schuster, M. E.; Stotz, E.; Hamilton, N. G.; Amrute, A. P.; Perez-Ramirez, J.; Lopez, N.; Teschner, D., *Phys. Chem. Chem. Phys.* **2013**, *15* (10), 3454-65.
- [24]. Gerward, L.; Olsen, J. S., *Powder Diffr.* **1993**, *8* (2), 127-129.
- [25]. Nakajima, A.; Yoshihara, A.; Ishigame, M., *Phys Rev B Condens Matter* **1994**, *50* (18), 13297-13307.
- [26]. Da Silva, J. L. F.; Ganduglia-Pirovano, M. V.; Sauer, J.; Bayer, V.; Kresse, G., *Physical Review B* **2007**, *75* (4).
- [27]. Fernández-Torre, D.; Kośmider, K.; Carrasco, J.; Ganduglia-Pirovano, M. V.; Pérez, R., *The Journal of Physical Chemistry C* **2012**, *116* (25), 13584-13593.
- [28]. Chen, K.; Mori, K.; Watanabe, H.; Nakagawa, Y.; Tomishige, K., *J. Catal.* **2012**, *294*, 171-183.
- [29]. Xi, Y. J.; Yang, W. Q.; Ammal, S. C.; Lauterbach, J.; Pagan-Torres, Y.; Heyden, A., *Catal. Sci. Technol.* **2018**, *8* (22), 5740-5752.



Scheme 2.1 Deoxydehydration + Hydrogenation (DODH + HG) of methyl α -D-mannopyranoside.

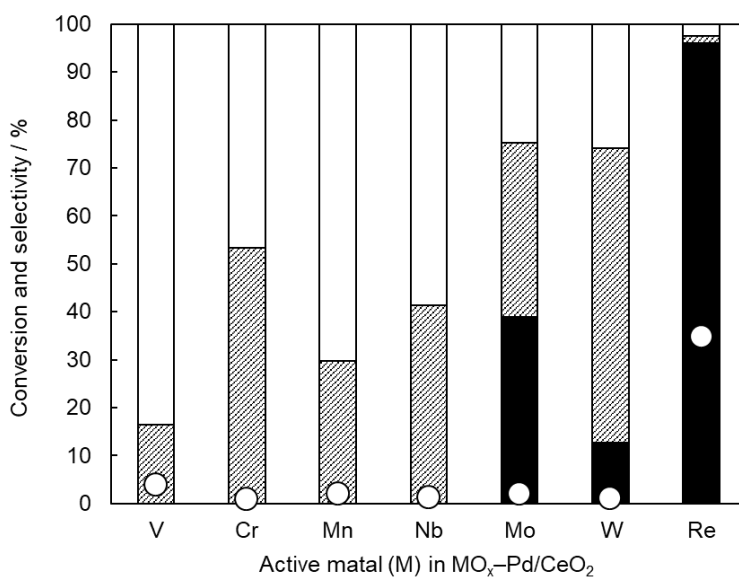


Figure 2.1 Screening of active metals for the DODH + HG of methyl α -D-mannopyranoside. (○: conversion of methyl α -D-mannopyranoside; black bar: selectivity to methyl α -D-mannopyranoside dideoxy product; diagonal bar: selectivity to methyl α -D-mannopyranoside DODH product; white bar: selectivity to other products.)

Reaction conditions: methyl α -D-mannopyranoside 1.3 mmol, $\text{MO}_x\text{-Pd/CeO}_2$ catalyst 0.15 g (M=2 wt%, Pd/M=0.25), 1,4-dioxane 10 g, 7.7 MPa H_2 at 413 K (initial 5.5 MPa H_2 at R.T.), 4 h.

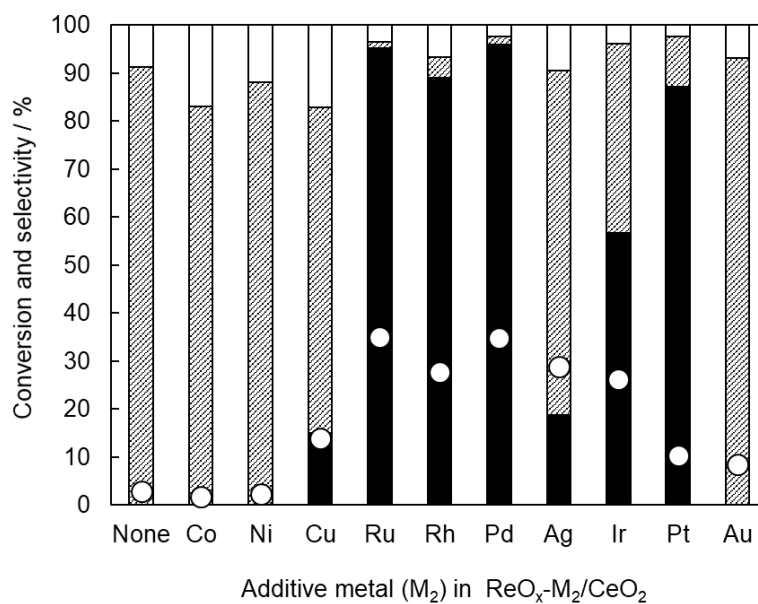


Figure 2.2. Screening of additive metals for the DODH + HG of methyl α -D-mannopyranoside. (○: conversion of methyl α -D-mannopyranoside; black bar: selectivity to methyl α -D-mannopyranoside dideoxy product; diagonal bar: selectivity to methyl α -D-mannopyranoside DODH product; white bar: selectivity to other products.)

Reaction conditions: methyl α -D-mannopyranoside 1.3 mmol, $\text{ReO}_x\text{-}M'/\text{CeO}_2$ catalyst 0.15 g ($\text{Re}=2$ wt%, $M_2/\text{Re}=0.25$), 1,4-dioxane 10 g, 7.7 MPa H_2 at 413 K (initial 5.5 MPa H_2 at R.T.), 4 h.

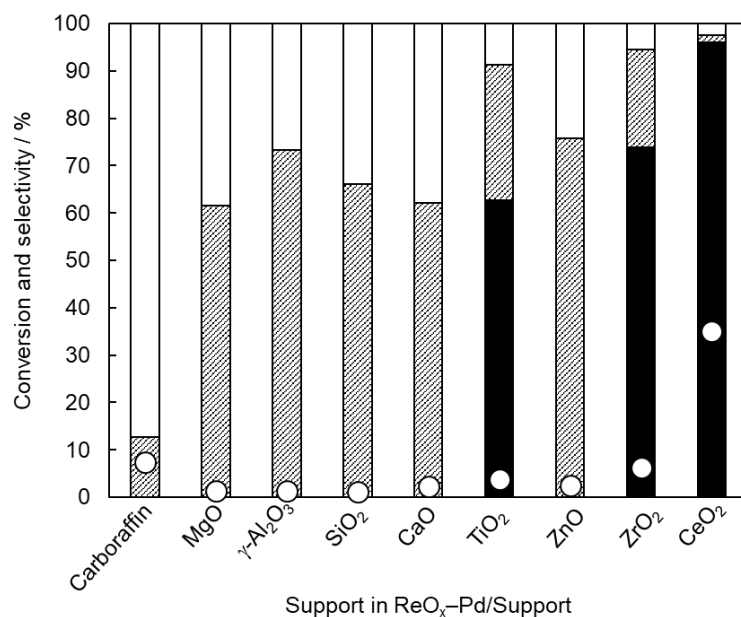


Figure 2.3. Screening of supports for the DODH + HG of methyl α -D-mannopyranoside. (○: conversion of methyl α -D-mannopyranoside; black bar: selectivity to methyl α -D-mannopyranoside dideoxy product; diagonal bar: selectivity to methyl α -D-mannopyranoside DODH product; white bar: selectivity to other products.)

Reaction conditions: methyl α -D-mannopyranoside 1.3 mmol, $\text{ReO}_x\text{-Pd/Support}$ catalyst 0.15 g (Re=2 wt%, Pd/Re=0.25), 1,4-dioxane 10 g, 7.7 MPa H_2 at 413 K (initial 5.5 MPa H_2 at R.T.), 4 h.

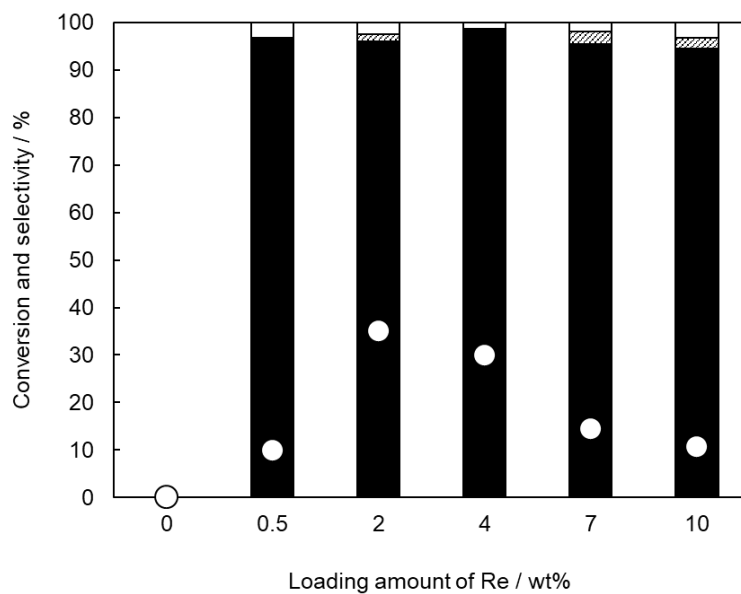


Figure 2.4. Re loading amount effect on the DODH + HG of methyl α -D-mannopyranoside. (○: conversion of methyl α -D-mannopyranoside; black bar: selectivity to methyl α -D-mannopyranoside dideoxy product; diagonal bar: selectivity to methyl α -D-mannopyranoside DODH product; white bar: selectivity to other products.)

Reaction conditions: methyl α -D-mannopyranoside 1.3 mmol, $\text{ReO}_x\text{-Pd/CeO}_2$ catalyst 0.15 g (Re=0-10 wt%, Pd/Re=0.25), 1,4-dioxane 10 g, 7.7 MPa H_2 at 413 K (initial 5.5 MPa H_2 at R.T.), 4 h.

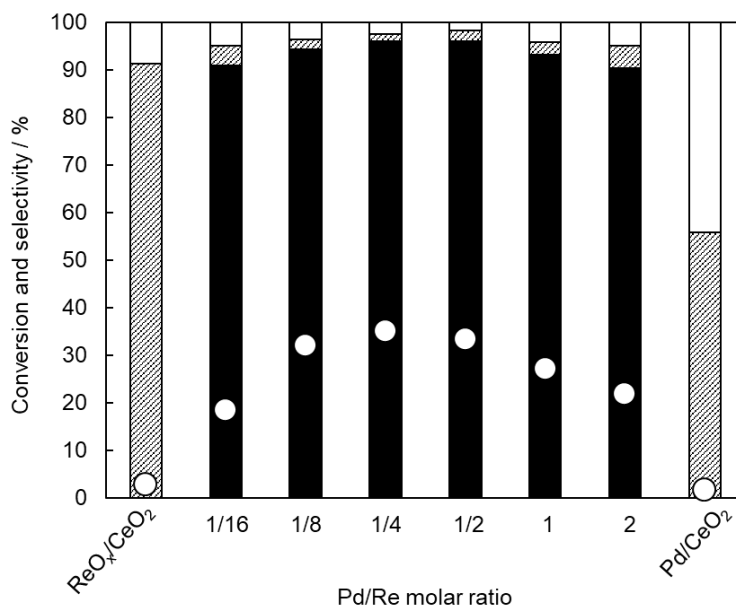


Figure 2.5 Pd/Re molar ratio effect on the DODH + HG of methyl α -D-mannopyranoside. (○: conversion of methyl α -D-mannopyranoside; black bar: selectivity to methyl α -D-mannopyranoside dideoxy product; diagonal bar: selectivity to methyl α -D-mannopyranoside DODH product; white bar: selectivity to other products.)

Reaction conditions: methyl α -D-mannopyranoside 1.3 mmol, $\text{ReO}_x\text{-Pd/CeO}_2$ catalyst 0.15 g (Re=2 wt%, Pd/Re=0-2), 1,4-dioxane 10 g, 7.7 MPa H_2 at 413 K (initial 5.5 MPa H_2 at R.T.), 4 h.

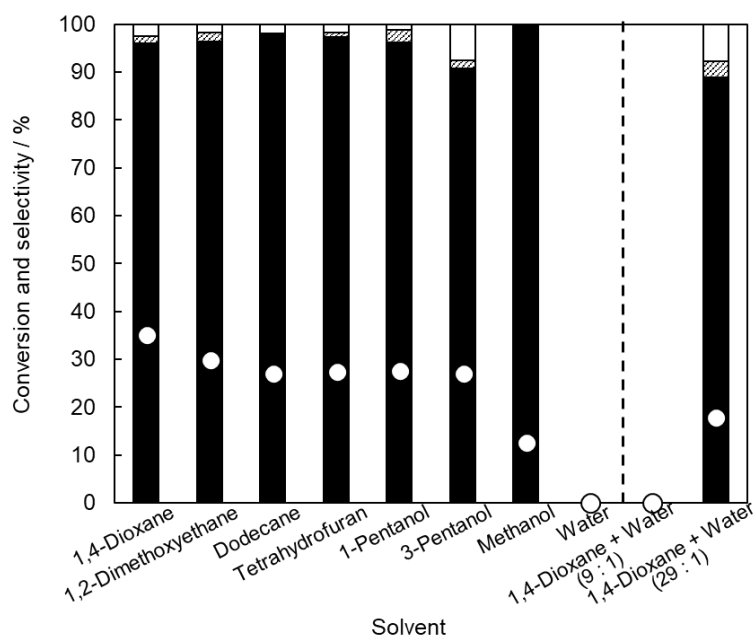


Figure 2.6 Solvent effects on the DODH+HG of methyl α -D-mannopyranoside over $\text{ReO}_x\text{-Pd/CeO}_2$. (\circ : conversion of methyl α -D-mannopyranoside; black bar: selectivity to methyl α -D-mannopyranoside dideoxy product; diagonal bar: selectivity to methyl α -D-mannopyranoside DODH product; white bar: selectivity to other products.)

Reaction conditions: methyl α -D-mannopyranoside 1.3 mmol, $\text{ReO}_x\text{-Pd/CeO}_2$ catalyst 0.15 g ($\text{Re}=2$ wt%, $\text{Pd/Re}=0.25$), solvent 10 g, 7.7 MPa H_2 at 413 K (initial 5.5 MPa H_2 at R.T.), 4 h.

Mechanistic study on deoxydehydration + hydrogenation of methyl glycosides to the dideoxy sugars over $\text{ReO}_x\text{-Pd/CeO}_2$ catalyst

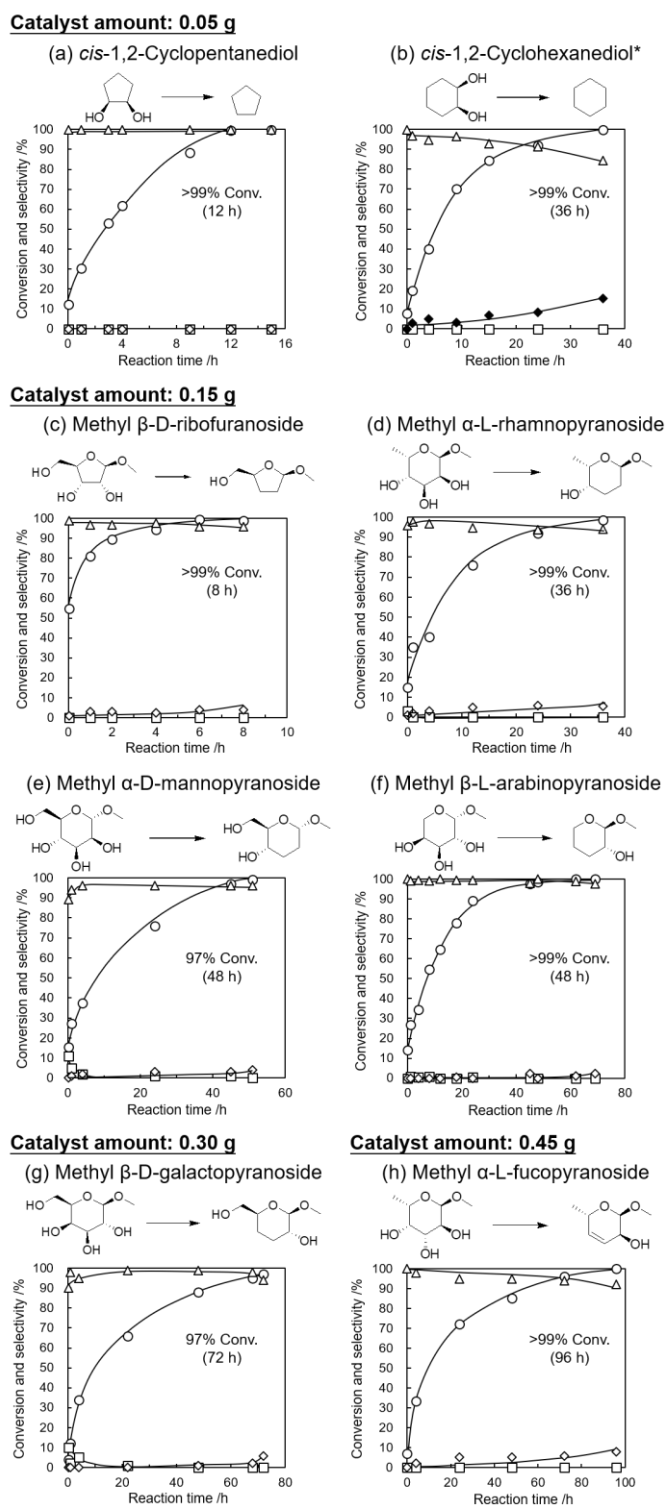


Figure 2.7 Time courses of related substrates over $\text{ReO}_x\text{-Pd/CeO}_2$ (○: conversion; △: selectivity to dideoxy product; □: selectivity to DODH product; ◇: selectivity to other products, *◆: selectivity to *trans*-1,2-cyclohexanediol). Others contain methanol and degradation products. The detailed data are listed in Table 2.1-2.8. Reaction conditions: substrate 1.3 mmol, $\text{ReO}_x\text{-Pd/CeO}_2$ catalyst (0.05 g for *cis*-1,2-cyclopentanediol and *cis*-1,2-cyclohexanediol; 0.15 g for methyl β -D-ribofuranoside, methyl α -L-rhamnopyranoside, methyl α -D-mannopyranoside and methyl β -L-arabinopyranoside; 0.30 g for methyl β -D-galactopyranoside; 0.45 g for methyl α -L-fucopyranoside), 1,4-dioxane 10 g, 7.7 MPa H_2 at 413 K (initial 5.5 MPa H_2 at R.T.).

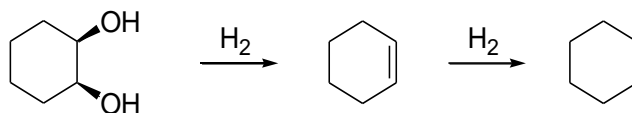
Table 2.1 The reaction of *cis*-1,2-cyclopentanediol over $\text{ReO}_x\text{-Pd/CeO}_2$ catalyst (Detail of Figure 2.7 (a))

$\text{cis-1,2-Cyclopentanediol} \xrightarrow{\text{H}_2} \text{Cyclopentene} \xrightarrow{\text{H}_2} \text{Cyclopentane}$

Entry	Reaction time. /h	Conv. /%	Selectivity /%		Carbon balance /%
			Cyclopentane	Cyclopentene	
1	0	12.5	>99	<1	104
2	1	30.6	>99	<1	101
3	3	53.3	>99	<1	101
4	4	62.1	>99	<1	100
5	9	85.5	>99	<1	98
6	12	>99.9	>99	<1	100
7	15	>99.9	>99	<1	99

Reaction conditions: $\text{ReO}_x\text{-Pd/CeO}_2$ (Re=2 wt%, Pd/Re=0.25) catalyst 0.050 g, substrate 1.3 mmol, 1,4-dioxane 10g, 7.7 MPa H_2 at 413 K (initial 5.5 MPa H_2 at R.T.), 500 rpm.

Table 2.2 The reaction of *cis*-1,2-cyclohexanediol over ReO_x-Pd/CeO₂ catalyst (Detail of Figure 2.7 (b))



cis-1,2-Cyclohexanediol

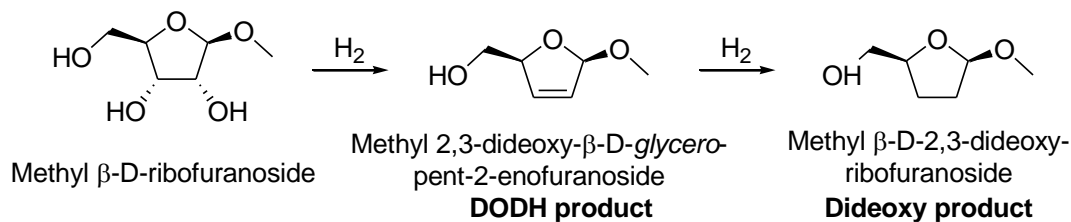
Cyclohexene

Cyclohexane

Entry	Reaction time /h	Conv. /%	Selectivity /%			Carbon balance /%
			Cyclohexane	Cyclohexene	<i>trans</i> -1,2-cyclohexanediol	
1	0	8.0	>99	<1	<1	104
2	1	19.2	97	<1	3	102
3	4	40.2	95	<1	5	98
4	9	70.5	97	<1	3	99
5	15	84.6	93	<1	7	99
6	24	92.3	92	<1	8	108
7	36	>99.9	85	<1	15	94

Reaction conditions: ReO_x-Pd/CeO₂ (Re=2 wt%, Pd/Re=0.25) catalyst 0.050 g, substrate 1.3 mmol, 1,4-dioxane 10g, 7.7 MPa H₂ at 413 K (initial 5.5 MPa H₂ at R.T.), 500 rpm.

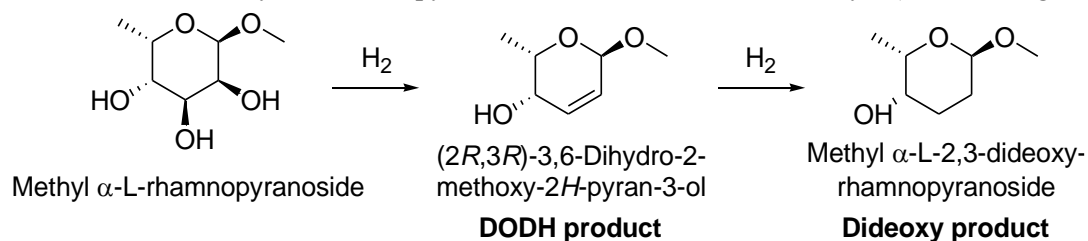
Table 2.3 The reaction of methyl β -D-ribofuranoside over $\text{ReO}_x\text{-Pd/CeO}_2$ catalyst (Detail of Figure 2.7 (c))



Entry	Reaction time /h	Conv. /%	Selectivity /%				Carbon balance /%
			Dideoxy product	DODH product	Methanol	Furfuryl alcohol	
1	0	54.7	99	<1	<1	1	101
2	1	81.4	97	<1	<1	2	102
3	2	89.9	97	<1	<1	2	100
4	4	94.6	98	<1	<1	2	103
5	6	99.7	96	<1	<1	3	97
6	8	99.2	96	<1	1	3	102

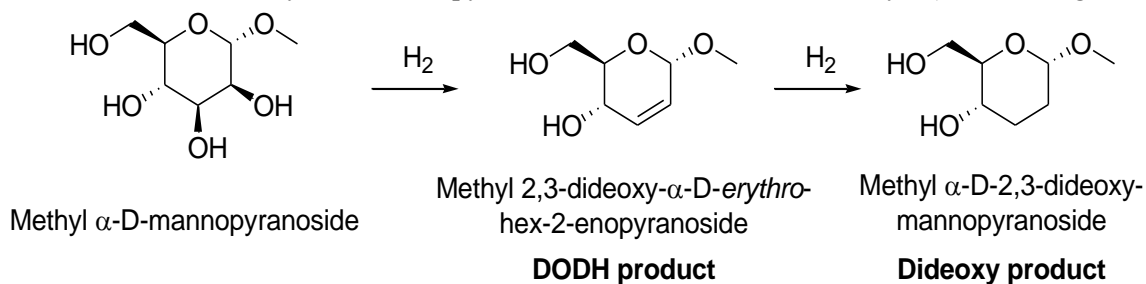
Reaction conditions: $\text{ReO}_x\text{-Pd/CeO}_2$ (Re=2 wt%, Pd/Re=0.25) catalyst 0.050 g, substrate 1.3 mmol, 1,4-dioxane 10g, 7.7 MPa H_2 at 413 K (initial 5.5 MPa H_2 at R.T.), 500 rpm.

Table 2.4 The reaction of methyl -L-rhamnopyranoside over ReO_x-Pd/CeO₂ catalyst (Detail of Figure 2.7 (d))



Entry	Reaction time /h	Conv. /%	Selectivity /%				Carbon balance /%
			Dideoxy product	DODH product	Methanol	Others	
1	0	15.0	96	3	<1	1	101
2	0.5	22.3	97	2	<1	1	100
3	1	35.1	98	<1	<1	2	99
4	4	40.0	97	<1	<1	3	104
5	12	76.3	95	<1	<1	5	102
6	24	92.2	94	<1	<1	6	103
7	36	98.9	94	<1	1	5	105

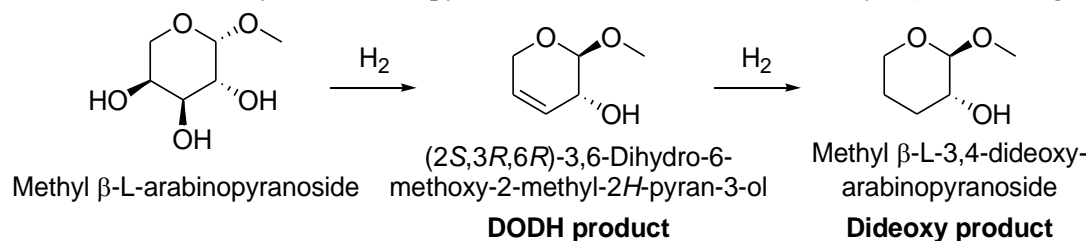
Reaction conditions: ReO_x-Pd/CeO₂ (Re=2 wt%, Pd/Re=0.25) catalyst 0.150 g, substrate 1.3 mmol, 1,4-dioxane 10g, 7.7 MPa H₂ at 413 K (initial 5.5 MPa H₂ at R.T.), 500 rpm. *: Others contain dehydration products from dideoxy product.

Table 2.5 The reaction of methyl α -D-mannopyranoside over $\text{ReO}_x\text{-Pd/CeO}_2$ catalyst (Detail of Figure 2.7 (e))

Entry	Reaction time. /h	Conv. /%	Selectivity %				Carbon balance /%
			Dideoxy product	DODH product	Methanol	Others	
1	0	15.4	89	11	<1	<1	99
2	1	27.1	94	5	<1	<1	97
3	4	37.5	96	2	<1	2	99
4	24	76.0	96	1	<1	2	102
5	45	96.8	96	1	1	2	98
6	51	99.0	96	<1	1	3	95

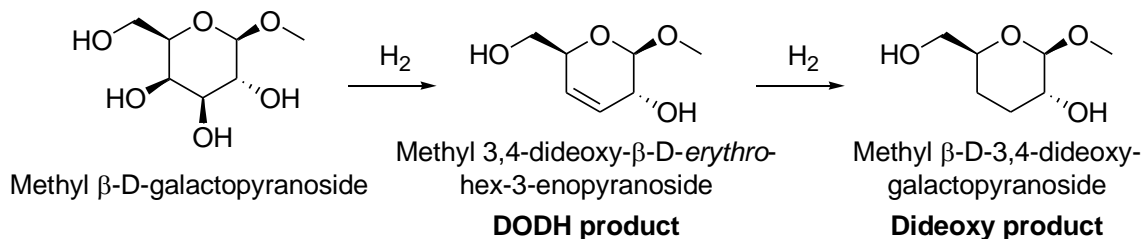
Reaction conditions: $\text{ReO}_x\text{-Pd/CeO}_2$ ($\text{Re}=2$ wt%, $\text{Pd/Re}=0.25$) catalyst 0.150 g, substrate 1.3 mmol, 1,4-dioxane 10g, 7.7 MPa H_2 at 413 K (initial 5.5 MPa H_2 at R.T.), 500 rpm. *: Others contain dehydration and/or hydrogenation products from dideoxy product.

Table 2.6 The reaction of methyl α -L-arabinopyranoside over ReO_x-Pd/CeO₂ catalyst (Detail of Figure 2.7 (f))



Entry	Reaction time /h	Conv. /%	Selectivity /%				Carbon balance /%
			Dideoxy product	DODH product	Methanol	Others	
1	0	14.1	>99	<1	<1	<1	100
2	1	26.8	99	1	<1	<1	100
3	4	34.3	99	1	<1	<1	99
4	8	54.6	99	1	<1	<1	103
5	12	64.7	>99	<1	<1	<1	96
6	18	77.8	99	<1	<1	1	104
7	24	89.1	99	1	<1	<1	104
8	45	97.6	98	<1	<1	2	99
9	48	98.4	100	<1	<1	<1	101
10	62	>99.9	99	<1	<1	1	100
11	69	>99.9	97	<1	1	2	94

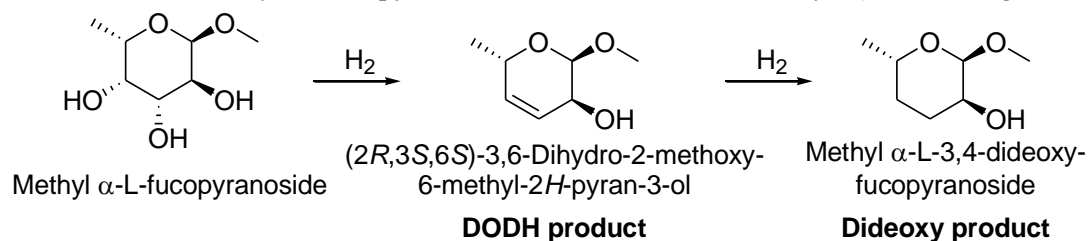
Reaction conditions: ReO_x-Pd/CeO₂ (Re=2 wt%, Pd/Re=0.25) catalyst 0.150 g, substrate 1.3 mmol, 1,4-dioxane 10g, 7.7 MPa H₂ at 413 K (initial 5.5 MPa H₂ at R.T.), 500 rpm. *: Others contain dehydration products from dideoxy product.

Table 2.7 The reaction of methyl β -D-galactopyranoside over $\text{ReO}_x\text{-Pd/CeO}_2$ catalyst (Detail of Figure 2.7 (g))

Entry	Reaction time. /h	Conv. /%	Selectivity %				Carbon balance /%
			Dideoxy product	DODH product	Methanol	Others*	
1	0	4.0	90	10	<1	<1	100
2	1	12.0	98	2	<1	<1	100
3	4	34.0	95	5	<1	<1	97
4	22	66.0	99	1	<1	<1	100
5	48	88.0	99	<1	<1	1	100
6	68	95.0	98	<1	<1	2	98
7	72	97.0	94	<1	1	5	95

Reaction conditions: $\text{ReO}_x\text{-Pd/CeO}_2$ ($\text{Re}=2$ wt%, $\text{Pd/Re}=0.25$) catalyst 0.300 g, methyl α -D-mannopyranoside 1.3 mmol, 1,4-dioxane 10g, 7.7 MPa H_2 at 413 K (initial 5.5 MPa H_2 at R.T.), 500 rpm. *: Others contain degradation products from dideoxy product. *: Others contain dehydration products from dideoxy product.

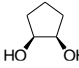

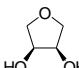
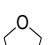
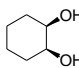
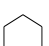
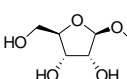
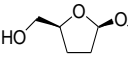
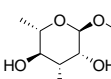
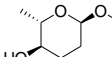
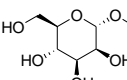
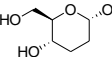
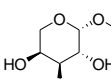
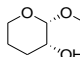
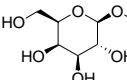
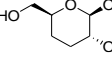
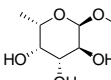
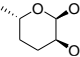
Table 2.8 The reaction of methyl -L-fucopyranoside over ReO_x-Pd/CeO₂ catalyst (Detail of Figure 2.7 (h))



Entry	Reaction time /h	Conv. /%	Selectivity /%				Carbon balance /%
			Dideoxy product	DODH product	Methanol	Others*	
1	0	7.0	100	<1	<1	<1	100
2	4	33.3	98	<1	<1	2	104
3	24	72.1	95	<1	<1	5	99
4	48	85.3	95	<1	1	4	102
5	72	96.1	94	<1	1	5	102
6	96	>99.9	92	<1	2	6	99

Reaction conditions: ReO_x-Pd/CeO₂ (Re=2 wt%, Pd/Re=0.25) catalyst 0.150 g, substrate 1.3 mmol, 1,4-dioxane 10g, 7.7 MPa H₂ at 413 K (initial 5.5 MPa H₂ at R.T.), 500 rpm. *: Others contain degradation products from dideoxy product.

Table 2.9 Reaction rate and reaction orders in related substrates over $\text{ReO}_x\text{-Pd/CeO}_2$

Entry	Substrate	Product	Reaction rate /mmol $\text{g}_{\text{cat}}^{-1} \text{h}^{-1}$	Reaction order	
				Concentration	H_2 Pressure
1	 <i>cis</i> -1,2-Cyclopentanediol	 Cyclopentane	20	-0.1	0.2
2	 1,4-Anhydroerythritol	 Tetrahydrofuran	9.0	-0.3	0.1
3	 <i>cis</i> -1,2-Cyclohexanediol	 Cyclohexane	7.2	0.0	0.1
4	 Methyl β -D-ribofuranoside	 Methyl β -D-2,3-dideoxy-ribofuranoside	4.5	0.1	0.1
5	 Methyl α -L-rhamnopyranoside	 Methyl α -L-2,3-dideoxy-rhamnopyranoside	1.9	0.1	0.2
6	 Methyl α -D-mannopyranoside	 Methyl α -D-2,3-dideoxy-mannopyranoside	1.7	-0.1	0.3
7	 Methyl β -L-arabinopyranoside	 Methyl β -L-3,4-dideoxy-arabinopyranoside	1.7	0.0	0.2
8	 Methyl β -D-galactopyranoside	 Methyl β -D-3,4-dideoxy-galactopyranoside	0.73	-0.1	0.2
9	 Methyl α -L-fucopyranoside	 Methyl α -L-3,4-dideoxy-fucopyranoside	0.38	0.0	0.3

Reaction conditions: $\text{ReO}_x\text{-Pd/CeO}_2$ catalyst 0.15 g (Re=2 wt%, Pd/Re=0.25), substrate amount 1.3 mmol (^asubstrate amount 3.9 mmol), 1,4-dioxane 10 g, 7.7 MPa H_2 at 413 K (initial 1.0 MPa H_2 at R.T.), 500 rpm. The detailed reaction rate data are shown in Figure 2.8, and detailed reaction order are shown in Figures 2.9, 2.10 (substrate concentration) and Figures 2.11, 2.12 (H_2 pressure).

Mechanistic study on deoxydehydration + hydrogenation of methyl glycosides to the dideoxy sugars over $\text{ReO}_x\text{-Pd/CeO}_2$ catalyst

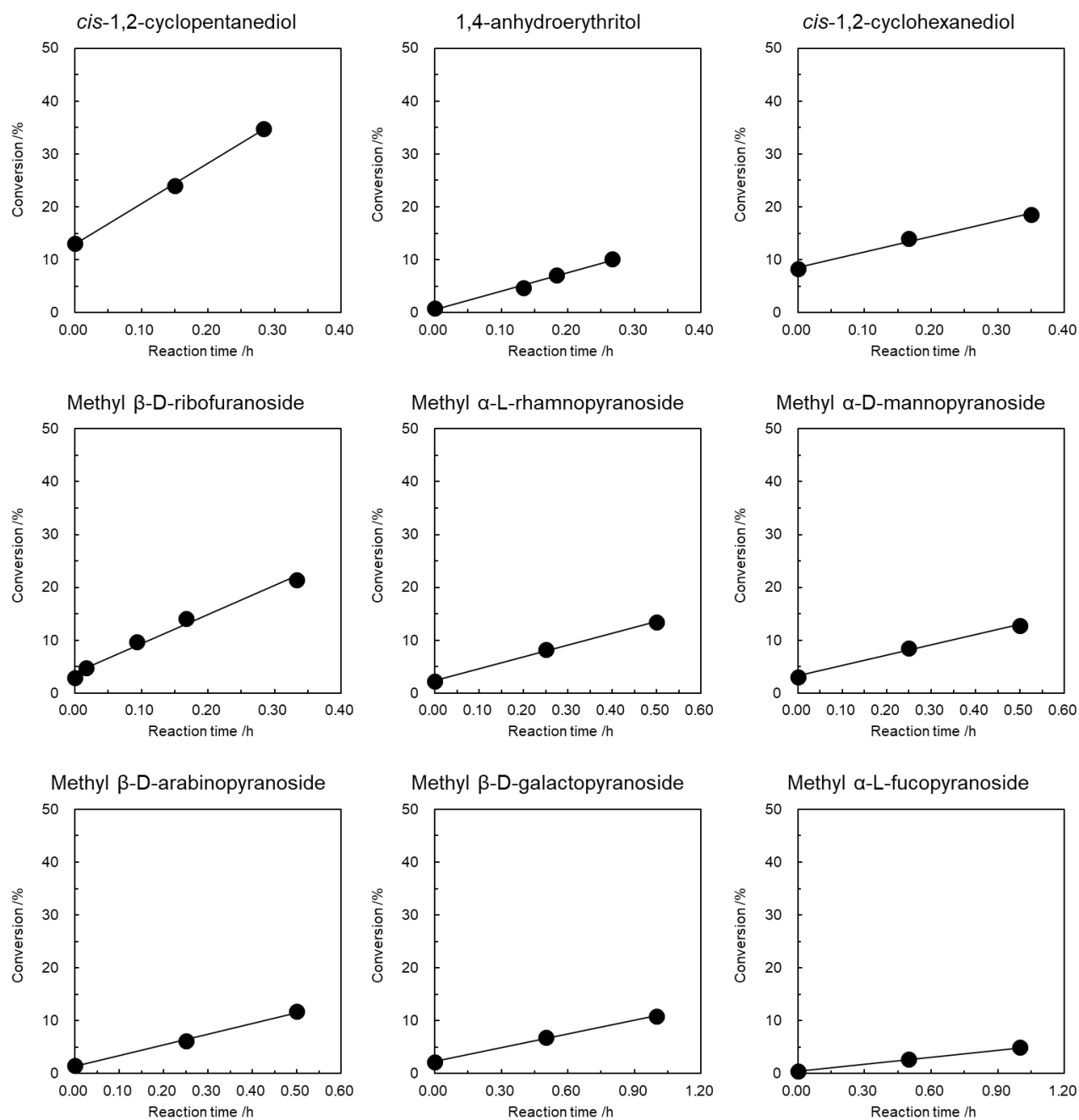


Figure 2.8 The detail of reaction rate of related substrates over $\text{ReO}_x\text{-Pd/CeO}_2$ catalyst

Reaction conditions: $\text{ReO}_x\text{-Pd/CeO}_2$ (Re=2 wt%, Pd/Re=0.25) catalyst, 1,4-dioxane 10 g, 7.7 MPa H_2 at 413 K (initial 1 MPa H_2 at R.T.), 500 rpm.

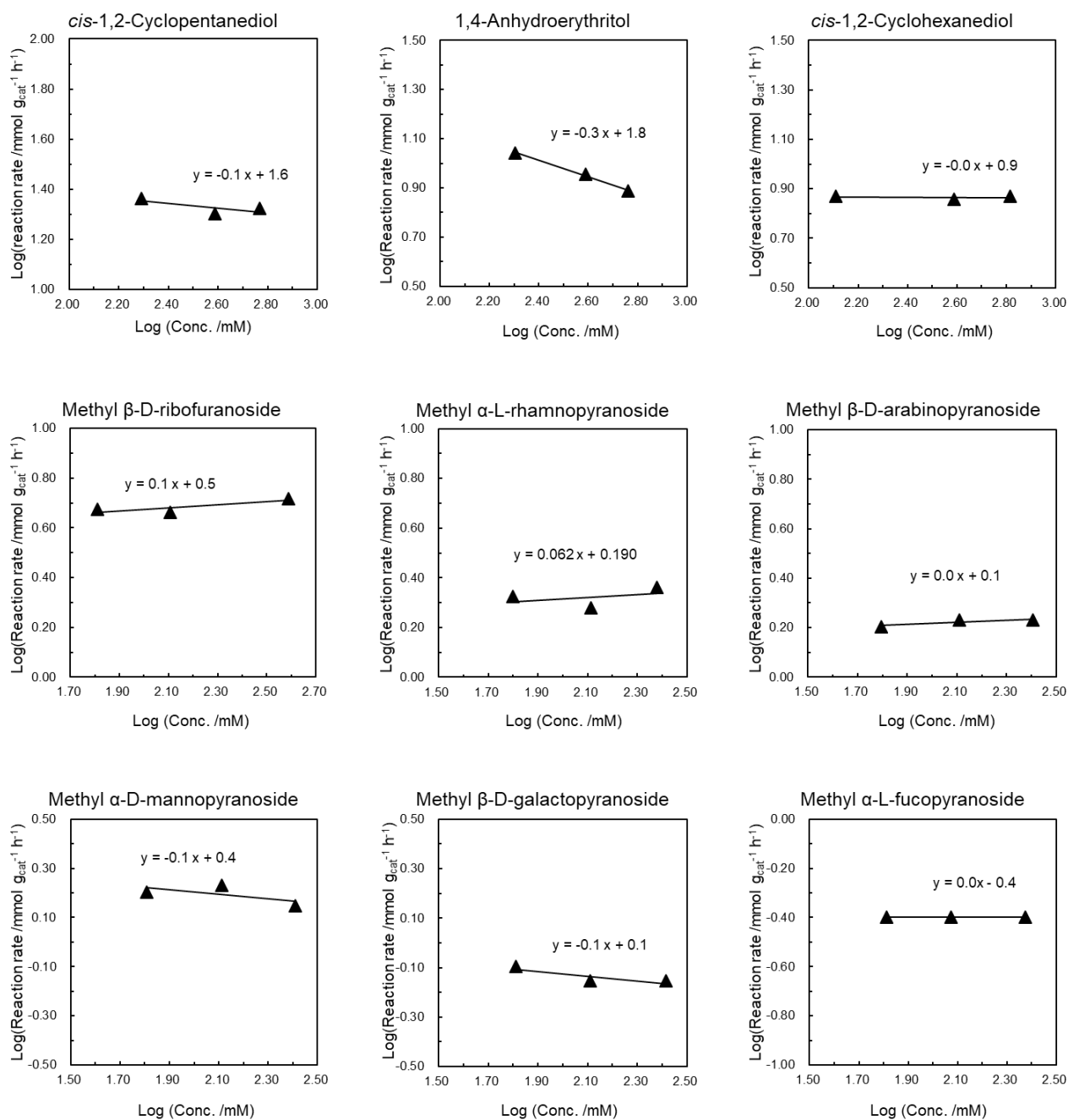


Figure 2.9 The effect of substrate concentration on the DODH + HG of related substrates over $\text{ReO}_x\text{-Pd/CeO}_2$.

Reaction conditions: $\text{ReO}_x\text{-Pd/CeO}_2$ catalyst 0.15 g (Re=2 wt%, Pd/Re=0.25), substrate amount 0.6-2.6 mmol (2.0-6.0 mmol for *cis*-1,2-cyclopentanediol, 1,4-anhydroerythritol and *cis*-1,2-cyclohexanediol), 1,4-dioxane 10 g, 7.7 MPa H_2 at 413 K (initial 1 MPa H_2 at R.T.), 500 rpm, 0-1 h.

Mechanistic study on deoxydehydration + hydrogenation of methyl glycosides to the dideoxy sugars over $\text{ReO}_x\text{-Pd/CeO}_2$ catalyst

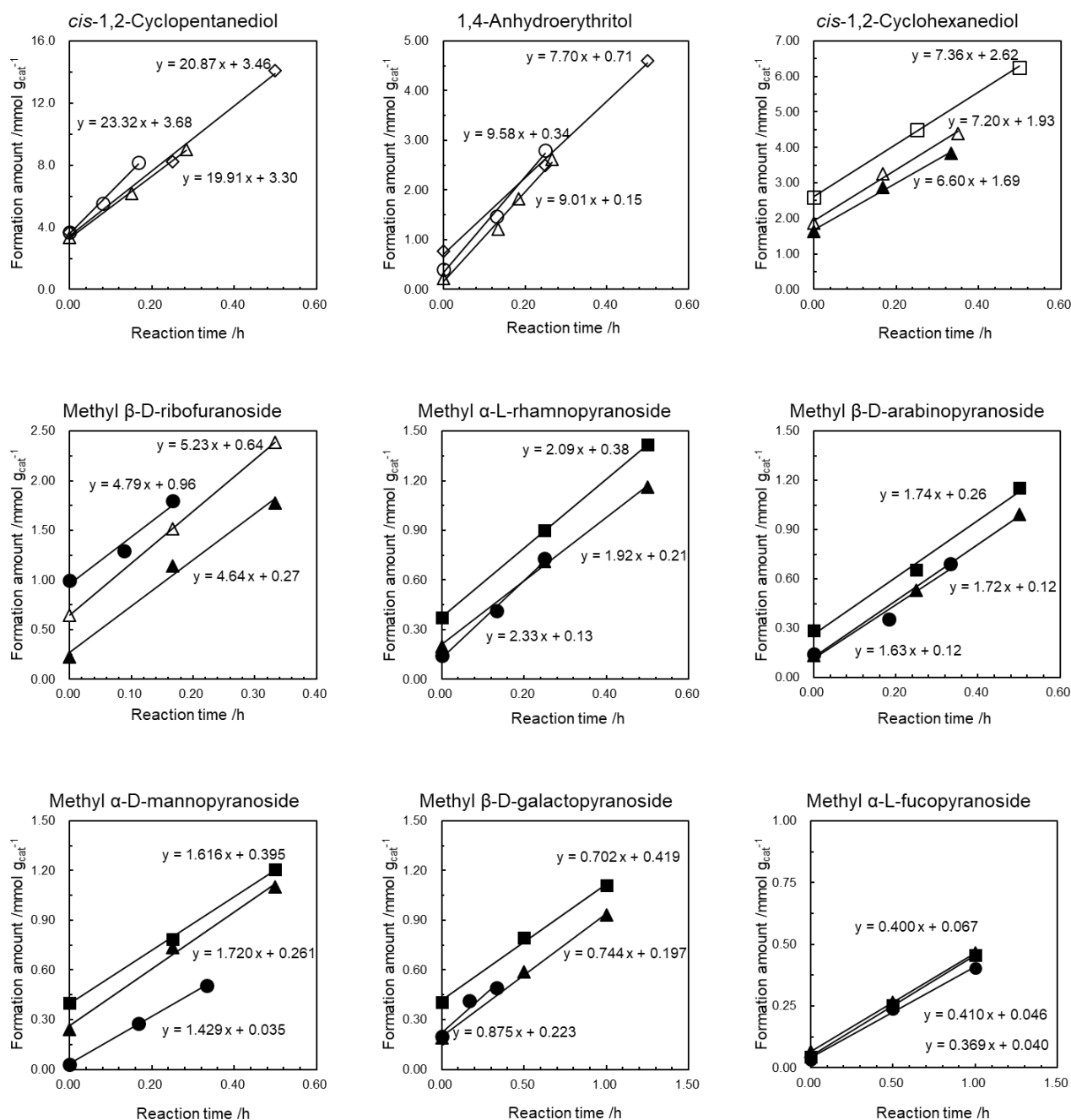


Figure 2.10 The detail of Figure 2.9 (effect of substrate concentration on the DODH + HG of related substrates. over $\text{ReO}_x\text{-Pd/CeO}_2$). (●: 0.65 mM; ▲: 1.3 mM; ○: 2.0 mM; ■: 2.6 mM; △: 3.9 mM; ◇: 6.5 mM)

Reaction conditions: $\text{ReO}_x\text{-Pd/CeO}_2$ catalyst 0.15 g (Re=2 wt%, Pd/Re=0.25), substrate amount 0.6-2.6 mmol (2.0-6.0 mmol for *cis*-1,2-cyclopentanediol, 1,4-anhydroerythritol and *cis*-1,2-cyclohexanediol), 1,4-dioxane 10 g, 7.7 MPa H_2 at 413 K (initial 1 MPa H_2 at R.T.), 500 rpm, 0-1 h.

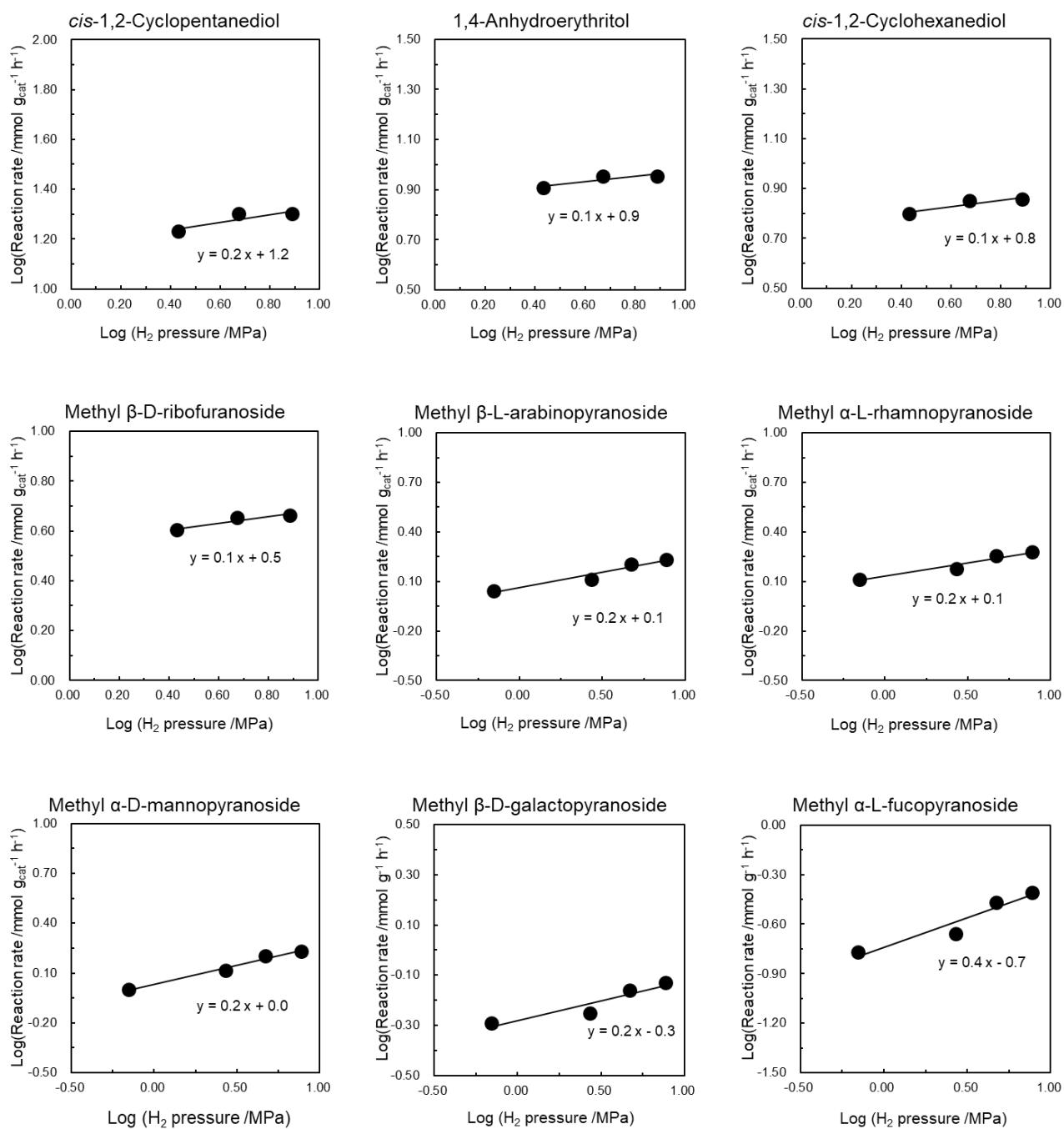


Figure 2.11 The effect of H_2 pressure on the DODH + HG of related substrates over $\text{ReO}_x\text{-Pd/CeO}_2$.

Reaction conditions: $\text{ReO}_x\text{-Pd/CeO}_2$ catalyst 0.15 g ($\text{Re}=2 \text{ wt\%}$, $\text{Pd/Re}=0.25$), substrate amount 1.3 mmol (3.9 mmol for *cis*-1,2-cyclopentanediol, 1,4-anhydroerythritol and *cis*-1,2-cyclohexanediol), 1,4-dioxane 10 g, 0.7-7.7 MPa H_2 at 413 K (typically initial 1.0 MPa H_2 at R.T., purge only for 0.7 MPa H_2), 500 rpm, 0-1 h.

Mechanistic study on deoxydehydration + hydrogenation of methyl glycosides to the dideoxy sugars over $\text{ReO}_x\text{-Pd/CeO}_2$ catalyst

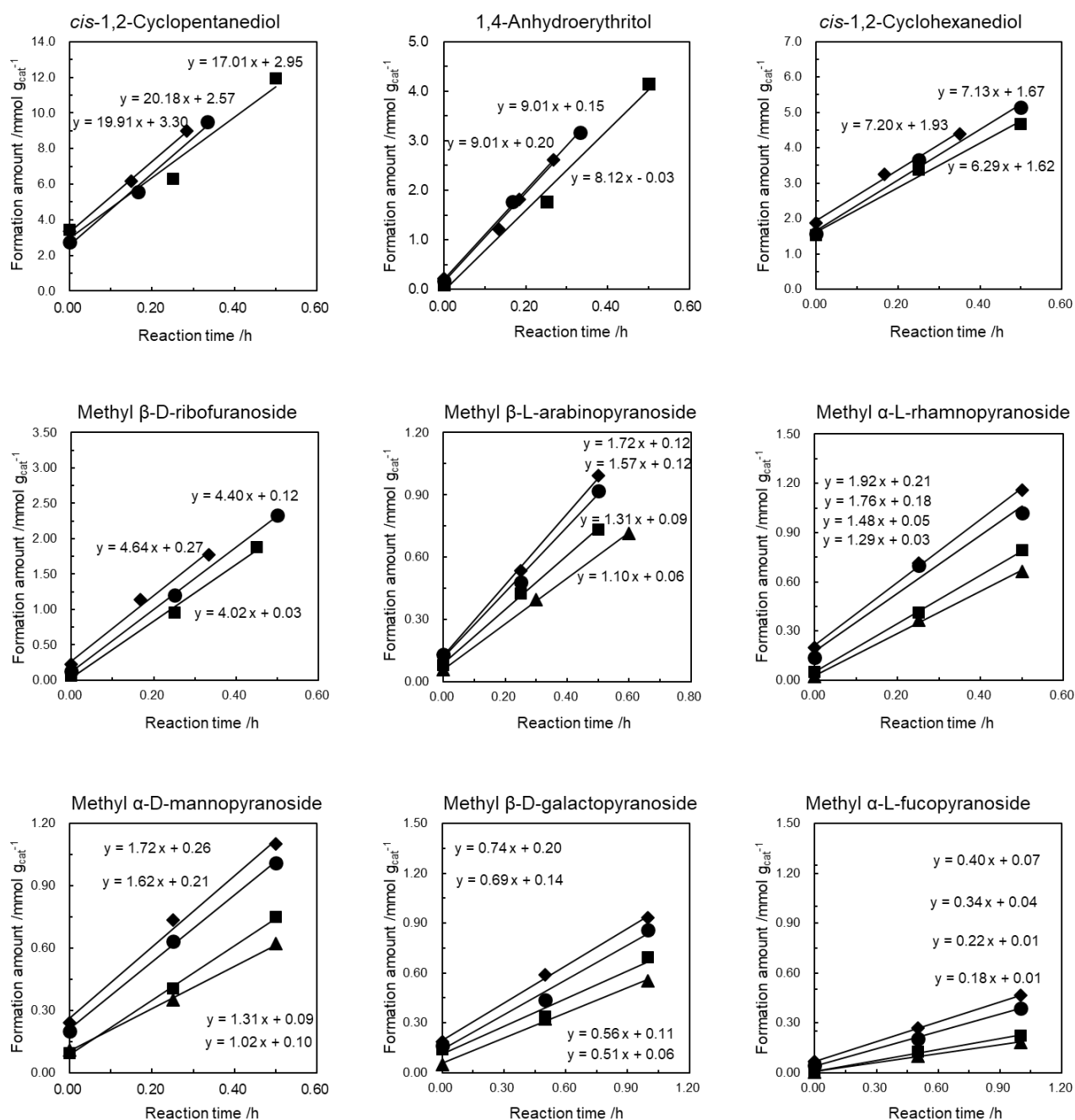
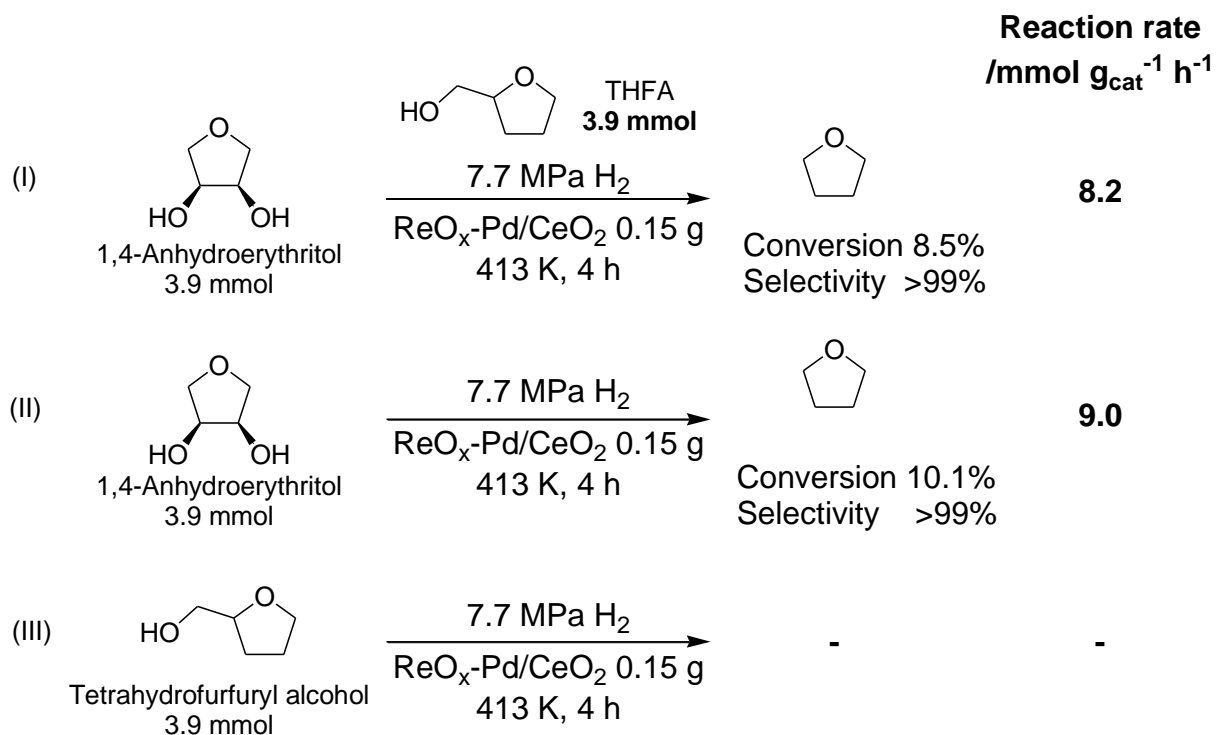


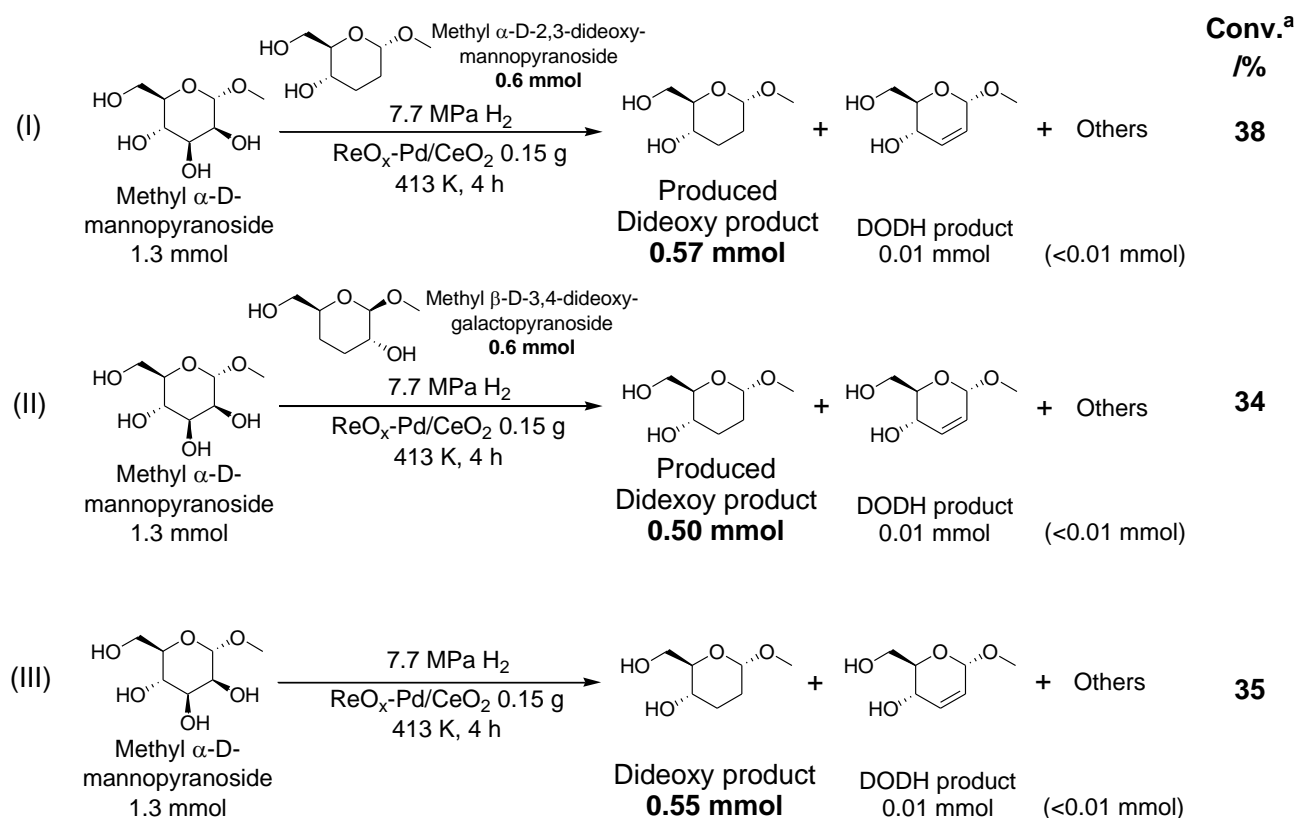
Figure 2.12 The detail of Figure 2.11 (effect of H_2 pressure on the DODH + HG of related substrates. over $\text{ReO}_x\text{-Pd/CeO}_2$). (▲: 0.7 MPa; ■: 2.7 MPa; ●: 4.7 MPa; ◆: 7.7 MPa)

Reaction conditions: $\text{ReO}_x\text{-Pd/CeO}_2$ catalyst 0.15 g (Re=2 wt%, Pd/Re=0.25), substrate amount 1.3 mmol (3.9 mmol for *cis*-1,2-cyclopentanediol, 1,4-anhydroerythritol and *cis*-1,2-cyclohexanediol), 1,4-dioxane 10 g, 0.7-7.7 MPa H_2 at 413 K (typically initial 1.0 MPa H_2 at R.T., purge only for 0.7 MPa H_2), 500 rpm, 0-1 h.



Scheme 2.2 Primary alcohol additive effect on the DODH + HG of 1,4-anhydroerythritol over ReO_x-Pd/CeO₂ (I): The mixture of tetrahydrofurfuryl alcohol and 1,4-anhydroerythritol was used as substrate; (II): 1,4-anhydroerythritol was used as substrate; (III): tetrahydrofurfuryl alcohol was used as substrate. Reaction conditions: ReO_x-Pd/CeO₂ catalyst 0.15 g (Re=2 wt%, Pd/Re=0.25), 3.9 mmol for each substrate, 1,4-dioxane 10 g, 7.7 MPa H₂ at 413 K (initial 1.0 MPa H₂ at R.T.), 0.5 h, 500 rpm.

Mechanistic study on deoxydehydration + hydrogenation of methyl glycosides to the dideoxy sugars over $\text{ReO}_x\text{-Pd/CeO}_2$ catalyst



Scheme 2.3 Product additive effect on the DODH + HG of methyl α -D-mannopyranoside over $\text{ReO}_x\text{-Pd/CeO}_2$ Reaction conditions: $\text{ReO}_x\text{-Pd/CeO}_2$ catalyst 0.15 g (Re=2 wt%, Pd/Re=0.25), methyl α -D-mannopyranoside 1.3 mmol, additive dideoxy product amount 0.6 mmol, 1,4-dioxane 10 g, 7.7 MPa H_2 at 413 K (initial 1.0 MPa H_2 at R.T.), 500 rpm. The detailed data were shown in Table 2.10. ^aCalculated on input methyl α -D-mannopyranoside basis.

Table 2.10 Product additive effect on the reaction of methyl α -D-mannopyranoside over $\text{ReO}_x\text{-Pd/CeO}_2$ (Detail of Scheme 2.3)

Reaction	Input product amount /mmol	Conv. * /%	Dideoxy product amount* /mmol	Dideoxy product amount* /mmol	DODH product amount* /mmol	Others* Carbon balance /%
Methyl α -D-mannopyranoside	--	34.9	0.55	0.55	0.01	<0.01 105
Methyl α -D-mannopyranoside +	0.66	38.2	1.23	0.57	0.01	<0.01 106
Methyl α -D-mannopyranoside dideoxy product						
Methyl α -D-mannopyranoside +	0.59	33.6	0.50	0.50	0.01	<0.01 106
Methyl β -D-galactopyranoside dideoxy product						

Reaction conditions: $\text{ReO}_x\text{-Pd/CeO}_2$ catalyst 0.15 g (Re=2 wt%, Pd/Re=0.25), methyl α -D-mannopyranoside 1.3 mmol, additive amount 0.6 mmol, 1,4-dioxane 10 g, 7.7 MPa H_2 at 413 K (initial 1 MPa H_2 at R.T.), 500 rpm. * Calculated on input methyl α -D-mannopyranoside basis.

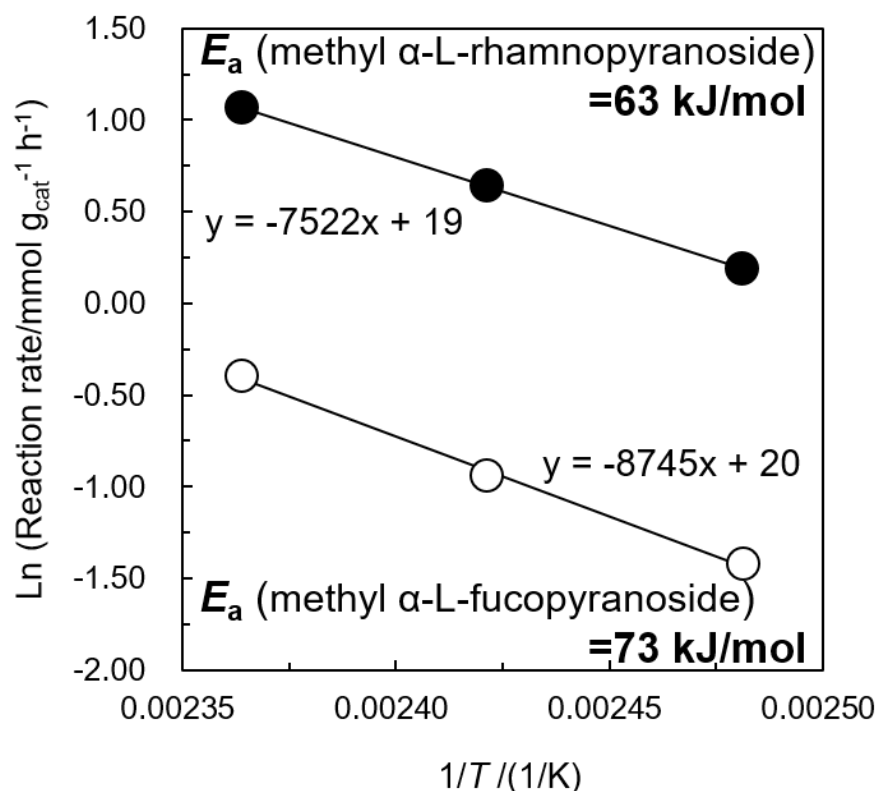


Figure 2.13 Activation energy of selective removal of *cis*-vicinal OH groups in methyl α -L-rhamnopyranoside (●) and methyl α -L-fucopyranoside (○) over $\text{ReO}_x\text{-Pd/CeO}_2$ catalyst. Reaction conditions: $\text{ReO}_x\text{-Pd/CeO}_2$ catalyst 0.15 g (Re=2 wt%, Pd/Re=0.25), substrate 1.3 mmol, 1,4-dioxane 10 g, 7.7 MPa H_2 (initial 1.0 MPa H_2 at R.T.), 500 rpm.

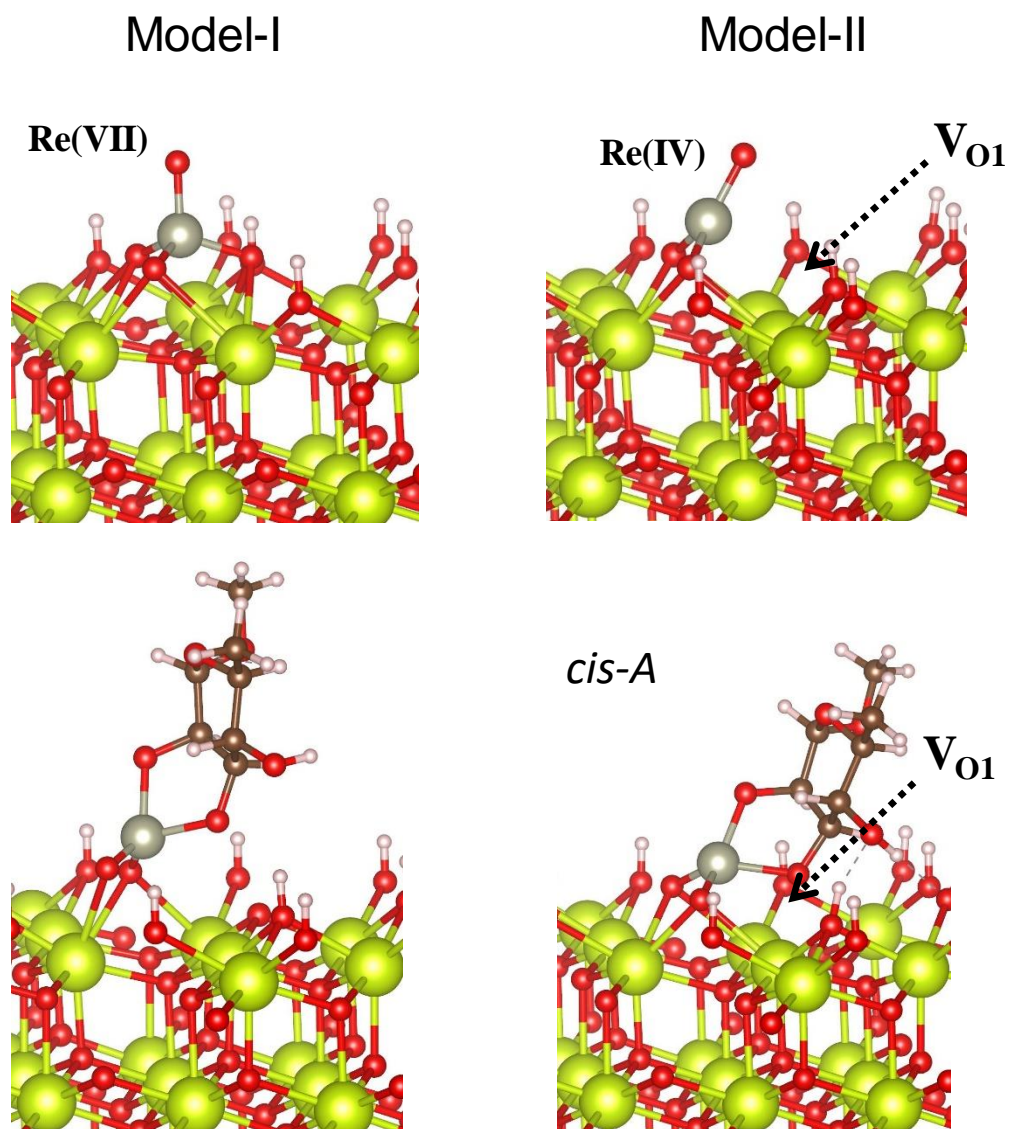


Figure 2.14. Structure of ReO species over CeO_2 in two surface models and diolate structures for methyl α -L-rhamnopyranoside over these models.

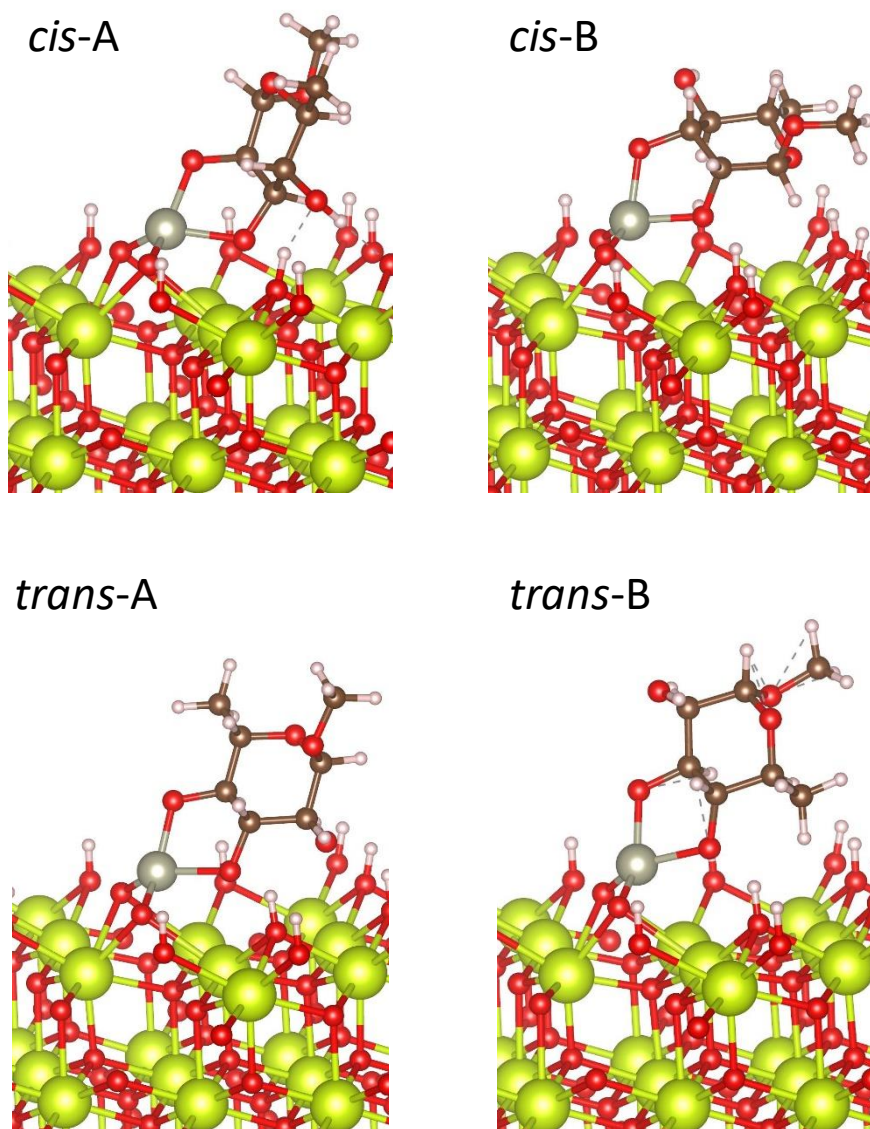


Figure 2.15. Structures of diolate adspecies in various conformation for methyl α -L-rhamnopyranoside.

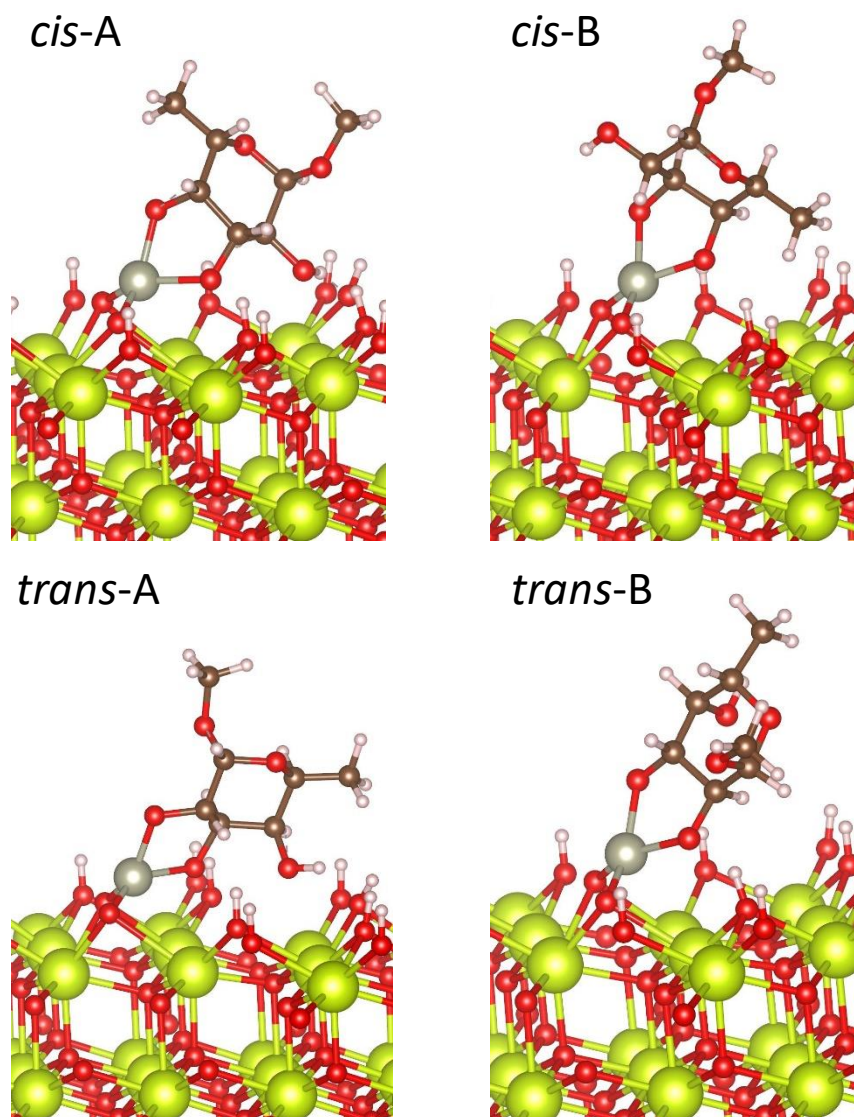


Figure 2.16 Structures of diolate adspecies in various conformation for methyl α -L-fucopyranoside.

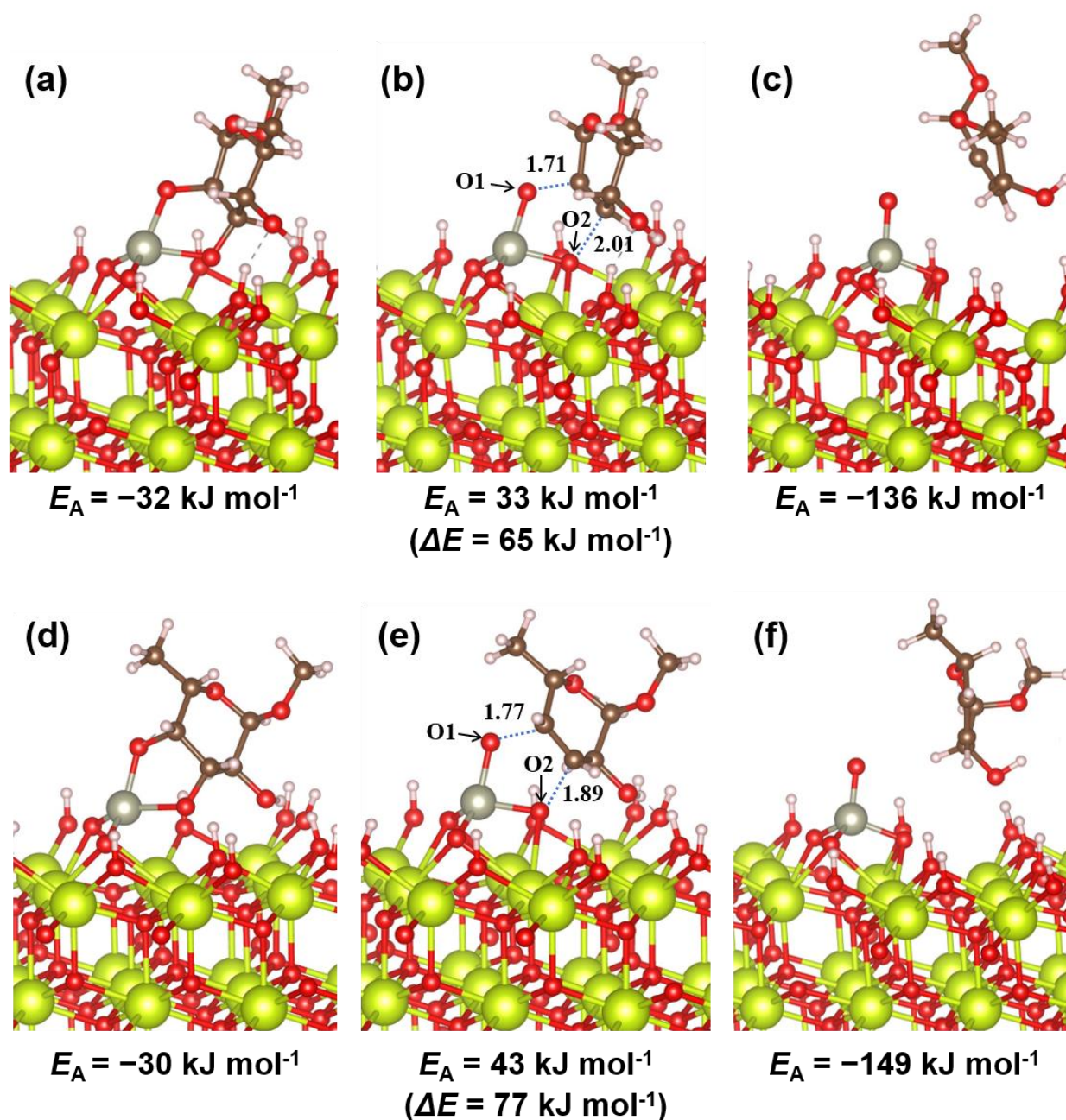


Figure 2.17. Structures of (a) diolate, (b) transition state and (c) the final product of methy α -L-f rhamnopyranoside, and (d) diolate, (e) transition state and (f) the final product of methy α -L-f fucopyranoside.

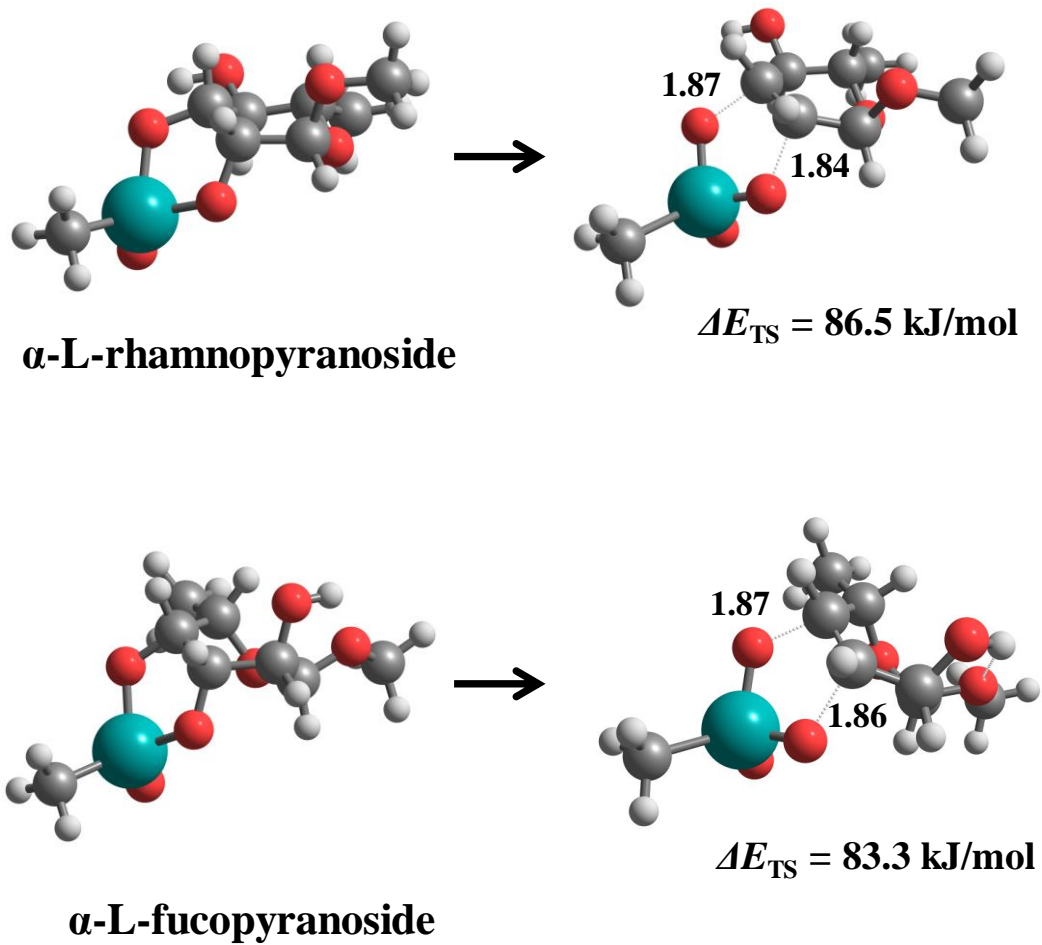


Figure 2.18 Transition state structure and the activation energy for the DODH reaction of methyl α -L-rhamnopyranoside and methyl α -L-fucopyranoside using the CH_3ReO_3 catalyst in the gas phase.

The calculations are performed by the B3LYP functional using the Gaussian 09 package.

Table 2.11 Relative energy of diolate structures of methyl α -L-rhamnopyranoside and methyl α -L-fucopyranoside obtained by DFT calculations.

Substrate	State	Energy / $\text{kJ}\cdot\text{mol}^{-1}$
methyl α -L-rhamnopyranoside	<i>cis</i> -A	-32
	<i>cis</i> -B	4.1
	<i>trans</i> -A	-18
	<i>trans</i> -B	84
methyl α -L-fucopyranoside	<i>cis</i> -A	-30
	<i>cis</i> -B	13
	<i>trans</i> -A	-0.8
	<i>trans</i> -B	8.3

Chapter 3

Direct synthesis of unsaturated sugars from methyl glycosides*

Reproduced from Ref “Ji Cao, Masazumi Tamura, Yoshinao Nakagawa, Keiichi Tomishige, ACS Catalysis. 9 (2019) 3725–3729” with permission from American Chemical Society

3.1 Introduction

Conversion of biomass to valuable chemicals is essential for sustainable society because biomass is the only renewable organic carbon resource^[1-2]. Sugars are the main components of lignocellulosic biomass^[3-5] and can be regarded as important intermediates for biomass conversion^[6-9]. Conventionally, sugars are transformed to furfurals by dehydration, followed by further transformations of furfurals to various chemicals^[10-11]. However, this method loses the original stereo-structure of sugars in spite of the unique stereo-structure being useful for the synthesis of valuable chemicals such as medicines and agrichemicals^[12-16]. Therefore, development of effective transformation methods of sugars without losing the original stereo-structure is desirable. Recently, effective transformation methods of sugars with maintaining the original stereo-structure have been developed. Gagné and co-workers reported an effective reaction system of $B(C_6F_5)_3$ and tertiary silane for selective transformation of silyl-protected polyols to chiral polyol synthons^[17-18] and reductive carbocyclization of unsaturated carbohydrates^[19], and very recently they reported that $B(C_6F_5)_3$ /catecholborane system was effective for selective C-O bond cleavage of sugar derivatives^[20]. Huber and co-workers demonstrated a novel transformation route of cellulose via formation of levoglucosenone, providing tetrahydrofuran dimethanol and 1,6-hexanediol in high selectivity^[21-23].

Among various target products from sugars, unsaturated sugars are one of promising chemicals because they are widely used for the biological active molecules^[24], and important intermediates^[25-34] for medicines, biomaterials and agrichemicals such as antibacterial agents^[30-31], antitumour agents^[32], mimics of specific amino acids in peptides^[33] and so on^[34]

Traditionally, these unsaturated sugars are synthesized^[35] by many reactions including Ferrier rearrangement^[36-39], *de novo* approach^[16,40-41], Achmatowicz rearrangement^[42-43], or heterocycloaddition^[44], which leads to large cost and low yield (Scheme 3.1). Reported methods for the synthesis of dideoxy unsaturated sugars from glucose need multiple steps (5-7 steps) and the yields are inadequate (18-75%) (Scheme 3.2). Therefore, direct transformation of sugars without protection of the OH groups to the unsaturated ones maintaining the original stereo-structure is highly required.

One promising strategy for that will be application of deoxydehydration (DODH) reaction, where the vicinal OH groups in polyols are simultaneously removed to produce C=C bond. DODH reactions have been actively investigated^[45-48], and effective Re, Mo and V complexes have been developed^[49-50]. Recently, heterogeneous catalysts such as $\text{ReO}_x/\text{TiO}_2$ ^[51] and $\text{ReO}_x/\text{Al}_2\text{O}_3$ ^[52-53] were reported to be effective for the reaction, and we also found that isolated ReO_x species over CeO_2 support was an effective heterogeneous catalyst for DODH reaction using H_2 as a reductant. We demonstrated effective catalyst systems of $\text{ReO}_x\text{-Pd/CeO}_2$ for DODH + hydrogenation of 1,4-anhydroerythritol to tetrahydrofuran^[57-58], $\text{ReO}_x\text{-Au/CeO}_2$ for DODH of glycerol to allyl alcohol^[54-55] and physical mixture of $\text{ReO}_x\text{-Au/CeO}_2$ and ReO_x/C for one-pot multi-step reactions including DODH from 1,4-anhydroerythritol to 1,4-butanediol^[56]. On the other hand, a few reports have been reported on application of the DODH reaction to transformation of sugars: Toste and co-workers reported a seminal work on the DODH of various sugar derivatives such as sugar alcohols (hexoses and tetroses) and inositols with CH_3ReO_3 catalyst to afford the corresponding polyenes in moderate to high yields^[59-60]. Moreover, the same research group demonstrated conversion of sugar acids to dicarboxylic acids with a combination catalyst system of KReO_4 and Pd/C ^[61]. NH_4ReO_4 , CH_3ReO_3 and $\text{MoO}_x/\text{Carbon black}$ were also applied to the conversion of sugar acids to dicarboxylic acids^[62-64]. However, these methods lose all the OH groups at the chiral carbons, and usually use organic reductants such as alcohols and phosphines. Recently, we substantiated direct transformation of methyl glycosides to dideoxy saturated methyl glycosides without protection of the OH groups using $\text{ReO}_x\text{-Pd/CeO}_2$ catalyst, where the *cis*-vicinal OH groups in methyl glycosides were

selectively removed^[65]. Methyl glycosides can be easily obtained by methanolysis of lignocellulosic biomass^[66] or methylation of monosaccharides with methanol. The corresponding dideoxy saturated methyl glycosides were obtained in high yields with maintaining the original stereo-structure of the OH groups over $\text{ReO}_x\text{-Pd/CeO}_2$ catalyst^[65], however, unsaturated methyl glycosides were not almost obtained, due to the high reactivity of C=C bond in unsaturated methyl glycosides over the catalyst under H_2 atmosphere. Therefore, development of effective heterogeneous catalysts for the selective synthesis of unsaturated sugars from methyl glycosides is desirable.

Herein, we demonstrated direct transformation of methyl glycosides to the corresponding unsaturated methyl glycosides with H_2 as a reductant over heterogeneous $\text{ReO}_x\text{-Au/CeO}_2$ catalyst, and high yields of the unsaturated methyl glycosides were obtained (up to 90%).

3.2 Experimental

3.2.1 Reagent information

All the methyl glycosides for deoxydehydration reactions were analytic reagents from chemical product corporations and were used without treatment: methyl α -D-mannopyranoside (>98%, FUJIFILM Wako Pure Chemical Co.), methyl β -D-galactopyranoside (>95% (NMR), FUJIFILM Wako Pure Chemical Co.), methyl β -L-arabinopyranoside (>97% (NMR), FUJIFILM Wako Pure Chemical Co.), methyl α -L-fucopyranoside (>98% (HPLC), Tokyo Chemical Industry Co., Ltd.), methyl α -L-rhamnopyranoside (>97% (NMR), FUJIFILM Wako Pure Chemical Co.) and methyl α -D-glucopyranoside (>98% (GC), Tokyo Chemical Industry Co., Ltd.).

All the metal precursors for catalyst preparation were analytic reagents from chemical product corporations: CeO_2 (Daiichi Kigenso Kagaku Kogyo Co., Ltd.), NH_4ReO_4 (Mitsuwa Chemicals Co., Ltd.) $\text{Pd}(\text{NO}_3)_2$ (Sigma-Aldrich Co., LLC.), $\text{Ru}(\text{NO})(\text{NO}_3)_{3-x}(\text{OH})_x$ (Sigma-Aldrich Co., LLC.), $\text{Pt}(\text{NH}_3)_4(\text{NO}_3)_2$ (Sigma-Aldrich Co., LLC.), H_2IrCl_6 (Furuya Metal Co., Ltd.), $\text{RhCl}_3 \cdot 3\text{H}_2\text{O}$ (FUJIFILM Wako Pure Chemical Co.), $\text{HAuCl}_4 \cdot 4\text{H}_2\text{O}$ (FUJIFILM Wako Pure Chemical Co.), AgNO_3 (FUJIFILM Wako Pure Chemical Co.), $\text{Cu}(\text{NO}_3)_2 \cdot 3\text{H}_2\text{O}$ (FUJIFILM

Wako Pure Chemical Co.).

All the solvents for the reaction and isolation of DODH products were also from chemical product corporations and were used without treatment: 1,4-dioxane (>99.5%, FUJIFILM Wako Pure Chemical Co.), diethyl ether (>99.8%, Kishida Chemical Co., Ltd.), diisopropyl ether (>99.0%, Nacalai Tesque, Inc.), methanol (>96%, FUJIFILM Wako Pure Chemical Co.) and hexane (>96%, FUJIFILM Wako Pure Chemical Co.).

3.2.2 Catalyst preparation

Sequential impregnation method

The catalyst prepared by this method was labeled as ^{imp} on the left side of additive metal. The $\text{ReO}_x/\text{CeO}_2$ (Re=1 wt%) and ^{imp}Au/CeO₂ (Au=0.3 wt%) catalyst were prepared by impregnating CeO₂ powder (calcined at 973 K for 1 h, BET surface area: 61 m² g⁻¹) with a 0.3 M aqueous solution of NH₄ReO₄ and HAuCl₄·4H₂O, respectively. After drying and stirring over a 353 K hot plate, the obtained mixture was dried at 383 K for 12 h and then calcined in air at 773 K for 3 h. The loading amount of Re and Au was 1 wt% and 0.3 wt%, respectively.

The $\text{ReO}_x\text{-}^{\text{imp}}\text{M}/\text{CeO}_2$ (M= Pd, Ru, Pt, Ir, Rh, Au, Ag, Cu, Re=1 wt%, M/Re=0.3 mol mol⁻¹) catalysts were prepared by impregnating the obtained $\text{ReO}_x/\text{CeO}_2$ (Re=1 wt%) with corresponding 0.1 M solution of Pd(NO₃)₂, Ru(NO)(NO₃)_{3-x}(OH)_x, Pt(NH₃)₄(NO₃)₂, H₂IrCl₆, RhCl₃·3H₂O, HAuCl₄·4H₂O, AgNO₃, Cu(NO₃)₂·3H₂O, respectively. After drying at 353 K over a hot plate, the catalysts were further dried at 383 K for 12 h. Then, the catalyst was calcined in air at 773 K for 3 h.

Deposition-precipitation method^[71-73]

The deposition-precipitation method was used for the ceria supported Au and ceria supported $\text{ReO}_x\text{-Au}$, and labeled as ^{dp} on the top left corner of Au. For ^{dp}Au/CeO₂ (Au=0.3 wt%) catalyst, a 0.01 M aqueous solution of HAuCl₄·4H₂O containing the suitable amount of Au (0.2 mmol in the case of preparation of 4 g ^{dp}Au/CeO₂) was heated by a hot plate with magnetic stirring, and the CeO₂ powder (calcined at 973 K for 1 h, BET surface area: 61 m² g⁻¹) was added to the solution at 323 K. After the solution temperature was raised to 343 K, the pH of the solution was

adjusted to 9 by addition of 0.1 M NH_3 aqueous solution dropwise using a cassette tube pump and the obtained mixture was stirred for 4 h at 343 K. The suspension of $^{\text{dp}}\text{Au}/\text{CeO}_2$ was filtered and washed several times with distilled water (1.5 L in the case of preparation of 4 g $^{\text{dp}}\text{Au}/\text{CeO}_2$) at room temperature. After drying at 383 K for 12 h, the catalyst was calcined in air at 673 K for 4 h.

The $\text{ReO}_x\text{-}^{\text{dp}}\text{Au}/\text{CeO}_2$ catalyst ($\text{Re}=1$ wt%, $\text{Au}/\text{Re}=0.3$) was prepared by impregnating the obtained $^{\text{dp}}\text{Au}/\text{CeO}_2$ ($\text{Au}=0.3$ wt%) with aqueous solution of NH_4ReO_4 . After drying at 383 K for 12 h, the catalyst was calcined in air at 673 K for 4 h.

3.2.3 Activity test

Activity tests were performed in a 190 mL stainless steel autoclave. The substrate, catalyst and solvent 1,4-dioxane were put into the autoclaves with a spinner. After sealing the reactor, the air content was purged three times with H_2 (>99.99%; Takachiho Trading Co., Ltd.), and the pressure was raised to appropriate value (typically 1.2 MPa, more information for H_2 pressure are shown in Table 3.1) by H_2 at room temperature (R.T.). Autoclaves were then heated to the reaction temperature. The temperature was monitored using a thermocouple inserted in the autoclave. The pressure at reaction temperature was recorded (typically 2.0 MPa at 413 K). The reaction time zero (0 h) was defined as the time when the temperature reached the set value (20 minutes). The stirring rate was fixed at 500 rpm (magnetic stirring). After an appropriate reaction time, the autoclave was cooled down to room temperature in water bath.

The autoclave content and the washing solvent (10 g mixed solution including 8 g distilled water and 2 g 1,4-dioxane) were transformed to vials, and the catalysts were separated by filtration. The both of gas and liquid products were collected and analyzed by FID-GC (Shimadzu GC-2014) and GC-MS (QP5050, Shimadzu) equipped with TC-WAX capillary column (diameter 0.25 mm, 30 m), and HPLC (Shimadzu LC-10A, refractive index detector) with Aminex HPX-87C column (diameter 7.8 mm, 300 mm) using water as the eluent. The amount of unreacted substrate was determined by the absolute calibration curve method based on the HPLC result, and the amounts of products was determined by the absolute calibration curve

method based on the GC result. The calibration curves were obtained by using corresponding chemicals and isolated products. Typical HPLC and GC charts of deoxydehydration of methyl α -D-mannopyranoside were shown in Figures 3.1 and 3.2.

The conversion and the selectivity were calculated on the methyl glycoside basis. The carbon balance was also confirmed in each result and the difference in carbon balance was always in the range of the allowed experimental error within $\pm 5\%$. The turnover frequency (TOF) and turnover number (TON) of catalyst on the reaction were based on total amount of Re.

All the formulas were listed as follow:

$$\text{Conversion (\%)} = [1 - \text{unreacted substrate (mol)} / \text{substrate (mol)}] \times 100$$

$$\text{Selectivity (\%)} = \text{product (mol)} \times n_{\text{carbon}} / (\text{reacted substrate (mol)} \times n_{\text{carbon}}) \times 100$$

$$\text{Carbon balance (\%)} = (\sum (\text{product (mol)} \times n_{\text{carbon}}) + \text{unreacted substrate (mol)} \times n_{\text{carbon}}) / (\text{substrate (mol)} \times n_{\text{carbon}}) \times 100$$

$$\text{TOF (h}^{-1}\text{)} = \text{produced DODH product (mol)} / (\text{Re amount (mol)} \times \text{reaction time (h)})$$

$$\text{TON} = \text{produced DODH product (mol)} / (\text{total Re amount (mol)})$$

Reusability test

The catalyst reusability test was operated in the following method: the $\text{ReO}_x\text{-}^{\text{dp}}\text{Au}^{0.3}/\text{CeO}_2$ catalyst after use was washed with methanol four times and dried at 383 K for 3 h, and then it was calcined in air at 573 K for 3 h. A slight loss (20% in weight in all of four-time uses) was observed during the recovery process, so the scale of the next run was adjusted according to the amount of recovered $\text{ReO}_x\text{-}^{\text{dp}}\text{Au}^{0.3}/\text{CeO}_2$ (catalyst (g): substrate (g): solvent (g)=2: 1 : 40).

3.2.4 Products isolation

Isolation of products was conducted by column chromatography on silica gel using diethyl ether and/or diisopropyl ether and/or methanol and/or hexane as eluents. The isolated products were then identified using GC-MS and NMR (^1H , ^{13}C , H-H COSY, H-C HMQC and H-C HMBC).

Methyl 2,3-dideoxy- α -D-erythro-hex-2-enopyranoside (Table 3.2, entry 1): diethyl ether:diisopropyl ether=2:1, R_f =0.32, HPLC and GC charts are shown in Figures 3.1 and 3.2,

NMR data are shown in supporting information, page 124-128.

Methyl 3,4-dideoxy- α -D-*erythro*-hex-3-enopyranoside (Table 3.2, entry 2): diisopropyl ether:methanol=8.5/1, R_f =0.30, NMR data are shown in supporting information, page 129-133.

(2*R*,3*R*)-3,6-Dihydro-2-methoxy-2*H*-pyran-3-ol, (Table 3.2, entry 3): diisopropyl ether:methanol=199/1, R_f =0.34, NMR data are shown in supporting information, page 134-138.

(2*S*,3*R*,6*R*)-3,6-Dihydro-6-methoxy-2-methyl-2*H*-pyran-3-ol, (Table 3.2, entry 4): diisopropyl ether: hexane=7/3, R_f =0.40, NMR data are shown in supporting information, page 139-143.

(2*R*,3*S*,6*S*)-3,6-Dihydro-2-methoxy-6-methyl-2*H*-pyran-3-ol, (Table 3.2, entry 5): diisopropyl ether: hexane=7/3), R_f =0.30, NMR data are shown in supporting information, page 144-148.

3.2.5 Catalyst characterization

X-ray diffraction (XRD)

The X-ray diffraction (XRD) patterns were recorded by a diffractometer (Rigaku MiniFlex600). The catalyst was filtered and washed by methanol, and then dried at 383 K for 3 h.

Inductively-coupled plasma atomic emission spectrometry (ICP-AES)

The amount of leaching elements from the catalysts into the reaction solution was analyzed by inductively-coupled plasma atomic emission spectrometry (ICP-AES, Thermo Fisher Scientific iCAP6500).

Transmission electron microscope (TEM)

Field emission transmission electron microscope (FE-TEM) images were obtained on a JEOL JEM-2100F instrument operated at 200 kV. The catalysts before reaction (calcined at 673 K) and after reaction were used as samples for the TEM observation. The samples were dispersed in ethanol by supersonic wave.

H₂-Temperature programmed reduction (H₂-TPR)

H₂-Temperature programmed reduction (H₂-TPR) was carried out in a fixed-bed reactor equipped with a thermal conductivity detector (TCD). A frozen trap containing acetone and liquid nitrogen was set up for trapping the produced water. The reduction gas (30 mL/min) was

the mixture of H₂ and Ar gas (5:95). The amount of catalyst was 50 mg, and temperature was increased from room temperature to 1273 K at a heating rate of 10 K/min.

X-ray absorption spectroscopy

The X-ray absorption (EXAFS and XANES) spectra were obtained at the BL01B1 station at SPring-8 with the approval of the Japan Synchrotron Radiation Research Institute (JASRI; Proposal No. 2016A1352, 2016B1410 and 2018B1805). The storage ring was operated at 8 GeV, and a Si (111) single crystal was used to obtain a monochromatic X-ray beam.

The detailed conditions of reference compounds (Au foil, Au₂O₃ and Re powder, ReO₂, ReO₃, Re₂O₇, NH₄ReO₄) for Au *L*₂-edge and Re *L*₃-edge measurements were as follows: Ion chambers for *I*₀ and *I* were filled with 100 % N₂ and 30% Ar + 70% N₂, respectively for both Au *L*₂-edge and Re *L*₃-edge measurement. The EXAFS and XANES data were collected in a transmission mode. The edge jumps of Au *L*₂-edge were 0.6 for Au foil and 0.4 for Au₂O₃, and the edge jumps of Re *L*₃-edge were 0.7 for Re powder, 0.9 for ReO₂, 1.1 for ReO₃, 0.5 for Re₂O₇ and 1.6 for NH₄ReO₄.

The detailed conditions of catalyst samples (ReO_x-^{dp}Au^{0.3}/CeO₂ sample before reaction (calcined at 673K) and ReO_x-^{dp}Au^{0.3}/CeO₂ sample after reaction) for Au *L*₂-edge and Re *L*₃-edge measurements were as follows: we prepared the ReO_x-^{dp}Au^{0.3}/CeO₂ sample before reaction (calcined at 673 K) by pressing the powder catalyst to a disk, and prepared the ReO_x-^{dp}Au^{0.3}/CeO₂ sample after reaction by transferring the used catalyst powder to a measurement bag in a glovebox filled with N₂ to avoid exposure to air. The samples were used for both of Au *L*₂-edge and Re *L*₃-edge measurement. The EXAFS and XANES data were collected in a fluorescence mode using a 19-element Ge solid-state detector (19-SSD). An ion chamber for *I*₀ was filled with 100 % N₂. The edge jumps of ReO_x-^{dp}Au^{0.3}/CeO₂ sample before reaction (calcined at 673 K) and ReO_x-^{dp}Au^{0.3}/CeO₂ sample after reaction were about 0.002.

For EXAFS analysis, the oscillation was first extracted from the EXAFS data using a spline method^[74]. Fourier transformation of the *k*³-weighted EXAFS oscillation from the *k* space to *r* space was carried out to obtain a radial distribution function. The inversely Fourier filtered data were analyzed using a usual curve-fitting method^[75-76]. For curve-fitting analysis, the empirical

phase shift and amplitude functions for the Au–Au and Re–O bonds were extracted from data for Au metal and NH_4ReO_4 , respectively. Analyses of EXAFS data were carried out using a computer program REX2000, ver. 2.6 (Rigaku Corp.). Error bars for each parameter was estimated by stepping each parameter, while optimizing the other parameters, until the residual factor becomes 2 times than its minimum value^[77].

In the analysis of XANES spectra, the normalized spectra were obtained by subtracting the pre-edge background from the raw data with a modified Victoreen equation and normalizing them by the edge height^[78-81]. The binding energy of the sample was defined by the inflection point^[82-83]. The chemical shift of the binding energy from Re metal powder was evaluated on each spectrum. The chemical shift of the binding energy is almost proportional to the valence of the Re species (Figure 3.8). In order to estimate the valence of Re species, we used the data of ReO_2 , ReO_3 , and NH_4ReO_4 as references. And the Re valence of the samples was estimated on the basis of the relation.

3.3 Results and discussion

3.3.1 Optimization of reaction conditions

At first, combination of ReO_x and metals (M) with H_2 activation ability over CeO_2 support was investigated in DODH of methyl α -D-mannopyranoside with H_2 as a model reaction (Table 3.3). The catalysts were prepared by impregnation method (labeled as ^{imp} on the left side of M) with 1 wt% Re loading amount and M/Re molar ratio of 0.3, which is the best composition of ReO_x -Au/ CeO_2 in our previous work on DODH of glycerol to allyl alcohol^[54-55]. The target product is methyl 2,3-dideoxy α -D-erythro-hex-2-enopyranoside (**1**), which is produced by removal of the *cis*-OH groups at C-2 and C-3 positions of methyl α -D-mannopyranoside, and the main by-product is methyl 2,3-dideoxy α -D-mannopyranoside (**2**), which is formed by over-hydrogenation of **1**. Au-, Ag- and Cu-loaded $\text{ReO}_x/\text{CeO}_2$ catalysts provided high selectivity to **1** (49->99%, entries 1-3), while Ir-, Pt-, Rh-, Ru- and Pd-loaded $\text{ReO}_x/\text{CeO}_2$ catalysts showed low selectivity to **1** (<10%) and high selectivity to **2** (entries 4-8). Among the catalysts tested, ReO_x -^{imp}Au^{0.3}/ CeO_2 showed the highest selectivity (>99%) to **1** with moderate conversion (10%,

entry 1). $\text{ReO}_x/\text{CeO}_2$, CeO_2 and $^{\text{imp}}\text{Au}/\text{CeO}_2$ catalysts (entries 9-11) showed no or low conversion ($\leq 2\%$), indicating that all the species of CeO_2 , ReO_x and Au are essential for the high performance.

Catalyst preparation method strongly influences formation of metal species, especially for Au catalysts^[67-68]. Generally, smaller Au particles have higher hydrogenation activity, and deposition-

precipitation method is often used for formation of small Au particles ($< 5 \text{ nm}$)^[69-70].

$\text{ReO}_x\text{-Au}/\text{CeO}_2$ was prepared by deposition-precipitation method ($\text{ReO}_x\text{-}^{\text{dp}}\text{Au}/\text{CeO}_2$, labeled as $^{\text{dp}}$ on the left side of Au), and the performance was compared with that of $\text{ReO}_x\text{-}^{\text{imp}}\text{Au}^{0.3}/\text{CeO}_2$ in the same reaction (Table 3.4). The $\text{ReO}_x\text{-}^{\text{dp}}\text{Au}^{0.3}/\text{CeO}_2$ showed higher conversion (27%, entry 2) than $\text{ReO}_x\text{-}^{\text{imp}}\text{Au}^{0.3}/\text{CeO}_2$, however the selectivity to **1** was a little low (96%) and **2** was formed, suggesting that the hydrogenation activity of Au was enhanced by the deposition-precipitation method. The effect of H_2 pressure was investigated with $\text{ReO}_x\text{-}^{\text{dp}}\text{Au}^{0.3}/\text{CeO}_2$ (Table 3.4, entries 2-8) and $\text{ReO}_x\text{-}^{\text{imp}}\text{Au}^{0.3}/\text{CeO}_2$ (Table 3.5). In the case of $\text{ReO}_x\text{-}^{\text{dp}}\text{Au}^{0.3}/\text{CeO}_2$, the conversion gradually decreased from 27% to 14% with decreasing the H_2 pressure from 7.7 to 0.2 MPa. The selectivity to **1** increased from 96 to $>99\%$ (entries 2-7), and the high selectivity ($>99\%$) was obtained at 0.2-1.7 MPa (entries 5-7). The conversion was adequately high (14%) even at low H_2 pressure of 0.2 MPa (entry 7), which was higher than that with $\text{ReO}_x\text{-}^{\text{imp}}\text{Au}^{0.3}/\text{CeO}_2$ at 7.7 MPa H_2 (10%, entry 1). In contrast, in the case of $\text{ReO}_x\text{-}^{\text{imp}}\text{Au}^{0.3}/\text{CeO}_2$, the conversion drastically decreased with lower H_2 pressure from 10 to $<1\%$ (7.7 to 0.2 MPa) (Table 3.5), meaning that low H_2 pressure is not applicable with $\text{ReO}_x\text{-}^{\text{imp}}\text{Au}^{0.3}/\text{CeO}_2$. High active Au particles over $\text{ReO}_x\text{-}^{\text{dp}}\text{Au}^{0.3}/\text{CeO}_2$ will enhance H_2 activation, leading to the high activity even at low H_2 pressure. Moreover, in order to confirm which is the best catalyst, $\text{ReO}_x\text{-}^{\text{dp}}\text{Au}^{0.3}/\text{CeO}_2$ or $\text{ReO}_x\text{-}^{\text{imp}}\text{Au}^{0.3}/\text{CeO}_2$, for high yield of **1**, the yield at high conversion level ($\sim 99\%$) was compared at the preferable H_2 pressure (entries 8 and 9). $\text{ReO}_x\text{-}^{\text{dp}}\text{Au}^{0.3}/\text{CeO}_2$ provided 92% selectivity at 99% conversion at 8 h and 1.7 MPa H_2 (entry 8), and $\text{ReO}_x\text{-}^{\text{imp}}\text{Au}^{0.3}/\text{CeO}_2$ provided 85% selectivity at 98% conversion at longer reaction time of 29 h despite of high H_2 pressure of 7.5

MPa (entry 9). Therefore, $\text{ReO}_x\text{-dpAu}^{0.3}/\text{CeO}_2$ catalyst at low H_2 pressure (≤ 1.7 MPa) was suitable for the reaction.

3.3.2 Catalyst characterization

The $\text{ReO}_x\text{-dpAu}^{0.3}/\text{CeO}_2$ before and after reaction was characterized by XRD, TEM and H_2 -temperature programmed reduction (H_2 -TPR). In XRD patterns (Figure 3.1), the signals due to Re species were not observed, suggesting that Re species were highly dispersed or amorphous. The particle size of Au over $\text{ReO}_x\text{-dpAu}^{0.3}/\text{CeO}_2$ was calculated to be about 3 nm. However, the Au particles were not observed by TEM, probably due to low contrast between CeO_2 and Au species (Figure 3.2), which also supports the formation of small Au particles. Reducibility of $\text{ReO}_x\text{-dpAu}^{0.3}/\text{CeO}_2$, $\text{ReO}_x/\text{CeO}_2$ and CeO_2 was studied by H_2 -TPR analysis (Figure 3.3 and Table 3.6). The sharp peak at 740 K over $\text{ReO}_x/\text{CeO}_2$ can be assigned to the reduction of Re species, and a part of CeO_2 was also reduced simultaneously, which was confirmed by the amount of H_2 consumption. The signal due to ReO_x reduction over $\text{ReO}_x\text{-dpAu}^{0.3}/\text{CeO}_2$ was observed at lower temperature than that over $\text{ReO}_x/\text{CeO}_2$, indicating that addition of Au species facilitated reduction of ReO_x species. Finally, XAS analyses were also conducted to confirm the state of Au and Re species (Figures 3.4-3.8, and Tables 3.7-3.9). From Au L_2 -edge and Re L_3 -edge XANES spectra (Figures 3.4 and 3.6), Au was in the metallic state, and Re species were in the oxidized state and the valences of Re species over $\text{ReO}_x\text{-dpAu}^{0.3}/\text{CeO}_2$ before and after reaction were calculated to be about +7.0 and +5.8, respectively (Table 3.8), indicating that ReO_x species were partially reduced by the reaction. From the curve-fitting analyses of Au L_2 -edge EXAFS spectra (Figure 3.5 and Table 3.7), only signal due to Au-Au bond was observed over $\text{ReO}_x\text{-dpAu}^{0.3}/\text{CeO}_2$ after reaction and the coordination number (CN) was 8.8, suggesting that small Au particles were formed. These results were consistent with the results of XRD and XANES. From the curve-fitting analyses of Re L_3 -edge XANES spectra (Figure 3.8 and Table 3.9), $\text{ReO}_x\text{-dpAu}^{0.3}/\text{CeO}_2$ before reaction provided only the bond due to $\text{Re}=\text{O}$, and the CN was ~ 4 . On the other hand, $\text{ReO}_x\text{-dpAu}^{0.3}/\text{CeO}_2$ after reaction provided the bonds due to $\text{Re}=\text{O}$ and $\text{Re}-\text{O}$, and the CN of $\text{Re}=\text{O}$ and $\text{Re}-\text{O}$ were ~ 1.7 and 3.9, respectively. These results indicate that

Re species were partially reduced by the reaction. Considering that the Re species are coordinated on the two surface oxygen species of CeO₂, the CN is in good accordance with the result of XANES. These results agreed with those in our previous report on ReO_x-^{dp}Au^{0.3}/CeO₂ in DODH of glycerol^[54-55], suggesting that similar active species like monomeric Re on CeO₂ catalyzes this reaction.

The time-course of DODH reaction of methyl α -D-mannopyranoside over ReO_x-^{dp}Au^{0.3}/CeO₂ is shown in Figure 3.9. The conversion smoothly increased with the time and reached almost 100% at 8 h. The selectivity to **1** was high (>90%) below 90% conversion and decreased at higher conversion due to over-hydrogenation of **1** to **2** and/or dehydration or hydration of **2** to others. The maximum yield of **1** reached 90% at 8 h. The turnover frequency (TOF) based on total Re amount was calculated to be 10 h⁻¹ in the initial stage (0-1 h). The value was lower than that of glycerol DODH reaction with ReO_x-^{imp}Au^{0.3}/CeO₂ at 8 MPa (16 h⁻¹), indicating that the reactivity of methyl α -D-mannopyranoside was a little lower than that of glycerol over ReO_x-^{dp}Au^{0.3}/CeO₂ catalyst. The high yield of **1** (88%) was also achieved even at low H₂ pressure of 0.7 MPa (Figure 3.10). Moreover, maximum turnover number (TON) per total Re atom of 270 was obtained by increasing the substrate (0.5 g) and reaction time (160 h) and by decreasing the catalyst amount (0.15 g) (Scheme 3.3).

The reusability of ReO_x-^{dp}Au^{0.3}/CeO₂ was tested. The catalyst could be reused three times without loss of activity and selectivity (Figure 3.11). The XRD patterns of the catalysts before and after reaction were not changed (Figure 3.12). The ICP-AES analysis of the reaction mixtures after the first reaction showed that the leaching amounts of Au and Re species were very small (Au: below the detection level (0.07%), Re: 1% to total metal species). Therefore, ReO_x-Au^{0.3}/CeO₂ is a reusable heterogeneous catalyst.

3.3.3 Substrate scope

The ReO_x-^{dp}Au^{0.3}/CeO₂ catalyst was applied to the reactions of various methyl glycosides, and the maximum yield of the DODH products was obtained by adjusting reaction time and catalyst amount (Table 3.2, and the detailed time-courses (Figure 3.15-3.18)). The substrates

with *cis*-vicinal OH groups could be converted to the corresponding unsaturated sugars in moderate to high selectivity (61-93%) such as methyl β -D-galactopyranoside, methyl β -L-arabinopyranoside, methyl α -L-rhamnopyranoside and methyl α -L-fucopyranoside (entries 1-5). On the other hand, methyl α -D-glucopyranoside with only *trans*-vicinal OH groups showed no conversion (entry 6). These results suggest that only *cis*-vicinal OH groups could be removed by the catalyst. Based on the result of the time-course (Table 3.2, Figures 3.15-3.18), the reactivities of the substrates are quite different and the reactivity order is as follows: methyl α -D-mannopyranoside \geq methyl β -L-arabinopyranoside $>$ methyl α -L-rhamnopyranoside $>$ methyl β -D-galactopyranoside $>$ methyl α -L-fucopyranoside. The reactivity tendency is similar to that of DODH +hydrogenation of methyl glycosides over $\text{ReO}_x\text{-Pd/CeO}_2$ catalyst in our previous work^[62-64]. The obtained yield of DODH product from methyl α -D-mannopyranoside (90%) was much higher than those in the previous literatures with 5-7 reaction steps (18-75%, Scheme 3.2). As for the reactive substrates, methyl α -D-mannopyranoside, methyl β -L-arabinopyranoside and methyl α -L-rhamnopyranoside (entries 1, 3 and 4), the position of the substituents next to the *cis*-vicinal OH groups is opposite to the *cis*-vicinal OH groups, suggesting that the high reactivity is due to the low steric hindrance around the *cis*-vicinal OH groups, and vice versa.

3.4 Conclusion

$\text{ReO}_x\text{-Au/CeO}_2$ prepared by deposition-precipitation method ($\text{ReO}_x\text{-}^{\text{dp}}\text{Au}^{0.3}/\text{CeO}_2$) was an effective and reusable heterogeneous catalyst for DODH of methyl glycosides without protection of the OH groups even at low H_2 pressure (0.2-1.7 MPa), providing the corresponding unsaturated sugars with the original stereo-structure in high selectivities and yields.

References

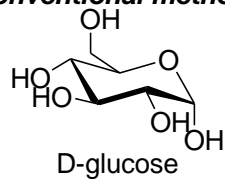
- [1] C. H. Christensen, J. Rass-Hansen, C. C. Marsden, E. Taarning, K. Egeblad, *ChemSusChem* **2008**, *1*, 283-289.
- [2] R. C. Saxena, D. K. Adhikari, H. B. Goyal, *Renew. Sust. Energ. Rev.* **2009**, *13*, 167-178.
- [3] B. Hahn-Hagerdal, M. Galbe, M. F. Gorwa-Grauslund, G. Liden, G. Zacchi, *Trends Biotechnol.* **2006**, *24*, 549-556.
- [4] J.-P. Lange, *Biofuels, Bioprod. Biorefin.* **2007**, *1*, 39-48.
- [5] F. H. Isikgor, C. R. Becer, *Polym. Chem.* **2015**, *6*, 4497-4559.
- [6] T. A. Bender, J. A. Dabrowski, M. R. Gagné, *Nat. Rev. Chem.* **2018**, *2*, 35-46.
- [7] J. B. Binder, R. T. Raines, *Proc. Natl. Acad. Sci. USA* **2010**, *107*, 4516-4521.
- [8] J. v. Haveren, E. L. Scott, J. Sanders, *Biofuels, Bioprod. Biorefin.* **2008**, *2*, 41-57.
- [9] G. Stephanopoulos, *Science* **2007**, *315*, 801-804.
- [10] J. B. Binder, R. T. Raines, *J. Am. Chem. Soc.* **2009**, *131*, 1979-1985.
- [11] G. Yi, S. P. Teong, Y. Zhang, *ChemSusChem* **2015**, *8*, 1151-1155.
- [12] A. Aljarilla, J. C. López, J. Plumet, *Eur. J. Org. Chem.* **2010**, *2010*, 6123-6143.
- [13] T. G. Frihed, M. Bols, C. M. Pedersen, *Chem. Rev.* **2015**, *115*, 3615-3676.
- [14] T. B. Granström, G. Takata, M. Tokuda, K. Izumori, *J. Biosci. Bioeng.* **2004**, *97*, 89-94.
- [15] W. R. Gunther, Y. Wang, Y. Ji, V. K. Michaelis, S. T. Hunt, R. G. Griffin, Y. Roman-Leshkov, *Nat. Commun.* **2012**, *3*, 1109.
- [16] W. Song, S. Wang, W. Tang, *Chem. Asian J.* **2017**, *12*, 1027-1042.
- [17] T. A. Bender, J. A. Dabrowski, M. R. Gagné, *ACS Catal.* **2016**, *6*, 8399-8403.
- [18] L. L. Adduci, T. A. Bender, J. A. Dabrowski, M. R. Gagné, *Nat. Chem.* **2015**, *7*, 576-581.
- [19] T. A. Bender, J. A. Dabrowski, H. Zhong, M. R. Gagné, *Org. Lett.* **2016**, *18*, 4120-4123.
- [20] J. M. Lowe, Y. Seo, M. R. Gagné, *ACS Catal.* **2018**, *8*, 8192-8198.
- [21] F. Cao, T. J. Schwartz, D. J. McClelland, S. H. Krishna, J. A. Dumesic, G. W. Huber, *Energ. Environ. Sci.* **2015**, *8*, 1808-1815.
- [22] P. U. Karanjkar, S. P. Burt, X. L. Chen, K. J. Barnett, M. R. Ball, M. D. Kumbhalkar, X. H. Wang, J. B. Miller, I. Hermans, J. A. Dumesic, G. W. Huber, *Catal. Sci. Technol.* **2016**, *6*, 7841-7851.
- [23] S. H. Krishna, D. J. McClelland, Q. A. Rashke, J. A. Dumesic, G. W. Huber, *Green Chem.* **2017**, *19*, 1278-1285.
- [24] S. J. Danishefsky, M. T. Bilodeau, *Angew. Chem. Int. Ed.* **1996**, *35*, 1380-1419; *Angew. Chem.* **1996**, *108*, 1482-1522.
- [25] J. M. Harris, M. D. Keranen, G. A. O'Doherty, *J. Org. Chem.* **1999**, *64*, 2982-2983.
- [26] A. Guaragna, C. Napolitano, D. D'Alonzo, S. Pedatella, G. Palumbo, *Org. Lett.* **2006**, *8*, 4863-4866.
- [27] J.-P. Joly, F. Roze, S. Banas, F. Quilès, *Tetrahedron Lett.* **2010**, *51*, 3236-3241.
- [28] M. F. Cuccarese, H.-Y. L. Wang, G. A. O'Doherty, *Eur. J. Org. Chem.* **2013**, *2013*, 3067-3075.
- [29] Y. Namito, K. Michigami, T. Nagahashi, R. Matsubara, M. Hayashi, *Org. Lett.* **2016**, *18*, 6058-6061.

- [30] S. J. Danishefsky, D. M. Armistead, F. E. Wincott, H. G. Selnick, R. Hungate, *J. Am. Chem. Soc.* **1989**, *111*, 2967-2980.
- [31] M. Saquib, I. Husain, S. Sharma, G. Yadav, V. K. Singh, S. K. Sharma, P. Shah, M. I. Siddiqi, B. Kumar, J. Lal, G. K. Jain, B. S. Srivastava, R. Srivastava, A. K. Shaw, *Eur. J. Med. Chem.* **2011**, *46*, 2217-2223.
- [32] A. M. Gómez, B. L. de Uralde, S. Valverde, J. Cristóbal López, *Chem. Commun.* **1997**, 1647-1648.
- [33] A. Montero, E. Mann, B. Herradón, *Eur. J. Org. Chem.* **2004**, 3063-3073.
- [34] A. M. Gómez, J. C. López, B. Fraser-Reid, *Synlett* **1993**, *1993*, 557-560.
- [35] A. M. Gómez, F. Lobo, S. Miranda, J. C. Lopez, *Molecules* **2015**, *20*, 8357-8394.
- [36] R. J. Ferrier, W. G. Overend, A. E. Ryan, *J. Chem. Soc.* **1962**, 3667.
- [37] R. J. Ferrier, N. Prasad, *J. Chem. Soc. C* **1969**, 575-580.
- [38] A. M. Gómez, F. Lobo, C. Uriel, J. C. López, *Eur. J. Org. Chem.* **2013**, *2013*, 7221-7262.
- [39] R. J. Ferrier, J. O. Hoberg, *Adv. Carbohydr. Chem. Biochem.* **2003**, *58*, 55-119.
- [40] M. Shan, Y. Xing, G. A. O'Doherty, *J. Org. Chem.* **2009**, *74*, 5961-5966.
- [41] A. Guaragna, D. D'Alonzo, C. Paoletta, C. Napolitano, G. Palumbo, *J. Org. Chem.* **2010**, *75*, 3558-3568.
- [42] D. Thiel, F. Blume, C. Jäger, J. Deska, *Eur. J. Org. Chem.* **2018**, *2018*, 2717-2725.
- [43] A. K. Ghosh, M. Brindisi, *RSC Adv.* **2016**, *6*, 111564-111598.
- [44] C. Bataille, G. Bégin, A. Guillam, L. Lemiègre, C. Lys, J. Maddaluno, L. Toupet, *J. Org. Chem.* **2002**, *67*, 8054-8062.
- [45] D. Lupp, N. J. Christensen, J. R. Dethlefsen, P. Fristrup, *Chem. Eur. J.* **2015**, *21*, 3435-3442.
- [46] J. R. Dethlefsen, D. Lupp, A. Teshome, L. B. Nielsen, P. Fristrup, *ACS Catal.* **2015**, *5*, 3638-3647.
- [47] M. Stalpaert, D. De Vos, *ACS Sustain. Chem. Eng.* **2018**, *6*, 12197-12204.
- [48] G. Chapman, Jr., K. M. Nicholas, *Chem. Commun.* **2013**, *49*, 8199-8201.
- [49] A. R. Petersen, P. Fristrup, *Chem. Eur. J.* **2017**, *23*, 10235-10243.
- [50] J. R. Dethlefsen, P. Fristrup, *ChemSusChem* **2015**, *8*, 767-775.
- [51] L. Sandbrink, E. Klindtworth, H.-U. Islam, A. M. Beale, R. Palkovits, *ACS Catal.* **2015**, *6*, 677-680.
- [52] B. E. Sharkey, A. L. Denning, F. C. Jentoft, R. Gangadhara, T. V. Gopaladasu, K. M. Nicholas, *Catal. Today* **2018**, *310*, 86-93.
- [53] Y. Kon, M. Araque, T. Nakashima, S. Paul, F. Dumeignil, B. Katryniok, *ChemistrySelect* **2017**, *2*, 9864-9868.
- [54] S. Tazawa, N. Ota, M. Tamura, Y. Nakagawa, K. Okumura, K. Tomishige, *ACS Catal.* **2016**, *6*, 6393-6397.
- [55] Y. Nakagawa, S. Tazawa, T. Wang, M. Tamura, N. Hiyoshi, K. Okumura, K. Tomishige, *ACS Catal.* **2017**, *8*, 584-595.
- [56] T. Wang, S. Liu, M. Tamura, Y. Nakagawa, N. Hiyoshi, K. Tomishige, *Green Chem.* **2018**, *20*, 2547-2557.
- [57] N. Ota, M. Tamura, Y. Nakagawa, K. Okumura, K. Tomishige, *Angew. Chem. Int. Ed.* **2015**, *54*, 1897-1900; *Angew. Chem.* **2015**, *127*, 1917-1920.

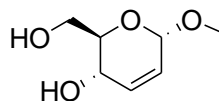
- [58] N. Ota, M. Tamura, Y. Nakagawa, K. Okumura, K. Tomishige, *ACS Catal.* **2016**, *6*, 3213-3226.
- [59] M. Shiramizu, F. D. Toste, *Angew. Chem. Int. Ed.* **2012**, *51*, 8082-8086; *Angew. Chem.* **2012**, *32*, 8206-8210.
- [60] M. Shiramizu, F. D. Toste, *Angew. Chem. Int. Ed.* **2013**, *52*, 12905-12909; *Angew. Chem.* **2013**, *125*, 13143-13147.
- [61] R. T. Larson, A. Samant, J. Chen, W. Lee, M. A. Bohn, D. M. Ohlmann, S. J. Zuend, F. D. Toste, *J. Am. Chem. Soc.* **2017**, *139*, 14001-14004.
- [62] J. Fu, E. S. Vasiliadou, K. A. Goulas, B. Saha, D. G. Vlachos, *Catal. Sci. Technol.* **2017**, *7*, 4944-4954.
- [63] N. Shin, S. Kwon, S. Moon, C. H. Hong, Y. G. Kim, *Tetrahedron* **2017**, *73*, 4758-4765.
- [64] H. Zhang, X. Li, X. Su, E. L. Ang, Y. Zhang, H. Zhao, *ChemCatChem* **2016**, *8*, 1500-1506.
- [65] M. Tamura, N. Yuasa, J. Cao, Y. Nakagawa, K. Tomishige, *Angew. Chem. Int. Ed.* **2018**, *57*, 8058-8062; *Angew. Chem.* **2018**, *130*, 8190-8194.
- [66] J. Feng, J. Jiang, J. Xu, Z. Yang, *RSC Adv.* **2015**, *5*, 38783-38791.
- [67] M. Haruta, *Catal. Today* **1997**, *36*, 153-166.
- [68] M. Haruta, *Angew. Chem. Int. Ed.* **2014**, *53*, 52-56; *Angew. Chem.* **2014**, *126*, 54-58.
- [69] R. Zanella, *J. Catal.* **2004**, *222*, 357-367.
- [70] A. Miyata, A. Mitoglu, P. Plochocka, O. Portugall, J. T.-W. Wang, S. D. Stranks, H. J. Snaith, R. J. Nicholas, *Nature Physics* **2015**, *11*, 582-587.
- [71] S. Tazawa, N. Ota, M. Tamura, Y. Nakagawa, K. Okumura, K. Tomishige, *ACS Catal.* **2016**, *6*, 6393-6397.
- [72] Y. Nakagawa, S. Tazawa, T. Wang, M. Tamura, N. Hiyoshi, K. Okumura, K. Tomishige, *ACS Catal.* **2017**, *8*, 584-595.
- [73] M. Haruta, *Gold Bull.* **2004**, *37*, 27-36.
- [74] J. W. Cook, D. E. Sayers, *J. Appl. Phys.* **1981**, *52*, 5024-5031.
- [75] K. Okumura, J. Amano, N. Yasunobu, M. Niwa, *J. Phys. Chem. B.* **2000**, *104*, 1050-1057.
- [76] K. Okumura, S. Matsumoto, N. Nishiaki, M. Niwa, *Appl. Catal. B.* **2003**, *40*, 151-159.
- [77] K. Tomishige, K. Asakura, Y. Iwasawa, *J. Catal.* **1994**, *149*, 70-80.
- [78] T. Kubota, K. Asakura, N. Ichikuni, Y. Iwasawa, *Chem. Phys. Lett.* **1996**, *256*, 445-448.
- [79] T. Kubota, K. Asakura, Y. Iwasawa, *Catal. Lett.* **1997**, *46*, 141-144.
- [80] A. N. Mansour, J. W. Cook, D. E. Sayers, *J. Phys. Chem.* **1984**, *88*, 2330-2334.
- [81] J. A. Horsley, *J. Chem. Phys.* **1982**, *76*, 1451-1458.
- [82] F. Hilbrig, C. Michel, G. L. Haller, *J. Phys. Chem. C.* **1992**, *96*, 9893-9899.
- [83] S. Koso, H. Watanabe, K. Okumura, Y. Nakagawa, K. Tomishige, *J. Phys. Chem. C.* **2012**, *116*, 3079-3090.
- [84] C. G. Vinson, J. J. Martin, *J. Chem. Eng. Data* **1963**, *8*, 74-75.
- [85] *Organic Syntheses* **1942**, *22*, 1.
- [86] H. Chen, T. Xian, W. Zhang, W. Si, X. Luo, B. Zhang, M. Zhang, Z. Wang, J. Zhang, *Carbohydr. Res.* **2016**, *431*, 42-46.

- [87] B. K. Gorityala, R. Lorpitthaya, Y. Bai, X.-W. Liu, *Tetrahedron* **2009**, *65*, 5844-5848.
- [88] *Organic Syntheses* **1942**, *22*, 1.
- [89] H. Chen, T. Xian, W. Zhang, W. Si, X. Luo, B. Zhang, M. Zhang, Z. Wang, J. Zhang, *Carbohydr. Res.* **2016**, *431*, 42-46.
- [90] S. Chittela, T. R. Reddy, P. Radha Krishna, S. Kashyap, *J. Org. Chem.* **2015**, *80*, 7108-7116.
- [90] A. Guaragna, C. Napolitano, D. D'Alonzo, S. Pedatella, G. Palumbo, *Org. Lett.* **2006**, *8*, 4863-4866.
- [91] A. Guaragna, D. D'Alonzo, C. Paolella, C. Napolitano, G. Palumbo, *J. Org. Chem.* **2010**, *75*, 3558-3568.

Conventional method

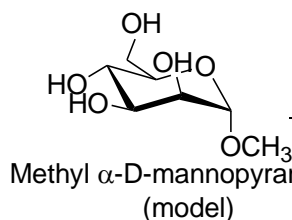


Multiple steps



Problems:
Multiple steps (5-7)
Many reagents
Low total yield

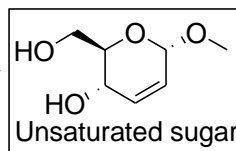
This work



$-2\text{H}_2\text{O}, \text{H}_2$
Deoxydehydration

Retention of original stereo-structure

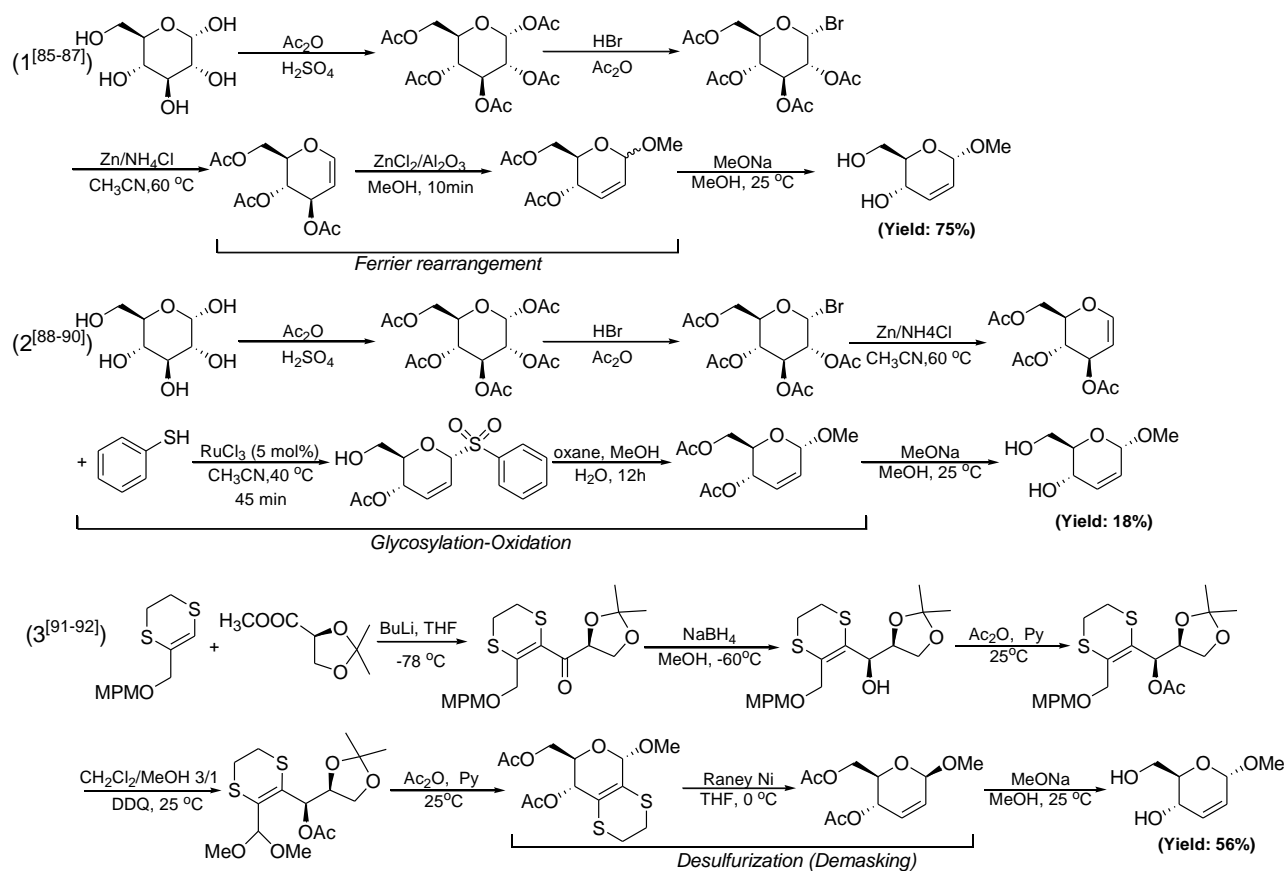
Target product



→ Medicines
→ Agrochemicals
→ Biomaterials
→ Food industries
etc.

Scheme 3.1. Synthesis method of unsaturated sugars from sugar derivatives.

**Synthesis of methyl 2,3-dideoxy- α -D-erythro-hex-2-enopyranoside
(DODH product of methyl α -D-mannopyranoside)**



Scheme 3.2. Conventional methods for the synthesis of unsaturated sugars.

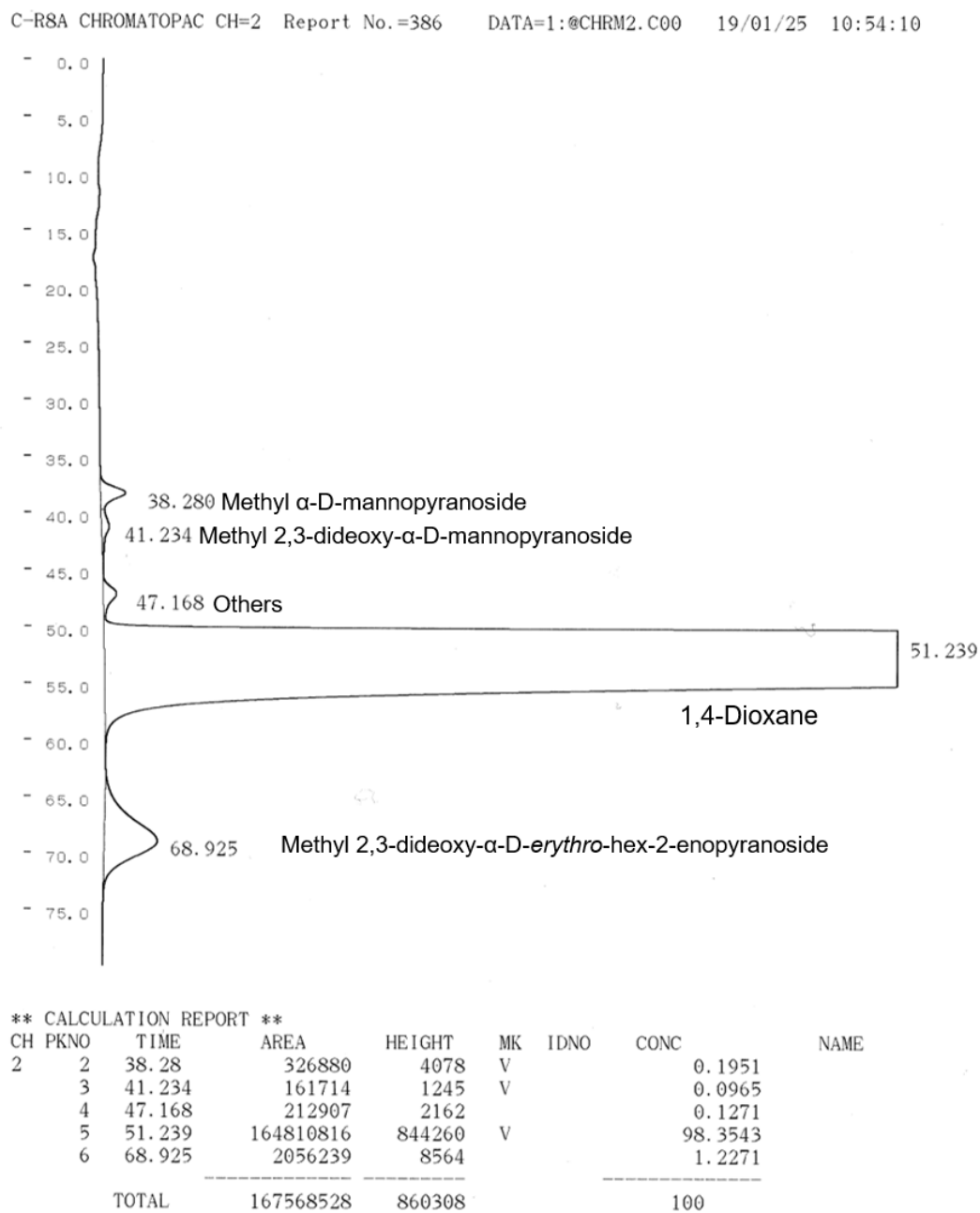
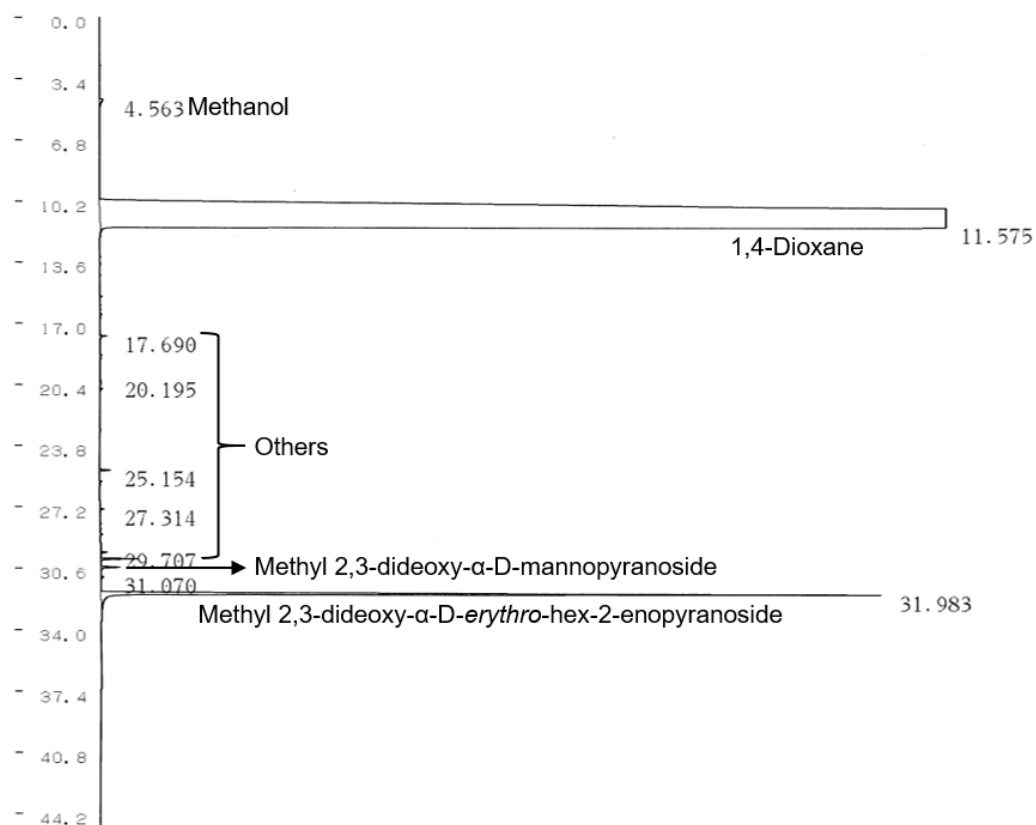


Figure 3.1. HPLC chart of the reaction mixture after reaction (Table 3.2, entry 1)

C-RSA CHROMATOPAC CH=1 Report No.=1128 DATA=1:@CHRM1.C00 19/01/24 10:46:34



** CALCULATION REPORT **

CH	PKNO	TIME	AREA	HEIGHT	MK	IDNO	CONC	NAME
1	5	4.563	3430	278			0.0158	
	6	11.575	21358858	603425			98.57	
	28	17.69	1634	503			0.0075	
	38	20.195	603	95			0.0028	
	41	20.626	745	174			0.0034	
	47	25.154	3048	843			0.0141	
	54	27.314	927	345	V		0.0043	
	68	29.707	1839	532			0.0085	
	69	30.061	8631	2817			0.0398	
	70	30.527	5755	1448			0.0266	
	71	31.07	974	174			0.0045	
	72	31.983	282275	58972			1.3027	
TOTAL			21668708	669607			100	

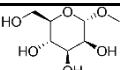
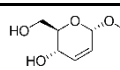
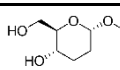
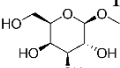
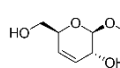
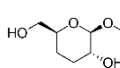
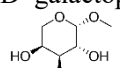
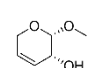
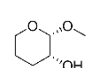
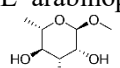
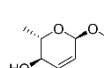
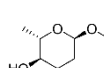
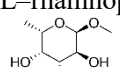
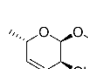
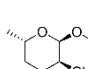
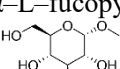
Figure 3.2. GC chart of the reaction mixture after reaction (Table 3.2, entry 1)

Table 3.1. Detail of H₂ pressure in autoclave during reaction

At 293 K			At 413 K			
$P_{\text{Total}}^{[a]}$ (Observed) [MPa]	$P_{1,4\text{-dioxane}}^{[b]}$ (Saturated vapor pressure) [MPa]	$P_{\text{H}_2}^{[c]}$ ($P_{\text{Total}} - P_{1,4\text{-dioxane}}$) [MPa]	$P_{\text{Total}}^{[a]}$ (Observed) [MPa]	$P_{1,4\text{-dioxane}}^{[b]}$ (Saturated vapor pressure) [MPa]	$P_{\text{H}_2}^{[d]}$ (Boyle's law) [MPa]	$P_{\text{H}_2}^{[c]}$ ($P_{\text{Total}} - P_{1,4\text{-dioxane}}$) [MPa]
0.1	0.004	0.1	0.5	0.3	0.1	0.2
0.5	0.004	0.5	1.0	0.3	0.7	0.7
1.2	0.004	1.2	2.0	0.3	1.7	1.7
2.6	0.004	2.6	4.0	0.3	3.6	3.7
4.0	0.004	4.0	6.0	0.3	5.6	5.7
5.4	0.004	5.4	8.0	0.3	7.6	7.7

[a] Observed from pressure gauge; [b] The data are cited from reference^[84]; [c] calculated by the difference pressure between total pressure and saturated vapor pressure of 1,4-dioxane; [d] calculated by Boyle's law.

Table 3.2 Deoxydehydration of various methyl glycosides over $\text{ReO}_x\text{-}^{\text{dp}}\text{Au}^{0.3}/\text{CeO}_2$ catalysts

Entry	Substrate	<i>t</i> (h)	Conv. (%)	Selectivity (%)		DODH product yield ^a (%)
				DODH product	Dideoxy product	
1	 Methyl α-D-mannopyranoside	8	99	 92	 1	90 (81)
2	 Methyl β-D-galactopyranoside	48	>99	 87	 9	87 (86)
3	 Methyl β-L-arabinopyranoside	8	97	 92	 4	90 (88)
4	 Methyl α-L-rhamnopyranoside	16	93	 84	 13	78 (78)
5 ^b	 Methyl α-L-fucopyranoside	24	67	 61	 34	41 (40)
6	 Methyl α-D-glucopyranoside	8	<1	—	—	—

Reaction conditions: $\text{ReO}_x\text{-}^{\text{dp}}\text{Au}^{0.3}/\text{CeO}_2$ (1 wt % Re, Au/Re=0.3) 0.50 g, methyl glycoside 1.29 mmol, 1,4-dioxane 10 g, H_2 pressure 1.7 MPa (at 413 K), 413 K. ^[a]GC yield of DODH product outside the brackets and isolated yields of DODH product inside the brackets. ^[b]Catalyst amount 1.00 g.

Table 3.3. Deoxydehydration of methyl α -D-mannopyranoside over various catalysts

<p> <chem>COC1OC(O)C(O)C(O)C1O</chem> $\xrightarrow[\text{Deoxydehydration}]{\text{H}_2, -2\text{H}_2\text{O}}$ <chem>COC1OC(O)C=CC1O</chem> $\xrightarrow[\text{Hydrogenation}]{\text{H}_2}$ <chem>COC1OC(O)CC(CO)C1O</chem> </p> <p> Methyl α-D-mannopyranoside α-D-erythro-hex-2-enopyranoside Methyl 2,3-dideoxy-α-D-mannopyranoside </p>					
Entry	Catalyst	Conv. [%]	Selectivity [%]		
			1	2	Others ^[a]
1	ReO _x - ^{imp} Au ^{0.3} /CeO ₂	10	>99	<1	<1
2	ReO _x - ^{imp} Ag ^{0.3} /CeO ₂	22	93	4	3
3	ReO _x - ^{imp} Cu ^{0.3} /CeO ₂	18	49	34	17
4	ReO _x - ^{imp} Ir ^{0.3} /CeO ₂	17	7	92	1
5	ReO _x - ^{imp} Pt ^{0.3} /CeO ₂	25	5	93	2
6	ReO _x - ^{imp} Rh ^{0.3} /CeO ₂	27	4	87	9
7	ReO _x - ^{imp} Ru ^{0.3} /CeO ₂	31	2	95	3
8	ReO _x - ^{imp} Pd ^{0.3} /CeO ₂	31	2	96	2
9	ReO _x /CeO ₂	2	90	<1	10
10	CeO ₂	<1	-	-	-
11	^{imp} Au/CeO ₂	<1	-	-	-

Reaction conditions: catalyst 0.15 g (Re=1 wt%, M/Re =0.3 in the case of ReO_x-^{imp}M^{0.3}/CeO₂, Au=0.3 wt% in the case of Au/CeO₂), methyl α -D-mannopyranoside 0.25 g (1.29 mmol), 1,4-dioxane 10 g, 413 K, 4 h, H₂ pressure 7.7 MPa (at 413 K). ^[a]Others contain methanol and degradation products.

Table 3.4. Deoxydehydration of methyl α -D-mannopyranoside over various $\text{ReO}_x\text{-Au/CeO}_2$ catalysts

Entry	Catalyst	P_{H_2} ^[a] [MPa]	Catalyst amount [g]	t [h]	Conv. [%]	Selectivity [%]		
						1	2	Others ^[b]
1	$\text{ReO}_x\text{-impAu}^{0.3}/\text{CeO}_2$	7.7	0.15	4	10	>99	<1	<1
2	$\text{ReO}_x\text{-dpAu}^{0.3}/\text{CeO}_2$	7.7	0.15	4	27	96	3	1
3	$\text{ReO}_x\text{-dpAu}^{0.3}/\text{CeO}_2$	5.7	0.15	4	24	99	1	<1
4	$\text{ReO}_x\text{-dpAu}^{0.3}/\text{CeO}_2$	3.7	0.15	4	22	99	1	<1
5	$\text{ReO}_x\text{-dpAu}^{0.3}/\text{CeO}_2$	1.7	0.15	4	20	>99	<1	<1
6	$\text{ReO}_x\text{-dpAu}^{0.3}/\text{CeO}_2$	0.7	0.15	4	16	>99	<1	<1
7	$\text{ReO}_x\text{-dpAu}^{0.3}/\text{CeO}_2$	0.2	0.15	4	14	>99	<1	<1
8	$\text{ReO}_x\text{-dpAu}^{0.3}/\text{CeO}_2$	1.7	0.5	8	99	92	1	7
9	$\text{ReO}_x\text{-impAu}^{0.3}/\text{CeO}_2$	7.7	0.5	29	98	85	8	7

Reaction conditions: $\text{ReO}_x\text{-Au/CeO}_2$ (Re=1 wt%, Au/Re =0.3) 0.15 g, methyl α -D-mannopyranoside 0.25 g (1.29 mmol), 1,4-dioxane 10 g, 413 K, 4 h. ^[a] H_2 pressure at 413 K.

^[b]Others contain methanol and degradation products.

Table 3.5. Effect of H₂ pressure on DODH of methyl α -D-mannopyranoside over ReO_x-impAu^{0.3}/CeO₂ catalysts

Entry	Catalyst	H ₂ pressure (413 K) /MPa	Conv. /%	Selectivity /%		
				1	2	Others ^[a]
1	ReO _x -impAu ^{0.3} /CeO ₂	7.7	10	>99	<1	<1
2	ReO _x -impAu ^{0.3} /CeO ₂	5.7	7	>99	<1	<1
3	ReO _x -impAu ^{0.3} /CeO ₂	3.7	5	>99	<1	<1
4	ReO _x -impAu ^{0.3} /CeO ₂	1.7	4	>99	<1	<1
5	ReO _x -impAu ^{0.3} /CeO ₂	0.7	2	>99	<1	<1
6	ReO _x -impAu ^{0.3} /CeO ₂	0.2	<1	>99	<1	<1

Reaction conditions: ReO_x-impAu^{0.3}/CeO₂ (Re=1 wt%, Au/Re =0.3) 0.150 g, methyl α -D-mannopyranoside 0.250 g (1.29 mmol), 1,4-dioxane 10 g, 413 K.

[a] Others contain methanol and degradation products.c

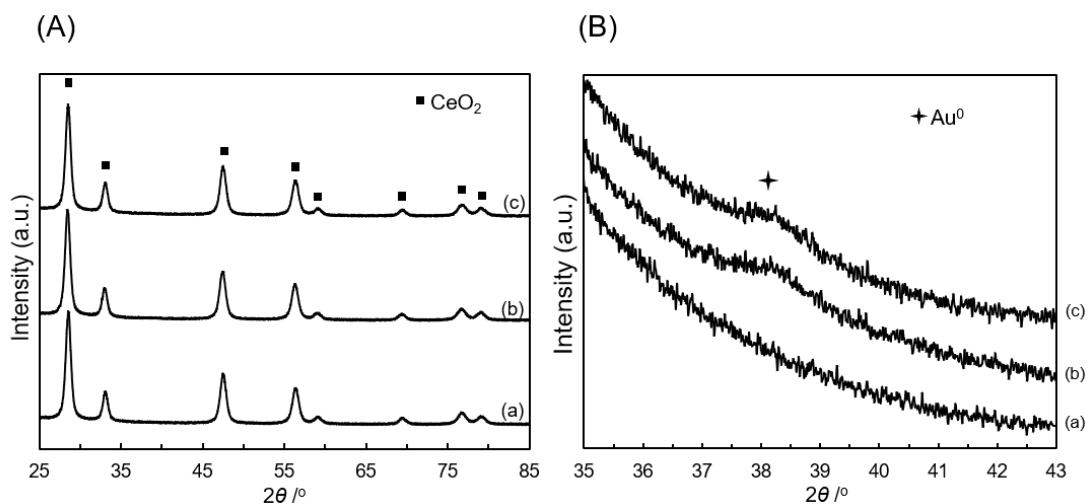


Figure 3.3. XRD patterns of $\text{ReO}_x/\text{CeO}_2$ (1 wt% Re) and $\text{ReO}_x\text{-Au}/\text{CeO}_2$ (Re=1 wt%, Au/Re=0.3) catalyst. (A) The full profiles of XRD patterns, (B) the enlarged profiles of (A). (a) $\text{ReO}_x/\text{CeO}_2$, (b) $\text{ReO}_x\text{-dpAu}^{0.3}/\text{CeO}_2$ catalyst before reaction (calcined at 673 K), (c) $\text{ReO}_x\text{-dpAu}^{0.3}/\text{CeO}_2$ after reaction.

Reaction conditions: methyl α -D-mannopyranoside 0.25 g, $\text{ReO}_x\text{-dpAu}^{0.3}/\text{CeO}_2$ 0.50 g, 1,4-dioxane 10 g, H_2 pressure 1.7 MPa, 1 h, 413 K.

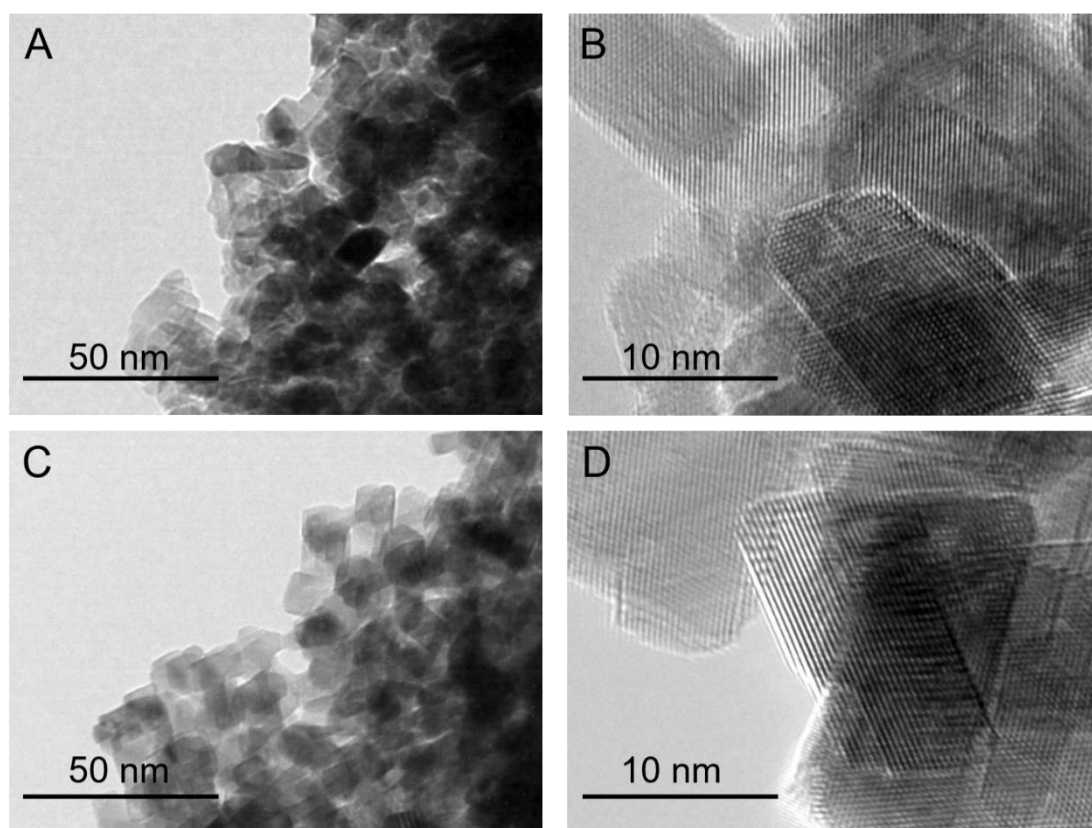


Figure 3.4. TEM images of $\text{ReO}_x\text{-dpAu}^{0.3}/\text{CeO}_2$ (1 wt% Re, $\text{Au/Re} = 0.3$) catalyst. (A) (B) $\text{ReO}_x\text{-dpAu}^{0.3}/\text{CeO}_2$ before reaction (calcined at 673 K), (C) (D) $\text{ReO}_x\text{-dpAu}^{0.3}/\text{CeO}_2$ after reaction.

Reaction conditions: methyl α -D-mannopyranoside 0.25 g, $\text{ReO}_x\text{-dpAu}^{0.3}/\text{CeO}_2$ 0.50 g, 1,4-dioxane 10 g, H_2 pressure 1.7 MPa, 1 h, 413 K.

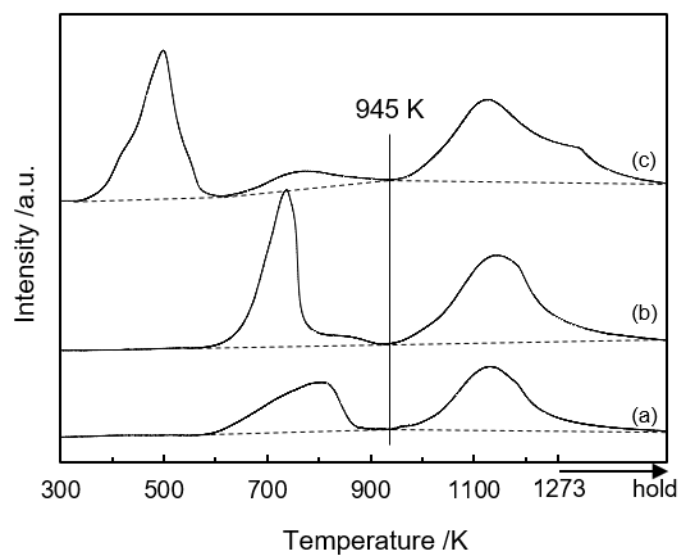


Figure 3.5. H₂-TPR profiles of catalysts. Dashed lines represent the baselines for integration.

(a) CeO₂, (b) ReO_x/CeO₂ (1 wt% Re), (c) ReO_x-^{dp}Au^{0.3}/CeO₂ (1 wt% Re, Au/Re = 0.3).

TPR conditions: catalyst (50 mg) and H₂/Ar (5% v/v, 30 mL min⁻¹) at heating rate of 10 K min⁻¹.

The calculated H₂ consumption is listed in Table 3.6.

Table 3.6. Re reduction degree from TPR profiles

Entry	Catalyst	Re amount [mmol]	H ₂ consumption [mmol]	
			298-945 K	298-1273 K
1	CeO ₂	-	0.014	0.038
2	ReO _x /CeO ₂	0.003	0.022	0.056
3	ReO _x - ^{dp} Au ^{0.3} /CeO ₂	0.003	0.031	0.072

TPR conditions: 50 mg catalyst and H₂/Ar (5% v/v, 30 mL min⁻¹) at heating rate of 10 K min⁻¹.

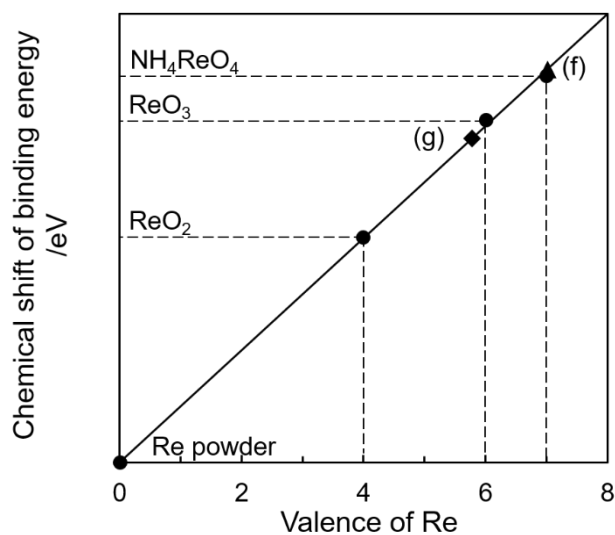


Figure 3.6. Linear relationship of chemical shift of binding energy with Re oxidation state from the Re L_3 -edge XANES spectra. (●: reference samples, ▲(f): $\text{ReO}_x\text{-dpAu}^{0.3}/\text{CeO}_2$ (Re=1 wt%, Au/Re=0.3) before reaction (calcined at 673 K), ◆(g): $\text{ReO}_x\text{-dpAu}^{0.3}/\text{CeO}_2$ (1 wt % Re, Au/Re=0.3) after reaction.

Reaction conditions: methyl α -D-mannopyranoside 0.25 g, $\text{ReO}_x\text{-dpAu}^{0.3}/\text{CeO}_2$ 0.50 g, 1,4-dioxane 10 g, H_2 pressure 1.7 MPa, 1 h, 413 K.

The calculated average valence of Re in $\text{ReO}_x\text{-dpAu}^{0.3}/\text{CeO}_2$ are shown in Table 3.7.

Table 3.7 The average valence of Re in $\text{ReO}_x\text{-dpAu}^{0.3}/\text{CeO}_2$ catalyst

Sample	Condition	Re average valance
(f) $\text{ReO}_x\text{-dpAu}^{0.3}/\text{CeO}_2$	Before reaction (calcined at 673 K)	7.0
(g) $\text{ReO}_x\text{-dpAu}^{0.3}/\text{CeO}_2$	After reaction	5.8

The observed linear correlation between the chemical shift binding energy of Re compounds relative to metallic Re powder and the Re oxidation state of Re reference samples is show in Figure 3.7.

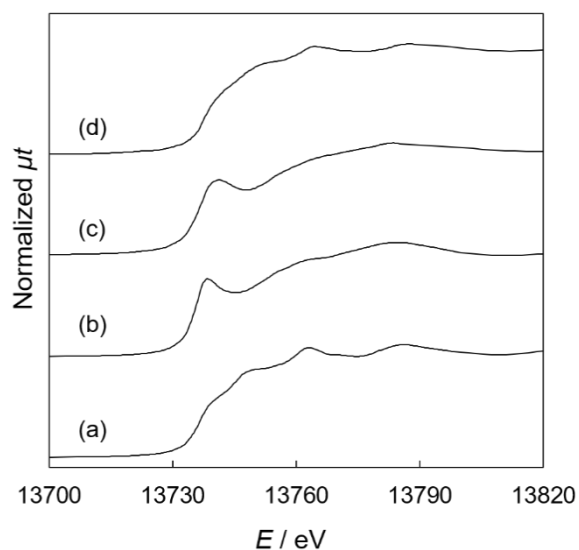


Figure 3.7. Au L_2 -edge XANES spectra.

(a) Au foil, (b) Au_2O_3 , (c) $\text{ReO}_x\text{-dpAu}^{0.3}/\text{CeO}_2$ (Re=1 wt%, Au/Re=0.3) before reaction (calcined at 673 K), (d) $\text{ReO}_x\text{-dpAu}^{0.3}/\text{CeO}_2$ (Re=1 wt%, Au/Re=0.3) after reaction.

Reaction conditions: methyl α -D-mannopyranoside 0.25 g, $\text{ReO}_x\text{-dpAu}^{0.3}/\text{CeO}_2$ 0.50 g, 1,4-dioxane 10 g, H_2 pressure 1.7 MPa, 1 h, 413 K.

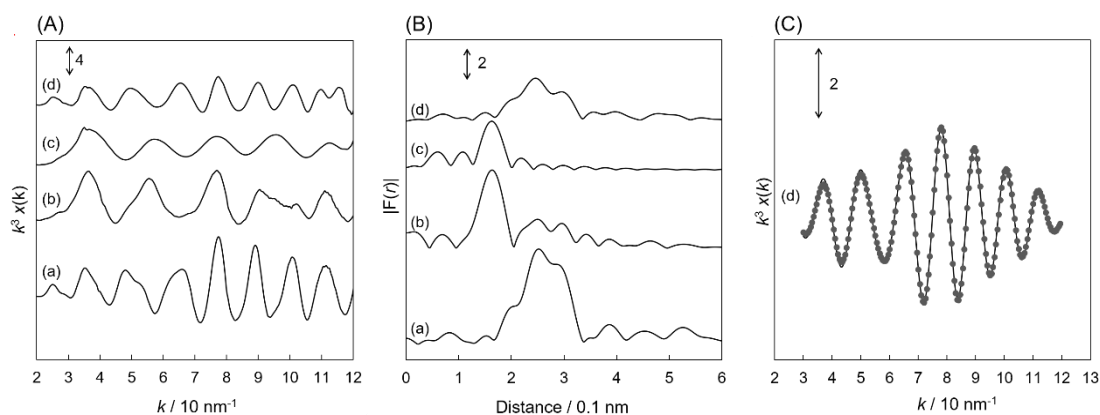


Figure 3.8. Au L_2 -edge EXAFS spectra. (A) k^3 -Weighted EXAFS oscillations, (B) Fourier transform of k^3 -weighted Au L_2 -edge EXAFS, FT range: 30-120 nm^{-1} , (C) Fourier filtered EXAFS data (solid line) and calculated data (dotted line) of $\text{ReO}_x\text{-dpAu}^{0.3}/\text{CeO}_2$ after reaction.

(a) Au foil, (b) Au_2O_3 , (c) $\text{ReO}_x\text{-dpAu}^{0.3}/\text{CeO}_2$ (Re=1 wt%, Au/Re=0.3) before reaction (calcined at 673 K), (d) $\text{ReO}_x\text{-dpAu}^{0.3}/\text{CeO}_2$ (Re=1 wt%, Au/Re=0.3) after reaction.

Reaction conditions: methyl α -D-mannopyranoside 0.25 g, $\text{ReO}_x\text{-dpAu}^{0.3}/\text{CeO}_2$ 0.50 g, 1,4-dioxane 10 g, H_2 pressure 1.7 MPa, 1 h, 413 K.

The details of Au L_2 -edge EXAFS curve fitting result are listed in Table 3.3.

Table 3.8. Curve fitting results of Au L_2 -edge EXAFS of $\text{ReO}_x\text{-}^{\text{dp}}\text{Au}^{0.3}/\text{CeO}_2$ catalyst

Sample	Shell	CN ^[a]	R ^[b] [10 ⁻¹ nm]	σ ^[c] [10 ⁻¹ nm]	ΔE ^[d] [eV]	R_f ^[e] [%]	FF range ^[f] [nm-nm]
$\text{ReO}_x\text{-}^{\text{dp}}\text{Au}^{0.3}/\text{CeO}_2$ after reaction	Au-Au	8.8±0.5	2.88±0.004	0.087±0.002	2.51±0.6	0.33	0.172-0.331
Au foil	Au-Au	12.0	2.88	0.060	0	-	-
$\text{ReO}_x\text{-}^{\text{dp}}\text{Au}^{0.3}/\text{CeO}_2$ after reaction ^[g]	Au-Au	8.9±1.5	2.83±0.02	0.064±0.001	-3.3±2.1	3.5	0.173-0.322

[a] CN = Coordination number; [b] R = Bond distance; [c] σ = Debye-Waller factor; [d] ΔE_0 = Difference in origin of photoelectron energy between the reference and the sample; [e] R_f = Residual factor; [f] FF range = Fourier filtering range; [g] The data are cited from refence [1a].

Reaction conditions: methyl α -D-mannopyranoside 0.25 g, $\text{ReO}_x\text{-}^{\text{dp}}\text{Au}^{0.3}/\text{CeO}_2$ (1 wt % Re, Au/Re=0.3) 0.50 g, 1,4-dioxane 10 g, H_2 pressure 1.7 MPa, 1 h, 413 K.

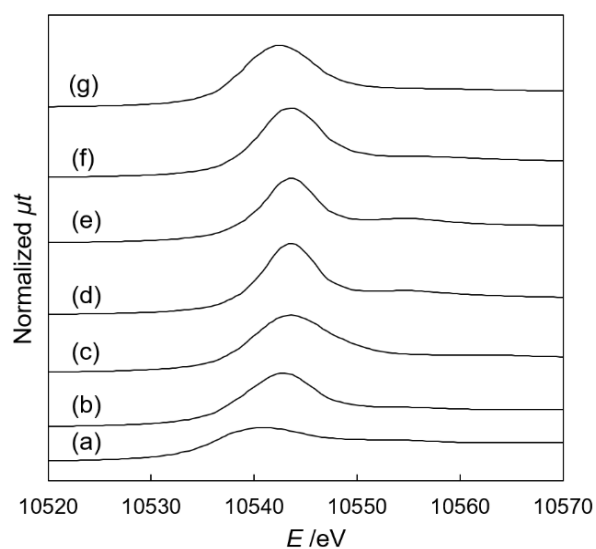


Figure 3.8. Re L_3 -edge XANES spectra.

(a) Re powder, (b) ReO_2 , (c) ReO_3 , (d) Re_2O_7 , (e) NH_4ReO_4 , (f) $\text{ReO}_x\text{-dpAu}^{0.3}/\text{CeO}_2$ (Re=1 wt%, Au/Re=0.3) before reaction (calcined at 673 K), (g) $\text{ReO}_x\text{-dpAu}^{0.3}/\text{CeO}_2$ (Re=1 wt%, Au/Re=0.3) after reaction.

Reaction conditions: methyl α -D-mannopyranoside 0.25 g, $\text{ReO}_x\text{-dpAu}^{0.3}/\text{CeO}_2$ 0.50 g, 1,4-dioxane 10 g, H_2 pressure 1.7 MPa, 1 h, 413 K.

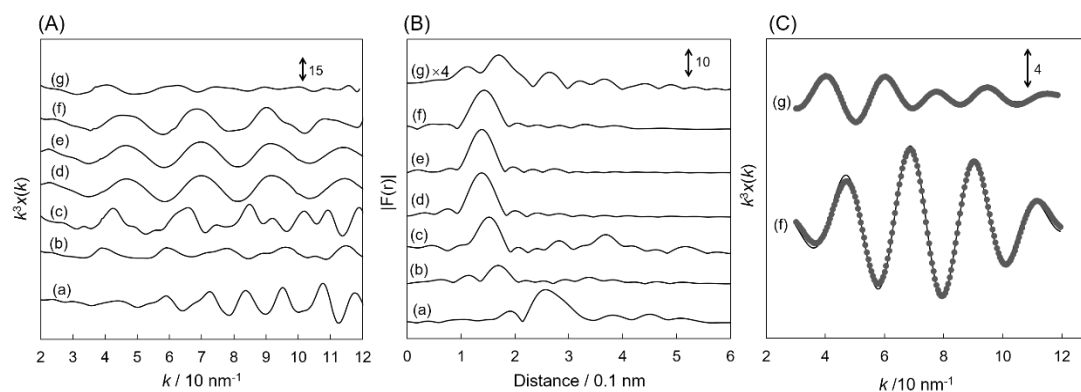


Figure 3.10. Re L_3 -edge EXAFS spectra. (A) k^3 -Weighted EXAFS oscillations, (B) Fourier transform of k^3 -weighted Au L_2 -edge EXAFS, FT range: 30-120 nm^{-1} , (C) Fourier filtered EXAFS data (solid line) and calculated data (dotted line) of $\text{ReO}_x\text{-dpAu}^{0.3}/\text{CeO}_2$ after reaction.

(a) Re powder, (b) ReO_2 , (c) ReO_3 , (d) Re_2O_7 , (e) NH_4ReO_4 , (f) $\text{ReO}_x\text{-dpAu}^{0.3}/\text{CeO}_2$ (Re=1 wt%, Au/Re=0.3) before reaction (calcined at 673 K), (g) $\text{ReO}_x\text{-dpAu}^{0.3}/\text{CeO}_2$ (Re=1 wt%, Au/Re=0.3) after reaction.

Reaction conditions: methyl α -D-mannopyranoside 0.25 g, $\text{ReO}_x\text{-dpAu}^{0.3}/\text{CeO}_2$ 0.50 g, 1,4-dioxane 10 g, H_2 pressure 1.7 MPa, 1 h, 413 K.

The details of Re L_3 -edge EXAFS curve fitting result are listed in Table 3.5.

Table 3.9. Curve fitting results of Re L_3 -edge EXAFS of $\text{ReO}_x\text{-dpAu}^{0.3}/\text{CeO}_2$ catalyst

Sample	Shell	CN ^[a]	$R^{[b]}$ [10 ⁻¹ nm]	$\sigma^{[c]}$ [10 ⁻¹ nm]	$\Delta E^{[d]}$ [eV]	$R_f^{[e]}$ [%]	FF range ^[f] [nm-nm]
$\text{ReO}_x\text{-dpAu}^{0.3}/\text{CeO}_2$	Re=O	1.7±0.2	1.75±0.01	0.092±0.007	-7.7±2.3	2.2	0.089-0.218
after reaction	Re-O	3.9±0.3	1.97±0.01	0.098±0.003	-4.4±1.7		
$\text{ReO}_x\text{-dpAu}^{0.3}/\text{CeO}_2$	Re=O	4.0±0.4	1.76±0.01	0.063±0.007	2.26±1.9	1.2	0.089-0.190
before reaction							
NH_4ReO_4	Re=O	4.0	1.73	0.060	0	-	-
$\text{ReO}_x\text{-dpAu}^{0.3}/\text{CeO}_2$	Re=O	1.7±0.2	1.74±0.01	0.060±0.007	-9.9±2.4	1.6	0.089-0.218
after reaction ^[g]	Re-O	4.0±0.4	1.96±0.01	0.064±0.006	-9.9±1.3		
$\text{ReO}_x\text{-dpAu}^{0.3}/\text{CeO}_2$	Re=O	4.0±0.4	1.74±0.01	0.064±0.007	-0.7±1.7	0.9	0.089-0.190
before reaction ^[g]							

[a] CN = Coordination number; [b] R = Bond distance; [c] σ = Debye-Waller factor; [d] ΔE_0 = Difference in origin of photoelectron energy between the reference and the sample; [e] R_f = Residual factor; [f] FF range = Fourier filtering range; [g] The data are cited from reference [1b].

Reaction conditions: methyl α -D-mannopyranoside 0.25 g, $\text{ReO}_x\text{-dpAu}^{0.3}/\text{CeO}_2$ (1 wt % Re, Au/Re=0.3) 0.50 g, 1,4-dioxane 10 g, H_2 pressure 1.7 MPa, 1 h, 413 K.

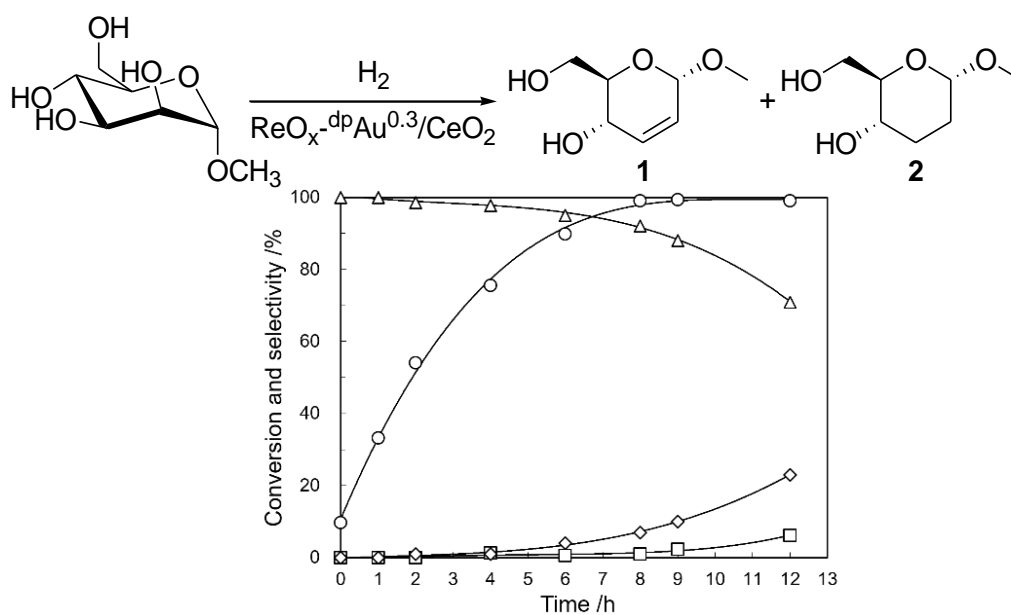


Figure 3.11 Time course of deoxydehydration of methyl α -D-mannopyranoside over $\text{ReO}_x\text{-dpAu}^{0.3}/\text{CeO}_2$ catalyst (\circ : conversion, \triangle : selectivity to 1, \square : selectivity to 2, \diamond : selectivity to others).

Reaction conditions: $\text{ReO}_x\text{-dpAu}^{0.3}/\text{CeO}_2$ (Re=1 wt%, Au/Re =0.3) 0.50 g; methyl α -D-mannopyranoside 0.25 g (1.29 mmol), 1,4-dioxane 10 g, 413 K, H_2 pressure 1.7 MPa (at 413 K).

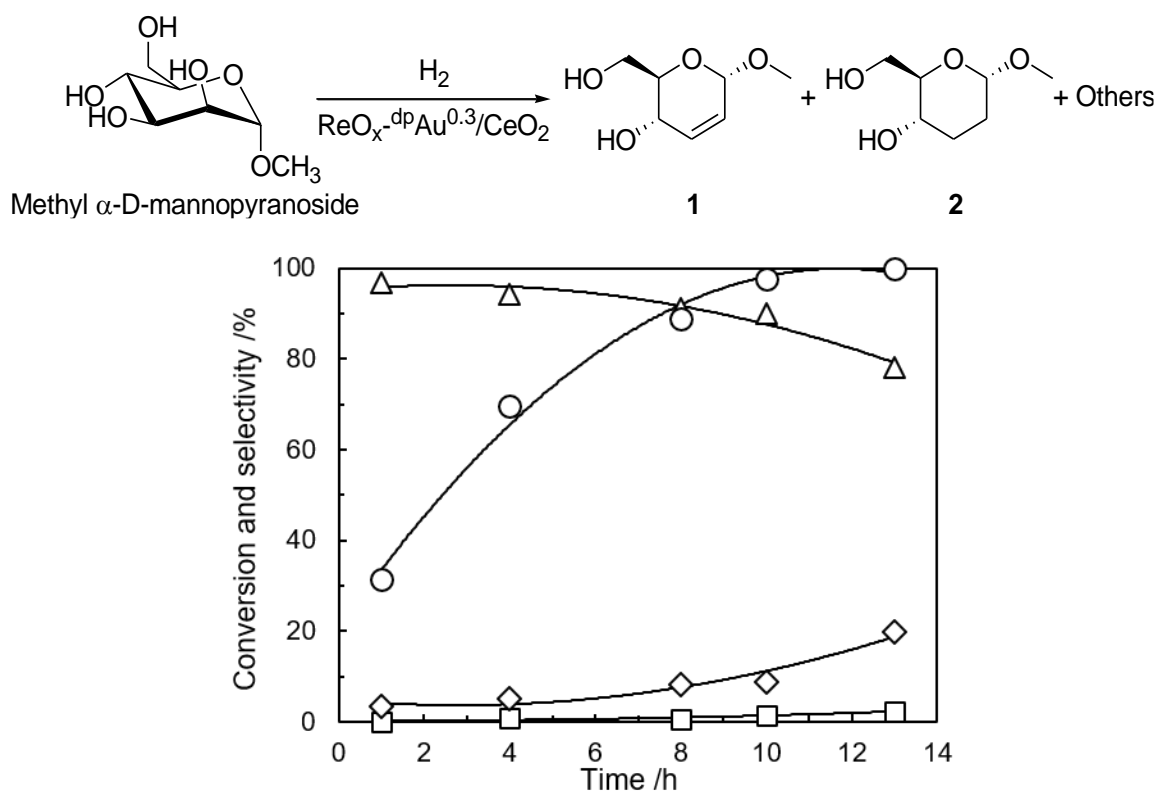
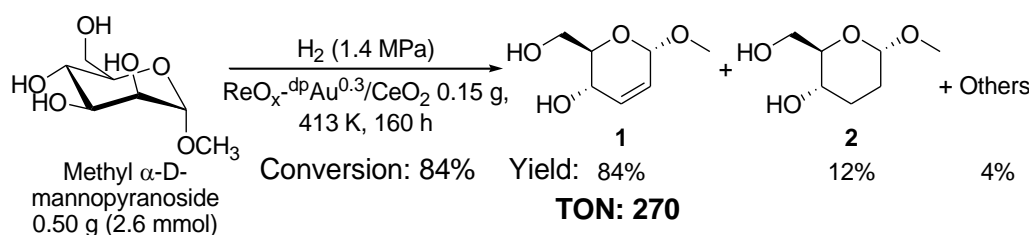


Figure 3.12. Time course of methyl α -D-mannopyranoside DODH over $\text{ReO}_x^{\text{dp}}\text{Au}^{0.3}/\text{CeO}_2$ (Re=1 wt%, Au/Re =0.3) catalyst (○: conversion, △: selectivity to 1, □: selectivity to 2, ◇: selectivity to other products).

Reaction conditions: $\text{ReO}_x^{\text{dp}}\text{Au}^{0.3}/\text{CeO}_2$ 0.50 g; methyl α -D-mannopyranoside 0.25 g (1.29 mmol), 1,4-dioxane 10 g, H_2 pressure 0.7 MPa, 413 K.



Scheme 3.3. Deoxydehydration of methyl α -D-mannopyranoside over $\text{ReO}_x\text{-}^{\text{dp}}\text{Au}^{0.3}/\text{CeO}_2$ catalyst with larger substrate/catalyst ratio.

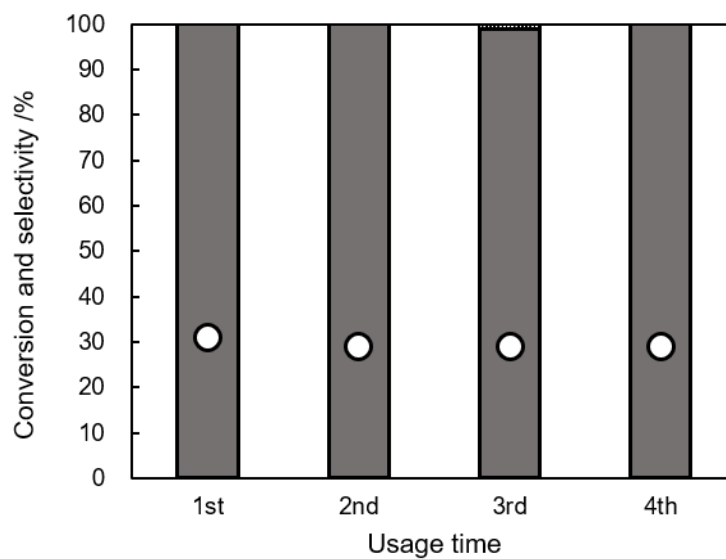


Figure 3.13. Reusability test of $\text{ReO}_x\text{-dpAu}^{0.3}/\text{CeO}_2$ catalyst in deoxydehydration of methyl α -D-mannopyranoside.

Reaction conditions: methyl α -D-mannopyranoside 0.20-0.25 g, $\text{ReO}_x\text{-dpAu}^{0.3}/\text{CeO}_2$ (1 wt % Re, Au/Re=0.3) 0.50-0.40 g, 1,4-dioxane 10-8 g, H_2 pressure 1.7 MPa, 1 h, 413 K.

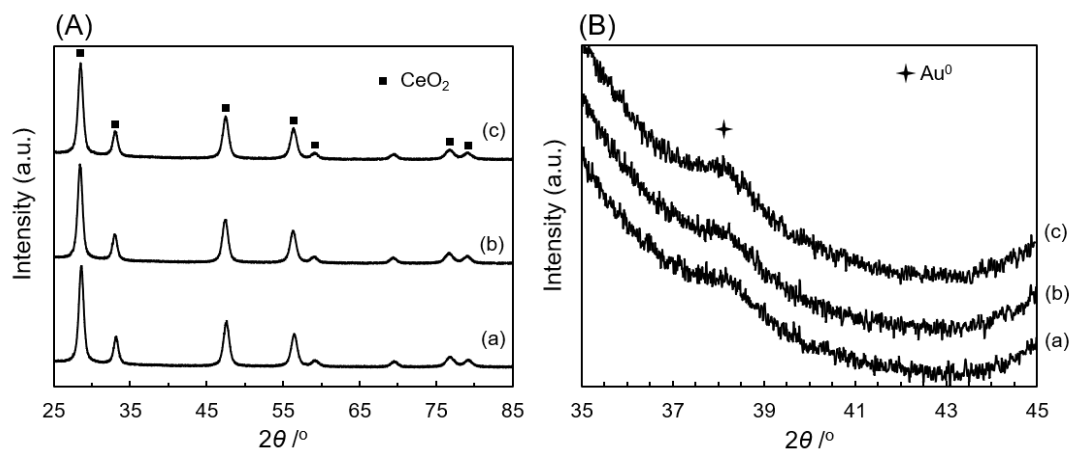


Figure 3.14. XRD patterns of $\text{ReO}_x\text{-dpAu}^{0.3}/\text{CeO}_2$ catalyst, (A) the full profiles of XRD patterns, (B) the enlarged profiles of (A).

(a) $\text{ReO}_x\text{-dpAu}^{0.3}/\text{CeO}_2$ (Re=1 wt%, Au/Re=0.3) before reaction (calcined at 673 K), (b) $\text{ReO}_x\text{-dpAu}^{0.3}/\text{CeO}_2$ (1 wt% Re, Au/Re = 0.3) after first use, (c) $\text{ReO}_x\text{-dpAu}^{0.3}/\text{CeO}_2$ (1 wt% Re, Au/Re = 0.3) after fourth use.

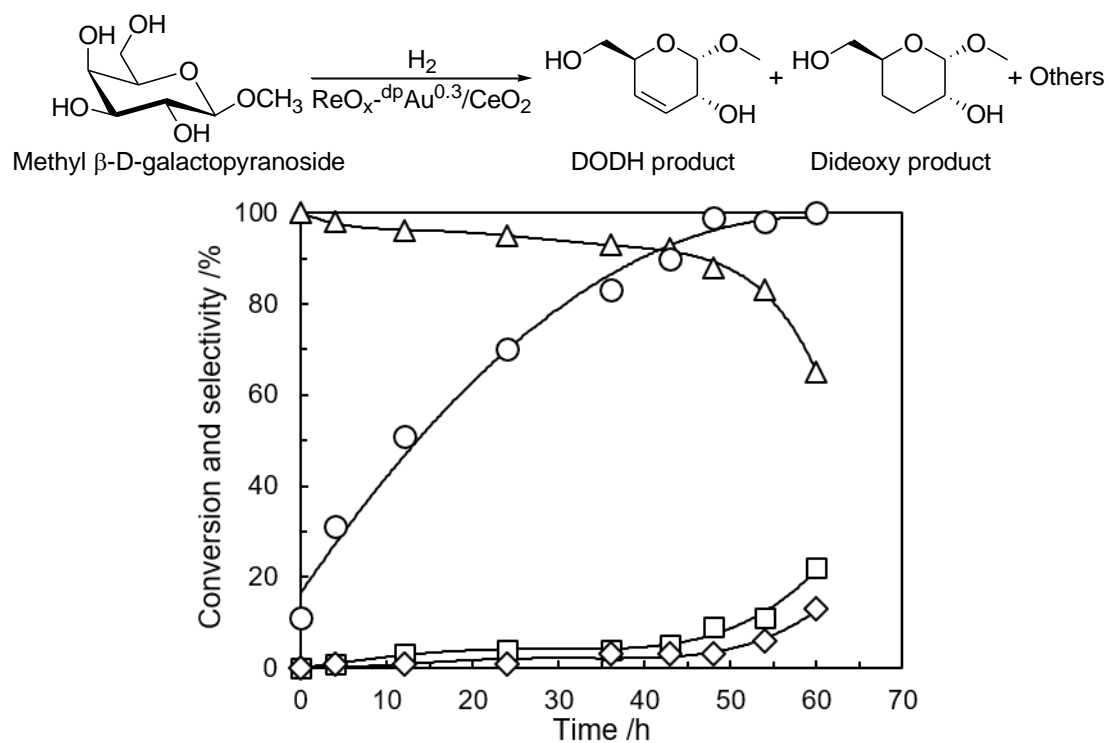


Figure 3.15. Time course of deoxydehydration of methyl β -D-galactopyranoside over $\text{ReO}_x\text{-dpAu}^{0.3}/\text{CeO}_2$ (1 wt% Re, Au/Re = 0.3) catalyst (○: conversion, △: selectivity to 1, □: selectivity to 2, ◇: selectivity to others).

Reaction conditions: $\text{ReO}_x\text{-dpAu}^{0.3}/\text{CeO}_2$ 0.50 g; methyl β -D-galactopyranoside 0.25 g (1.29 mmol), 1,4-dioxane 10 g, H_2 pressure 1.7 MPa, 413 K.

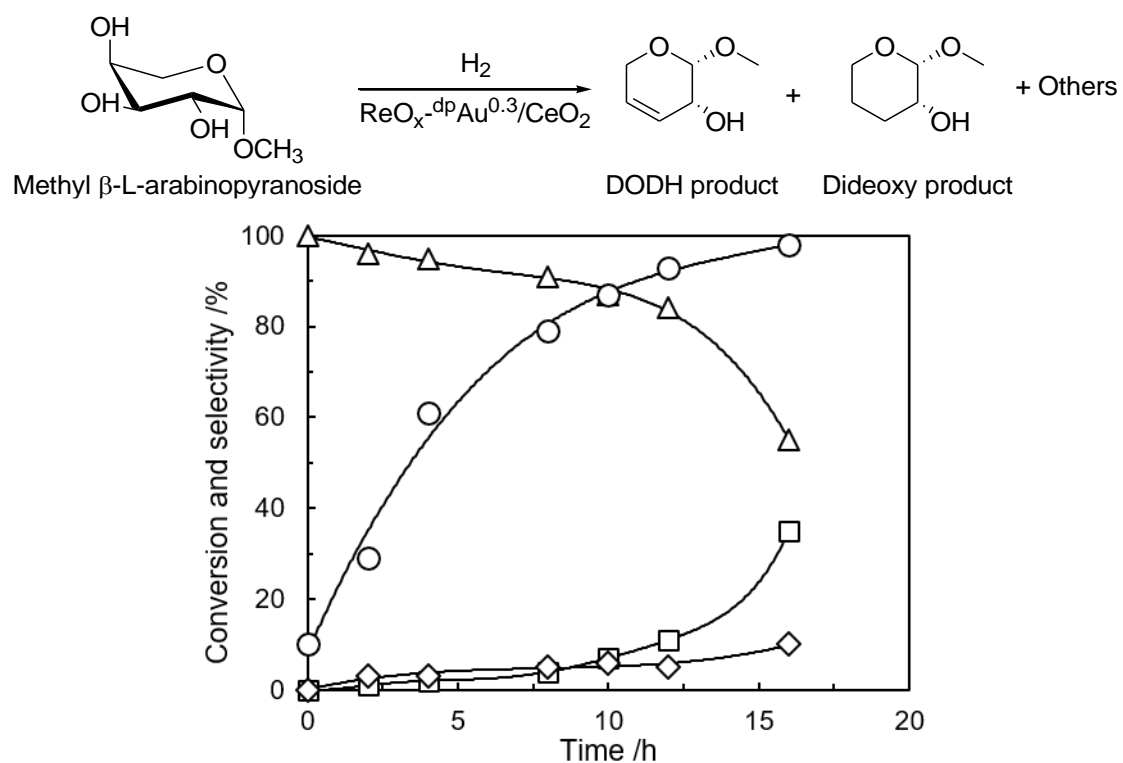


Figure 3.16. Time course of deoxydehydration of methyl β-L-arabinopyranoside over $\text{ReO}_x\text{-dpAu}^{0.3}/\text{CeO}_2$ (1 wt% Re, Au/Re=0.3) catalyst (○: conversion, △: selectivity to 1, □: selectivity to 2, ◇: selectivity to others).

Reaction conditions: $\text{ReO}_x\text{-dpAu}^{0.3}/\text{CeO}_2$ 0.50 g; β-L-arabinopyranoside 0.21 g (1.29 mmol), 1,4-dioxane 10 g, H_2 pressure 1.7 MPa, 413 K.

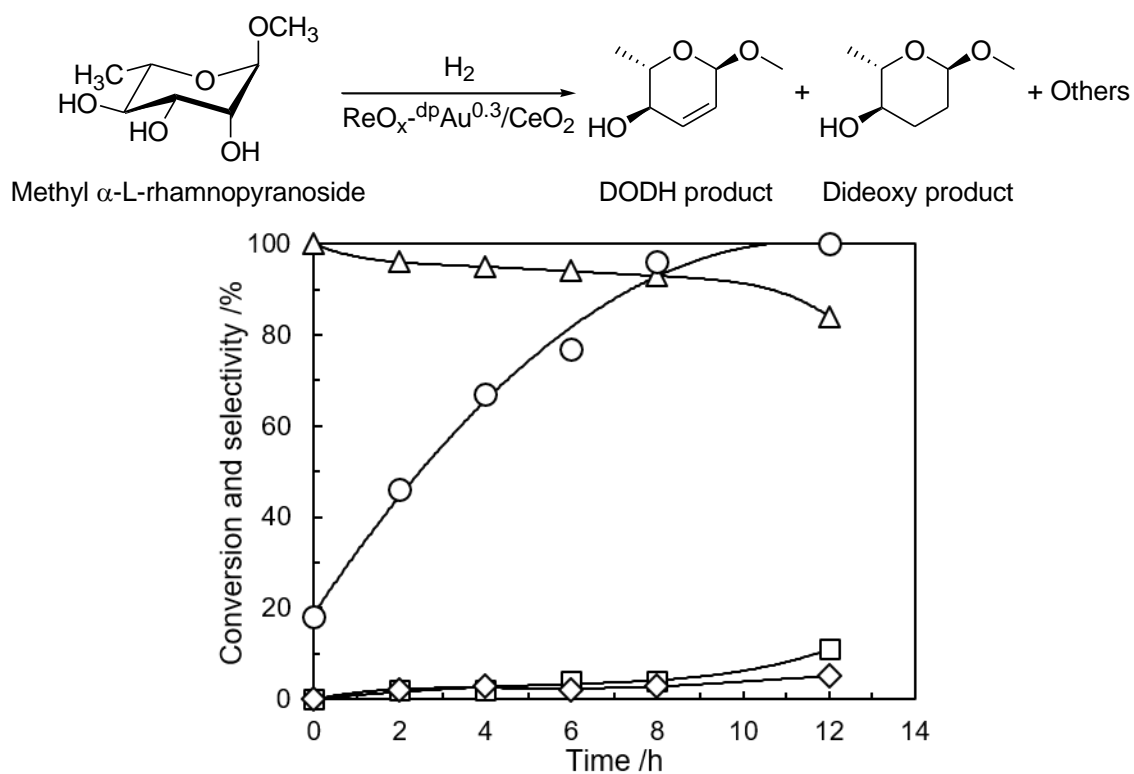


Figure 3.7 Time course of deoxydehydration of methyl α -L-rhamnopyranoside over $\text{ReO}_x\text{-dpAu}^{0.3}/\text{CeO}_2$ (1 wt% Re, Au/Re=0.3) catalyst (○: conversion, △: selectivity to 1, □: selectivity to 2, ◇: selectivity to others).

Reaction conditions: $\text{ReO}_x\text{-dpAu}^{0.3}/\text{CeO}_2$ 0.50 g; methyl α -L-rhamnopyranoside 0.23 g (1.29 mmol), 1,4-dioxane 10 g, H_2 pressure 1.7 MPa, 413 K.

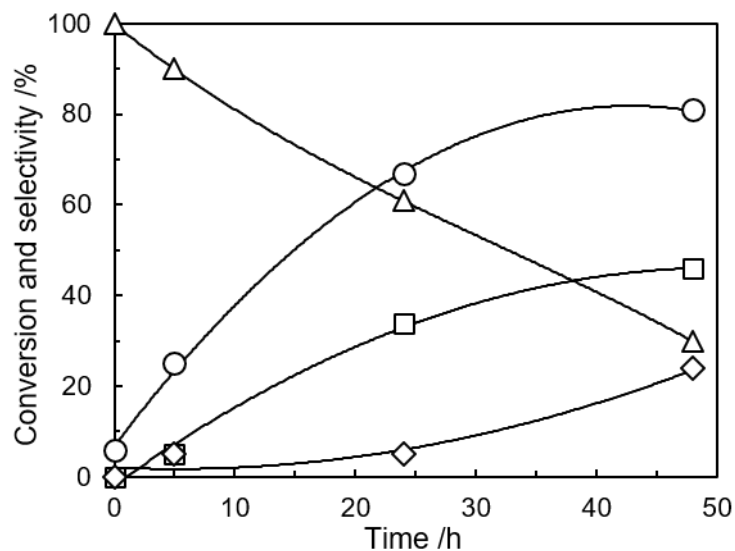
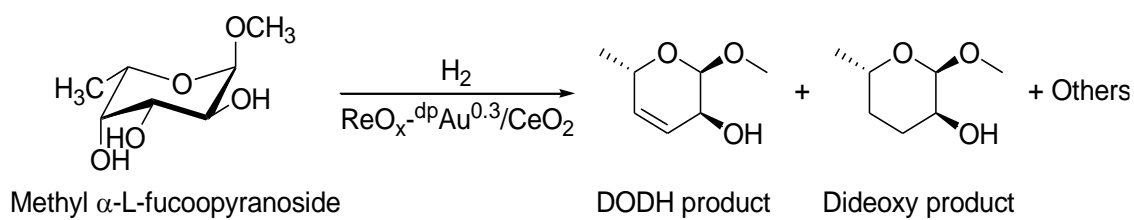
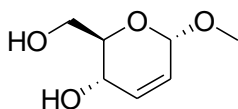


Figure 3.18. Time course of deoxydehydration of methyl α -L-fucoopyranoside over $\text{ReO}_x\text{-dpAu}^{0.3}/\text{CeO}_2$ (1 wt% Re, Au/Re=0.3) catalyst (○: conversion, △: selectivity to 1, □: selectivity to 2, ◇: selectivity to others).

Reaction conditions: $\text{ReO}_x\text{-dpAu}^{0.3}/\text{CeO}_2$ 1.00 g; methyl β -D-fucoopyranoside 0.23 g (1.29 mmol), 1,4-dioxane 10 g, H_2 pressure 1.7 MPa, 413 K.

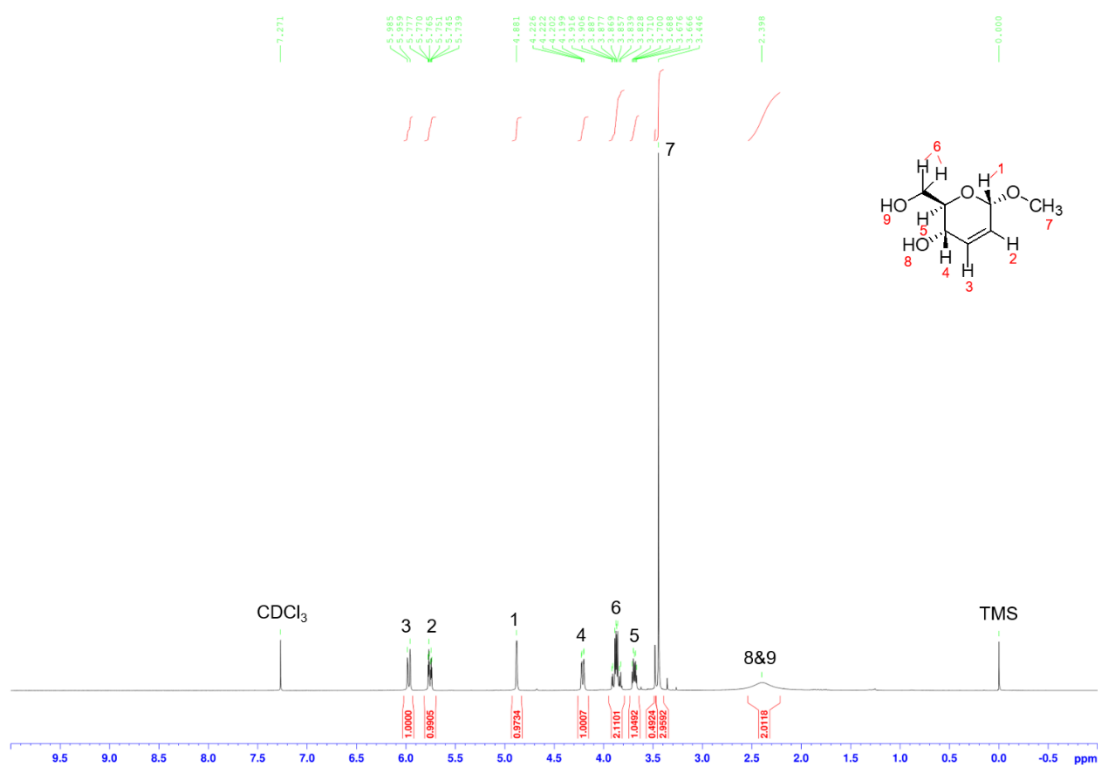
NMR spectra of isolated DODH product from methyl glycosides



Methyl 2,3-dideoxy- α -D-erythro-hex-2-enopyranoside

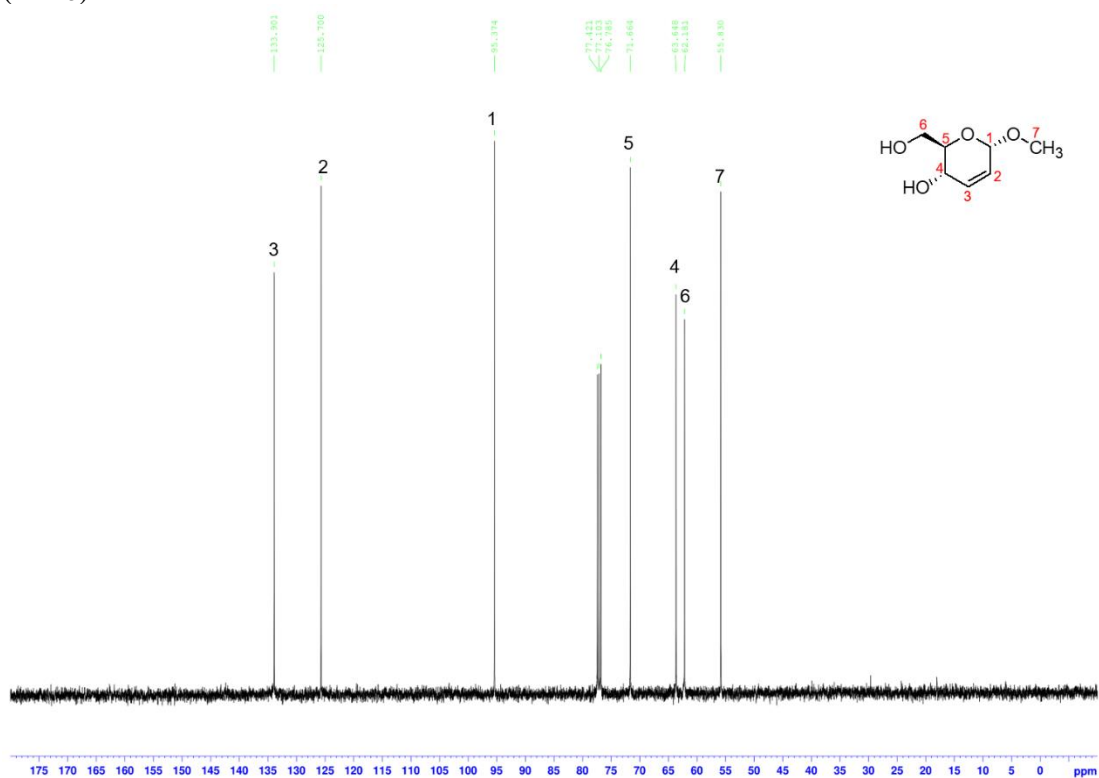
^1H NMR (400 MHz, CDCl_3 , r.t.):

δ 5.97 (d, $J=10.2$ Hz, 1H, H^3), δ 5.76 (dt, $J=10.2, 2.4$ Hz, 1H, H^2), δ 4.88 (s, 1H, H^1), δ 4.21 (dd, $J=7.6, 1.4$ Hz, 1H, H^4), δ 3.92-3.83 (m, 2H, H^6), δ 3.69 (dt, $J=9.1, 4.0$ Hz, 1H, H^5), δ 3.45 (s, 3H, H^7), δ 2.40 (bs, 2H, H^8 & H^9).

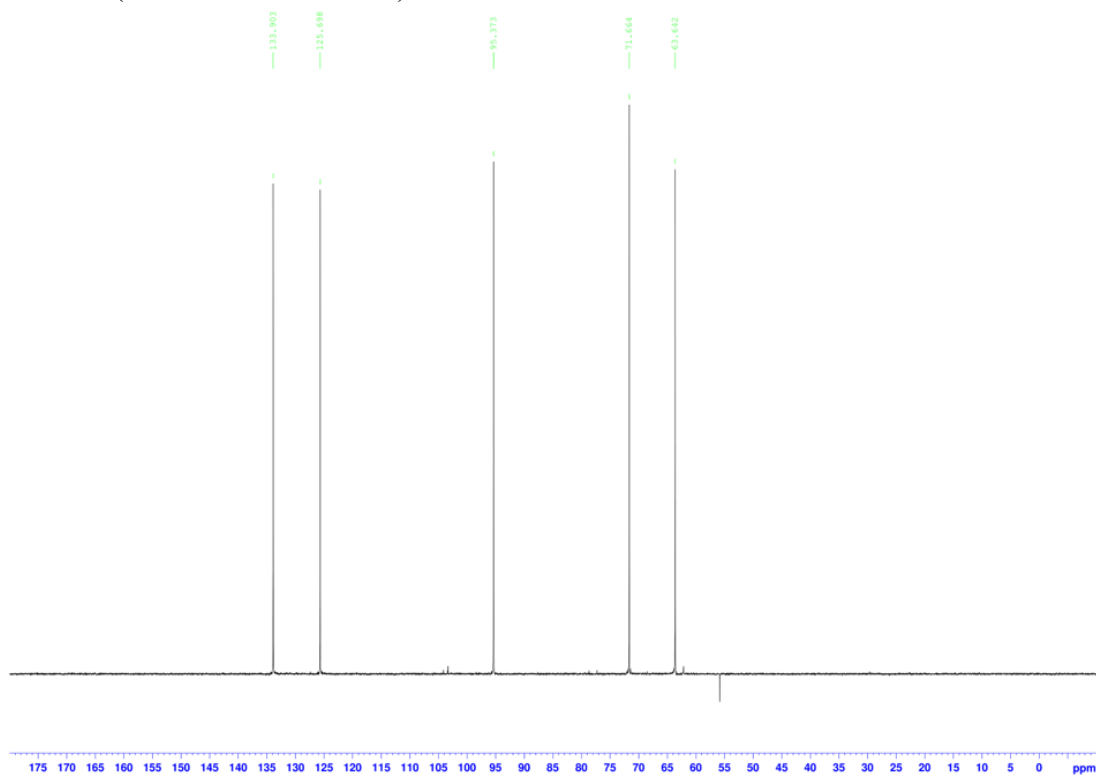


^{13}C NMR (400 MHz, CDCl_3 , r.t.):

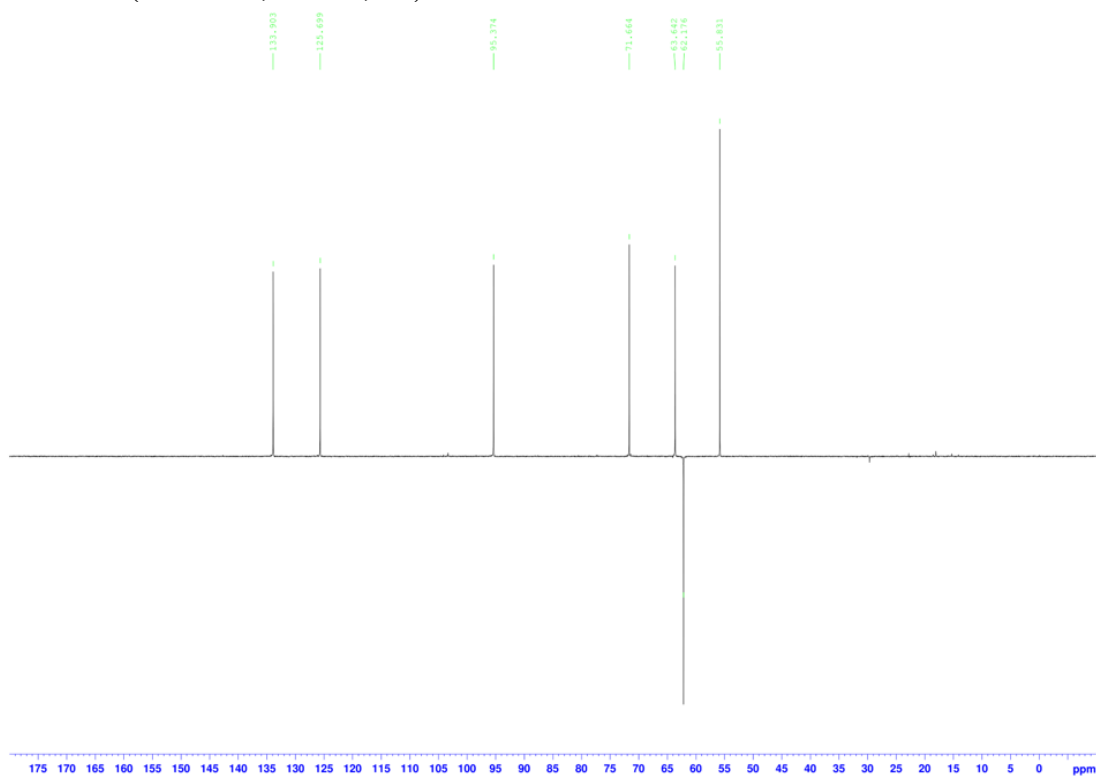
δ 133.90 (C^3H), δ 125.70 (C^2H), δ 95.37 (C^1H), δ 71.66 (C^5H), δ 63.65 (C^4H), δ 62.18 (C^6H_2), δ 55.83 (C^7H_3).

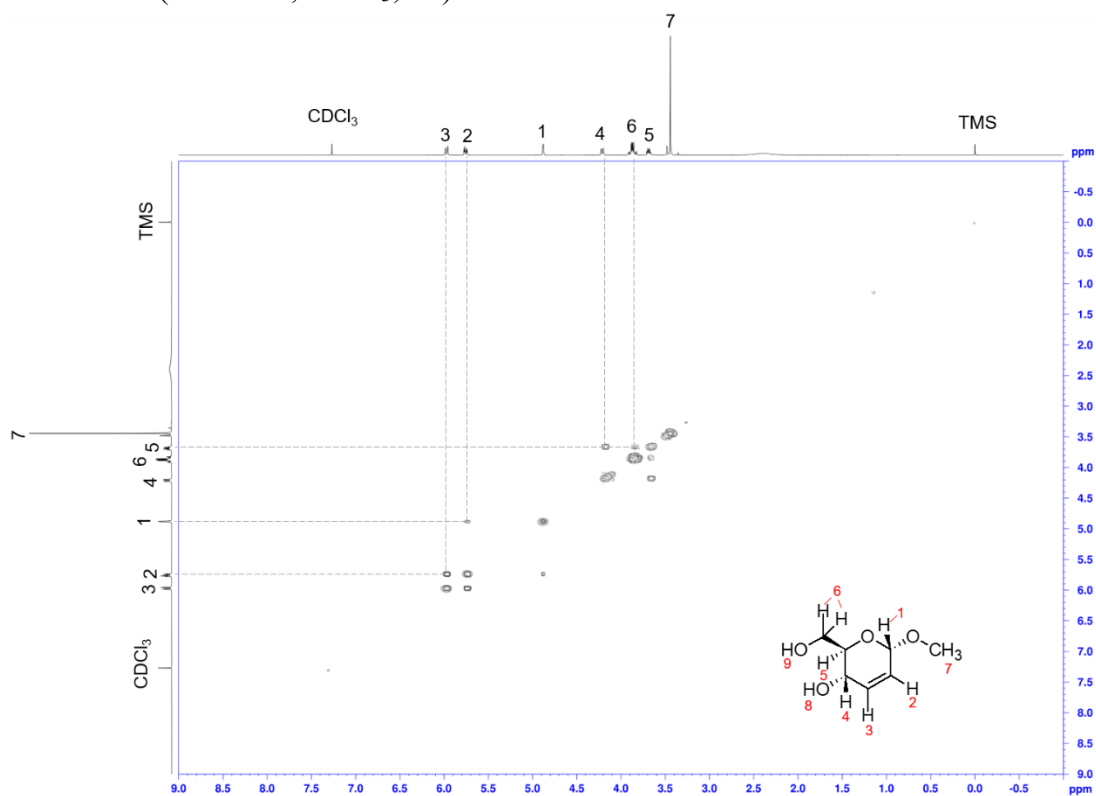
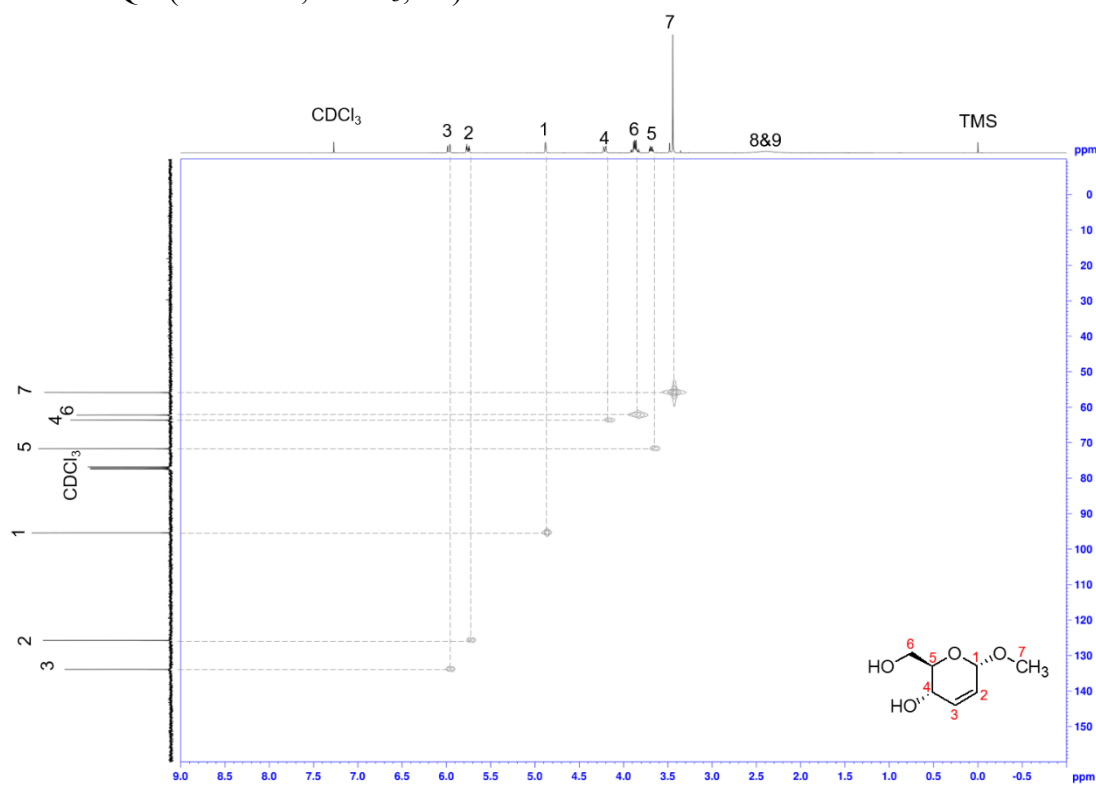


DEPT90(400 MHz, CDCl₃, r.t.):

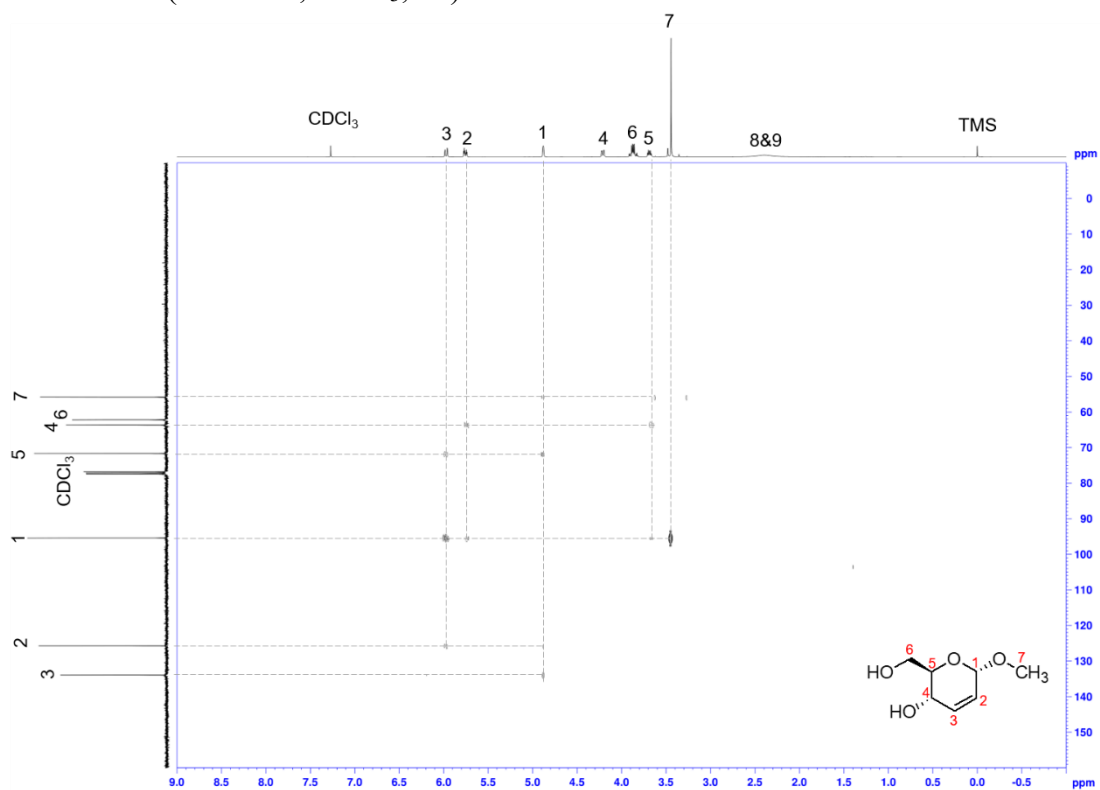


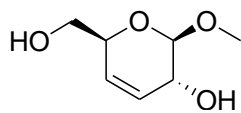
DEPT135(400 MHz, CDCl₃, r.t.):



H-H COSY (400 MHz, CDCl₃, r.t.):H-C HMQC (400 MHz, CDCl₃, r.t.):

H-C HMBC (400 MHz, CDCl₃, r.t.):

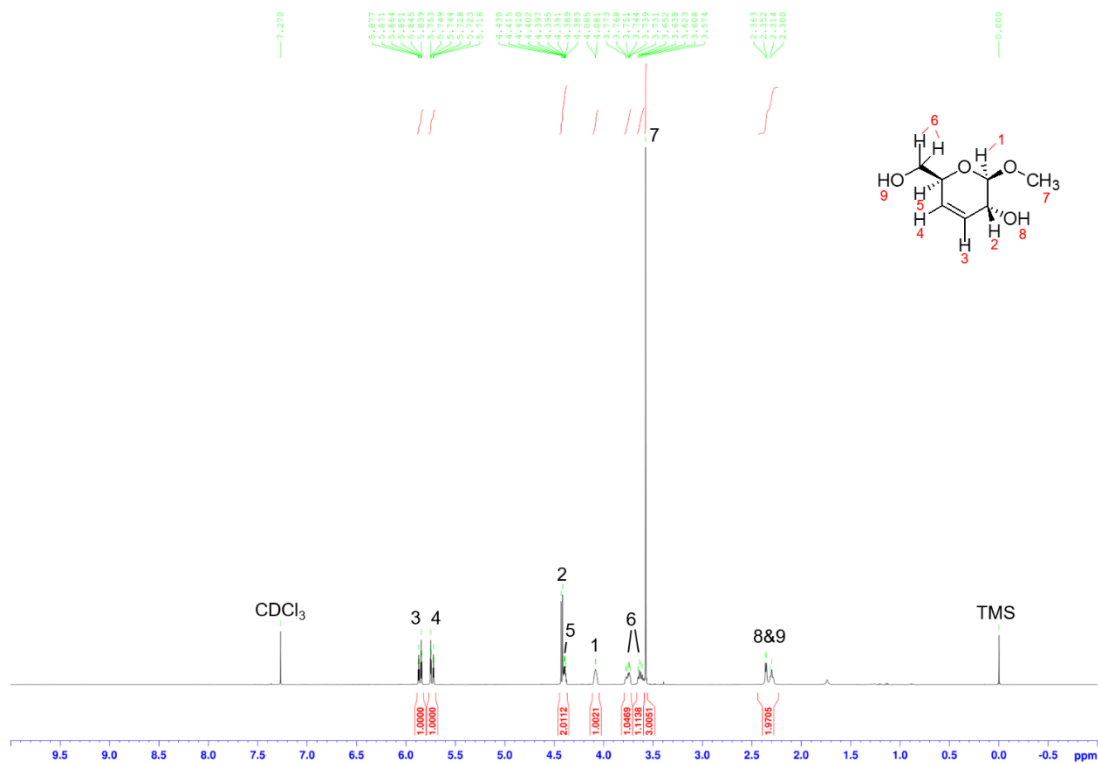




Methyl 3,4-dideoxy- α -D-erythro-hex-3-enopyranoside

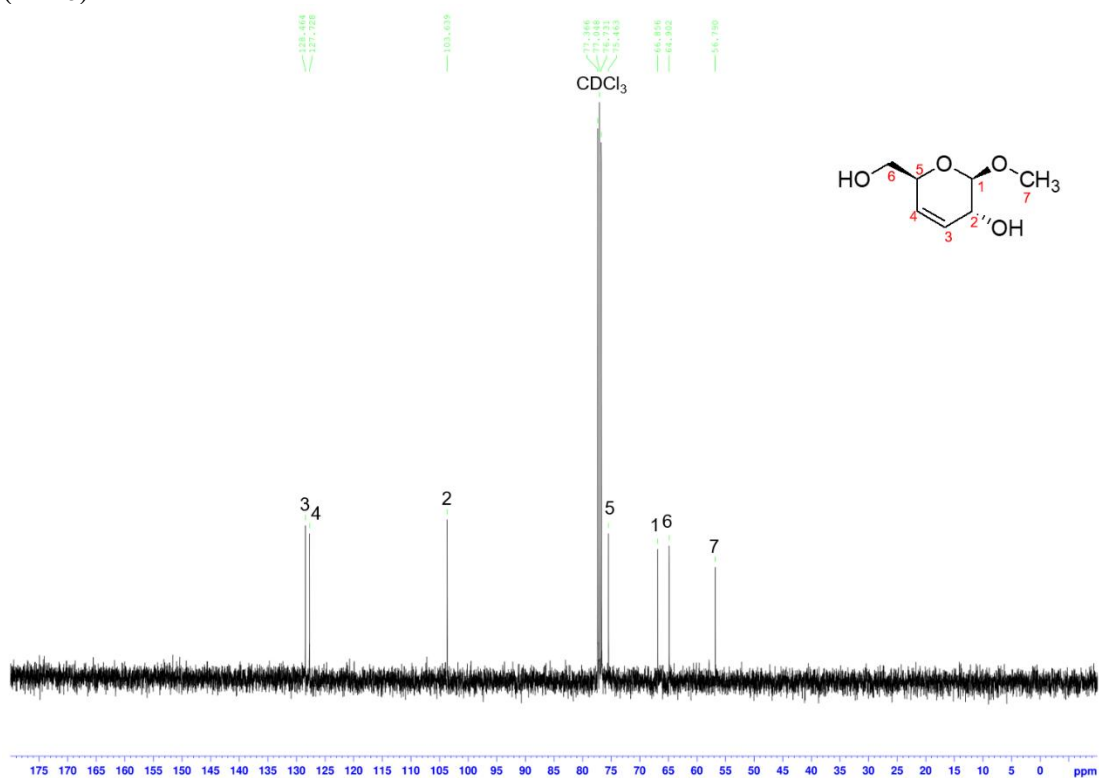
^1H NMR (400 MHz, CDCl_3 , r.t.):

δ 5.86 (dt, $J=10.2$ Hz, 1H, H^3), δ 5.74 (dt, $J=10.2$, 2.4 Hz, 1H, H^4), δ 4.43-4.38 (m, 2H, H^4 & H^5), δ 4.08 (s, 1H, H^1), δ 3.77-3.60 (m, 2H, H^6), δ 3.58 (s, 3H, H^7), δ 2.24 (bs, 2H, H^8 & H^9).

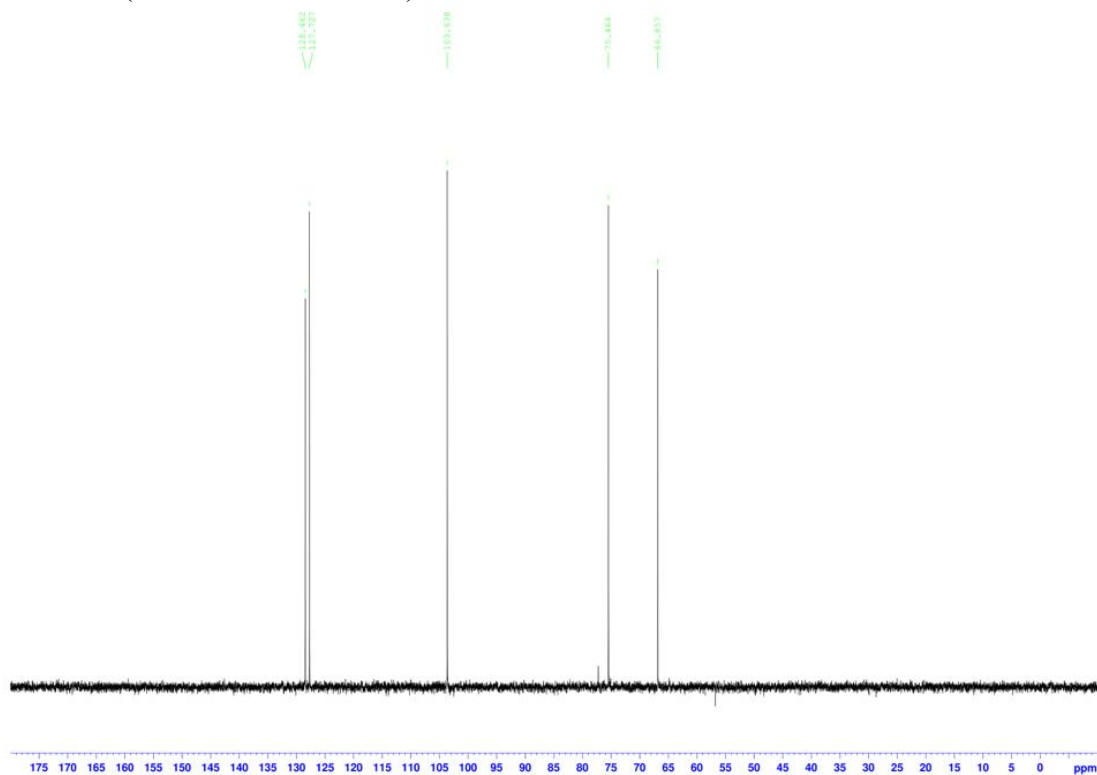


^{13}C NMR (400 MHz, CDCl_3 , r.t.):

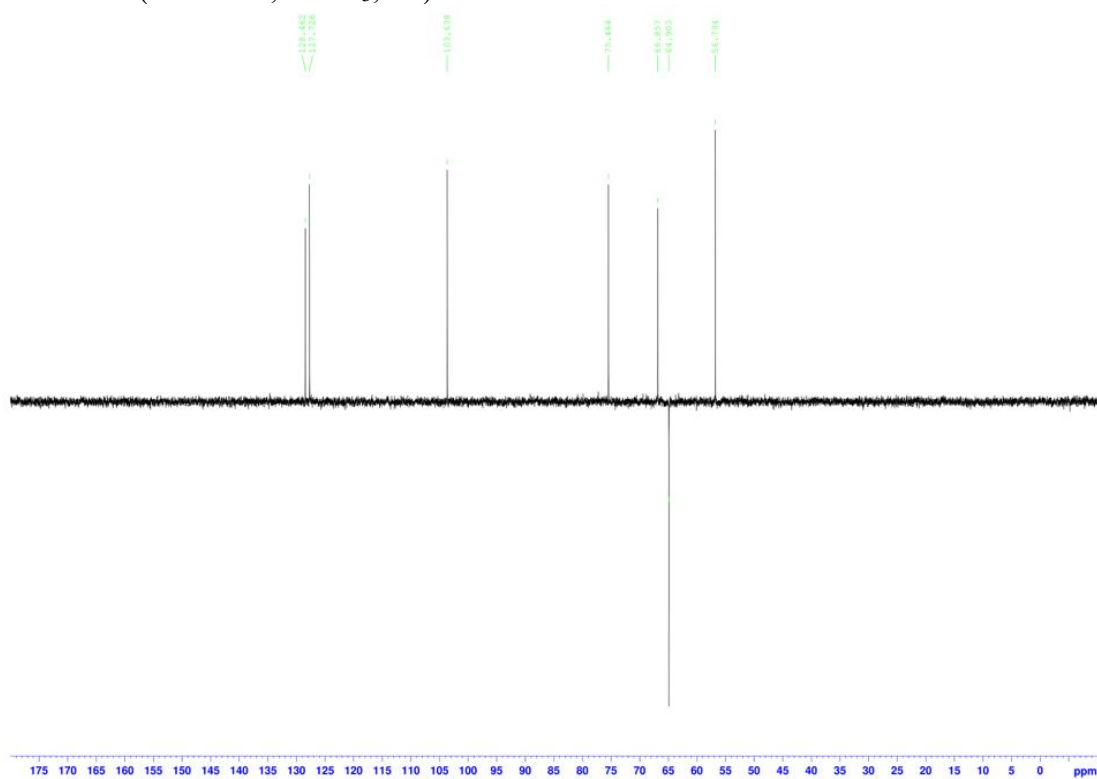
δ 128.46 (C^3H), δ 127.73 (C^4H), δ 103.64 (C^2H), δ 75.46 (C^5H), δ 66.86 (C^1H), δ 64.90 (C^6H_2), δ 56.79 (C^7H_3).



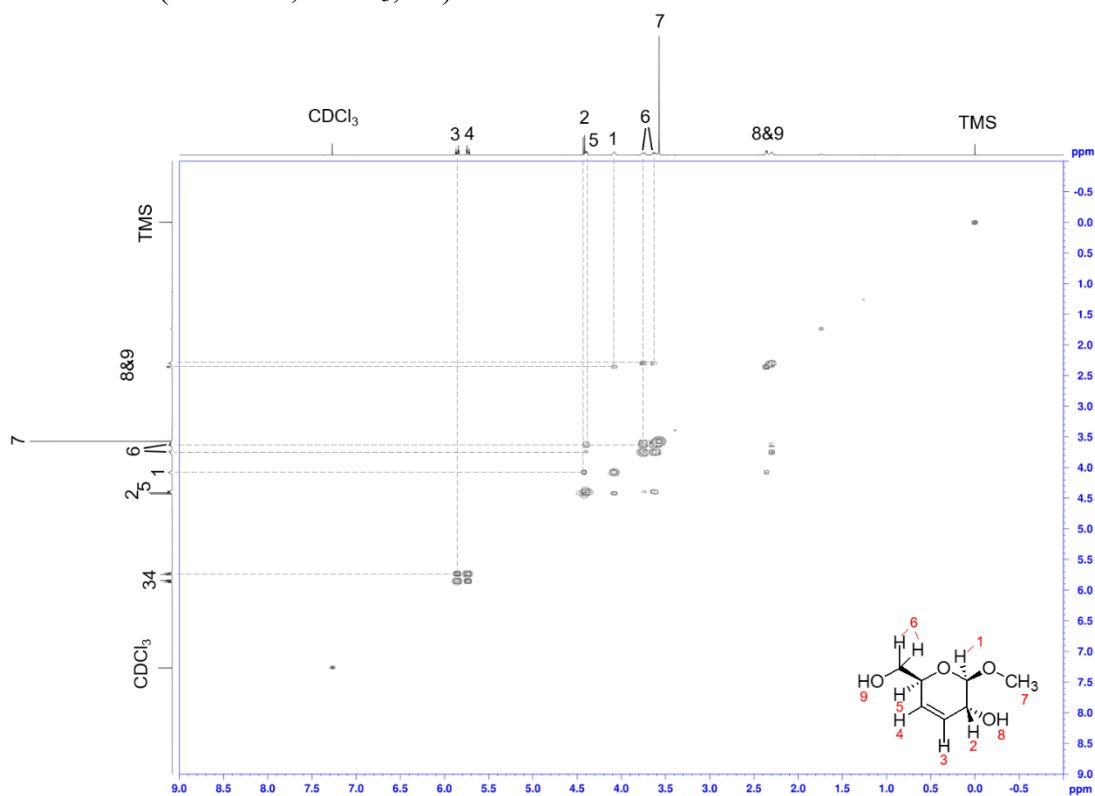
DEPT90 (400 MHz, CDCl₃, r.t.):



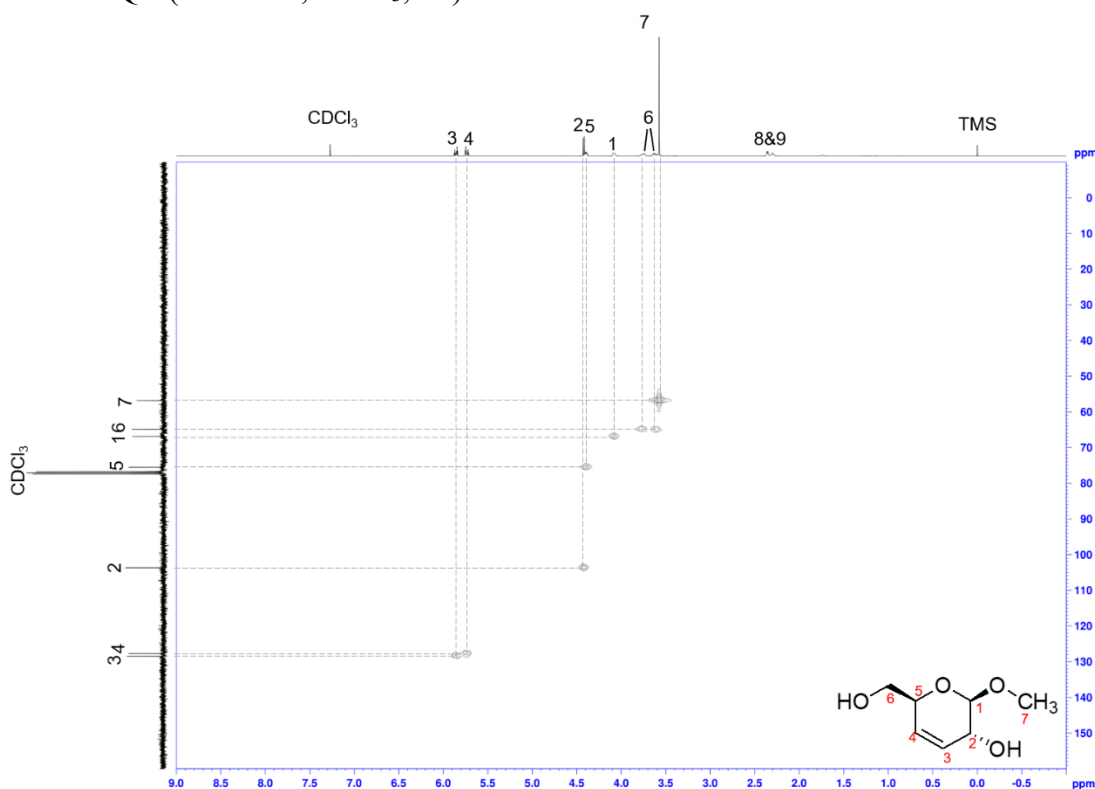
DEPT135 (400 MHz, CDCl₃, r.t.):



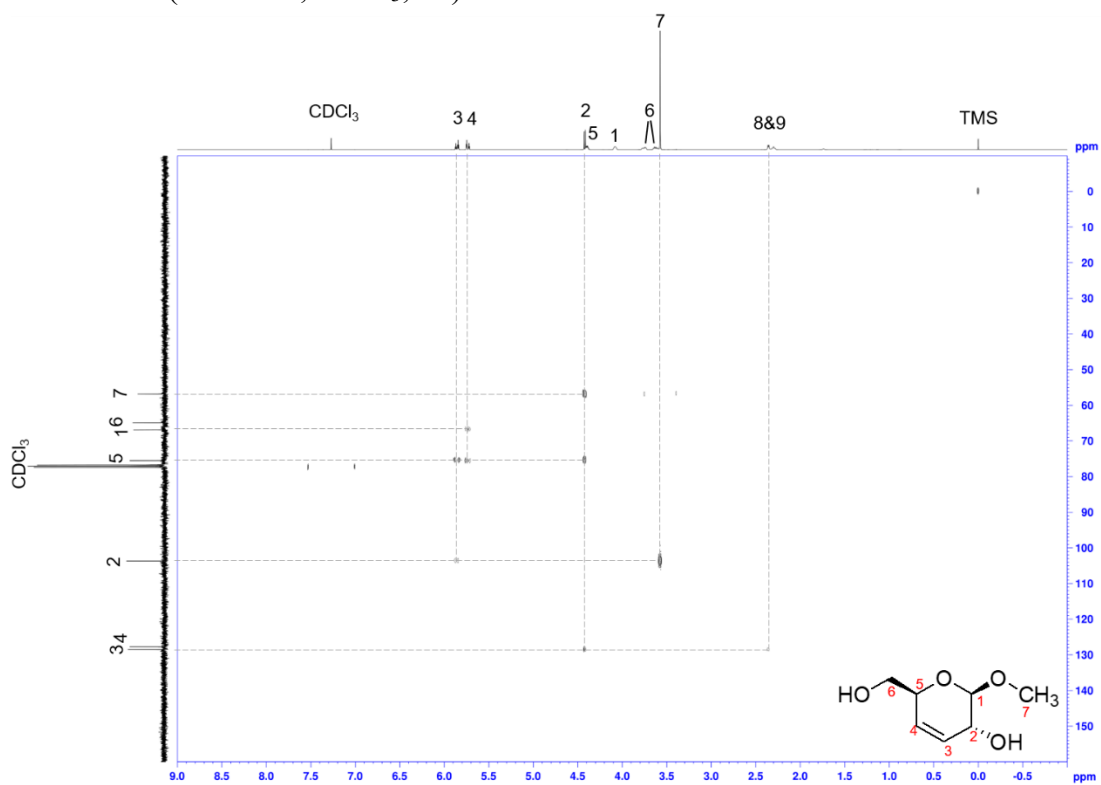
H-H COSY (400 MHz, CDCl₃, r.t.):

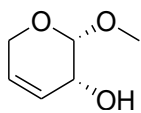


H-C HMQC (400 MHz, CDCl₃, r.t.):



H-C HMBC (400 MHz, CDCl₃, r.t.):

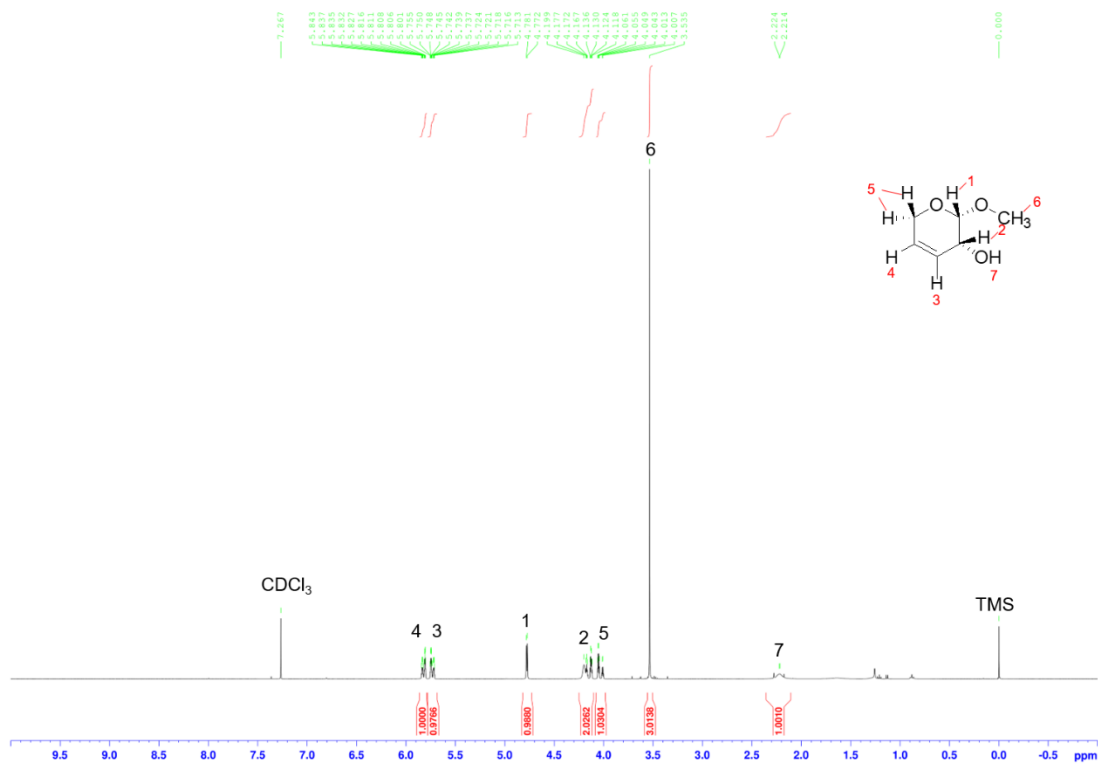




(2*R*,3*R*)- 3,6-Dihydro-2-methoxy-2*H*-pyran-3-ol

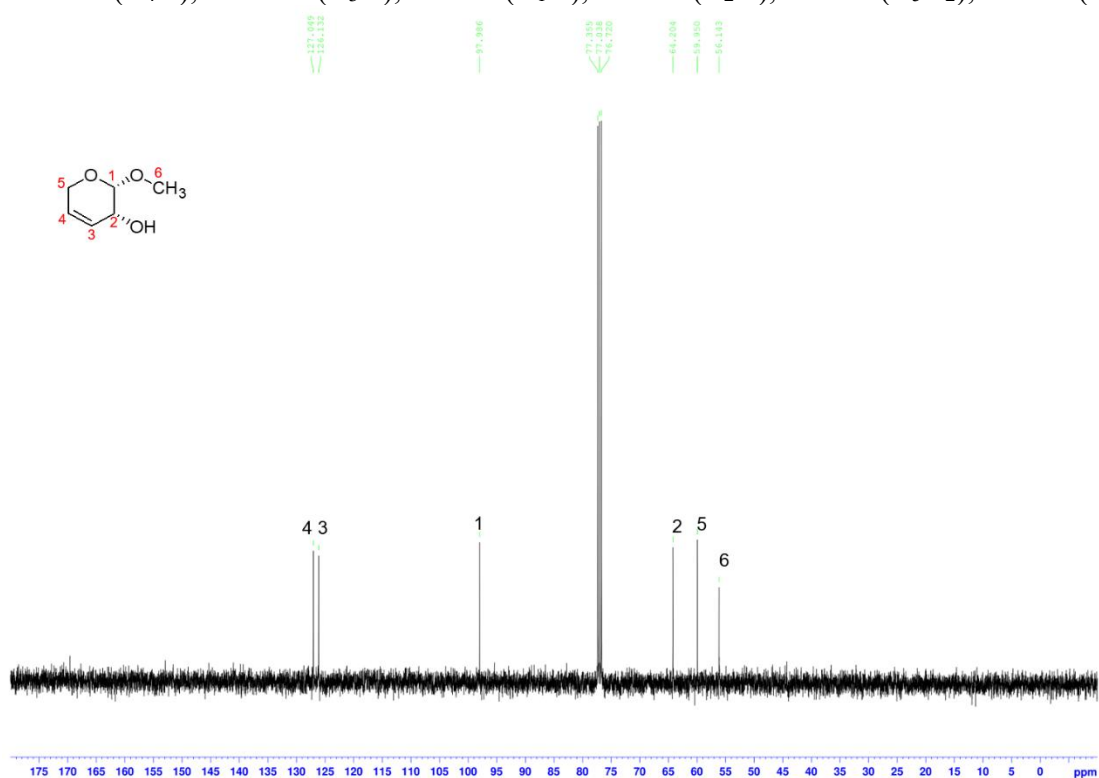
^1H NMR (400 MHz, CDCl_3 , r.t.):

δ 5.84-5.80 (m, 1H, H^4), δ 5.76-5.74 (m, 1H, H^3), δ 4.77 (d, $J=3.84$ Hz, 1H, H^1), δ 4.20-4.12 (m, 2H, H^5), δ 4.06-4.01 (m, 1H, H^2), δ 3.54 (s, 3H, H^6), δ 2.22 (bs, 1H, H^7).

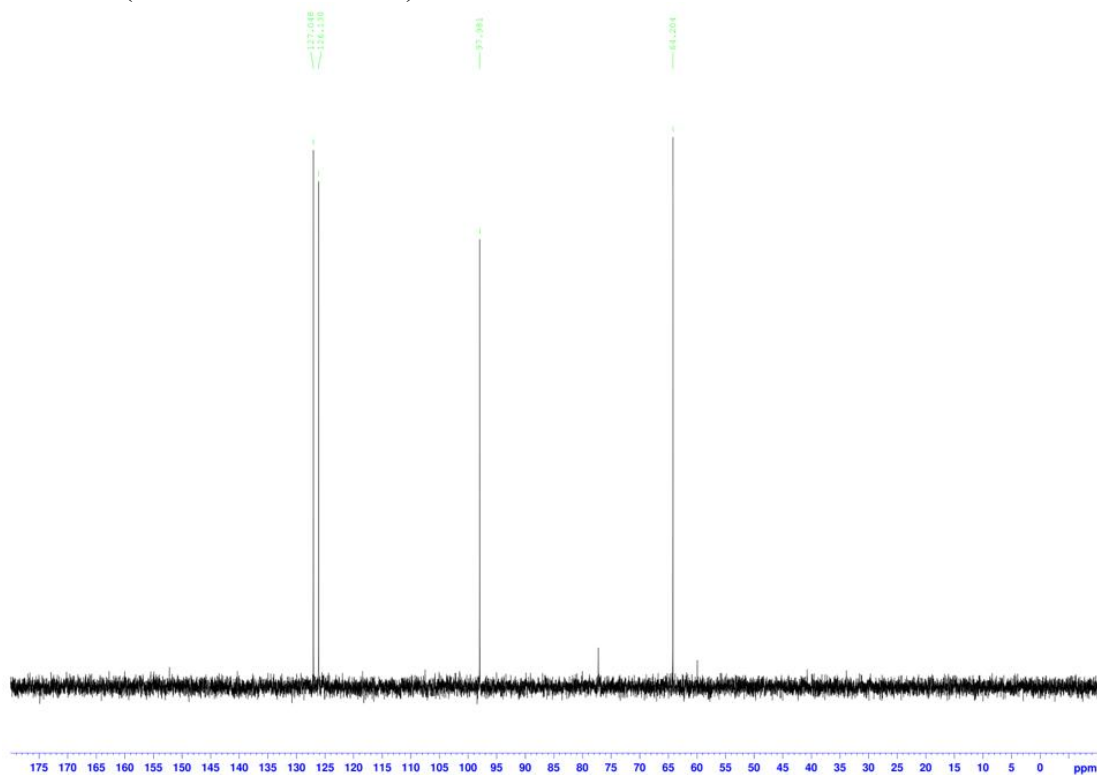


^{13}C NMR (400 MHz, CDCl_3 , r.t.):

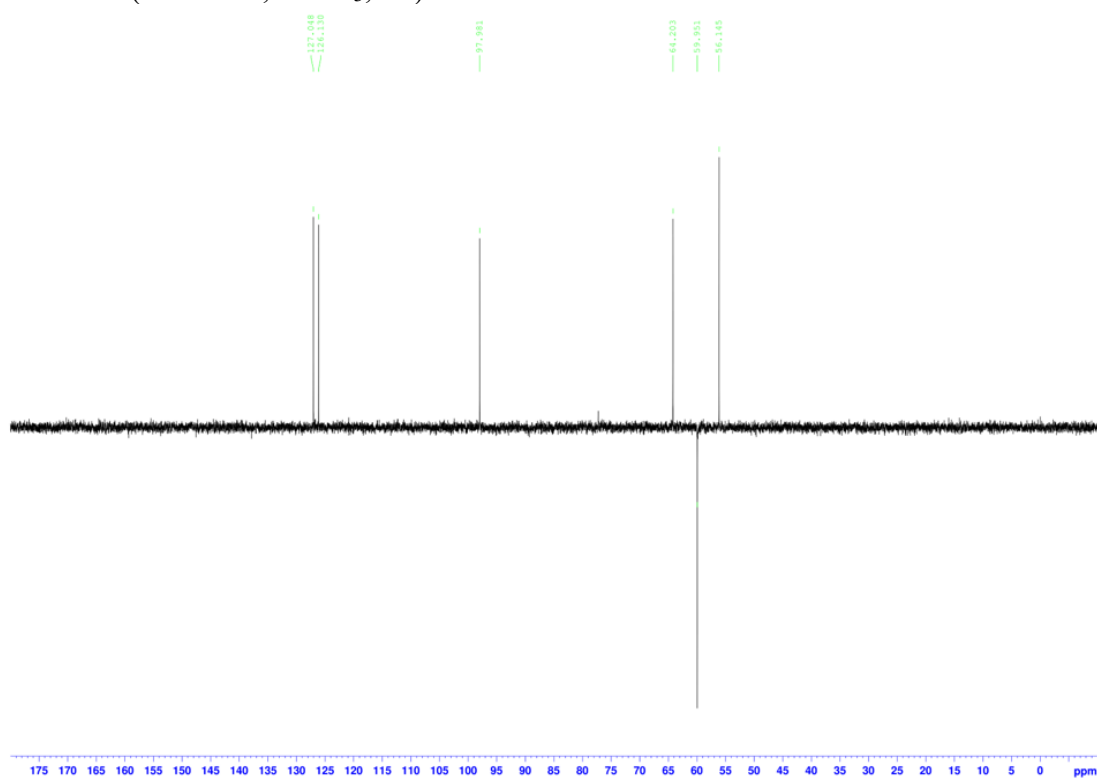
$\delta 127.05$ (C_4H), $\delta 126.13$ (C_3H), $\delta 97.99$ (C_1H), $\delta 64.20$ (C_2H), $\delta 59.95$ (C_5H_2), $\delta 56.14$ (C_6H_3).



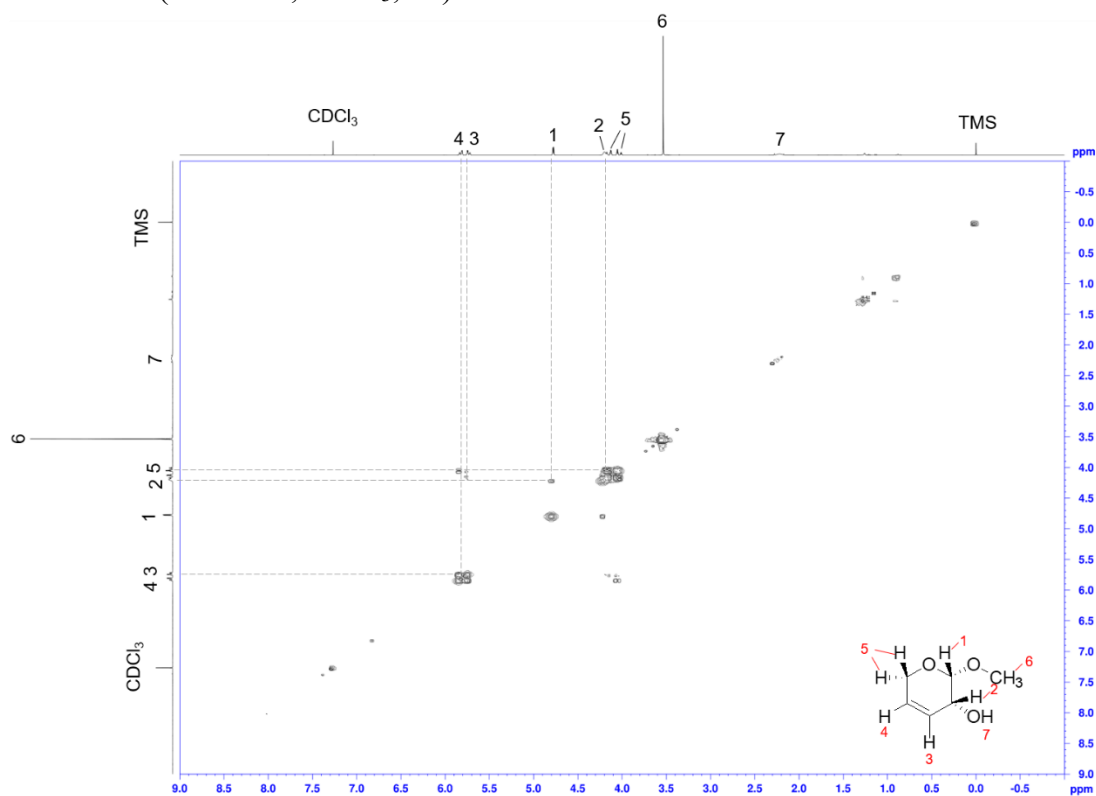
DEPT90 (400 MHz, CDCl₃, r.t.):



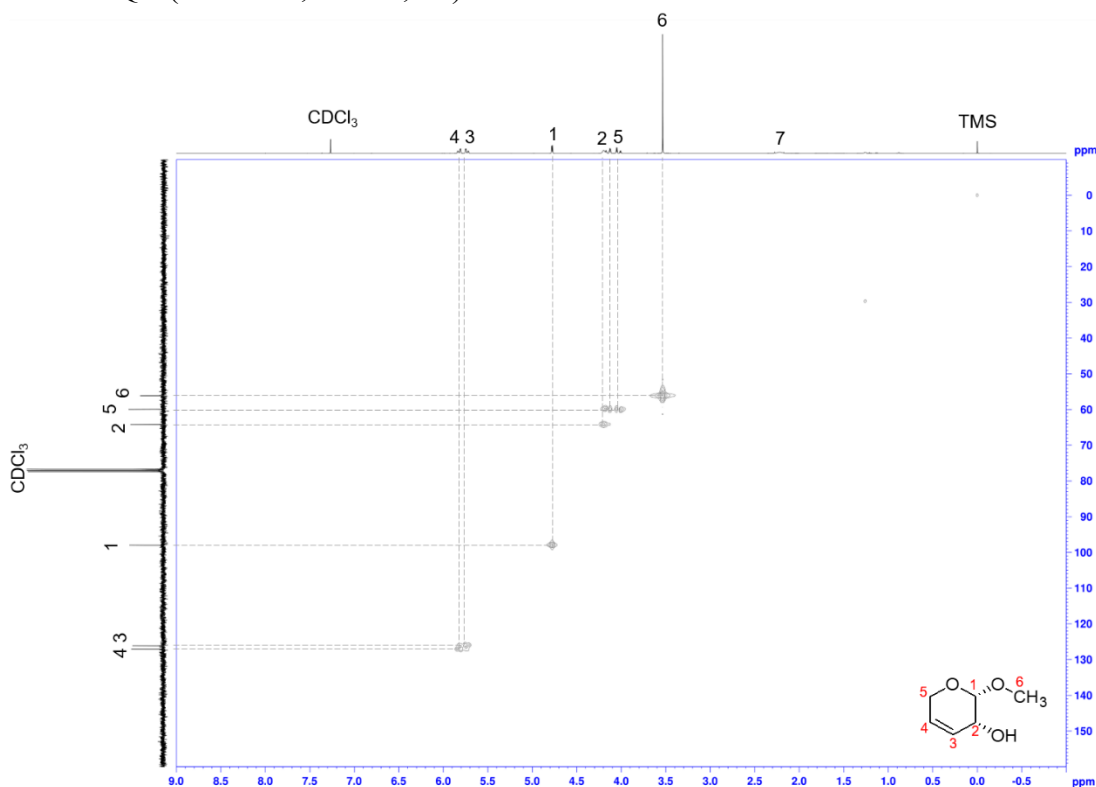
DEPT135(400 MHz, CDCl₃, r.t.):



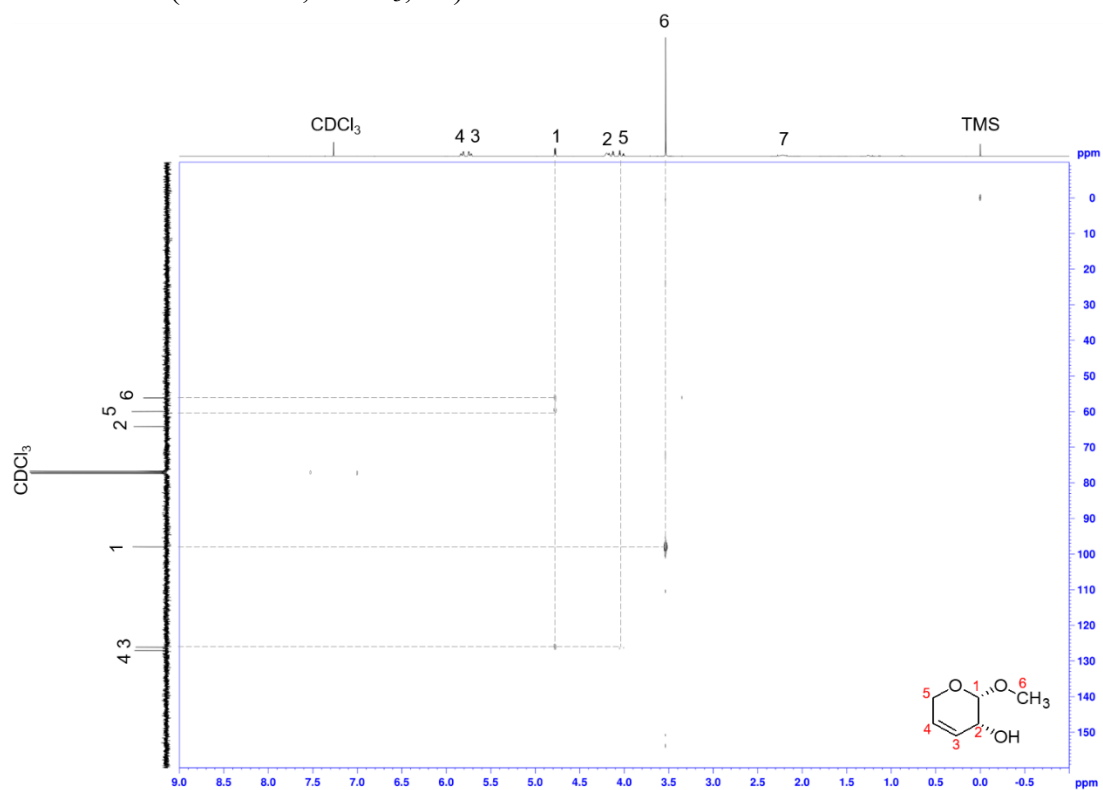
H-H COSY (400 MHz, CDCl₃, r.t.):

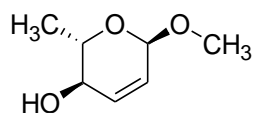


H-C HMQC (400 MHz, CDCl₃, r.t.):



H-C HMBC (400 MHz, CDCl₃, r.t.):

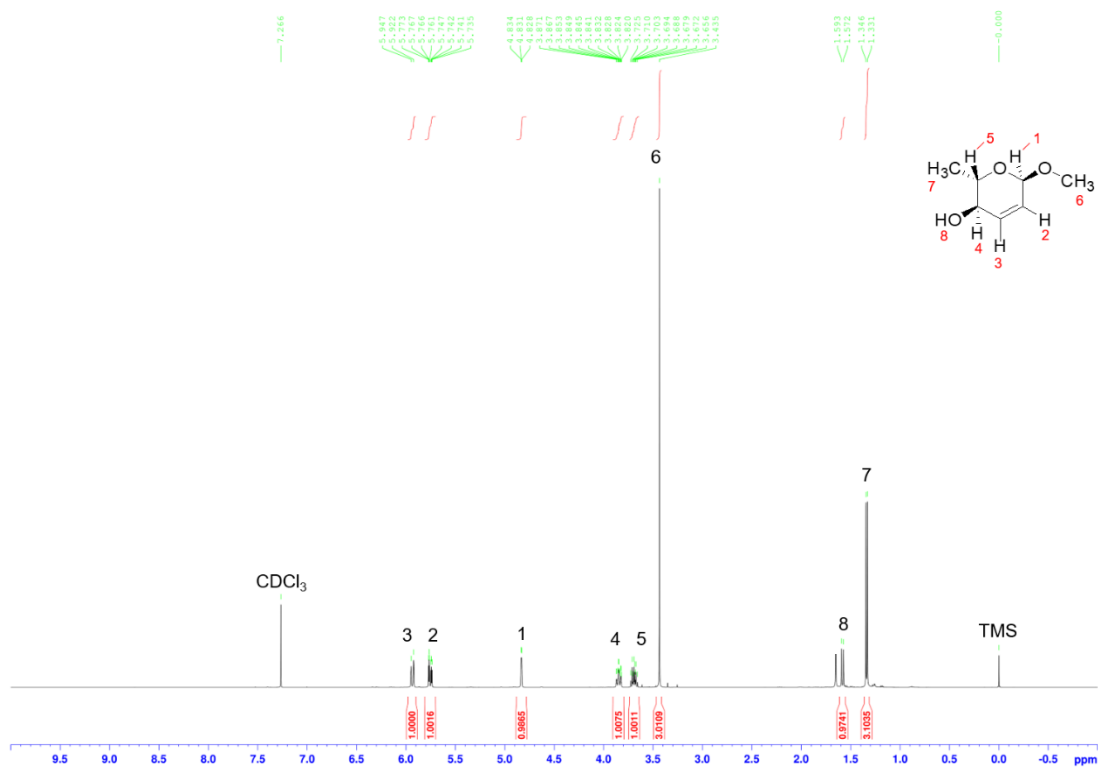




(2*S*,3*R*,6*R*)-3,6-Dihydro-6-methoxy-2-methyl-2*H*-pyran-3-ol

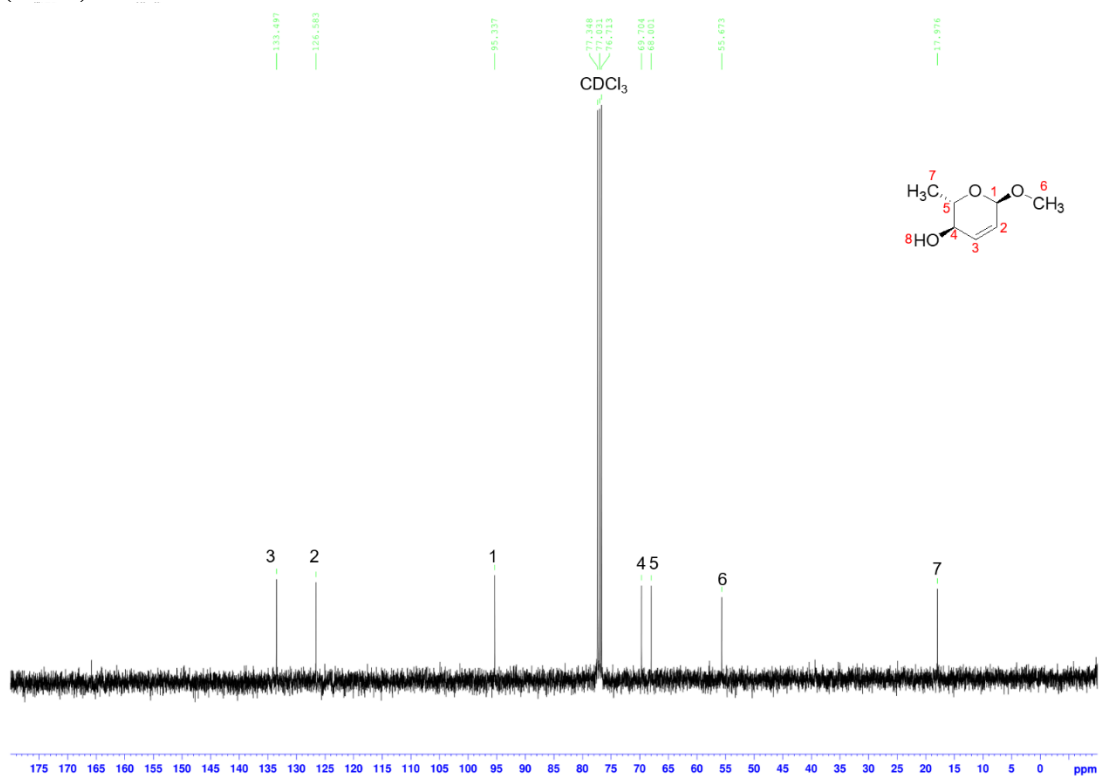
^1H NMR (400 MHz, CDCl_3 , r.t.):

δ 5.93 (d, $J=10.0$ Hz, 1H, H^3), δ 5.75 (dt, $J=10.2, 2.4$ Hz, 1H, H^2), δ 4.83 (s, 1H, H^1), δ 3.82 (dd, $J=8.9, 1.5$ Hz, 1H, H^4), δ 3.71-3.66 (m, 1H, H^5), δ 3.53 (s, 1H, H^6), δ 2.26 (bs, 1H, H^8), δ 1.33 (d, $J=6.2$ Hz, 3H, H^7).

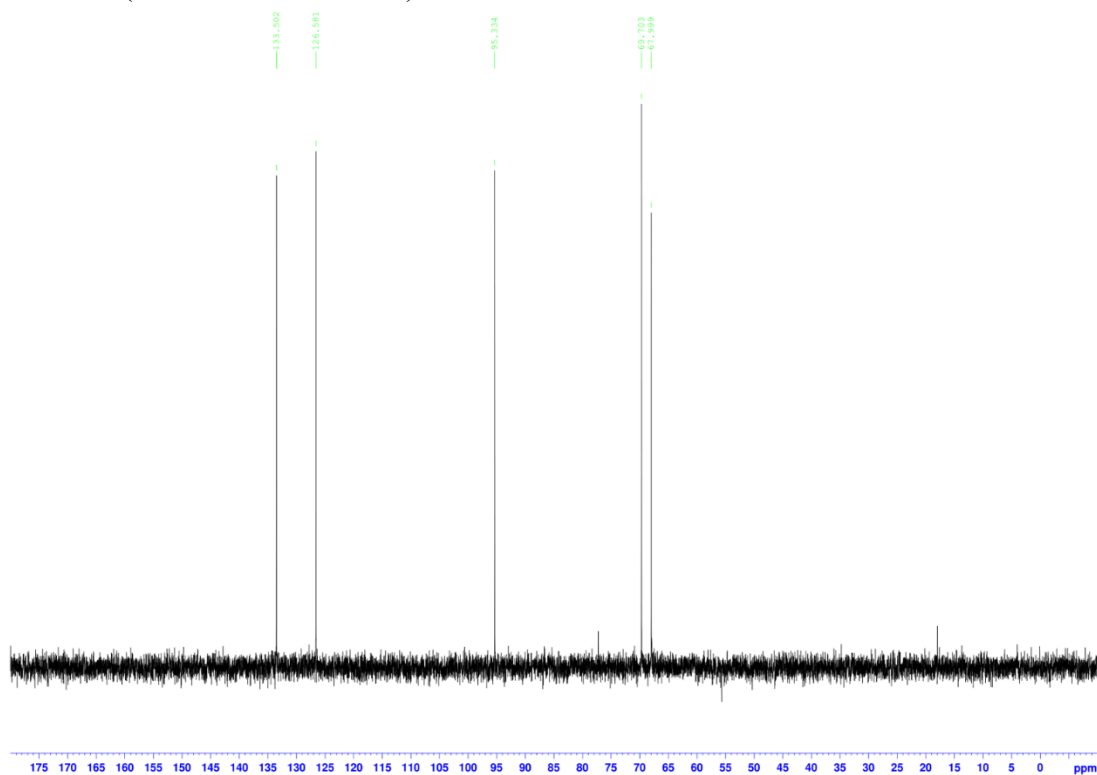


^{13}C NMR (400 MHz, CDCl_3 , r.t.):

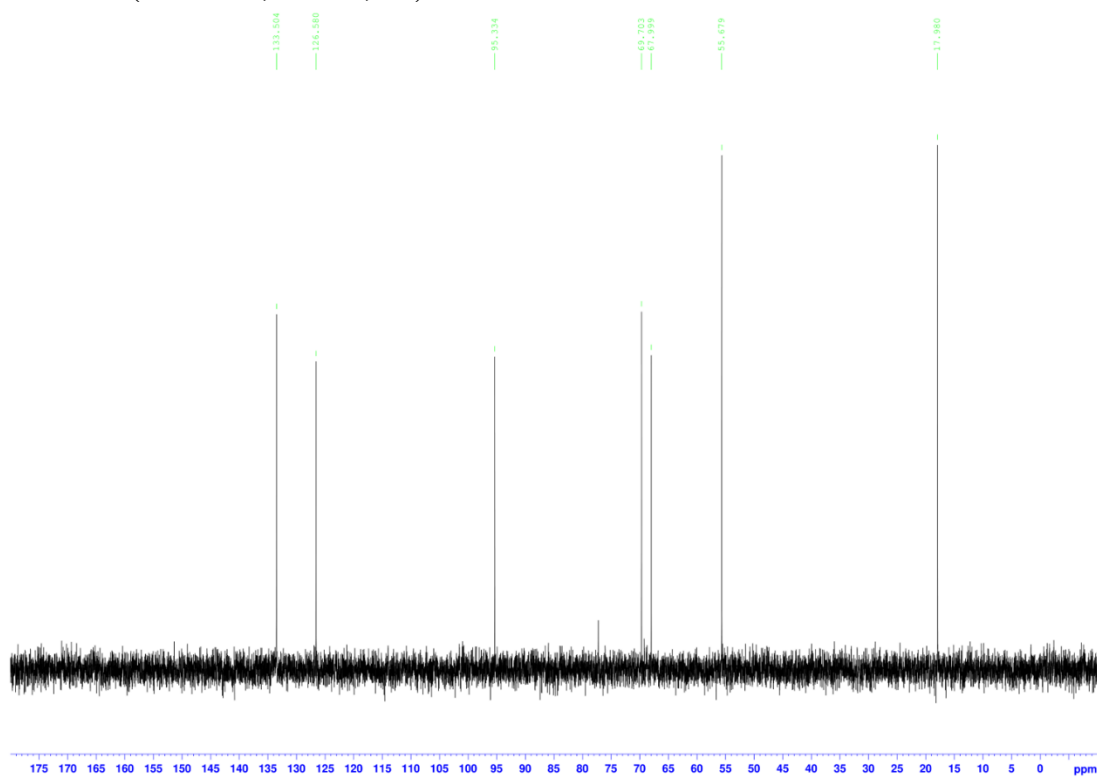
δ 133.50 (C^3H), δ 126.58 (C^2H), δ 95.34 (C^1H), δ 69.70 (C^4H), δ 68.00 (C^5H), δ 55.67 (C^6H_3), δ 17.98 (C^7H_3).



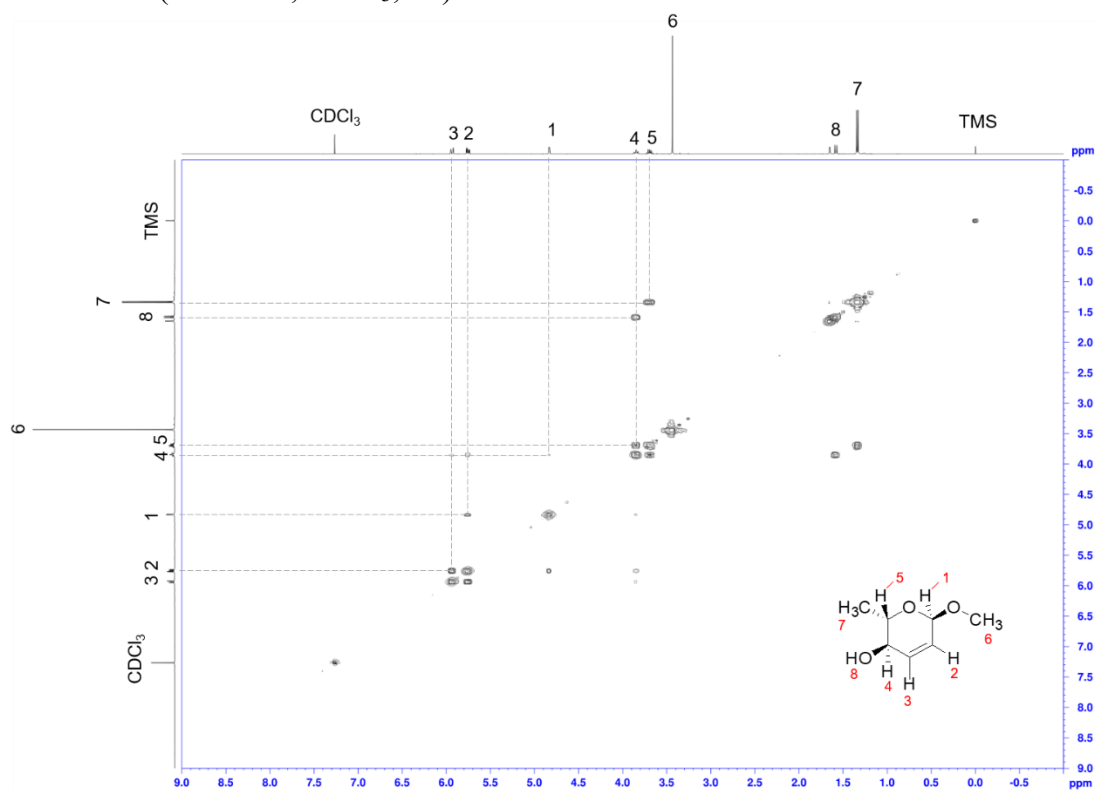
DEPT90 (400 MHz, CDCl₃, r.t.):



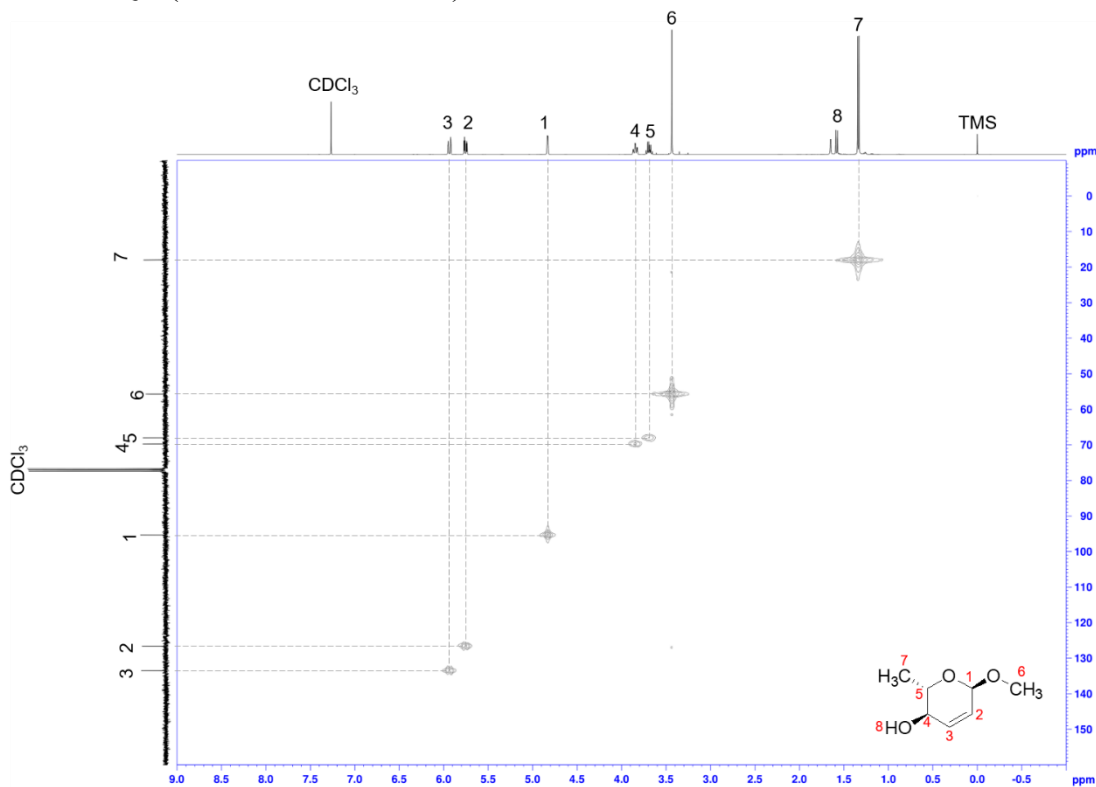
DEPT135(400 MHz, CDCl₃, r.t.):

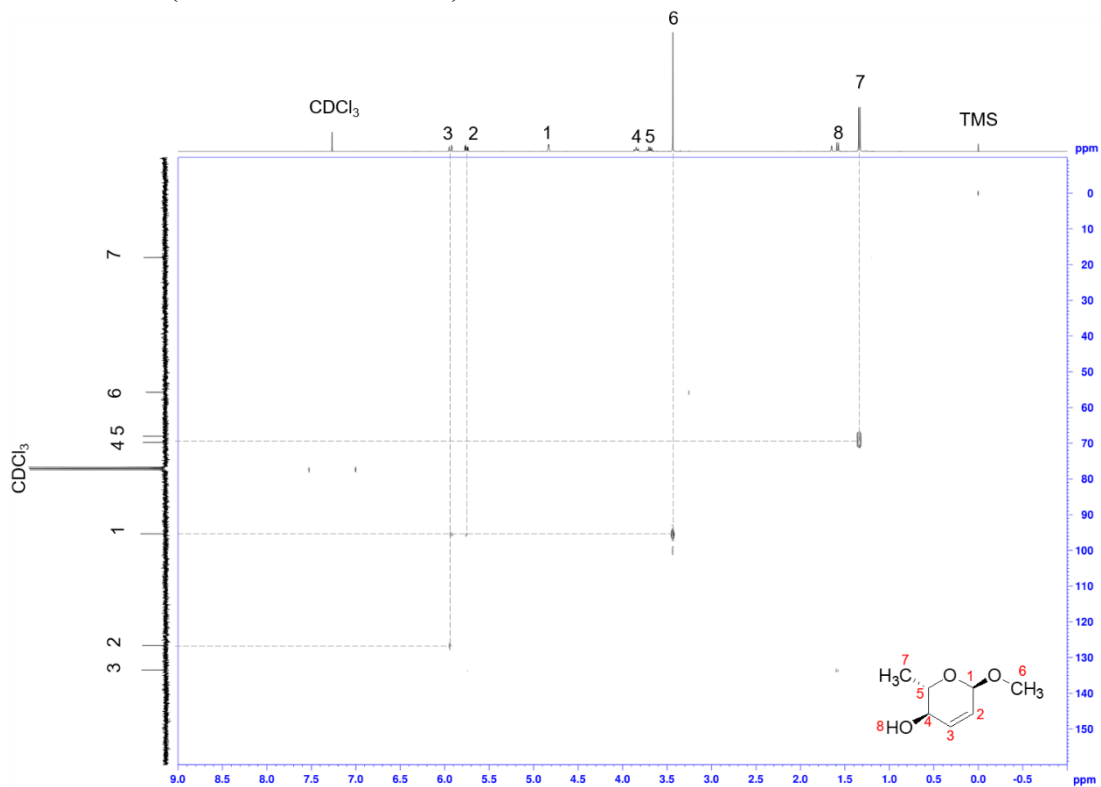


H-H COSY (400 MHz, CDCl₃, r.t.):



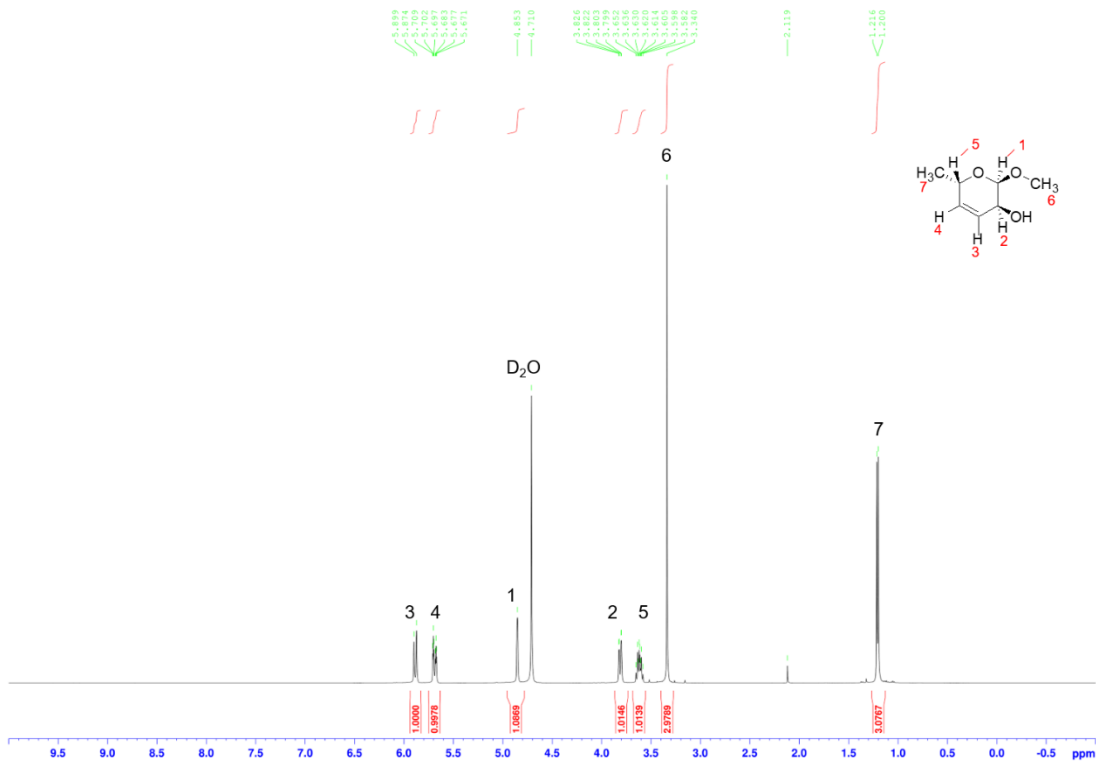
H-C HMQC (400 MHz, CDCl₃, r.t.):



H-C HMBC (400 MHz, CDCl₃, r.t.):

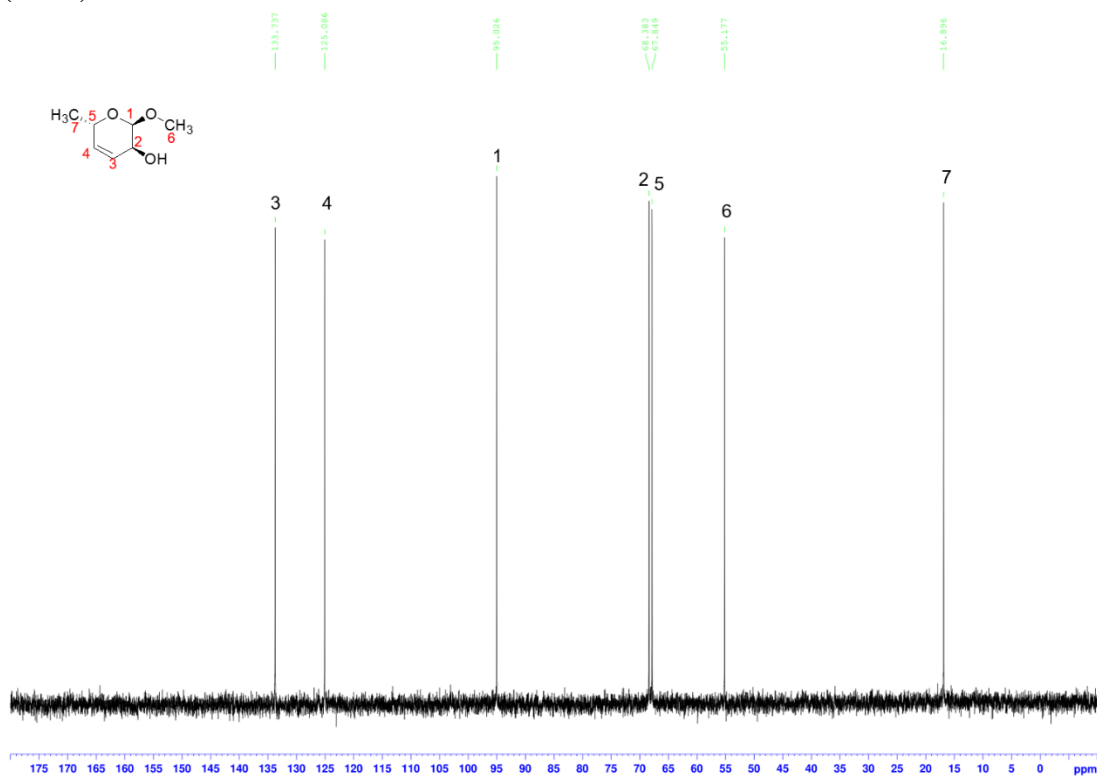
¹H NMR (400 MHz, D₂O, r.t.):

85.89 (d, $J=10.0$ Hz, 1H, H³), 85.69 (dt, $J=10.2, 2.4$ Hz, 1H, H²), 84.85 (s, 1H, H¹), 83.81 (dt, $J=9.2, 1.6$ Hz, 1H, H²), 83.65-3.58 (m, 1H, H⁵), 83.34 (s, 3H, H⁶), 81.21 (d, $J=6.4$ Hz, 3H, H⁷).

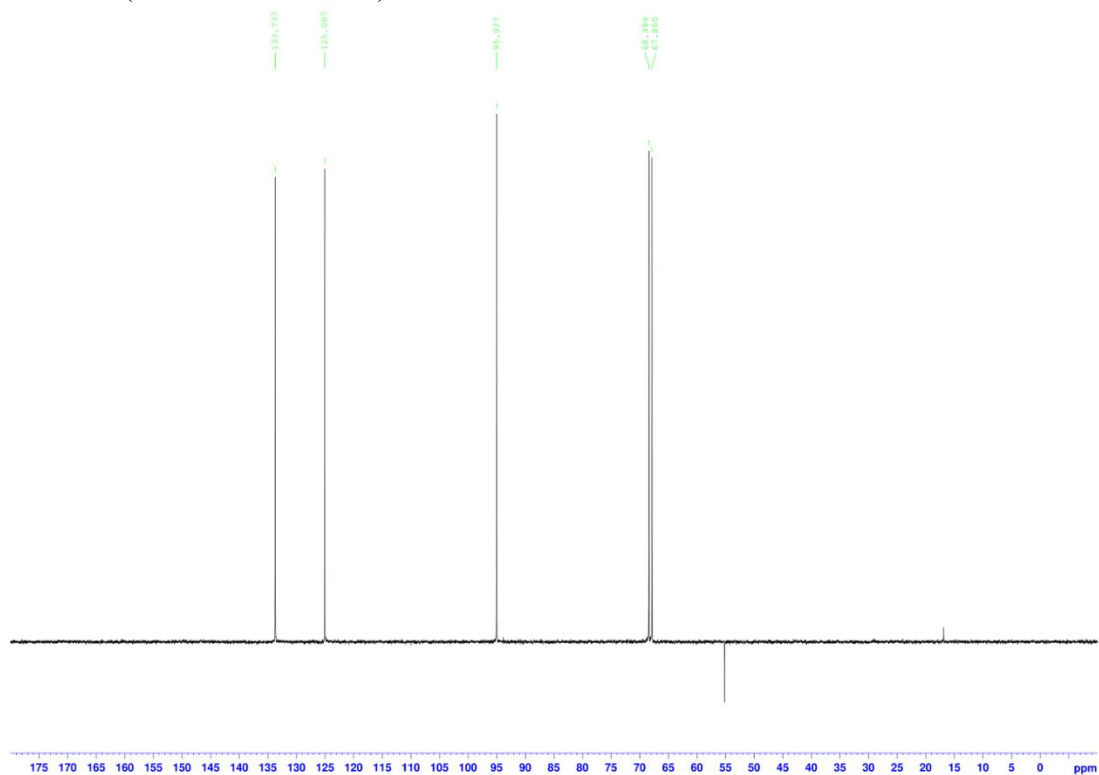


^{13}C NMR (400 MHz, D_2O , r.t.):

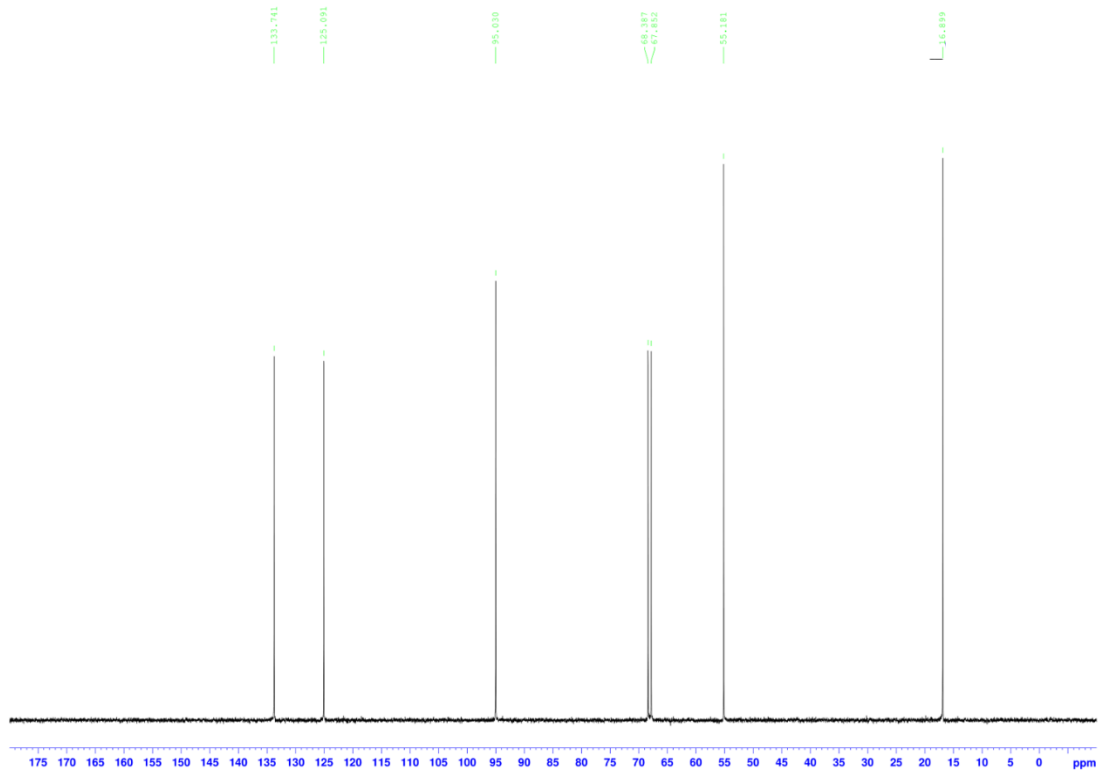
$\delta 133.74$ (C^3H), $\delta 125.09$ (C^4H), $\delta 95.03$ (C^1H), $\delta 68.38$ (C^2H), $\delta 67.85$ (C^5H), $\delta 55.18$ (C^6H_3), $\delta 16.90$ (C^7H_3).



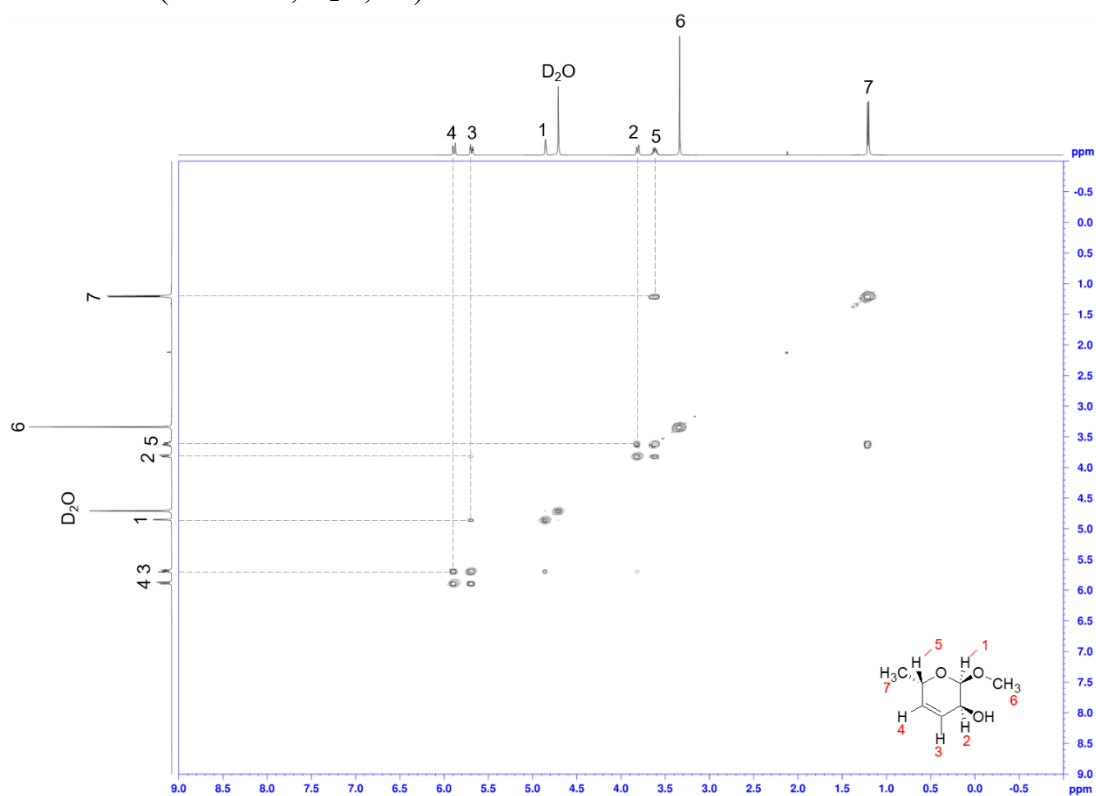
DEPT90 (400 MHz, D₂O, r.t.):



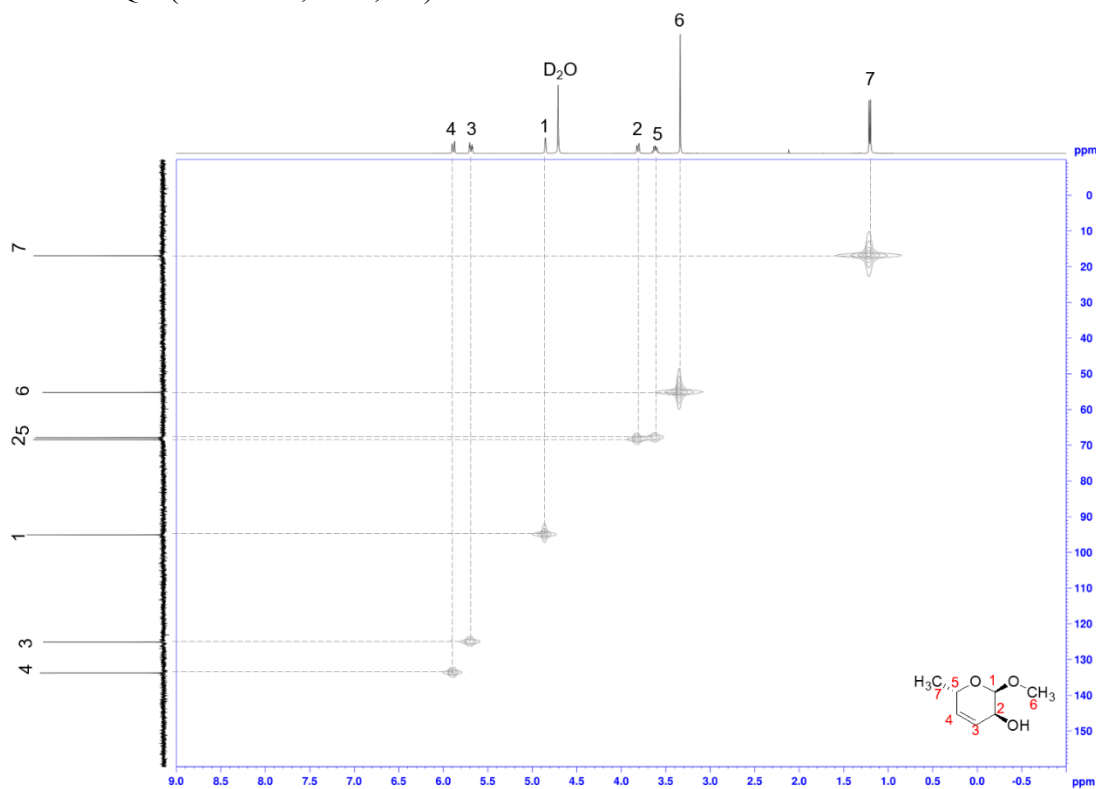
DEPT135(400 MHz, D₂O, r.t.):



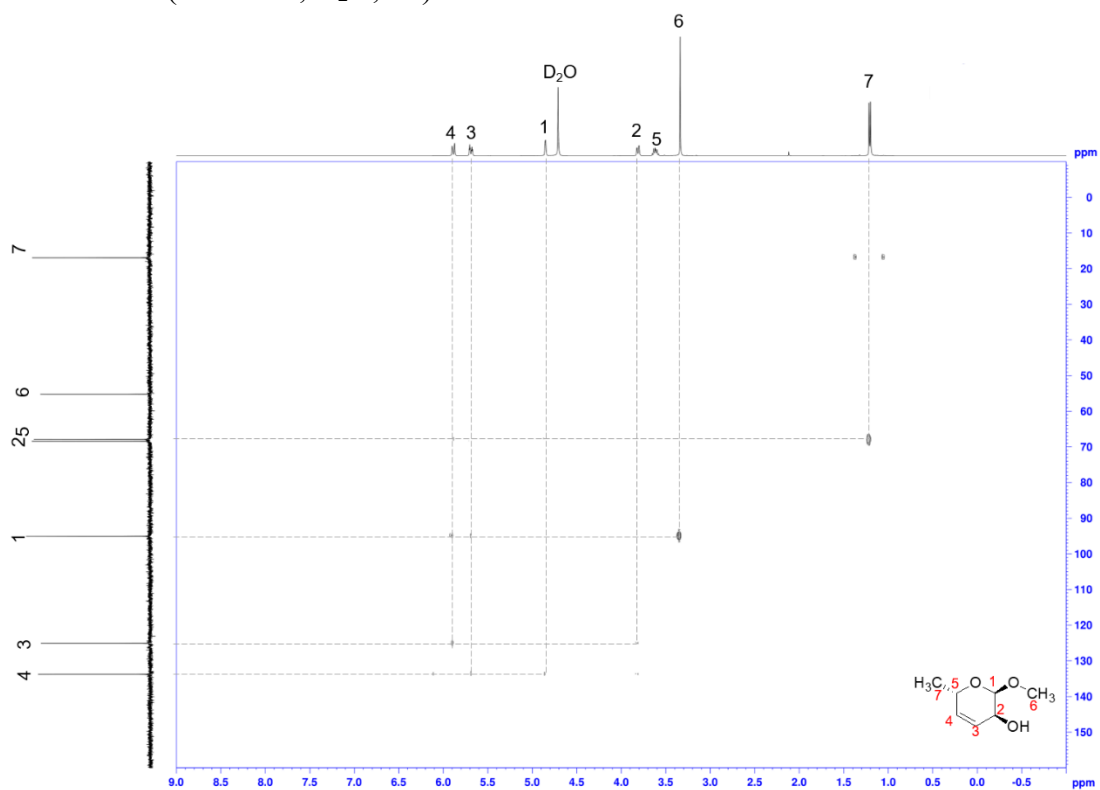
H-H COSY (400 MHz, D₂O, r.t.):



H-C HMQC (400 MHz, D₂O, r.t.):



H-C HMBC (400 MHz, D₂O, r.t.):



Chapter 4

One-pot selective synthesis of chiral polyols from methyl glycosides via deoxydehydration

4.1 Introduction

Carbohydrates are the main component of biomass, the utilization and development of them offer many possibilities to the chemical industry because of their stereo structural diversity^[1]. Lignocellulosic biomass-derived products, for example, polyols and partially reduced polyols, are useful precursors^[2-10] for biochemistry, medicine chemistry, and agricultural chemistry, and they can be obtained by hydrodeoxygenation over heterogeneous metal-acid catalysts^[11-13]. In addition, the properties of polyols can be influenced by their stereostructure, and the stereochemistry of polyols is critical for applications. Optically active polyols and partially deoxy polyols are important intermediates and chemicals for the production of fine chemicals, such as perfume and alcoholic beverage, cosmetics, food additives, polymers and medicines^[1, 13-16]. For example, polyol-based nonionic surfactants, comprised of a hydrophilic polyol head group and hydrophobic tail gap, are widely used for cosmetics and pharmaceuticals applications because of their stereo structural diversity, biodegradability and nontoxicity. It would be highly desirable to selectively produce polyols with fixed hydroxyl group positions and stereochemistry.

However, conventional transformation processes of carbohydrates to such polyols are typically not regio-selective because of the indiscriminate cleavage of hydroxyl groups, which results in a complex mixture of polyols, and the stereocenters present in the original carbohydrate feedstocks were also erased^[17-18]. Recently, a large number of papers on the stereoselective preparation of bioactive carbohydrates and hydroxylated alkaloids were reported^[19]. Most commonly, they can be synthesized from carbohydrates depending on the chiral centre(s). Since their chemical conversions and asymmetric inductions are sometimes inefficient, it is evidently desirable to develop more facile and stereoselective synthetic routes^[20]. Huber and coworkers reported on a new route to produce a

mixture of (2*R*,5*S*)-1,2,5,6-hexaneterol and (2*S*,5*S*)-1,2,5,6-hexaneterol from levoglucosan in up to 90% yield^[21-23].

One-pot reaction is a sequence of chemical transformations which is operated in a single reactor. It is convenient and economical, and can improve the efficiency of a chemical reaction. In a one-pot reaction, the separation and purification of the intermediates can be avoided between the individual reactions, which minimizes the chemical waste, as well as save energy, labor, and time. In some cases, the concentration of unstable intermediates can be kept low during the reaction in one-pot system which can suppress side reactions of intermediates and increase the yield of final products. Difficulties for one-pot process include the control of reaction conditions: each step has different optimized conditions and therefore some steps proceed under not-best conditions^[24-25].

Recently, our laboratory found that Pd- modified CeO₂ supported Re catalysts (ReO_x-Pd/CeO₂) was effective heterogeneous DODH catalysts^[26-29] for direct and selective transformation of vicinal OH groups in methyl glycosides without protection of OH groups reaction by using gaseous H₂, providing the corresponding dideoxy polyols via DODH + hydrogenation (DODH + HG)^[30-31]. The obtained dideoxy methyl glycosides have asymmetric carbon atoms, fixed hydroxyl group positions and original stereostructure in the molecules. On the other hand, Rh-ReO_x/SiO₂^[32-33] and Ir-ReO_x/SiO₂^[34-36] catalyst exhibits unique catalytic properties in the hydrogenolysis of C–O bonds of various biomass-based substrates^[37-38]. And Ir-ReO_x/SiO₂ also acted as a highly active and selective heterogeneous catalyst for the hydrogenation of unsaturated aldehydes to unsaturated alcohols in water^[39].

In this work, we conducted the hydrolysis and hydrogenation of dideoxy product which obtained from methyl glycosides (such methyl α-D-mannopyranoside, methyl β-L-arabinopyranoside and methyl β-D-ribofuranoside) via DODH reaction in one-pot.

4.2 Experimental

4.2.1 Reagent information

All the methyl glycosides for deoxydehydration reactions were analytic reagents from chemical product corporations and were used without treatment: methyl α-D-mannopyranoside (>98%,

FUJIFILM Wako Pure Chemical Co.), methyl β -D-galactopyranoside (>95% (NMR), FUJIFILM Wako Pure Chemical Co.), methyl β -L-arabinopyranoside (>97% (NMR), FUJIFILM Wako Pure Chemical Co.), methyl α -L-fucopyranoside (>98% (HPLC), Tokyo Chemical Industry Co., Ltd.), methyl α -L-rhamnopyranoside (>97% (NMR), FUJIFILM Wako Pure Chemical Co.) and methyl α -D-glucopyranoside (>98% (GC), Tokyo Chemical Industry Co., Ltd.).

All metal precursors for catalyst preparation were analytic reagents from chemical product corporations: CeO_2 (Daiichi Kigenso Kagaku Kogyo Co., Ltd.), SiO_2 (G-6, Fuji Silysia Chemical Ltd.), NH_4ReO_4 (Mitsuwa Chemicals Co., Ltd.), $\text{Pd}(\text{NO}_3)_2$ (Sigma-Aldrich Co., LLC.), H_2IrCl_6 (Furuya Metal Co., Ltd.), $\text{RhCl}_3 \cdot 3\text{H}_2\text{O}$ (FUJIFILM Wako Pure Chemical Co.), $\text{HAuCl}_4 \cdot 4\text{H}_2\text{O}$ (FUJIFILM Wako Pure Chemical Co.).

The information of the commercial catalyst used in this work was as below: Pt/C ($S_{\text{BET}}=485 \text{ m}^2 \text{ g}^{-1}$), Rh/C ($S_{\text{BET}}=485 \text{ m}^2 \text{ g}^{-1}$), Ru/C ($S_{\text{BET}}=485 \text{ m}^2 \text{ g}^{-1}$) and Pt/C ($S_{\text{BET}}=478 \text{ m}^2 \text{ g}^{-1}$) with 5 wt % metal loading were purchased from FUJIFILM Wako Pure Chemical Co. A cation exchange resins functionalized with sulfonic groups: Amberlyst70 (4.78 eq/kg resin dried, highest operating temperature 463 K, highly cross-linked styrene-divinyl benzene copolymer beads) were from Morton International Ltd..

All solvents were from chemical product corporations and were used without treatment: 1,4-dioxane (>99.5%, FUJIFILM Wako Pure Chemical Co.), diethylene glycol dimethyl ether (>99.0% Tokyo Chemical Industry Co., Ltd.) and methanol (>96%, FUJIFILM Wako Pure Chemical Co.).

4.2.2 Catalyst preparation

The $\text{ReO}_x\text{-Pd/CeO}_2$ ^[29] (Re=2 wt%, Pd/Re=0.25 mol mol⁻¹) catalysts were prepared by impregnating the CeO_2 powder (calcined at 873 K for 1 h) with a 0.1 M aqueous solution of NH_4ReO_4 , after drying and stirring over a 353 K hot plate and drying at 383 K for 12 h, the obtained mixture was impregnated with 0.1 M aqueous solution of $\text{Pd}(\text{NO}_3)_2$. After drying and at 353 K over a hot plate, the catalysts were further dried at 383 K for 12 h. Then, the mixture was calcined in air at 773 K for 3 h.

Ir-ReO_x/SiO₂^[40] and Rh-ReO_x/SiO₂^[41] catalysts were prepared as follows: Rh/SiO₂ and Ir/SiO₂ catalysts were prepared by impregnating SiO₂ with an aqueous solution of RhCl₃·3H₂O and H₂IrCl₆, respectively. After the impregnation procedure and drying at 383 K for 12 h, the prepared catalysts were calcined under air at 773 K for 3 h.

Rh-ReO_x/SiO₂ (Rh=4 wt%, Re/Rh=0.5 mol mol⁻¹) catalyst was prepared by impregnating Rh/SiO₂ after drying procedure with aqueous solutions of NH₄ReO₄. After the impregnation procedure and drying at 383 K for 12 h, the prepared catalysts were calcined under air at 773 K for 3 h.

Ir-ReO_x/SiO₂ (Ir=4 wt%, Re/Ir=1) catalyst was prepared by impregnating Ir/SiO₂ after drying procedure with aqueous solutions of NH₄ReO₄. After the impregnation procedure and drying at 383 K for 12 h, the prepared catalysts were calcined under air at 773 K for 3 h.

4.2.3 Synthesis of dideoxy product from methyl glycosides

Activity tests were performed in a 190 mL stainless steel autoclave. The substrate, catalyst and 1,4-dioxane were put into the autoclave with a spinner. After sealing the reactor, the air content was purged three times with H₂ (>99.99%; Takachiho Trading Co., Ltd.), and the pressure was raised to an appropriate value by H₂ at room temperature (RT). Autoclaves were then heated to the reaction temperature and its temperature was monitored using a thermocouple inserted in the autoclave. The pressure at reaction temperature was recorded (8.0 MPa in the case of DODH + HG reaction and 2.0 MPa in the case of DODH reaction at 413 K). The reaction time zero (0 h) was defined as the time when the temperature reached the set value (413 K) and the heating-up time was about 40 mins. The stirring rate was fixed at 500 rpm (magnetic stirring). After an appropriate reaction time, the autoclave was cooled down to RT in cold water bath. The gases in the autoclave were collected in a gas bag. The autoclave contents and the washing solvent (10 g mixed solution including 8 g distilled water and 2 g 1,4-dioxane) were transformed into vials.

4.2.4 Synthesis of chiral polyols from dideoxy methyl glycosides

After the DODH + HG reaction of methyl glycosides, the catalyst was removed by centrifugation and filtration, the filtrate, 10 g H₂O and catalyst were added into the autoclave. After sealing the autoclave, the air content was purged by flushing three times with 1 MPa H₂ at R.T., and H₂ pressure was increased to 5.5 MPa. The autoclave was heated to 393 K, and the temperature was maintained under 8 MPa H₂. The stirring rate was fixed at 500 rpm (magnetic stirring). After an appropriate reaction time, the autoclave was cooled down to the S7 room temperature in water bath.

4.2.5 One-pot synthesis of chiral polyols from methyl glycosides

After the DODH+HG reaction of methyl glycosides was conducted as described in 4.2.3, 10 g water was added into the obtained reaction mixture without the removal of catalyst. After sealing the autoclave, the air content was purged by flushing three times with 1 MPa H₂ at R.T., and H₂ pressure was increased to 5.5 MPa. The autoclave was then heated to 393 K, and the temperature was maintained under 8 MPa H₂. The stirring rate was fixed at 500 rpm (magnetic stirring). After an appropriate reaction time, the autoclave was cooled down to the room temperature in water bath.

4.2.6 Product analysis

The both of gas and liquid products were collected and analyzed by FID-GC (Shimadzu GC-2014) and GC-MS (QP5050, Shimadzu) equipped with TC-WAX capillary column (diameter 0.25 mm, 30 m), and HPLC (Shimadzu LC-10A, refractive index detector) with Aminex HPX-87C column (diameter 7.8 mm, 300 mm) using water as the eluent. The stereopurity of obtained polyols was checked by chiralyser-HPLC and FIC-GC with a chiralsil column.

The calibration curves were obtained by using corresponding chemicals and isolated products. The conversion and the selectivity were calculated on the methyl glycoside basis. The carbon balance was also confirmed in each result and the difference in carbon balance was always in the range of the allowed experimental error within $\pm 5\%$.

All the formulas were listed as follow:

$$\text{Conversion (\%)} = [1 - \text{unreacted substrate (mol)} / \text{substrate (mol)}] \times 100$$

$$\text{Selectivity (\%)} = \text{product (mol)} \times n_{\text{carbon}} / (\text{reacted substrate (mol)} \times n_{\text{carbon}}) \times 100$$

$$\text{Carbon balance (\%)} = (\sum (\text{product (mol)} \times n_{\text{carbon}}) + \text{unreacted substrate (mol)} \times n_{\text{carbon}}) / (\text{substrate (mol)} \times n_{\text{carbon}}) \times 100$$

4.2.7 Catalyst characterization

Inductively-coupled plasma atomic emission spectrometry (ICP-AES)

The amount of leaching elements from the catalysts into the reaction solution was analyzed by inductively-coupled plasma atomic emission spectrometry (ICP-AES, Thermo Fisher Scientific iCAP6500).

4.3 Results and discussion

4.3.1 Synthesis of saturated chiral polyols from dideoxy methyl glycosides

Methyl β -D-ribofuranoside, a 5-membered ring methyl glycoside, was selected as a model substrate for the ring-opening (hydrolysis + hydrogenation) reaction of dideoxy methyl glycosides (Scheme 4.1). The hydroxyl groups at C2 and C3 position of methyl β -D-ribofuranoside were removed and methyl β -D-2,3-dideoxy-ribofuranoside was obtained over $\text{ReO}_x\text{-Pd/CeO}_2$ via a 25 h DODH + HG reaction (Chapter 2) firstly. In this step, methyl β -D-ribofuranoside showed a >99% conversion and the yield of methyl β -D-2,3-dideoxy-ribofuranoside was 96%. The eluted metal amounts of $\text{ReO}_x\text{-Pd/CeO}_2$ catalyst in reaction liquids after reaction under air atmosphere and N_2 atmosphere were detected. The leaching amount of Pd was below 0.1% in both atmospheres, and that of Re was below 0.1% under N_2 atmosphere was 0.5% when collected in the air (Table 4.1). After the DODH + HG reaction of methyl β -D-ribofuranoside, $\text{ReO}_x\text{-Pd/CeO}_2$ was removed by filtration. The activity of some catalysts, including prepared $\text{Rh-ReO}_x/\text{SiO}_2$ ($\text{Rh}=4$ wt%, $\text{Re/Rh}=0.5$), $\text{Ir-ReO}_x/\text{SiO}_2$ ($\text{Ir}=4$ wt%, $\text{Re/Ir}=1$) catalyst, commercial catalyst (Rh/C , Ru/C , Pd/C , Pt/C with 5 wt% metal loading amount) and cation exchange resin (Amberlyst 70) catalysts, were investigated with the filtrate and water by using H_2 as a reductant at 393 K (Figure 4.1). The target product is 1,2,5-pentanetriol, which is produced by hydrolysis + hydrogenation of methyl β -D-2,3-dideoxy-ribofuranoside, and the main by-product is dideoxy ribose and methanol, which is formed by hydrolysis of methyl β -D-2,3-dideoxy-ribofuranoside. Otherwise, diols such as 1,2-pentanediol, 1,4-pentanediol and

1,5-pentanediol, and mono-ols such as 1-pentanol, 2-pentanol and tetrahydrofurfuryl alcohol (THFA) were formed by the dehydration and/or hydration and/or hydrogenolysis of methyl β -D-2,3-dideoxy-ribofuranoside and/or 1,2,5-pentanediol. The catalyst screening results (Figure 4.1) showed that methyl dideoxy ribofuranoside was easily transformed into the corresponding dideoxy ribose with high yield (97 %) in 4 h in the case of no catalyst addition. Among all the catalysts, only Pd/C showed lower conversion (44%) of dideoxy methyl ribofuranoside, and Rh-ReO_x/SiO₂, Ir-ReO_x/SiO₂ and Ru/C catalysts showed high yield to 1,2,5-pentanediol (72%, 95%, 89%, respectively), while Rh-ReO_x/SiO₂ provided some selectivities to pentanediols. Cation exchange resin, Amberlyst 70, was also applied to this reaction to increase the reactivity of commercial carbon supported catalyst, but they still showed low selectivity to 1,2,5-pentanetriol, and Pd/C showed high yield (83%) to THFA in the presence of Amberlyst 70.

Rh-ReO_x/SiO₂ and Ir-ReO_x/SiO₂ catalysts were picked up and 24h reactions were carried out to investigate the additional solvent effect (water, *n*-heptane, methanol) on the synthesis of saturated chiral polyols from dideoxy methyl ribofuranoside at 393 K (Figure 4.2). The solvent in this reaction was marked as [1,4-dioxane] [1,4-dioxane + 1,4-dioxane], [water], [1,4-dioxane + water], [1,4-dioxane + *n*-heptane] and [1,4-dioxane + methanol], because 1,4-dioxane was used as solvent in 1st step DODH + HG reaction. In the case of [1,4-dioxane], no solvent was added before 2nd step reaction, and in the case of [water], 1,4-dioxane (the solvent of 1st step reaction) was removed by rotary evaporator and 20 mL water was added before 2nd step reaction. In general, the reactions in [1,4-dioxane + methanol] solvent showed lower conversion of dideoxy methyl ribofuranoside, because methanol could suppress the hydrolysis of dideoxy methyl ribofuranoside. For the reactions with no catalyst addition in these solvents, dideoxy methyl ribofuranoside was totally converted into dideoxy ribose with high selectivity in [1,4-dioxane + water] solvent, but the reaction did not occur in the cases of using [1,4-dioxane + *n*-heptane] or [1,4-dioxane + methanol] as solvent. For the reactions over Ir-ReO_x/SiO₂ catalyst, high selectivity of 1,2,5-pentanediol was maintained in [1,4-dioxane + water] solvent, and in the cases of using [1,4-dioxane + *n*-heptane] or [1,4-dioxane + methanol] as solvent, low conversion of dideoxy methyl ribofuranoside was showed with the produce of some pentanediols. In the cases of using Rh-ReO_x/SiO₂ as catalyst, 73% selectivity of

1,2,5-pentanetriol was obtained in [1,4-dioxane + methanol] solvent, but the result in [1,4-dioxane + water] solvent showed that 42% selectivity of 1,5-pentanediol was produced (the selectivity to pentanediol was 56%), comparing with the 1 h active result of Rh-ReO_x/SiO₂ in Figure 4.1, this could be owing to the hydrogenolysis of 1,2,5-pentanediol over Rh-ReO_x/SiO₂ catalyst. Particularly, THFA was mainly obtained with 91% selectivity in [1,4-dioxane + n-heptane] solvent, and the same reaction also occurred in [1,4-dioxane + 1,4-dioxane] and [1,4-dioxane] solvent, the selectivity to THFA was 78% and 86%, respectively, on the contrary, in the case of [water] as solvent, the reaction showed high selectivity to 1,2,5-pentanetriol (87%). The speculated formation route of THFA from methyl β-D-dideoxy-ribofuranoside could be due to the consecutive reactions of hydrolysis, hydrogenation, and dehydration (Scheme 4.2) of dideoxy methyl ribofuranoside.

Then, the temperature effect on the catalyst that showed high selectivity to 1,2,5-pentanetriol (Rh-ReO_x/SiO₂, Ir-ReO_x/SiO₂ and Ru/C) was investigated in 1,4-dioxane and water solvent, and the stereopurity of obtained chiral polyols was also investigated (Figure 4.3). The result showed that all these three catalysts showed high yield and optical selectivity of (2*S*)-1,2,5-pentantriol at low temperature (353 K), the original stereo structure of methyl β-D-ribofuranoside was maintained. In details, 98% yield with 94% e.e. and 98% yield with 96% e.e. of (2*S*)-1,2,5-pentantriol was obtained over Ru/C and Rh-ReO_x/SiO₂ catalyst, respectively, at 353 K for 1 h; and 95% yield with 96% e.e. and 97% yield with 95% e.e. of (2*S*)-1,2,5-pentantriol was obtained over Ir-ReO_x/SiO₂ catalyst at 353 K for 4 h or 393 K for 1 h, respectively. Compared with other two catalysts, Ir-ReO_x/SiO₂ catalyst showed higher selectivity to (2*S*)-1,2,5-pentantriol at higher reaction temperature (393 K), and it showed 87% (2*S*)-1,2,5-pentanetriol yield with 94% e.e. even when the reaction time was prolonged to 24 h, while Rh-ReO_x/SiO₂ showed an 87% (2*S*)-1,2,5-pentanetriol yield with a 94% e.e. under same reaction conditions.

The synthesis of (2*R*)-1,2,5-pentanetriol from methyl β-L-arabinopyranoside was investigated by DODH-HG over ReO_x-Pd/CeO₂ and subsequent hydrolysis and hydrogenation over Rh-ReO_x/SiO₂ by adjusting the reaction temperature and reaction time. The 95 % yield with a 95 % e.e. of (2*R*)-1,2,5-pentanetriol was achieved (Table 4.2). Therefore, the enantiomers of 1,2,5-pentanetriol could be individually synthesized from glycosides by using the appropriate substrate. Moreover,

methyl α -L-rhamnopyranoside is converted to (4*R*,5*S*)-1,4,5-hexanetriol in 92% yield over Rh-ReO_x/SiO₂ catalyst via DODH + HG reaction.

4.3.2 Synthesis of saturated chiral polyols from dideoxy methyl glycosides over Pt-based catalyst^[42]

For other applications, our laboratory cooperated with Huber group in University of Wisconsin, to synthesize saturated chiral polyols from dideoxy methyl glycosides. We prepared the dideoxy products from methyl glycosides over ReO_x-Pd/CeO₂ catalyst via DODH+HG, and they focused on the work about hydrolysis and hydrogenation of saturated dideoxy product of methyl glycosides. Various methyl glycosides with *cis*-vicinal OH groups were converted into the corresponding chiral dideoxy polyols in high yields (69–93%) with largely preserving the original stereochemistry. Using a 5% Pt/SiO₂ catalyst in water, methyl α -D-mannopyranoside is converted to (2*R*,3*S*)-1,2,3,6-hexanetetrol in 91% yield and >99% e.e., and methyl α -L-rhamnopyranoside is converted to (4*R*,5*S*)-1,4,5-hexanetriol in 85% yield and >99% e.e.. And over 5% Pt/Al₂O₃-SiO₂, methyl- β -D-galactopyranoside is converted to (2*R*,5*S*)-1,2,5,6-hexanetetrol with 77% yield and 98% e.e., and methyl α -L-fucopyranoside could be converted to (2*S*,5*S*)-1,2,5-hexanetriol in 69% yield and 92% e.e. at the same reaction conditions.

4.3.2 One-pot synthesis of saturated chiral polyols from methyl glycosides

Moreover, the one-pot synthesis of (2*S*)-1,2,5-pentanetriol from methyl β -D-ribofuranoside was investigated. After the 25 h DODH+HG reaction of methyl β -D-ribofuranoside over ReO_x-Pd/CeO₂ catalyst (methyl β -D-ribofuranoside conversion >99%, methyl β -D-2,3-dideoxy-ribofuranoside yield \approx 96%), water was then added into the reaction mixture and without removal of the ReO_x-Pd/CeO₂ catalyst. The obtained mixture was reacted at 393 K, and the results are shown in Figure 4.4 and Table 4.3.

The time course result showed that (2*S*)-1,2,5-pentanetriol can be produced by one-pot DODH+HG and hydrolysis + HG of methyl β -D-ribofuranoside over ReO_x-Pd/CeO₂ catalyst, while maintaining the configuration of the original methyl β -D-ribofuranoside. The racemization of 1,2,5-pentanetriol was suppressed and methyl β -D-2,3-dideoxy-ribofuranoside was converted

smoothly to reach greater than 99 % conversion in 48 h and the selectivity for (2*S*)-1,2,5-pentanetriol was high, thus providing (2*S*)-1,2,5-pentanetriol in 94 % yield with 96% e.e. (see e.e in Table 4.3).

4.4 Conclusions

The combination of $\text{ReO}_x\text{-Pd/CeO}_2$ catalyst and hydrogenation catalyst ($\text{Rh-ReO}_x/\text{SiO}_2$, $\text{Ir-ReO}_x/\text{SiO}_2$, Pt/SiO_2 , $\text{Pt/SiO}_2\text{-Al}_2\text{O}_3$ and commercial Ru/C catalyst) showed high yield with high stereopurity to obtain the corresponding dideoxy chiral polyols from methyl glycosides. Chiral dideoxy polyols also can be one-pot synthesized from methyl glycosides over $\text{ReO}_x\text{-Pd/CeO}_2$ catalyst by DODH+HG and hydrolysis + HG reaction, while maintaining their configuration of the original stereostructure of methyl glycosides.

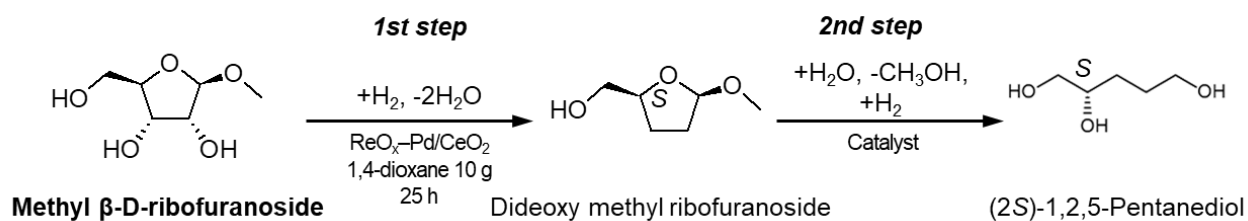
References

- [1]. Kennedy, J. F., *Carbohydrate Chemistry: Volume 14*. Royal Society of chemistry: 2007.
- [2]. Danishefsky, S. J.; Bilodeau, M. T., *Angew. Chem. Int. Ed. Engl.* **1996**, 35 (13-14), 1380-1419.
- [3]. Harris, J. M.; Keranen, M. D.; O'Doherty, G. A., *J. Org. Chem.* **1999**, 64 (9), 2982-2983.
- [4]. Allen, J. R.; Harris, C. R.; Danishefsky, S. J., *J. Am. Chem. Soc.* **2001**, 123 (9), 1890-7.
- [5]. Montero, A.; Mann, E.; Herradón, B., *Eur. J. Org. Chem.* **2004**, 2004 (14), 3063-3073.
- [6]. Boysen, M. M., *Chemistry* **2007**, 13 (31), 8648-59.
- [7]. Willfor, S.; Sundberg, K.; Tenkanen, M.; Holmbom, B., *Carbohydr. Polym.* **2008**, 72 (2), 197-210.
- [8]. Luley-Goedl, C.; Nidetzky, B., *Biotechnol J* **2010**, 5 (12), 1324-38.
- [9]. Rosatella, A. A.; Simeonov, S. P.; Frade, R. F. M.; Afonso, C. A. M., *Green Chem.* **2011**, 13 (4), 754.
- [10]. Nahain, A. A.; Ignjatovic, V.; Monagle, P.; Tsanaktsidis, J.; Ferro, V., *Med Res Rev* **2018**, 38 (5), 1582-1613.
- [11]. Tomishige, K.; Nakagawa, Y.; Tamura, M., *Green Chem.* **2017**, 19 (13), 2876-2924.
- [12]. Chheda, J. N.; Huber, G. W.; Dumesic, J. A., *Angew. Chem. Int. Ed.* **2007**, 46 (38), 7164-7183.
- [13]. Corma, A.; Iborra, S.; Velty, A., *Chem. Rev.* **2007**, 107 (6), 2411-2502.
- [14]. Node, M.; Nishide, K.; Shigeta, Y.; Shiraki, H.; Obata, K., *J. Am. Chem. Soc.* **2000**, 122 (9), 1927-1936.
- [15]. Kang, S. H.; Choi, H.-W., *Chem. Commun.* **1996**, (13), 1521-1522.
- [16]. Young, R. J.; Lovell, P. A., *Introduction to polymers*. CRC press: 2011.
- [17]. Amada, Y.; Watanabe, H.; Hirai, Y.; Kajikawa, Y.; Nakagawa, Y.; Tomishige, K., *ChemSusChem* **2012**, 5 (10), 1991-1999.
- [18]. Kühne, B.; Vogel, H.; Meusinger, R.; Kunz, S.; Kunz, M., *Catal. Sci. Technol.* **2018**, 8 (3), 755-767.
- [19]. Casiraghi, G.; Zanardi, F.; Rassu, G.; Spanu, P., *Chem. Rev.* **1995**, 95 (6), 1677-1716.
- [20]. Henderson, A. S.; Bower, J. F.; Galan, M. C., *Org Biomol Chem* **2016**, 14 (17), 4008-17.
- [21]. Cao, F.; Schwartz, T. J.; McClelland, D. J.; Krishna, S. H.; Dumesic, J. A.; Huber, G. W., *Energ. Environ. Sci.* **2015**, 8 (6), 1808-1815.
- [22]. Karanjkar, P. U.; Burt, S. P.; Chen, X. L.; Barnett, K. J.; Ball, M. R.; Kumbhalkar, M. D.; Wang, X. H.; Miller, J. B.; Hermans, I.; Dumesic, J. A.; Huber, G. W., *Catal. Sci. Technol.* **2016**, 6 (21), 7841-7851.
- [23]. Krishna, S. H.; McClelland, D. J.; Rashke, Q. A.; Dumesic, J. A.; Huber, G. W., *Green Chem.* **2017**, 19 (5), 1278-1285.
- [24]. Liu, S.; Tamura, M.; Nakagawa, Y.; Tomishige, K., *ACS Sustain. Chem. Eng.* **2014**, 2 (7), 1819-1827.
- [25]. Hayashi, Y., *Chem Sci* **2016**, 7 (2), 866-880.
- [26]. Nakagawa, Y.; Tazawa, S.; Wang, T.; Tamura, M.; Hiyoshi, N.; Okumura, K.; Tomishige, K., *ACS Catal.* **2017**, 8 (1), 584-595.

- [27]. Tazawa, S.; Ota, N.; Tamura, M.; Nakagawa, Y.; Okumura, K.; Tomishige, K., *ACS Catal.* **2016**, 6 (10), 6393-6397.
- [28]. Ota, N.; Tamura, M.; Nakagawa, Y.; Okumura, K.; Tomishige, K., *ACS Catal.* **2016**, 6 (5), 3213-3226.
- [29]. Ota, N.; Tamura, M.; Nakagawa, Y.; Okumura, K.; Tomishige, K., *Angew. Chem. Int. Ed. Engl.* **2015**, 54 (6), 1897-900.
- [30]. Cao, J.; Tamura, M.; Nakagawa, Y.; Tomishige, K., *ACS Catal.* **2019**, 3725-3729.
- [31]. Tamura, M.; Yuasa, N.; Cao, J.; Nakagawa, Y.; Tomishige, K., *Angew. Chem. Int. Ed. Engl.* **2018**, 57 (27), 8058-8062.
- [32]. Takeda, Y.; Shoji, T.; Watanabe, H.; Tamura, M.; Nakagawa, Y.; Okumura, K.; Tomishige, K., *ChemSusChem* **2015**, 8 (7), 1170-8.
- [33]. Tamura, M.; Tamura, R.; Takeda, Y.; Nakagawa, Y.; Tomishige, K., *Chemistry* **2015**, 21 (7), 3097-107.
- [34]. Nakagawa, Y.; Mori, K.; Chen, K.; Amada, Y.; Tamura, M.; Tomishige, K., *Applied Catalysis A: General* **2013**, 468, 418-425.
- [35]. Chen, K.; Tamura, M.; Yuan, Z.; Nakagawa, Y.; Tomishige, K., *ChemSusChem* **2013**, 6 (4), 613-21.
- [36]. Chen, K.; Mori, K.; Watanabe, H.; Nakagawa, Y.; Tomishige, K., *J. Catal.* **2012**, 294, 171-183.
- [37]. Tomishige, K.; Tamura, M.; Nakagawa, Y., *Chem Rec* **2014**, 14 (6), 1041-54.
- [38]. Tamura, M.; Nakagawa, Y.; Tomishige, K., *Journal of the Japan Petroleum Institute* **2019**, 62 (3), 106-119.
- [39]. Tamura, M.; Tokonami, K.; Nakagawa, Y.; Tomishige, K., *Chem Commun (Camb)* **2013**, 49 (63), 7034-6.
- [40]. Nakagawa, Y.; Shinmi, Y.; Koso, S.; Tomishige, K., *J. Catal.* **2010**, 272 (2), 191-194.
- [41]. Shinmi, Y.; Koso, S.; Kubota, T.; Nakagawa, Y.; Tomishige, K., *Applied Catalysis B: Environmental* **2010**, 94 (3-4), 318-326.
- [42]. S. Krishna, J. Cao, M. Tamura, Y. Nakagawa, M. De bruyn, G. S Jacobson, B. M. Weckhuysen, J. A. Dumesic, K. Tomishige, and G. W. Huber, *ACS Sustainable Chem. Eng.* **2019**, <https://doi.org/10.1021/acssuschemeng.9b04634>.

Table 4.1 Eluted amount of metals in $\text{ReO}_x\text{-Pd/CeO}_2$ catalyst

Separation method of catalyst	Conv. / %	Selectivity / %		Eluted amount of metal / %	
		Dideoxy product	Others	Re	Pd
Air atmosphere	>99	94	6	0.5	<0.1
N_2 atmosphere	>99	94	6	<0.1	<0.1



Scheme 4.1 Synthesis of chiral polyol from methyl-β-D-ribofuranoside via DODH + HG reaction

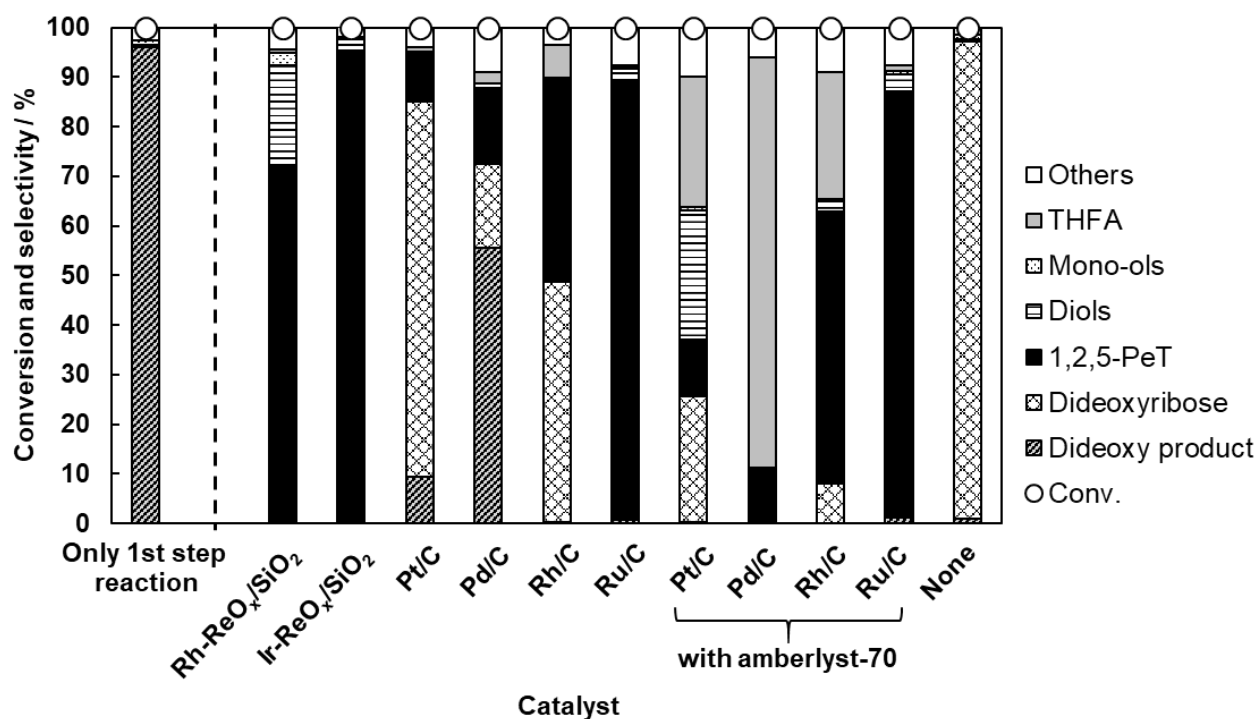


Figure 4.1 Catalyst screening for synthesis of 1,2,5-pentanetriol from methyl- β -D-ribofuranoside via DODH + HG reaction

Reaction conditions:

1st step: Methyl β -D-ribofuranoside 0.25 g, ReO_x-Pd/CeO₂ (Re=2 wt%, Pd/Re=1/4) 100 mg, 1,4-dioxane 10 g,

$T=413$ K, $P_{H_2}=8$ MPa, $t=25$ h.

2nd step: Reaction solution of 1st step 10 mL, catalyst 100 mg, (amberlyst 100 mg), water 10 g,

$T=393$ K, $P_{H_2}=8$ MPa, $t=4$ h.

Reduction conditions (Ir-ReO_x/SiO₂): Water 2 g, $T=473$ K, $P_{H_2}=8$ MPa, $t=1$ h.

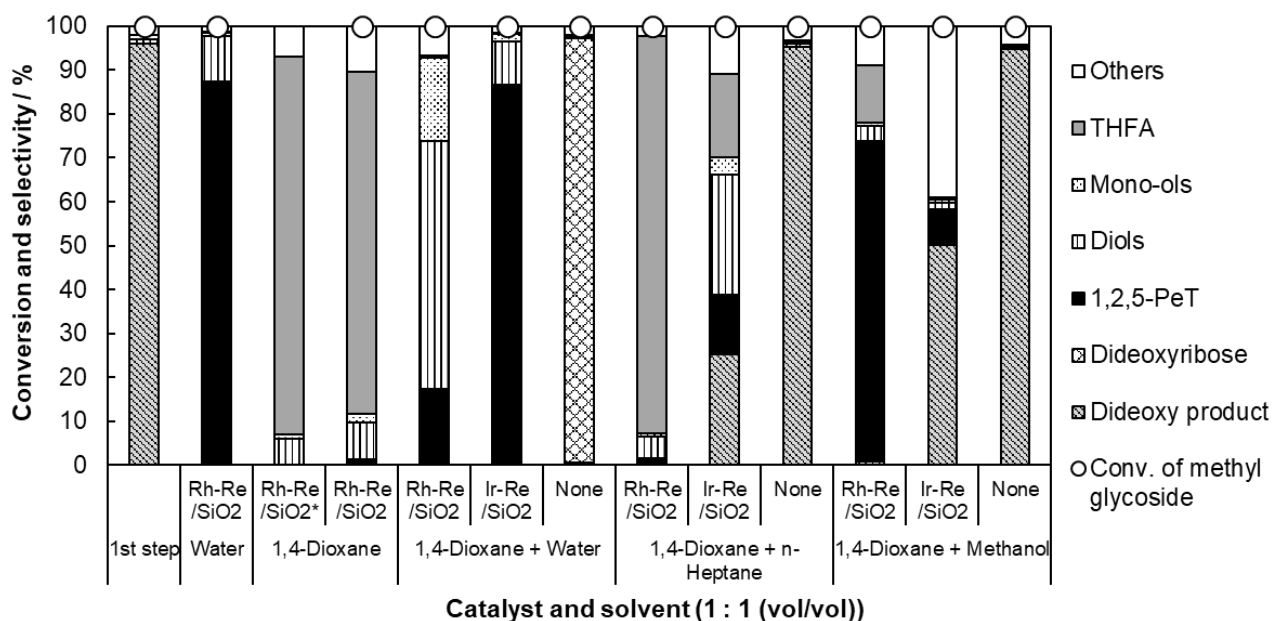


Figure 4.2 Solvent effect on the synthesis of 1,2,5-pentanetriol from methyl-β-D-ribofuranoside via DODH + HG reaction

Reaction conditions:

1st step: Methyl β-D-ribofuranoside 0.25 g, ReO_x-Pd/CeO₂ 100 mg, 1,4-dioxane 10 g,

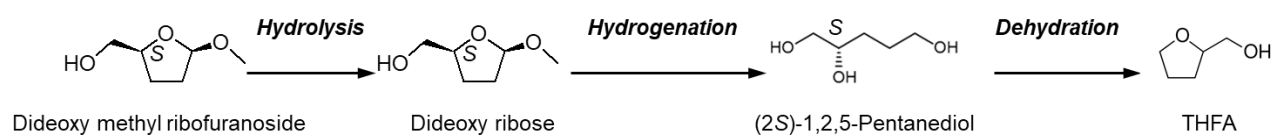
$T=413\text{ K}$, $PH_2=8\text{ MPa}$, $t=25\text{ h}$.

2nd step : Reaction solution of 1st step 10 mL, catalyst 100 mg, additive solvent 10 mL,

$T=393\text{ K}$, $PH_2=8\text{ MPa}$, $t=24\text{ h}$.

Reduction conditions (Ir-ReO_x/SiO₂) : Solvent 2 mL, $T=473\text{ K}$, $PH_2=8\text{ MPa}$, $t=1\text{ h}$.

(*) New solvent (1,4-dioxane) was not added before 2nd step reaction.



Scheme 4.2 Speculated formation route of tetrahydrofurfuryl alcohol from methyl β -D-dideoxy-ribofuranoside.

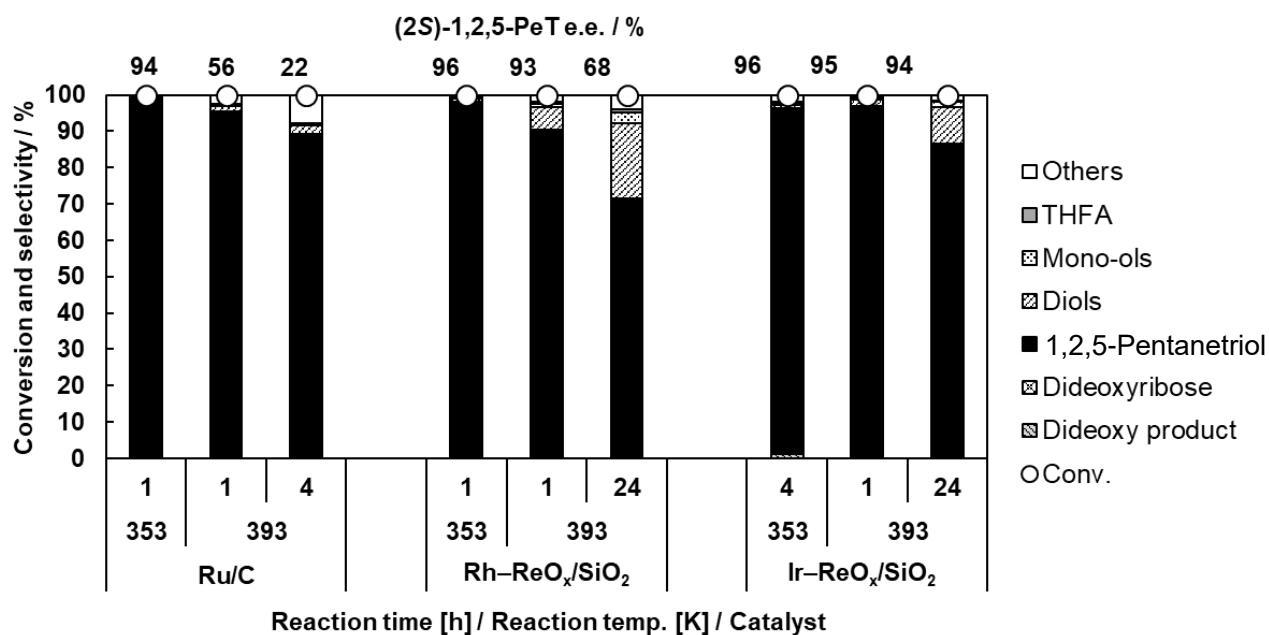


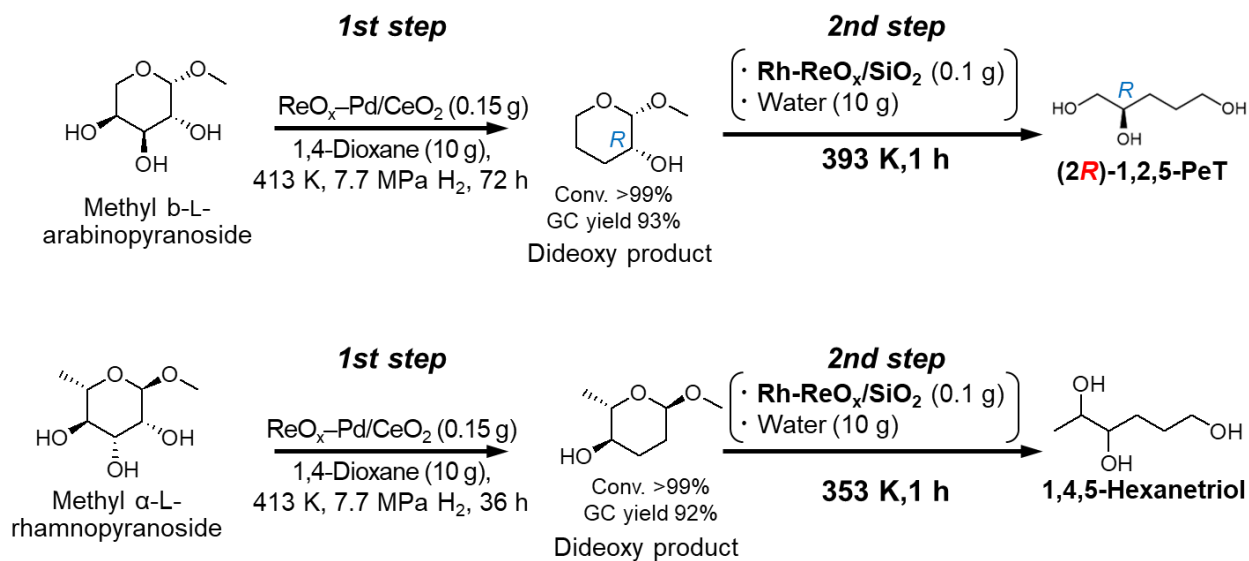
Figure 4.3 Reaction temperature effect on the synthesis of 1,2,5-pentanetriol from methyl- β -D-ribofuranoside via DODH + HG reaction

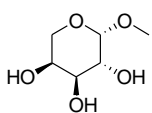
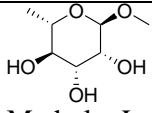
Reaction conditions:

1st step : Methyl β -D-ribofuranoside 0.25 g, ReO_x-Pd/CeO₂ 100 mg, 1,4-dioxane 10 g, $T=413$ K, $P_{H_2}=8$ MPa, $t=25$ h.

2nd step : Reaction solution of 1st step 10 mL, catalyst 100 mg, water 10 g, $T=353$ or 393 K, $P_{H_2}=8$ MPa, $t=1 - 24$ h.

Reduction conditions (Ir-ReO_x/SiO₂) : Water 2 g, $T=473$ K, $P_{H_2}=8$ MPa, $t=1$ h.

Table 4.1 Synthesis of chiral product from methyl glycosides over Rh–ReO_x/SiO₂ via DODH + HG reaction

Substrate	Temp. / K	Time / h	Conv. / %	Selectivity / %					(2S)-1,2,5-PeT e.e. / %
				Dideoxy product	Target product	Diols	Mono-ols	Others	
 Methyl β-L-arabinopyranoside	353	1	>99	97	1	<1	<1	1	-
	373	1	>99	63	34	1	<1	2	-
	393	1	>99	1	95	1	1	2	95
		24	>99	2	94	2	<1	2	82
 Methyl α-L-rhamnopyranoside	353	1	>99	<1	97	<1	<1	3	-

Reaction conditions:

1st step: Methyl β-L-arabinopyranoside or methyl α-L-rhamnopyranoside 0.25 g, ReO_x-Pd/CeO₂ 150 mg, 1,4-dioxane 10 g, *T*=413 K, *P*H₂=8 MPa, *t*=72 or 36 h.2nd step: Reaction solution of 1st step 10 mL, Rh–ReO_x/SiO₂ 100 mg, water 10 g *P*H₂=8 MPa

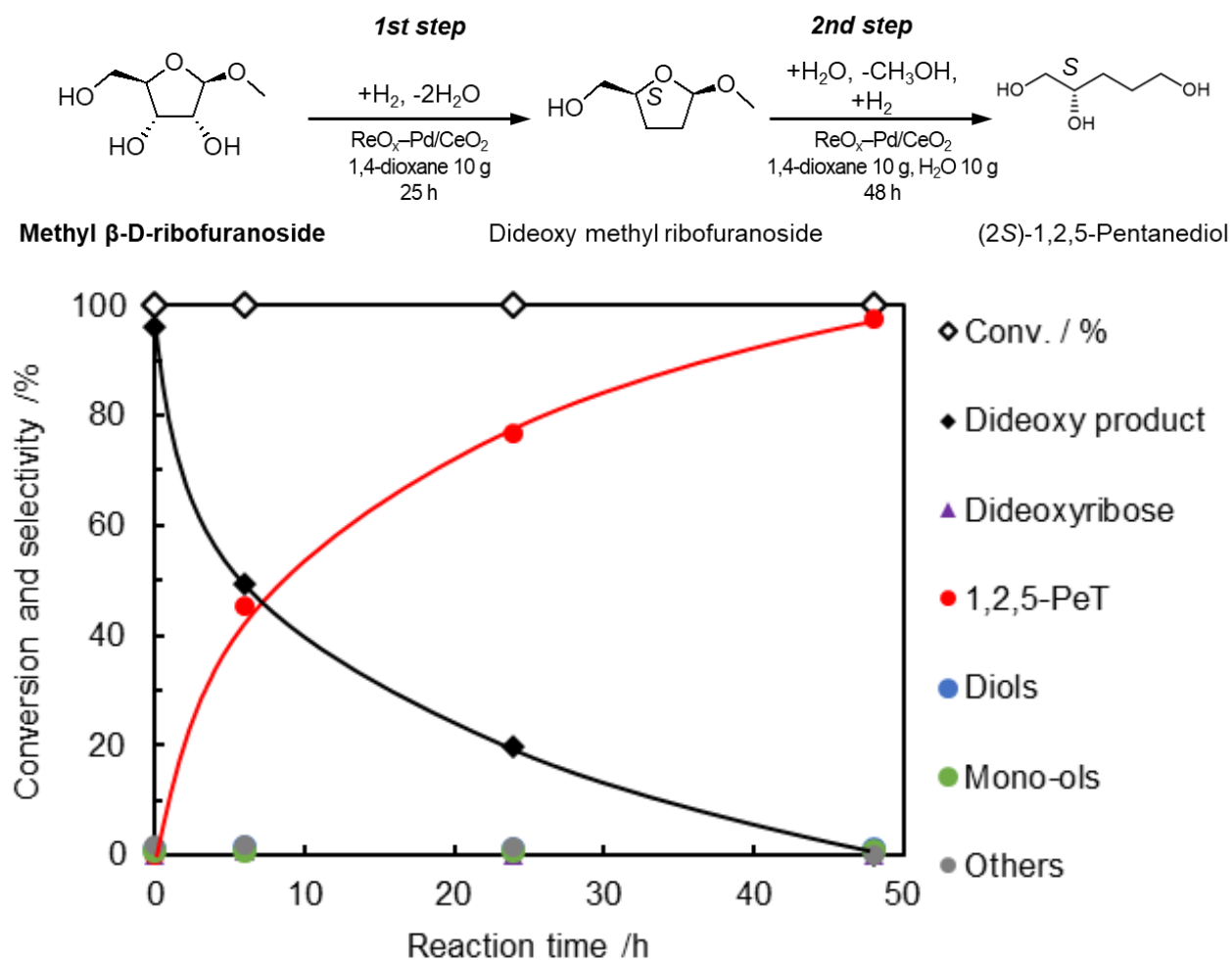


Figure 4.4 One-pot synthesis of 1,2,5-pentanetriol from methyl-β-D-ribofuranoside over $\text{ReO}_x\text{-Pd/CeO}_2$

Reaction conditions :

1st step : Methyl β-D-ribofuranoside 0.25 g, $\text{ReO}_x\text{-Pd/CeO}_2$ 100 mg, 1,4-dioxane 10 g, $T=413\text{ K}$, $P\text{H}_2=8\text{ MPa}$, $t=25\text{ h}$.

2nd step : Reaction solution of 1st step(without separation of $\text{ReO}_x\text{-Pd/CeO}_2$) 10 mL, water 10 g, $T= 393\text{ K}$, $P\text{H}_2=8\text{ MPa}$, $t=6 - 48\text{ h}$.

Table 4.3 One-pot synthesis of 1,2,5-pentanetriol from methyl- β -D-ribofuranoside over $\text{ReO}_x\text{-Pd/CeO}_2$

Time / h	Conv. / %	Selectivity / %							(2S)-1,2,5-PeT e.e. / %
		Dideoxy product	Dideoxyribose	1,2,5-PeT	Diols	Mono-ols	THFA	Others	
0	>99	96	<1	<1	1	1	<1	2	-
6	>99	49	1	45	2	1	<1	2	-
24	>99	20	<1	77	1	1	<1	1	96
48	>99	<1	<1	97	1	1	<1	<1	96

Reaction conditions :

1st step : Methyl β -D-ribofuranoside 0.25 g, $\text{ReO}_x\text{-Pd/CeO}_2$ 100 mg, 1,4-dioxane 10 g, $T=413$ K, $P_{\text{H}_2}=8$ MPa, $t=25$ h.

2nd step : Reaction solution of 1st step(without separation of $\text{ReO}_x\text{-Pd/CeO}_2$) 10 mL, water 10 g, $T= 393$ K, $P_{\text{H}_2}=8$ MPa, $t=6 - 48$ h.

Chapter 5

Summary and Conclusions

5.1 Summary

The development of direct and selective transformation of monosaccharides without the protection of the OH groups and keeping the original stereostructure is an ideal method for saccharide transformation and a powerful tool for biomass transformation.

$\text{ReO}_x\text{-Pd/CeO}_2$ ($\text{Re}=2$ wt%, $\text{Pd/Re}=0.25$) was an effective catalyst for the direct and selective transformation of methyl glycosides having *cis*-vicinal OH groups into the corresponding dideoxy products in high yields with maintaining the original structure using H_2 as a reductant. From the kinetic results, the reactivity of methyl glycosides is lower than that of simple cyclic diols, which can be attributed to the presence of the substituents in the methyl glycosides except the *cis*-vicinal diols. Moreover, the reactivity of the methyl glycosides depended on the structure, and the low activity is related to the direction of the substituents adjacent to the *cis*-vicinal diols in methyl glycosides. The kinetic parameters regarding substrate concentration and H_2 pressure are almost zero in DODH+HG of methyl glycosides and simple cyclic diols over $\text{ReO}_x\text{-Pd/CeO}_2$ catalyst, suggesting that the reaction mechanisms of the methyl glycosides and simple cyclic diols is similar. DFT calculations of the adsorption state and the transition state of methyl glycosides on isolated Re species over CeO_2 showed that the activation energy of these methyl glycosides is different, which was also supported by Arrhenius plots based on the experimental results. The reactivity difference of methyl glycosides may be due to their activation energy differences, and the difference of these substrates is derived from the intricate interactions between the adjacent functional groups to *cis*-vicinal OH groups and the surface hydroxy groups (Chapter 2).

$\text{ReO}_x\text{-Au/CeO}_2$ ($\text{Re}=1$ wt%, $\text{Au/Re}=0.3$) prepared by deposition-precipitation method ($\text{ReO}_x\text{-}^{\text{dp}}\text{Au}^{0.3}/\text{CeO}_2$) was an effective and reusable heterogeneous catalyst for DODH of methyl glycosides without protection of the OH groups even at low H_2 pressure (0.2-1.7 MPa),

providing the corresponding unsaturated monosaccharides with the original stereo-structure in high selectivities and yields. (Chapter 3)

The combination of $\text{ReO}_x\text{-Pd/CeO}_2$ catalyst and hydrogenation catalyst ($\text{Rh-ReO}_x/\text{SiO}_2$, $\text{Ir-ReO}_x/\text{SiO}_2$, Pt/SiO_2 , $\text{Pt/SiO}_2\text{-Al}_2\text{O}_3$, and commercial Ru/C) showed high yield and high stereoselectivity to the corresponding dideoxy chiral polyols from methyl glycosides. (2*S*)-1,2,5-Pentanetriol could be produced by the one-pot DODH+HG and hydrolysis + HG conversion of methyl β -D- ribofuranoside over $\text{ReO}_x\text{-Pd/CeO}_2$ catalyst with maintaining the configuration of the original methyl β -D-ribofuranoside. (Chapter 4)

5.2 Conclusions

Methyl glycosides with *cis*-vicinal OH groups could be directly and selectively transformed to the corresponding saturated dideoxy products over $\text{ReO}_x\text{-Pd/CeO}_2$ catalyst via DODH +HG reaction, and the methyl glycosides could be transformed to the corresponding unsaturated dideoxy products in high yields over $\text{ReO}_x\text{-Au/CeO}_2$ catalyst via DODH reaction without protection of the OH groups and with keeping the original stereostructure. Chiral polyols were selectively synthesized from methyl glycosides in high total yield and high e.e. by DODH, hydrolysis, and hydrogenation reactions.

Acknowledgements

This thesis originated in the time between October 2016 and March 2020 at the Tomishige Laboratory, Department of Applied Chemistry, School of Engineering, Tohoku University, with the financial support from the China Scholarship Council (CSC). This thesis would not have been possible without the generous contributions of many people that I have had the privilege to work with and learn from.

First of all, my sincere thanks go to my supervisor, Professor Keiichi Tomishige, for giving me the opportunity to be a member of this legendary research group, for this challenging research topic, for the invaluable scientific discussion, for the tireless guidance, for the kind encouragements and for all the support which were crucial for the success of this thesis. My heartfelt thanks go to Professor Yoshinao Nakagawa for providing me numerous academic advices and valuable support during my doctoral degree. I also want to send my unlimited gratitude to Prof. Masazumi Tamura, for the excellent discussions, for the uncountable advices in my experiment and for his patience with my English grammar. I'm proud of having shared more than 3 years with these three distinguished experts on my way to complete the doctoral degree.

My heartfelt grateful go out to:

Prof. Kasai and Prof. Hattori for their participation in the degree committee.

All members in the laboratory, both past and present, for lending valuable advice and encouragement, for the help during the experiments, and for providing great experiences in the laboratory.

Mr. Naoto Yuasa, I really appreciate the time he spent on training my experiment skills and the supports for my experiment, and I really admire his enormously conscientious and hard-working.

Also, I would like to express my gratitude to Prof. Guoqing Guan, who gave me a chance to study at Hirosaki University with a very good study environment, and I really very grateful to his guidance and supports throughout my master's and doctoral course. He gave me many invaluable comments and advices to solve those complicated problems during my research and life.

Finally, I would like to thank my family and friends for their unwavering support over these years.

Summary

I love you all for now and forever! In particular, I want to thank my family for their unconditional love. I would not be where I am today without them, they always support me and encourage me to strive the best that I can.

January 2020

School of Engineering

Tohoku University

Ji Cao

List of Publications

(1) Masazumi Tamura, Naoto Yuasa, **Ji Cao**, Yoshinao Nakagawa, Keiichi Tomishige
Transformation of Sugars to Chiral Polyols over a Heterogeneous Catalyst
Angewandte Chemie-International Edition, 57 (2018) 8058-8062

(2) **Ji Cao**, Masazumi Tamura, Yoshinao Nakagawa, Keiichi Tomishige
Direct Synthesis of Unsaturated Sugars from Methyl Glycosides
ACS Catalysis, 9 (2019) 3725-3729

(3) Siddarth Krishna, **Ji Cao**, Masazumi Tamura, Yoshinao Nakagawa, Mario De bruyn,
Graeme S Jacobson, Bert M. Weckhuysen, James A. Dumesic, Keiichi Tomishige, and George
W. Huber
Synthesis of Hexane-Tetrols and -Triols with Fixed Hydroxyl Group Positions and
Stereochemistry from Methyl Glycosides over Supported Metal Catalysts
ACS Sustainable Chemistry & Engineering, (2019), in publication